

UNIVERSITÉ LILLE 1 SCIENCES ET TECHNOLOGIES

Année : 2009

N₀ d'ordre :

THÈSE

présentée en vue d'obtenir le grade de

DOCTEUR

en

Spécialité: CHIMIE

par

Mei WANG

DOCTORAT DELIVRE EN COTUTELLE

PAR L'UNIVERSITÉ LILLE 1 SCIENCES ET TECHNOLOGIES ET

L'UNIVERSITÉ DE SHANDONG

FONCTIONNALISATION DES SURFACES DE DIAMANT DOPÉ AU BORE ET APPLICATIONS EN BIOSCIENCES

Soutenue le 15.06.2009 devant le jury d'examen:

M. Bo Tang	Rapporteur	Professeur	Université normale de Shandong
M. Kezheng Chen	Rapporteur	Professeur	Université des sciences et technologies de Qingdao
Mme. Sabine Szunerits	Examinatrice	Professeure	INP Grenoble
M. Guanghui Min	Examineur	Professeur	Université de Shandong
M. Longwei Yin	Examineur	Professeur	Université de Shandong
M. Musen Li	Directeur de thèse	Professeur	Université de Shandong
M. Rabah Boukherroub	Directeur de thèse	Directeur de recherche	Institut de Recherche Interdisciplinaire

Thèse préparée au Laboratoire de Biointerfaces Group d'Interdisciplinary Research
Institute(IRI)-IEMN, FRE 2963

RÉSUMÉ

Le diamant est un matériau caractérisé par ses propriétés physiques très spécifiques bien que son utilisation en sciences et en ingénierie est longtemps freinée par le coût élevé des substrats monocristallins. Avec les développements récents des techniques de dépôt de couches minces de diamant sur différents substrats, il est possible d'exploiter ses propriétés pour des applications très variées.

Le diamant présente des caractéristiques physique, chimique et mécanique exceptionnelles : une grande conductivité thermique, une dureté très élevée, une large bande, une transparence optique (de l'UV à l'IR) et une grande stabilité chimique. C'est un semi-conducteur à grand gap (5.45eV) possédant de bonnes propriétés mécaniques et caractérisé par ses propriétés de biocompatibilité. Le dopage de celui-ci lui confère de bonnes propriétés de conduction électrique et donc ouvre des perspectives pour son utilisation en bioélectronique. Pour cette fin, il est devenu urgent de développer une chimie de surface spécifique pour introduire des fonctions chimiques ou biologiques sur la surface.

Mon travail de thèse s'inscrit dans cette perspective. D'un point de vue technologique, le diamant cristallin est très cher et donc notre étude a été limitée au diamant polycristallin. Dans cette thèse, on a contribué à la mise au point de nouvelles méthodes de fonctionnalisation de la surface de diamant. Ces méthodes sont basées sur des concepts chimique, photochimique et électrochimique et permettent d'introduire des groupements fonctionnels sur la surface de diamant de façon contrôlée.

La première partie de ma thèse concerne la réaction d'oxydation de la surface de diamant hydrogéné en utilisant trois différentes techniques : plasma d'oxygène, voie électrochimique et UV/ozone. Nous avons utilisé les techniques de caractérisation par spectrométrie de photoélectrons induits par rayons X (XPS) et mesures électrochimiques (Mott-Schottky) pour comparer la composition chimique des surfaces de diamant oxydé. Il en ressort que le rapport entre les différentes composantes (C-OH, C-O-C et C=O) varie selon la technique d'oxydation utilisée. La réactivité des groupes -OH de surface a été exploitée pour coupler le 3-aminopropyltriéthoxysilane (APTES) et l'acide trifluoroacétique (CF₃COOH) afin d'évaluer la densité de greffage de ces molécules sur les différentes surfaces. Les résultats obtenus indiquent que les surfaces de diamant qui ont une densité de greffage plus élevée ont un potentiel de bande plate déplacé positivement. Ce comportement (déplacement du potentiel

de la bande plate vers des valeurs positives) suggère une terminaison chimique dominée par des groupements C-OH sur la surface de diamant oxydé.

Cette étude a permis de mettre en évidence l'effet de la terminaison chimique sur la conductivité de diamant dopé au bore. Les résultats obtenus sont très importants au regard des questions fondamentales débattues dans la littérature concernant le rôle de la surface sur la conductivité de diamant.

Dans la deuxième partie de ma thèse, j'ai utilisé pour la première fois la réaction de couplage par « click ». Cette technique connue sous le nom de « click chemistry » est très versatile et permet de coupler des alcynes et des azides dans des conditions douces avec de bons rendements. Nous avons, par cette méthode, greffé des groupes « thiophène, ferrocène ou cyclophane » sur la surface de diamant terminée par des fonctions « azide » (N_3). La fonction azide est obtenue par réaction de la surface de diamant oxydée avec l'acide 4-azidobenzoïque. Les résultats de spectrométrie de photoélectrons induits par rayons X (XPS), angles de contact et mesures électrochimiques permettent de conclure : i) succès de la réaction de cycloaddition [3+2] azide-alcyne pour l'incorporation de groupements thiophène et la formation d'une structure hybride : diamant/polythiophène, suite à une réaction de polymérisation électrochimique des groupements 'thiophène' terminaux avec du thiophène monomère en solution ; ii) greffage de groupements 'ferrocène' électroactifs sur la surface de diamant terminée 'azide' avec une grande sélectivité et un rendement élevé ; iii) immobilisation d'une molécule de cyclophane comportant un groupe alcyne terminal.

La troisième partie de ma thèse concerne l'étude de la réactivité des surfaces de diamant oxydé avec un liquide ionique (IL, 1-(Methyl carboxylic acid)-3-octylimidazolium-bis (tri fluoromethyl sulfonyl) imide). Le couplage du liquide ionique a été réalisé par réaction d'estérification des groupements -OH de surface avec les fonctions « acide » du liquide ionique. Les différentes étapes sont caractérisées par spectrométrie de photoélectrons induits par rayons X (XPS), angle de contact et mesures électrochimiques.

Ensuite, nous avons réalisé l'échange anionique des groupements $(CF_3SO_3)_2N^-$ de la surface de diamant fonctionnalisée par le liquide ionique avec les anions BF_4^- , NO_3^- and PF_6^- . L'évolution des propriétés de mouillage de la surface de diamant fonctionnalisée par le liquide ionique suite à l'échange anionique a été mis en évidence par les mesures d'angle de contact.

Finalement, nous avons mis au point une nouvelle technique d'halogénéation de la surface de diamant hydrogéné. A l'inverse des techniques décrites dans la littérature (utilisation de gazes très réactifs tels que Cl_2 et Br_2 à haute température pour préparer des surfaces terminées C-Cl et C-Br), on a développé une méthode simple et facile à mettre en œuvre pour préparer

des surfaces halogénées. Nous avons exploité la réactivité des liaisons C-H de surface avec la *N*-chlorosuccimide (NCS) et la *N*-bromosuccimide (NBS) en présence d'un initiateur de radicaux, le peroxyde de benzoyle.

La réactivité chimique des surfaces halogénées a été exploitée par réaction de la surface bromée avec les réactifs de Grignard. De plus, une terminaison « azide » est obtenue par substitution nucléophile de -Br par -N₃ suite à une réaction de la surface bromée avec NaN₃. La présence de la fonction « azide » terminale a été mise en évidence par la réaction chimique par « click » avec l'éthynyle ferrocène. Les différentes étapes sont caractérisées par spectrométrie de photoélectrons induits par rayons X (XPS), angles de contact et mesures électrochimiques.

Mots clés : diamant dopé au bore; fonctionnalisation; oxydation; chimie par « click »; liquide ionique; halogénéation

ABSTRACT

Diamond display some of the most extreme physical properties even though its practical use in science and engineering has been restricted due its scarcity and expense. With the recent developments of techniques for the deposition of thin films of diamond on various substrates, it is now possible to explore these superior properties in various exciting applications.

Diamond, owing to its combination of specific physical, chemical and mechanical properties such as high thermal conductivity, high hardness, large band gap, optical transparency over a wide wavelength region (from UV to IR), stability against chemical reagents, high mechanical stability, corrosion resistance and biocompatibility has been regarded as one of the most promising industrial materials in various fields. Diamond display a very large band-gap (5.45eV), but can be made conducting by doping with certain elements. On basis of all above properties, diamond is a particularly attractive substrate for robust chemical and biochemical modification for sensor applications.

In this thesis, we have contributed to the development of easy, controllable and specific surface functionalization methods for the introduction of different functional groups on the diamond surface. These methods are based on chemical, photochemical, and electrochemical concepts.

The initial phase of the study includes the oxidation of hydrogen-terminated boron-doped diamond (BDD) surfaces using three different approaches, and the resulting surfaces were characterized by X-ray photoelectron spectroscopy (XPS) and Mott-Schottky analysis. Chemical coupling of 3-aminopropyltriethoxysilane (APTES) and trifluoroacetic acid (CF_3COOH) to the oxidized surfaces were used to verify the difference in terms of grafting density. These organic molecules were investigated for their specific reactivity with hydroxyl groups. It is concluded that diamond interfaces exhibiting better grafting efficiency also show a more positive flat band position. This behaviour suggests strongly that a positive shift of the flat band potential is related to the formation of a higher density of C-OH bonds rather than C-O-C groups. Based on this result, the electrochemical oxidation is one of the preferred methods, forming the highest amount of C-OH groups without graphitizing the diamond interface, as observed in the case of oxygen plasma treatment. However, for APTES modified BDD surface , photochemical oxidation for short times (5 to 15min) results in high N/O

ratios together with an increase in electron transfer kinetics (for 15min treatment) and is an alternative for undoped diamond samples.

In the second part of my work, “click chemistry” was used for the first time to covalently attach acetylene-bearing molecules (thiophene, ferrocene as well as cyclophane) to azide-terminated BDD surfaces. The azide termination was obtained through an esterification reaction between 4-azidobenzoic acid and the terminal hydroxyl groups of oxidized BDD surfaces. The resulting surfaces were characterized using X-ray photoelectron spectroscopy (XPS), water contact angle and electrochemical measurements. As a result, 1) the applicability of azide-alkyne [3+2] cycloaddition was successfully demonstrated with ethynyl thiophene and further electrochemical polymerization of terminal “thiophene” units with thiophene monomers in solution led to the formation of a polythiophene film covalently linked to the BDD surface; 2) the attachment of an electroactive ferrocene moiety on azide terminated BDD surface was achieved in high selectivity and yield; 3) alkyne-functionalized cyclophane can undergo click chemistry to conveniently attach these units onto a preformed azide-functionalized BDD surface.

Another aspect regarding the reactivity of the oxidized BDD surfaces concerns its chemical coupling with an ionic liquid (IL, 1-(Methylcarboxylacid)-3-octylimidazolium-bis (trifluoromethyl sulfonyl) imide) through an esterification reaction. The resulting surface was characterized and confirmed by X-ray photoelectron spectroscopy, water contact angle and electrochemical measurements. Anion exchange of $(\text{CF}_3\text{SO}_3)_2\text{N}^-$ with BF_4^- , NO_3^- and PF_6^- of the IL modified BDD surface was investigated subsequently. Contact angles of IL modified BDD varied alternatively in the process of anion exchange reactions between $(\text{CF}_3\text{SO}_3)_2\text{N}^-$ and BF_4^- , NO_3^- and PF_6^- , suggesting successful anion exchange.

Finally, a versatile strategy for chemical halogenation of hydrogenated boron-doped diamond (H-BDD) surfaces was proposed. Brominated and chlorinated boron-doped diamond electrodes were prepared in a controlled way through a radical substitution reaction using *N*-halogenosuccinimide (*N*-chloro or *N*-bromosuccinimide) in the presence of benzoyl peroxide. This versatile strategy was developed for chemically functionalizing hydrogenated boron-doped diamond (H-BDD) surfaces in a manner that stabilizes the underlying diamond against oxidation and allows subsequent chemical or electrochemical functionalization of the surface. The chemical reactivity of the halogenated BDD surfaces was confirmed by exposing the brominated BDD surface to a Grignard reagent. Furthermore, an azide termination was obtained through a nucleophilic substitution reaction of the brominated BDD surface with sodium azide. Ferrocene was linked with the azide-terminated BDD surface using click

chemistry. The resulting surfaces were characterized and confirmed by X-ray photoelectron spectroscopy, water contact angle and electrochemical measurements.

Key words: boron-doped diamond; surface functionalization; surface oxidation; click chemistry; Ionic liquid; halogenation

ACKNOWLEDGEMENTS

I would like to give my sincere thanks to my advisor Professors-Rabah Boukherroub and Musen Li for their patience, guidance, stimulating discussion, continued advice permanent support over past three years on this project, teaching me thoroughness in scientific thinking, and the time and patience they have spent reading and editing the manuscript of this dissertation. Working with them on this study has been an excellent learning experience with many challenges and responsibilities. Thank Professor Rabah Boukherroub for giving me the opportunity to join his group. Thank Professor Musen Li for supporting the Co-tutelle and all preparation for my graduation. It was a great pleasure and privilege to study under their mentorships.

My special thanks go to Professor Sabine Szunerits. If I only have one-sentence to say about her, I would like to say that she is the most kind, generous, optimistic and knowledgeable person I ever met and I was so lucky to have her as my teacher. She is such a great teacher: she provided me with invaluable opportunities to know surface chemistry and to enjoy this research; she provided me with abundant guidance and support, and always believed in me and encouraged me to do my best; she is always there for me to help me with my research, my career plans, my language and my life in France.

I thank all people from my collaborative research group IRI-IEMN in France for all the help, discussions, and sharing. It is my honor to work with all of you: Dr. Yannick Coffinier, Dr. Manash R. Das, Dr. Vera G. Praig, Dr. Manjusha Shelke, Dr. Elisabeth galopin, Dr. Joanna Niedziółka-Jönsson, Dr. Paolo Actis, Dr. Martin Jönsson-Niedziolka, Gaëlle. Piret, Florian Lapierre, Phuong Nhung Nguyen, Maël Manesse, Hana Ferkous, HongQin Liu, Chiboub Nawel, and Keith.Fahnestock.

My thanks go to my office: Dr. Gong Jian-hong, Dr. Su Qing-cai, Dr. Qi Yong-xin, Dr. Li Li, Cao Ning, Li He-sheng, Tian Bin, Liu Lei, Wang Cheng-xiang, Zheng Ke-fang, Li Hong-yan, Chen Hua-ying.

I would like to express my thanks to Professor Xu Bin, Professor Yin Long-wei, Professor Lv Yu-peng, and Professor Gong Zhi-guang for all the help. Thank Dr. David Guerin for information about cleanroom and his invaluable discussions about chemistry, which was very valuable for my research. I would like to express my thanks to Professor Deresmes Dominique for AFM training; Professor Boyaval Christophe for SEM measurement and

Professor Liu Yu-xian for TEM measurement.

I want to thank my parents. Thanks for their care and interaction with me in my life. I thank my brother for taking care of my parents. I also want to thank all my friends for always being there for me. I wish to share this accomplishment with my boyfriend, Yang Dapeng. Without him, I can not imagine what my life would be now. He has been with me all the way and has always enjoyed discussing my research with me.

In particular, I want to give my thanks to Chinese government for the China Scholarship Council Award.

Mei WANG

Villeneuve d'ascq, France

16th April, 2009

TABLE OF CONTENTS

RÉSUMÉ	i
ABSTRACT	v
ACKNOWLEDGEMENTS	ix
TABLE OF CONTENTS	I
CHAPTER 1 INTRODUCTION	1
1.1. Diamond: a potential candidate in bioelectronics	1
1.2. Preparation of diamond films	4
1.3. Properties of diamond	6
1.3.1. General properties of diamond	6
1.3.2. Properties of doped diamond electrodes	6
1.3.2.1. Dopants for diamond electrodes and their electrical properties	6
1.3.2.2. Electrochemical properties in aqueous electrolytes	7
1.3.2.3. Photoelectrochemistry	9
1.3.3. Stability of diamond electrodes	10
1.3.4. Biocompatibility of diamond electrodes	12
1.4. Functionalization of diamond electrodes	12
1.4.1. Functionalization of hydrogen-terminated diamond surfaces through C-C bond formation	13
1.4.1.1. Direct reaction of hydrogen-terminated diamond surfaces with alkenes under photochemical conditions.....	13
1.4.1.2. Diazonium chemistry	14
1.4.2. Functionalization of hydrogen-terminated diamond surfaces through C-O bond formation	17
1.4.3. Oxidation of H-terminated diamond surfaces	18
1.4.4. Halogenation of H-terminated diamond surfaces.....	21
1.4.5. Amination of H-terminated diamond surfaces	23
1.4.6. Reactivity of oxidized diamond surfaces	23
1.4.6.1 Silanization reactions on oxygen-terminated diamond surfaces	23
1.4.6.2 Esterification reactions of oxygen-terminated diamond surfaces	25
1.4.7. Reactivity of halogenated surfaces.....	26
1.4.8. Reactivity of aminated diamond surfaces	28
1.5. Scope of the thesis.....	29
1.6. References	31
CHAPTER 2 MATERIAL AND METHODS	41

2.1. Materials and reagents.....	41
2.1.1. Chemicals	41
2.1.2. Deionized water.....	41
2.1.3. Glassware and containers	42
2.1.4. Safety considerations.....	42
2.2. Synthesis of alkyne-functionalized cyclophane 6	42
2.2.1. Synthesis of solid 3	42
2.2.2. Synthesis of alkyne-functionalized cyclophane 6	42
2.3. Preparation of the substrates	43
2.3.1. Hydrogen terminated boron-doped diamond samples	43
2.3.2. Hydrogen-terminated free-standing boron-doped diamond films.....	44
2.3.3. Hydrogen-terminated porous silicon substrates	46
2.4. Functionalization of the substrates	46
2.4.1. Functionalization of oxygen-terminated boron-doped diamond.....	47
2.4.1.1. Oxidation of hydrogen-terminated boron-doped diamond.....	47
2.4.1.1.1. Electrochemical oxidation.....	47
2.4.1.1.2. Photochemical Oxidation	47
2.4.1.1.3. Oxygen-plasma.....	47
2.4.1.2. Modification of three kinds of oxygen terminated boron-doped diamond.....	47
2.4.1.2.1. Silanization.....	47
2.4.1.2.2. Esterification	47
2.4.1.3. Click chemistry	47
2.4.1.3.1. Azide termination.....	47
2.4.1.3.2. “Clicking” ferrocene on azide-terminated BDD surface.....	48
2.4.1.3.3. “Clicking” thiophene on azide-terminated BDD surface.....	48
2.4.1.3.4. “Clicking” cyclophane on azide-terminated BDD surface	48
2.4.1.4 Esterification between hydroxyl groups of oxygenated boron doped diamond (HO-BDD) and ionic liquid (IL)	48
2.4.1.4.1 Anion exchange reactions	48
2.4.2. Halogenation of hydrogen terminated boron-doped diamond	49
2.4.2.1. Reaction halogenated boron-doped diamond surfaces with Grignard reagents.....	49
2.4.2.2. Reaction of the brominated boron-doped diamond (Br-BDD) with sodium azide.....	49
2.4.2.3. Azide-alkyne Huisgen cycloaddition reaction between ethynyl ferrocene and azide-terminated boron-doped diamond (N ₃ -BDD)	50
2.4.3. Functionalization of porous silicon surfaces with thiophene groups	50
2.4.3.1. Amine termination.....	50
2.4.3.2. Azide termination.....	50
2.4.3.3. “Clicking” thiophene on azide-terminated PSi surface.....	50
2.4.3.4. Polymerization of the surface linked thiophene units	50

2.5. Surface characterization	51
2.5.1. Contact angle measurements	51
2.5.2. X-ray photoelectron spectroscopy (XPS).....	51
2.5.3. Electrochemistry.....	51
2.5.3.1. Electrochemistry conditions used in Chapter.3.....	52
2.5.3.2. Electrochemistry conditions used in Chapter.4.....	52
2.5.3.3. Electrochemistry conditions used in Chapter.5.....	52
2.5.3.4. Electrochemistry conditions used in Chapter.6.....	52
2.5.4. Scanning electron microscopy (SEM) imaging	53
2.5.5. Atomic force microscopy (AFM) imaging.....	53
2.6. References	53
CHAPTER 3 OXIDATION OF HYDROGEN TERMINATED BORON DOPED DIAMOND ELECTRODES.....	55
3.1. Introduction	55
3.2. Objectives.....	56
3.3. Results and discussion.....	57
3.3.1 Electrochemical Oxidation.....	57
3.3.2 Investigation of photochemical oxidized diamond	59
3.3.2.1 Contact angle measurements	60
3.3.2.2 Electrochemical Characterization	62
3.3.2.3 XPS analysis.....	65
3.3.3 Investigation of oxygen plasma oxidized diamond.....	67
3.3.4 Silanization of the three interfaces	68
3.3.5 Esterification of the oxidized interfaces.....	72
3.4 Conclusion.....	74
3.5 Perspectives	75
3.6 References	76
CHAPTER 4 “CLICKING” ORGANIC MOLECULES BEARING ACETYLENE GROUP TO AZIDE-TERMINATED BORON-DOPED DIAMOND SURFACES	79
4.1. Introduction	79
4.2. Objectives.....	81
4.3. Results and discussion.....	82
4.3.1. Characterization of azide-terminated BDD surfaces.....	82
4.3.1.1. X-ray photoelectron spectroscopy (XPS) analysis.....	83
4.3.1.2. Electrochemistry measurement	83
4.3.2 Characterization of ferrocene-terminated BDD surfaces	84
4.3.3 Clicking thiophene to the azide-terminated BDD	89

4.3.4. Clicking of cyclophane to azide terminated BDD surfaces	95
4.4. Functionalization of porous silicon surfaces with thiophene groups	96
4.4.1. Grafting of ethynyl thiophene on porous silicon.....	97
4.4.2. Surface characterization	98
4.4.3. Electrochemical polymerization.....	100
4.4.4. Formation of polythiophene films on thiophene-modified PSi.....	101
4.5 Conclusion.....	104
4.6 Perspectives	105
4.7 References	106
CHAPTER 5 FUNCTIONALIZATION OF OXYGENATED BORON-DOPED	
DIAMOND SURFACE WITH AN IONIC LIQUID	111
5.1. Introduction	111
5.2. Objectives.....	112
5.3. Results and discussion.....	112
5.3.1. XPS characterization	112
5.3.2. Electrochemical investigation	116
5.4. Anion exchange reactions	117
5.5. Conclusion.....	120
5.6. Perspectives.....	121
5.7. References	121
CHAPTER 6 PREPARATION OF HALOGENATED BORON-DOPED DIAMOND	
ELECTRODES AND THEIR REACTIVITY	123
6.1. Introduction	123
6.2. Objectives.....	124
6.3. Results and discussion.....	124
6.3.1. Contact angle.....	124
6.3.2 Electrochemical characterisation.....	127
6.3.3. X-ray photoelectron spectroscopy (XPS) analysis.....	129
6.4. Reaction mechanism	134
6.4.1. Halogenation reaction	134
6.4.2. Nucleophilic substitution.....	134
6.4.3. Click reaction	136
6.5. Conclusion.....	136
6.6. Perspectives	137

6.7. References	137
CHAPTER 7 CONCLUSION AND PERSPECTIVES	139
7.1. Functionalization of oxygen-terminated diamond surfaces	140
7.1.1. “Clicking” organic and biological molecules bearing acetylene group to azide terminated boron-doped diamond surfaces	140
7.1.2. Chemical functionalization of oxygenated boron-doped diamond using ionic liquids	141
7.2. Functionalization of hydrogen-terminated diamond surfaces	141
7.3. Perspectives	142
APPENDIX	143
Appendix 1. Ultrasonic bath.....	143
Appendix 2. Orbital platform shaker.....	143
Appendix 3. UV-ozone	143
Appendix 4. Oxygen plasma	145
Appendix 5. Contact angle	146
Appendix 6. Scanning electron microscopy (SEM).....	147
Appendix 7. Atomic force microscopy (AFM)	149
Appendix 8. Fourier-Transform Infrared Spectroscopy (FTIR)	150
Appendix 9. Cyclic voltammetry	151
Appendix 10. X-ray Photoelectron Spectroscopy (XPS)	154
Appendix reference	156
CURRICULUM VITAE.....	159
Personal	159
Education.....	159
PUBLICATIONS	159

CHAPTER 1

INTRODUCTION

1.1. Diamond: a potential candidate in bioelectronics

Functionalization of semiconductor surfaces is a fast growing field, in particular due to potential applications in biosciences. Biosensors have been developed to detect a variety of biomolecular complexes and their interactions, including oligonucleotides [1-5], antibody-antigen [6,7], hormone-receptor [8], enzyme-substrate [9,10], and lectin glycoprotein interactions [11]. In general, a biosensor has two components: a receptor and a detector. The receptor is responsible for the selectivity of the sensor. Examples include enzymes, antibodies, and lipid layers. The detector, which plays the role of the transducer, translates the physical or chemical change by recognizing the analyte and relaying it through an electrical signal. The detector is not selective. For example, it can be a pH-electrode, an oxygen electrode or a piezoelectric crystal. **Figure 1.1** describes a typical biosensor configuration that allows measurement of a target-analyte interaction without using reagents. The device incorporates a biological-sensing element with a traditional transducer. The biological-sensing element selectively recognizes a particular biological molecule through a reaction, specific adsorption, or other physical or chemical process, and the transducer converts the result of this recognition into a usable signal, which can be quantified.

Common transduction systems are optical, electro-optical, or electrochemical. This variety offers many opportunities to tailor biosensors for specific applications [13-18]. For example, the glucose concentration in a blood sample can be measured directly by a biosensor (which is made specifically for glucose measurement) by simply dipping the sensor into the sample.

A successful biosensor must possess at least some of the following beneficial features:

- ✧ The biocatalyst must be highly specific for the purpose of the analyses and it should have high stability (including chemical, electrochemical, thermal stability) under normal storage conditions.

- ✧ The reaction should be as independent of such physical parameters as stirring, pH and temperature as is manageable. This would allow the analysis of samples with minimal pre-treatment. If the reaction involves cofactors or coenzymes these should, preferably, also be co-immobilized with the enzyme.
- ✧ The response should be accurate, precise, reproducible and linear over the useful analytical range, without dilution or concentration. It should also be free from electrical noise.
- ✧ If the biosensor is to be used for invasive monitoring in clinical situations, the probe must be tiny and biocompatible, having no toxic or antigenic effects. If it is to be used in fermenters it should be sterilisable. This is preferably performed by autoclaving, but no enzyme biosensor can presently withstand such drastic wet-heat treatment. In either case, the biosensor should not be prone to fouling or proteolysis.

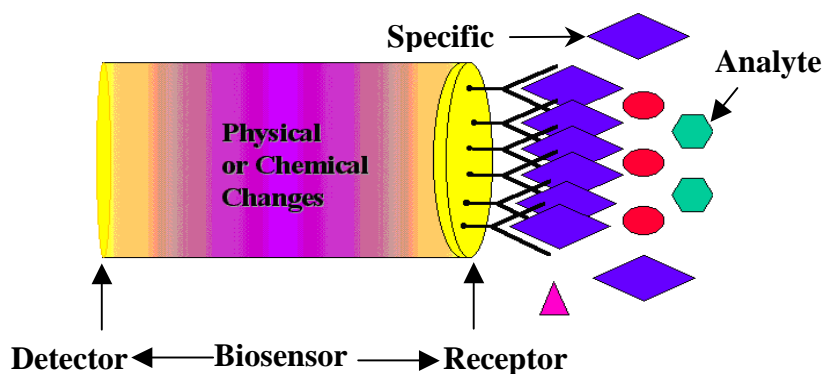


Figure 1.1. Schematic illustration of a biosensor device [12]

The present level of research on new biosensors as well as the development of currently available biosensors (e.g. glucose sensors) has increased dramatically over the past decade. The main driving force for this enhanced research activity is the booming demand for miniaturised biosensors, particularly for diagnostic applications. These however, impose rather strict requirements on the size of the device, selective response of the analyte, fast response time and compatibility with the peripheral electronic circuitry. Although the active interest in developing these small sensing devices for biomedical use is growing rapidly, some of the presently available biosensors are inadequate in these respects and several new and improved materials are desired to overcome some of these limitations. Self-assembled

monolayers (SAM) of alkanethiols and alkylsulfide on metal substrates (Au, Ag etc.) offer several attractive features for these kinds of applications. The easy procedure for SAM formation and compatibility with metal substrates for electrochemical measurements enable special benefits for biosensor applications involving current or potential measurements [19]. However, the thermal and chemical instability of the resulting SAMs and the unpleasant smell of the starting alkanethiols seriously limit their application domain. Porous silicon (PSi) has been used for highly sensitive detection of small molecules (biotin and the steroid digoxigenin), short DNA oligonucleotides (16-nucleotide oligomers), and proteins (streptavidin and antibodies). Most notably, the sensor can be highly effective in detecting multiple layers of biomolecular interactions, termed "cascade sensing," including sensitive detection of small molecules [5]. Anyway, silicon has attracted widespread attention because of the importance of silicon in microelectronics. However, hydrolysis reactions may limit the overall stability of functionalized silicon surfaces in aqueous solutions [20-25]. Another drawback for using silicon/organic monolayer as a biochip substrate and fluorescence for the detection scheme of biomolecular interactions on the surface is the fluorescence quenching in the close vicinity of the semiconductor. Finally, the improvement of the monolayers quality to resist biofouling is a real challenge to design selective and sensitive devices for monitoring biomolecular interactions.

Therefore, diamond, tetrahedrally bonded carbon atoms, which crystallizes into the face centred cubic diamond lattice structure, owing to its combination of specific physical, chemical and mechanical properties such as high thermal conductivity, high hardness, large band gap, optical transparency over a wide wavelength region (from UV to IR), stability against chemical reagents, high mechanical stability, corrosion resistance and biocompatibility has been regarded as one of the most promising industrial materials in various fields. With the current introduction of doped diamond, we are witnessing a technological leap. In the last years, several review articles [26-34] and a book on diamond electrodes have been published [35]. The high strength of C-C bonds and the well-established biocompatibility of diamond make it a particularly attractive substrate for robust chemical and biochemical modifications for sensor applications [25, 36-40]. Another interest for using diamond substrates is that thin diamond films can now be easily deposited on microelectronic

compatible substrates using methane/hydrogen gas mixtures by the Chemical Vapour Deposition (CVD) method.

1.2. Preparation of diamond films

Because of its large bandgap of more than 5 eV undoped diamond is normally electrically insulating and cannot be used as an electrode material. But as other large band-gap materials diamond can be made conducting by doping it with certain elements. Currently, in most cases boron is used as dopant, resulting in a p-type semiconducting properties. If phosphorus [41] or nitrogen is used as dopant, a n-type semiconductor is produced. Two major methods for the production of doped diamond materials have been developed: chemical vapour deposition (CVD) of thin films doped-diamond and high pressure, high temperature (HPHT) doped-diamond particle production [42-44]. However, the drawback of the HPHT method is that it still produces diamond in the form of single crystals ranging in size from nanometres to millimetres, and this limits the range of applications for which it can be used [34]. Other methods reported for the production of conducting diamond electrodes are vacuum annealing of undoped diamond [45, 46] and so-called surface transfer doping of undoped diamond [47]. The practical usefulness of these approaches to produce diamond electrodes remains questionable. Anyway, the majority of doped-diamond electrodes currently in use are thin film boron-doped diamond electrodes produced by CVD.

Similar to platinized electrodes, the doped diamond film is deposited on a conducting substrate [27, 48]. The deposition technique is plasma-assisted CVD. The plasma necessary for the deposition is activated either by hot filaments [27, 48, 49] or by microwave radiation [50]. In both cases, the gas phase (about 10 to 50mbar) typically consists of hydrogen as the carrier gas, methane (0.5-3% CH₄ in H₂) or acetone/methane mixture [50] as carbon source and other gases which provide the dopants [27,48-50]. By use of either microwave or thermally by hot filaments (temperature of filaments: about 2200-2800°C) the gas phase is activated to form a plasma. For the coating of larger substrates currently only the hot filament process can be used. In this case multiple filaments are applied.

Before diamond coating the substrate has to be pre-treated properly [27, 48]. One important pre-treatment step is activation of the surface with nanoscale diamond particles [48]. These tiny diamond crystallites are the nucleation sites for the growth of the thin diamond film during CVD process. The surface activation (seeding pre-treatment) can e.g. be performed by substrate polishing with diamond powder or by immersing the substrate into a suspension of nanoscale diamond particles accompanied by ultrasonication.

Substrate temperature during diamond film production is about 750 to 825°C. Typical growth rates are between 0.2 and 3µm/h [27]. The thickness of diamond thin films is usually between 1 and 10 µm but other thicknesses are possible. The diamond thin films have a nanocrystalline or microcrystalline structure and a rough surface. Substrates for doped diamond film deposition are usually either silicon (both single-crystalline and polycrystalline) or self-passivating metals such as titanium, tantalum, tungsten, molybdenum and niobium. Niobium seems to be the best suited of the metal substrate materials because it can withstand the deposition conditions (high temperature with hydrogen containing atmosphere) with the least changes in material structure. The use of silicon as a substrate leads to more perfect, pore-free films. But for many practical applications the brittleness of silicon is prohibitive. In this case doped-diamond films on metal substrates are used. Another advantage of the use of metal substrates is the possibility to produce large area electrodes up to the square meter range. This is not possible with silicon substrates because they are not available in this size. However, large area diamond electrodes based on silicon substrates can be produced by a mosaic-like arrangement of diamond-coated silicon wafers on a metal substrate with subsequent passivation of the metal portions not protected by the silicon/doped diamond pieces [34, 51].

Doped diamond films can be deposited directly onto silicon without any interlayer [30]. If the doped diamond films shall be deposited onto self-passivating metal substrates, often interlayers (e.g. the corresponding metal carbide) are applied to enhance the adhesion of the diamond film at the substrate and to protect the substrate against hydrogen in the deposition gas mixture (danger of hydrogen embrittlement of the substrate) [30].

Other substrate materials for deposition of doped diamond are carbon materials such as graphite [30, 52], glassy carbon [30] or carbon fibre materials. CVD thin film diamond electrodes can be modified in multitude of ways to change their properties.

Free-standing doped-diamond films can be produced by deposition of relatively thick conductive diamond films on silicon or other substrates and subsequent removal of the substrate e.g. by chemical etching. The production of single-crystalline doped-diamond by CVD is also possible. For this purpose natural nonconducting diamond single crystals have been used as a substrate for CVD thin film deposition [53, 54].

1.3. Properties of diamond

1.3.1. General properties of diamond

Diamond is well known for its unusual material properties such as the high hardness ($1 \times 10^4 \text{ kg mm}^{-2}$), high thermal conductivity ($2600 \text{ W m}^{-1} \text{ K}^{-1}$) and high charge carrier mobility (electron mobility: $2200 \text{ cm}^2 \text{ V}^{-1} \text{ s}^{-1}$, hole mobility: $1600 \text{ cm}^2 \text{ V}^{-1} \text{ s}^{-1}$). With a bandgap of 5.45 eV, undoped diamond is an excellent electrical insulator with resistivity in the order of $10^{20} \Omega \text{ cm}$.

1.3.2. Properties of doped diamond electrodes

1.3.2.1. Dopants for diamond electrodes and their electrical properties

Boron is by far the most widely used dopant to produce conducting diamond electrodes [30]. This is because boron has low charge carrier activation energy of 0.37 eV [30]. Boron doping leads to a p-type semiconductor. At low doping levels, the diamond acts as an extrinsic semiconductor. At high doping levels, the material acts as a semimetal. To introduce boron into the diamond material during film growth, a boron containing substance has to be added to the deposition gas mixture. Substances such as diborane (B_2H_6) or trimethyl borane ($(\text{CH}_3)_3\text{B}$) can be used. The majority of studies with doped diamond electrodes use boron-doped diamond.

But other dopants are also possible. They provide n-type conductivity: nitrogen (charge carrier activation energy 1.6–1.7 eV) [30, 55, 56], phosphorus (charge carrier activation energy 0.6 eV) [41, 56] and sulfur [32, 33]. Also co-doped diamond thin film electrodes have

been produced, such as nitrogen-boron [30] or boron-sulfur co-doped [56, 57] electrodes. Sulfur can only be introduced as a dopant into diamond in the presence of boron [56, 57]. At low boron concentrations, an n-type semiconductor is obtained [56, 57]. It has also been suggested that heavily boron-doped CVD diamond can switch its conductivity from p-type to n-type after deuterium plasma treatment [41]. The alternative dopants are introduced into the CVD diamond films by adding an appropriate gas to the deposition atmosphere. This is ammonia [30] or N_2 [55] in case of nitrogen doping, PH_3 for phosphorus [41] and H_2S for sulfur doping [56, 57]. **Figure 1.2** shows an energy diagram of diamond with some selected states in the band gap.

The conductivity of doped diamond electrodes depends on the doping level. For boron-doped diamond electrodes with resistivities between 5 and $100\text{m}\Omega\text{ cm}$ are usually produced [30, 48]. Typical and useful boron concentrations in diamond are between 500ppm to about 10,000ppm [30] or 10^{19} - $10^{21}\text{atoms cm}^{-3}$ [48]. Interestingly, boron-doped diamond has also been found to be superconducting at very low temperatures [58] with T_c depending on doping level.

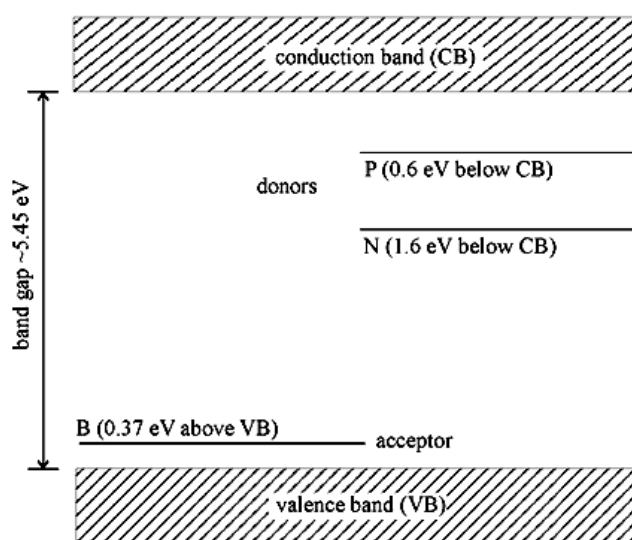


Figure 1.2. Energy diagram of selected states in the band gap of diamond [34].

1.3.2.2. Electrochemical properties in aqueous electrolytes

Doped-diamond has been introduced into electrochemistry by Pleskov et al. [59]. Since then, mainly the electrochemical behaviour of diamond electrodes in aqueous electrolytes has

been investigated. The most striking feature here is their very high overpotential for both oxygen and hydrogen evolution [26, 27, 31, 33, 48, 60-63]. **Figure 1.3** shows cyclic voltammograms of platinum and diamond electrodes in 0.2M H₂SO₄ in the region between hydrogen and oxygen evolution. The much higher overpotential of diamond electrode for both reactions is obvious. This leads to a wide potential window (approx. 3.5V), which can be used for other electrochemical reactions in aqueous electrolytes. Diamond electrodes have indeed the largest potential window so far measured in aqueous electrolytes. This makes them also totally different to common electrode materials such as gold, platinum or mixed metal oxide type electrodes.

Diamond electrodes are also distinguished from these conventional electrode materials by their very low capacitance and by the absence of surface oxide formation and reduction reactions which are found at conventional metal or metal oxide electrode materials between oxygen and hydrogen evolution (see also **Figure 1.3**). The electrochemical properties of diamond electrodes depend to some extent on doping level, on surface termination and nondiamond carbon content.

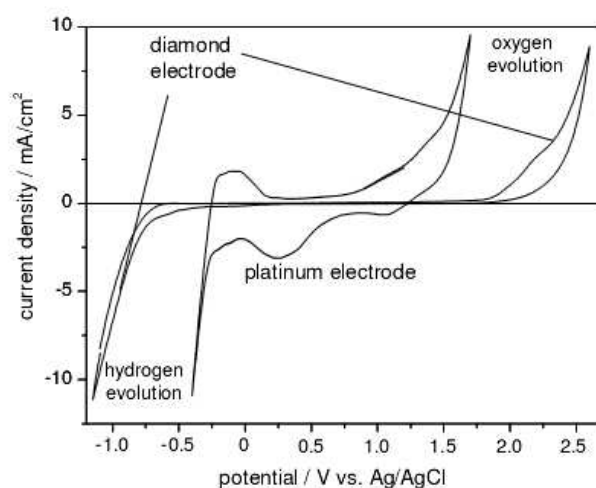


Figure 1.3. Cyclic voltammogram of a platinum and a diamond electrode in 0.2M H₂SO₄, $v=100\text{mV/s}$ [34].

High overpotentials on diamond electrodes are also found for halide (I, Br, Cl) oxidation [26, 64] and for the reduction of the corresponding halogens (I^- , Br^- , Cl^-) [64] as well as for oxygen reduction. In general, electrochemical reactions which require adsorption of reaction

intermediates have a high overvoltage on diamond electrodes. **Figure 1.4** displays cyclic voltammograms of diamond electrode in comparison with platinum electrode for the redox couples I/I_2 showing the much higher overpotential on diamond electrodes for this reaction.

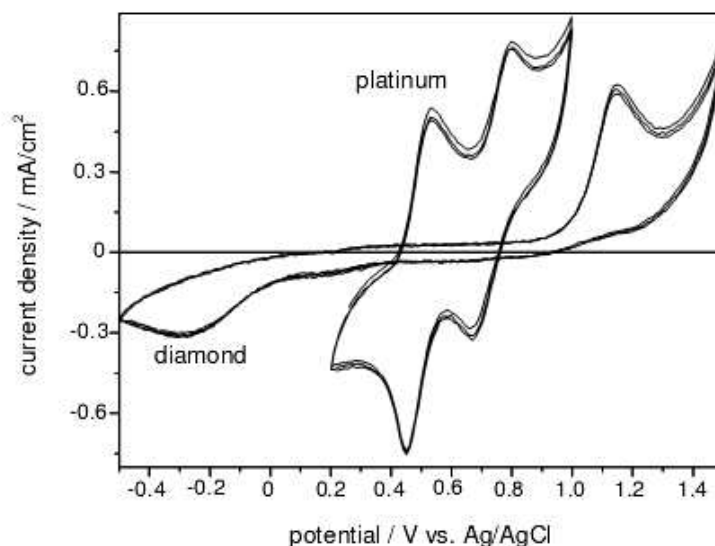


Figure 1.4. Cyclic voltammograms of a platinum and a diamond electrode in 5×10^{-3} M KI + 1 M KCl, $v=100$ mV/s [64].

A totally different electrochemical behaviour can be found in the case of simple outersphere, one-electron transfer processes in which no adsorbed intermediates are involved. They can precede more or less quasi-reversible on diamond electrodes [26, 54, 64]. This could e.g. be shown for $Fe(CN)_6^{3-/4-}$ [26, 29, 55, 65, 67-73], $Ru(NH_3)_6^{2+/3+}$ [26, 29, 52, 55, 64, 66-69, 71], $IrCl_6^{2-/3-}$ [55, 67], $Fe^{2+/3+}$ [67, 71], $Ce^{3+/4+}$ [74,75] and $Eu^{2+/3+}$ [76] among others. **Figure 1.5** displays cyclic voltammograms of a platinum and a diamond electrode with the redox couple $Fe(CN)_6^{3-/4-}$, showing that the electrochemical behaviour of both electrode materials is comparable in this case, although platinum is more reversible. Doping level and pre-treatment of the diamond electrode have a considerable influence on the kinetics of charge transfer reactions of this material. Therefore, a more irreversible behaviour of diamond electrodes especially at low doping levels and with oxygen terminated surface is possible [70, 73].

1.3.2.3. Photoelectrochemistry

Doped-diamond electrodes display also interesting photoelectrochemical properties [77-79]. Since diamond has a very wide bandgap, visible and long-wavelength ultraviolet (UV) radiation should not be able to excite electrons from the valence into conduction band. Nevertheless, some studies show significant photocurrents even with sub bandgap illumination [59, 77], presumably due to impurities or surface states within the bandgap. Fujishima and co-workers [78] showed that on high-quality diamond electrodes with very low nondiamond carbon content only irradiation with supra bandgap illumination is able to excite electrons into the conduction band. They studied the photoelectrochemical behaviour of boron-doped diamond electrodes in 0.1M KH_2PO_4 solution with excimer lasers of 3 different wavelengths: ArF (193nm, 6.4eV), KrF (248nm, 5.0eV), and XeF (351nm, 3.53eV). The photocurrent observed using the ArF laser was much greater than those observed with the KrF and XeF lasers. In addition, the photoelectrochemical properties of semiconducting diamond were found to be highly sensitive to the surface conditions [79].

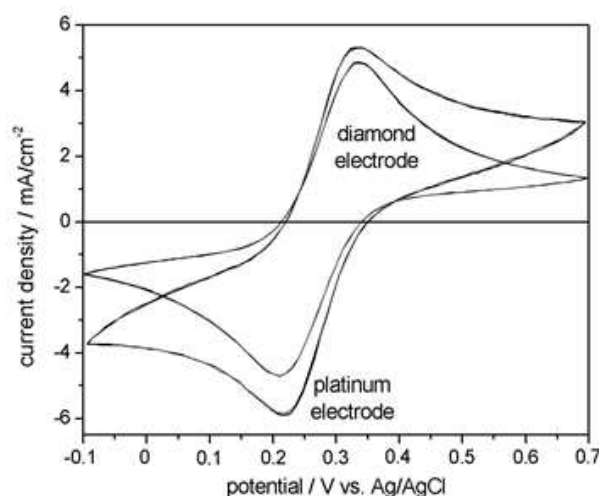


Figure 1.5. Cyclic voltammograms of a platinum and a diamond electrode in 10^{-2} M $\text{K}_3[\text{Fe}(\text{CN})_6]/\text{K}_4[\text{Fe}(\text{CN})_6] + 1$ M KCl, $v=100$ mV/s [67].

1.3.3. Stability of diamond electrodes

The high chemical and electrochemical stabilities of diamond electrodes have been taken for granted for some years. Especially the high electrochemical stability under severe conditions has been emphasized [31, 33, 48, 62]. It has been considered as one of the major advantages of doped-diamond electrodes compared to conventional electrode materials.

However, in the last years in some investigations it has been shown that diamond electrodes are etched electrochemically under certain experimental conditions [61, 80-82].

Until today, investigations on the anodic corrosion of doped-diamond were only performed in acidic aqueous electrolytes [61, 80-82]. Panizza et al. [80] did not find any loss of diamond material of diamond anodes during electrolysis in 1M H₂SO₄ (1A/cm², 40°C). But if the electrolysis experiments were performed in 1M H₂SO₄ + 3M acetic acid, a strong decrease of surface roughness has been measured. But more detailed investigations with diamond thin film electrodes on silicon substrates by Katsuki et al. [61] and Comninellis [81] did show that in sulfuric acid electrolytes corrosion rates of 0.4µg [61] or 0.3µg diamonds per Ah [81] can be measured. Comninellis [81] did also show that the corrosion rate strongly depends on electrolyte composition. If organic compounds are added to electrolytes such as 1M sulfuric acid or 1M perchloric acid, corrosion rates are dramatically increasing up to 12µg diamond per Ah in 1M H₂SO₄ + 3M acetic acid (at 1A/cm², 40°C).

Schafer et al. [82] reported that during electrolysis with thin film diamond anodes on niobium substrates (at 4A/cm², 70°C) in 1.3M H₂SO₄, corrosion rates of about 0.4µg/Ah cm⁻² are reached. In this long-term electrolysis experiment in certain time intervals 1g/L organic material has been added to the electrolyte (5 times). This organic material was destroyed during the electrolysis. Therefore, in this experiment only part of the electrolysis time organic material was present in the acidic electrolyte. The corrosion rate measured by Schafer et al. equals a loss of diamond film thickness of about 1µm diamond per 900Ah/cm². This means, that under these conditions and a current density of 200mA/cm², an electrode lifetime (diamond film thickness of 1µm) of 0.5years can be expected. Lowering the current density to only 20mA/cm² would give an electrode lifetime of roughly 5years for a 1µm thick electrode.

These corrosion rates of the diamond layer during anodic polarization are comparable to corrosion rates which are usually found with platinized or mixed metal oxide coated titanium electrodes [81]. By applying thicker diamond films (10µm are possible) also with high current densities acceptable electrode lifetimes are possible. However, certain electrolyte compositions lead to increased corrosion rates. The corrosion rate of 12µg diamond per Ah (in 1M H₂SO₄ + 3M acetic acid at 1A/cm², 40°C) reported by Comninellis [81] would result in an electrode lifetime of 6 days at 200mA/cm² or 6 months at 20mA/cm² (thickness of the

diamond film: 1 μ m). In this case even a 10-fold increase of diamond film thickness would only allow working with low current densities to reach acceptable service life.

Besides electrochemical etching also the detachment of diamond material from the substrate can be problematic. The mechanisms that can cause diamond film detachment are complex [83]. In addition to the nondiamond carbon content, also cracks and pores, the initial diamond nucleus density, the diamond film thickness, interlayer thickness, the nature of the substrate and the bonding between the substrate and the diamond film may affect electrode stability [83]. All these factors are associated with production conditions. Therefore, a proper selection and careful control of preparation conditions is very important in order to obtain long-term stable doped diamond thin film electrodes.

1.3.4. Biocompatibility of diamond electrodes

Doped diamond electrodes have been widely reported for their biocompatible applications. Martin and co workers used diamond electrodes for the study of neurodynamics in an animal model [84, 85]. Implantable diamond microelectrodes provide a unique opportunity to integrate neural stimulation and amperometric sensing (e.g. of dopamine, adenosine and serotonin) in the same implantable device. And biomolecules immobilized at the doped diamond surface are often still fully functional and active. Examples are an amperometric biosensor based on covalent immobilization of tyrosinase on a boron-doped diamond electrode [86] or catalase modified diamond electrode [87]. These biosensors could be used to detect phenolic compounds [86] or hydrogen peroxide [87], respectively. Also diamond electrodes modified with DNA oligonucleotides have been produced with the aim to create field-effect biological sensors [88]. It has also been found that boron-doped diamond activated by anodic oxidation is a highly active material providing appropriate contact of laccase enzyme molecules with the electrode surface and leading to direct bioelectrocatalysis of the dioxygen reduction which could be useful in biofuel cells [89].

1.4. Functionalization of diamond electrodes

1.4.1. Functionalization of hydrogen-terminated diamond surfaces through C-C bond formation

1.4.1.1. Direct reaction of hydrogen-terminated diamond surfaces with alkenes under photochemical conditions

H-terminated polycrystalline films exhibit a number of usual properties, including the ability to emit electrons from the valence band directly into a vacuum when illuminated with 254nm light [90]. Ultraviolet irradiation of hydrogen-terminated diamond covered with liquid films of an appropriate alkene is an additional approach to produce functionalized diamond (**Figure 1.6**). This scheme has been first proposed by Hamers et al. [25, 91-95] and is now used by different groups [96-101]. UV irradiation of hydrogen-terminated diamond surface in the presence of a liquid film of appropriate alkenes (e.g., 12-amino-dec-1-ene protected with a trifluoroacetic acid group, perfluorodecene, trifluoroethyl ester of ω -undecenoic acid, etc.) results in the formation of an organic layer covalently grafted to the surface through C-C bonds. While the stability of the formed monolayer has been proven [102-104], many questions remain about how the reaction proceeds mechanistically and how the organic film is organized on the surface. Hamers et al. carried out mechanistic and structural studies on photochemical functionalized diamond surfaces [105, 106]. They demonstrated that the modification process is not controlled by grain boundaries and that the functionalization is a surface-mediated reaction initiated by the photoejection of electrons from the diamond surface into the liquid phase [105].

Figure 1.6 displays the strategy used to incorporate terminal -NH₂ functional groups onto a diamond surface. To provide chemically reactive amine groups, the trifluoroacetamide protecting group was chemically removed, and DNA was linked to the amine-terminated diamond surfaces using a heterobifunctional cross-linker as discussed above. Comparing the DNA-modified diamond with a silicon surface modified in the similar way showed no loss of DNA over 15 hybridization/denaturation cycles on diamond and a loss of 1.8% on silicon [23].

The direct photochemical coupling using undecylenic acid was recently reported to form a higher density of carboxylic acid groups on the diamond compared to

trifluoroethylundecenoate [101]. **Figure 1.7** shows the fluorescence image of fluorescein isothiocyanate (FITC)-labeled DNA immobilized on acid-modified diamond subjected to three denaturation-rehybridization cycles. While the photochemical derivatization allows the introduction of several functional groups on the surface, the reaction time required is rather long (in the range of 12-15h), and most of organic molecules absorb at the used wavelength. Nevertheless, glycol compounds could be linked to diamond allowing the study of nonspecific binding of proteins [98]. Electrochemical impedance spectroscopy (EIS) was used to characterize the modified interfaces and showed that the monolayer strongly inhibits electron transfer, but the detection of biological binding events in real time, as a consequence of the field effect induced in the diamond by the charged DNA, is possible [88]. EIS measurements, together with cyclic voltammetry were performed on horseradish-peroxidase-modified nanocrystalline diamond films [100]. The proximity of the haem groups to the diamond surface allowed direct electron transfer between them.

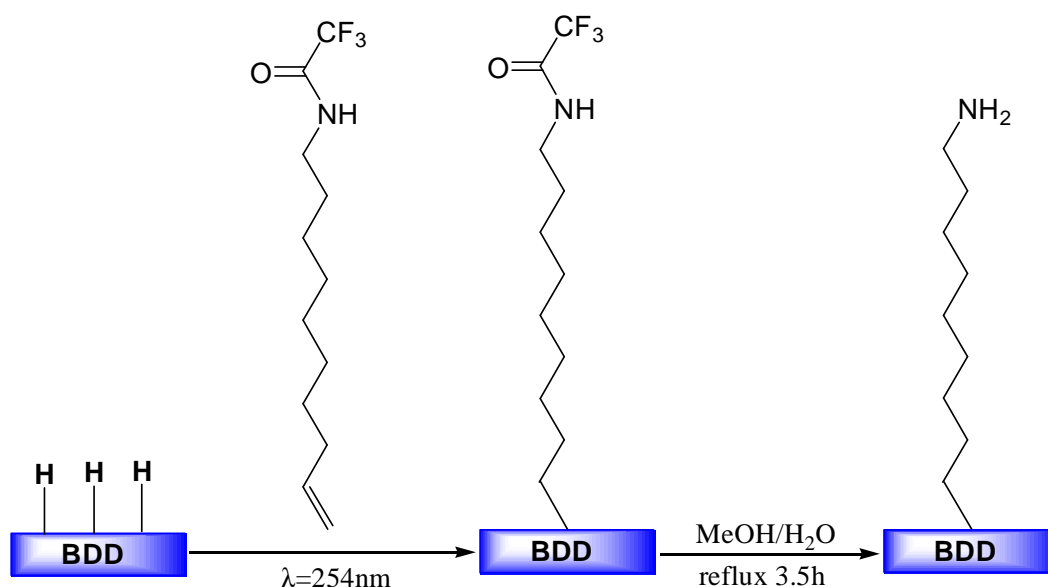


Figure 1.6. Photochemical linking of organic molecules to H-terminated diamond.

1.4.1.2. Diazonium chemistry

Another method available for the formation of a strong C–C bond between diamond and an organic molecule was first reported by McCreery and Swain [107] and consists of the electrochemical reduction of diazonium salts (**Figure 1.8**) [107,108]. Different diazonium salts are commercially available, but they can also easily be prepared in one step from a wide

range of aromatic amines. The technique offers the advantage of the availability of a wide range of functional groups ($-\text{COOH}$, X, NO_2 , etc.) that can be introduced onto the surface in one step.

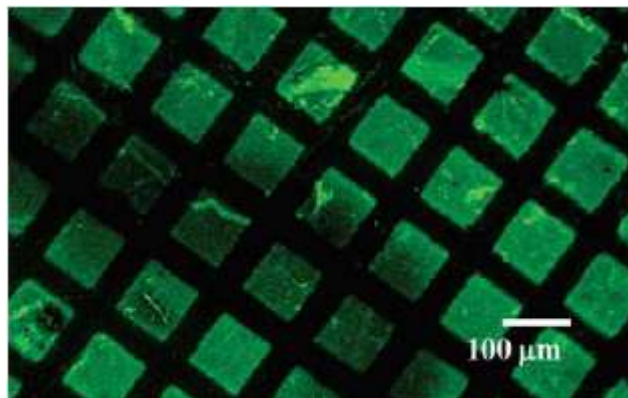


Figure 1.7. Fluorescence images of patterned FITC-labeled DNA immobilized on diamond which has been biofunctionalized with undecylenic acid and subjected to repeated denaturation / rehybridization cycles (three cycles; reprint with permission from [101]).

The method, intensively used for other carbon-based materials [109], is quite simple and can be performed in acetonitrile ($\text{CH}_3\text{CN} + 0.1\text{M Bu}_4\text{BF}_4$) and acidic aqueous solutions ($0.1\text{ M H}_2\text{SO}_4$) through electrochemical reduction of diazonium salts. Covalent bonds between the diamond and the diazonium salt can, in addition, be formed through a spontaneous binding (in the absence of external bias) of the diazonium salt in the presence of 1% sodium dodecyl sulfate [110]. We recently showed that solvent-free functionalization of hydrogen-terminated boron-doped diamond surfaces with aryldiazonium salts using ionic liquids (1-butyl-3-methylimidazolium hexafluorophosphate or 1-butyl-3-methylimidazolium methyl sulphate) can be achieved in high yield [111]. The electrons necessary for the reduction of the diazonium salt are, in these cases, most likely provided by the diamond itself [112]. This purely chemical grafting is attractive, as it does not require electrochemical equipment or doped diamond interfaces. The authors have also showed from ellipsometric measurements that the chemical approach results more readily in monolayers rather than multilayers observed under electrochemical conditions. AFM measurements have evidenced the formation of multilayers using the electrochemical route, and the formation of a real monolayer was only reported on pyrolyzed photoresist [113]. Phenyl radical species are

formed next to nitrogen during the grafting process, which react directly with the diamond surface. The formation of multilayers is due to an attack of the first grafted aryl group by another aryl radical. The principal interest in diazonium-based diamond modification is that the diamond-tethered functional groups are used for the covalent linking of biomolecules. This is due to the reported biocompatible and bio-inert character of diamond electrodes making them promising platforms for biosensing. The most intensively studied diazonium salt derivative is the nitrophenyl salt. The key to biomolecular functionalization lies in the ability to selectively reduce nitro groups to primary amines to which DNA and other biomolecules can chemically be linked. In aqueous solution, an irreversible multi-electron and multi-proton reaction of the nitro group to amine ($-NH_2$) or hydroxyaminophenyl ($-NHOH$) groups takes place [109]. The covalent linking of enzymes (glucose oxidase and tyrosinase) was achieved on the amine-terminated diamond surfaces. Carlisle et al. [108] reacted the amine terminal groups on the BDD with succinic anhydride and *N*-hydroxysulfosuccinimide to link glucose oxidase. Glucose was detected through the oxidation of biocatalytically formed H_2O_2 . An amperometric biosensor for phenol, *p*-cresol and 4-chlorophenol was developed by Zhin et al. [114]. It is based on covalent immobilization of tyrosinase on amine-terminated BDD via carbodiimide coupling by forming an amide bond between the carboxylic acid of the tyrosine and the NH_2 of the BDD. They reported that 90% of the enzyme activity was retained for 5 weeks when storing the sensor at 4°C in PBS. On the other hand, DNA immobilization was achieved by immersing the amine-terminated diamond into a heterobifunctional cross-linker (sulfo-succinimidyl 4-(*N*-maleimidomethyl) cyclohexan-1-carboxylate) to which thiol-modified DNA was linked [108,115,116]. Experiments on single crystalline diamond electrodes showed that the DNA chains are tilted by 31° with a DNA density of 6×10^{12} molecules cm^{-2} . The results are not affected by the variation of the buffer salinity [115]. The structural and mechanical properties of a DNA double helix bonded to NH_2 -terminated single crystalline diamond surfaces, prepared via photochemical or electrochemical routes, were evaluated using contact mode AFM. It was shown that DNA molecules can be irreversibly removed from the diamond surface by contact mode AFM with forces $N > 45nN$ and $> 76nN$ on photochemically and electrochemically functionalized diamonds, respectively [116]. Covalent linking of anthraquinone diazonium salt to BDD through electrochemical

reduction was recently shown by Foord [117]. In basic solution, the quinone-catalyzed reduction of oxygen was seen at -0.8V/SCE .

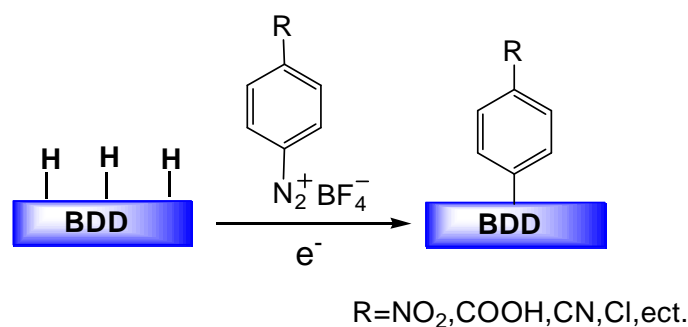


Figure 1.8. Attachment of organic layers by reduction of aryl diazonium salts.

1.4.2. Functionalization of hydrogen-terminated diamond surfaces through C-O bond formation

Tsubota et al. [118,119] investigated the modification of H-terminated diamond using alkyl-radicals. Among various radical initiators, benzoylperoxide was found to be the most effective in abstracting hydrogen on the surface (**Figure 1.9**). Due to their low dissociation energy, the O–O bond in these peroxides breaks easily, generating radicals [119-127]. When benzoyl peroxide is thus heated up to temperatures of about $T=60\text{-}80^\circ\text{C}$, it decomposes into benzoyl radicals. In the presence of an H-terminated diamond surface in toluene (under argon atmosphere, at $T=348\text{K}$ for $t=2\text{h}$), the benzoyl radicals formed can abstract a hydrogen atom on the diamond surface and bind to it. Further studies using benzoyl peroxide showed that the radical reaction is highly solvent dependent. While the radical substitution reaction works well in THF and DMF, the reaction in toluene depends on the reaction conditions [121,122]. The same group has demonstrated that aliphatic and aromatic carboxylic acids can be tethered to diamond surface through C–O bond formation by carrying out the thermal decomposition of benzoyl peroxide radical initiator in the presence of aliphatic and aromatic carboxylic acids [123,125,127]. In this case, R–COO radicals are formed and bind to the diamond surface. The final chemical state of the diamond surface is determined by the kinetics of the reaction.

The number of hydrogen atoms displaced on the diamond surface depends, however, strongly on the acid used. In the case of the large pyrene-carboxylic acid, rather low abstraction fraction was observed.

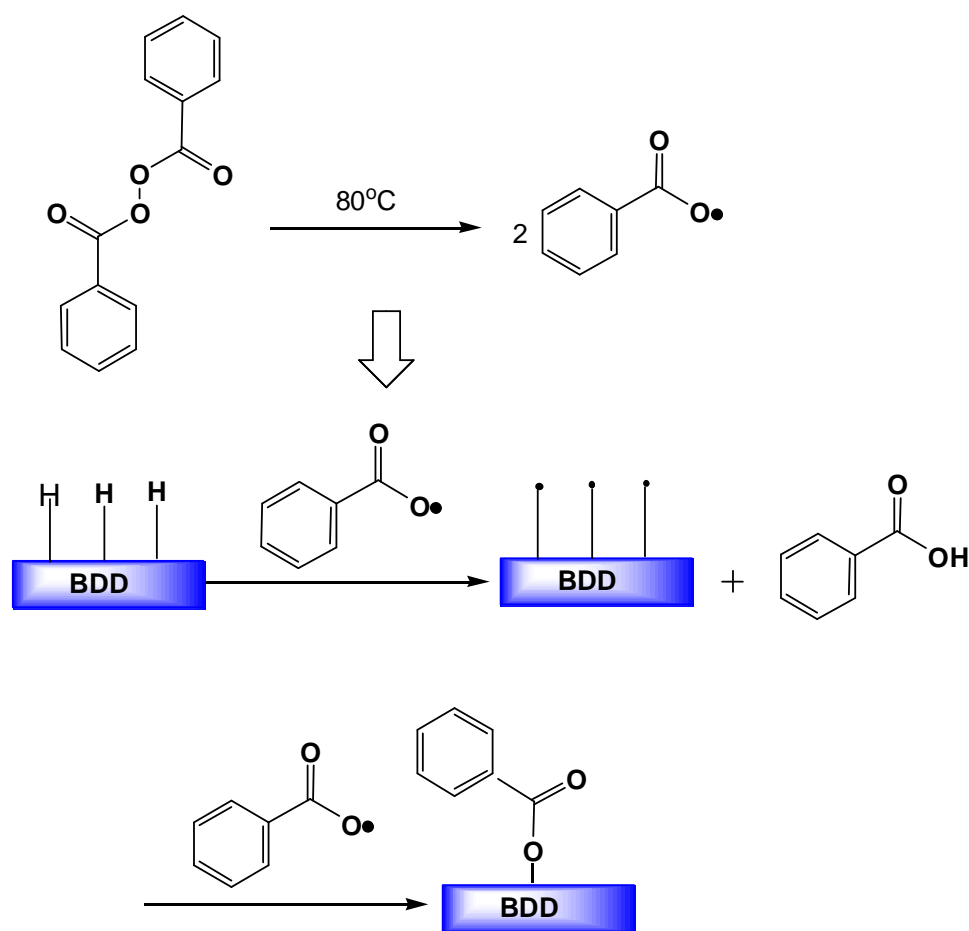


Figure 1.9. Liquid phase modification of hydrogenated diamond surfaces using a radical initiator.

1.4.3. Oxidation of H-terminated diamond surfaces

Freshly synthesized H-terminated diamond interfaces can be left without special precautions on the bench for several months. In spite of the high stability of diamond, oxidation of the hydrogenated surface is relatively easy to perform. The resulting oxidized surface is so stable that it can be recovered only by hydrogen plasma treatment at elevated temperatures. Diverse procedures have been reported for the oxidation of H-terminated surfaces including thermal [128-130], plasma [131, 132], and electrochemical techniques [133-136], as well as the use of singlet oxygen [133], irradiation with vacuum ultraviolet light (VUV, $\lambda = 172\text{nm}$, $t = 3\text{h}$ in the presence of O_2 and H_2O) [137] and ozone treatment [138-140]. Oxygen-terminated diamond surface shows hydrophilic character [60]. Independent of the activation method used, the presence of oxygen on the diamond surface

has a significant influence on the chemical reactivity [135], electrical conductivity [141, 142], field emission [143,144] and Schottky barrier heights [145].

Figure 1.10 shows typical high resolution X-ray photoelectron spectra of a hydrogen-terminated and a photochemically oxidized boron-doped (BDD) polycrystalline diamond surface [138]. The high-resolution XPS spectrum of the C1s of a hydrogenated BDD sample displays a main peak at $\sim 285\text{eV}$. The peak is unsymmetrical. The presence of a shoulder at higher binding energy ($\sim 286\text{eV}$) is most likely due to the presence of amorphous carbon at the grain boundaries. After photochemical oxidation, the XPS spectrum displays three different features: a peak at 285eV due to C1s from the bulk and two peaks at 286 and 289eV due to the surface C-O features. Based on the diamond structure, it is expected that the sp^3 C-H bonds on the (111) facets will be terminated with hydroxyl groups while the CH_2 bonds on the (100) facets will be transformed to carbonyl (C=O) and ether (C-O-C) functional groups. The signals from surface hydroxyl and ether groups are undistinguishable ($\sim 286\text{eV}$) [138]. The peak at 289eV results most likely from a contribution of carbonyl groups on the surface.

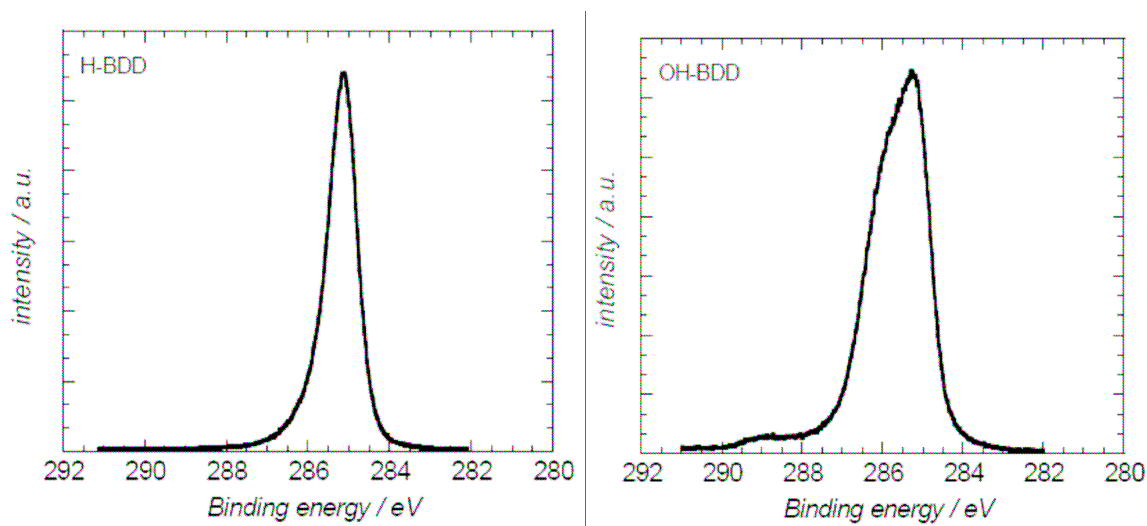


Figure 1.10. High resolution XPS spectra of C 1s of hydrogenated and photochemically oxidized boron-doped diamond surfaces [138].

The change of the chemical termination can affect the electrochemical properties of the diamond electrode. Surface oxidation treatment changes the electrochemical character of diamond electrodes by means of electrostatic interactions between the electrode surface and

redox ions. The potential windows of the oxygenated diamond electrodes became somewhat wider than that of the as-grown electrode (**Figure 1.11**) [146] and the electron transfer rates in various redox species were also changed, providing in some cases enhanced electroanalytical selectivity [147,148].

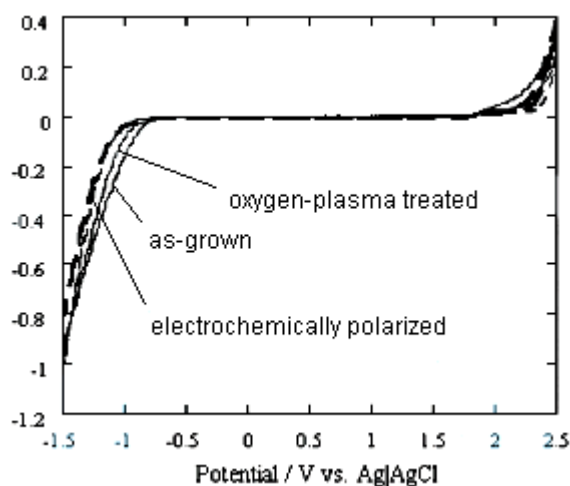


Figure 1.11. Cyclic voltammograms in 0.1M sulfuric acid solution for as-grown, electrochemically polarized and oxygen-plasma treated diamond electrodes; scan rate: 100mVs^{-1} .

Oxygenated diamond surface exhibit modified properties such as a different adsorbing behavior [149] which facilitates the subsequent functionalization of diamond electrodes [146, 147]. Actually, surface functional groups, which are introduced onto the diamond electrode by the surface oxidation treatment, facilitate the introduction of many kinds of functional materials [133, 146, 149]. Generally, because the hydrogen-terminated diamond electrode has low chemical reactivity and high hydrophobicity, it is difficult to functionalize its surface [67]. However, oxygenated diamond electrodes have hydroxyl groups on the surface, various functional groups including amino, vinyl, epoxide, mercapto, and phenyl groups can be introduced onto the oxidized boron doped diamond (BDD) surfaces to modify their chemical and physical properties. Additionally, a wide range of molecules with useful functionalities, such as redox activity, chemical selectivity, catalytic activity, and photosensitizability, can be attached onto electrode surfaces via silane coupling agents. Thus, the potential applications of boron-doped diamond (BDD) can be dramatically extended.

The decrease of surface conductivity has been observed at the semiconducting diamond

surface by converting the H-terminated surface to O-termination due to the removal of the surface conductive layer formed on the H-terminated diamond surface [150]. However, in the case of the heavily boron-doped diamond films, the effect of the removal of the surface conductive layer on the surface conductivity seems not to be significant. It was confirmed by the four-point probe method that the film resistivity of the diamond surface ($\sim 10^{-3} \Omega \text{ cm}$) did not change after surface oxidation treatment [146]. As expected from the change of the surface hydrophobicity and the enhancement of the surface roughness at the nanometer scale, the background current for the O-terminated surface became larger than that of the as-grown electrode, but the change of the chemical termination did not appear to cause a remarkable change in the electrochemical properties. In addition, it was also confirmed by the four-point probe method as above [132].

1.4.4. Halogenation of H-terminated diamond surfaces

A practical method for surface modification of nonoxidized diamond is the direct reaction with radical species in the gas phase. The radical moieties known to react directly with diamond include hydrogen [151], fluorine [152] and chlorine atoms [153]. The diamond surface is unreactive to the corresponding molecular species H_2 , F_2 and Cl_2 [154]. This implies that vigorous and corrosive (e.g. $\text{Cl}_2/400\text{-}500^\circ\text{C}$; $\text{F}_2/470^\circ\text{C}$) [155] reaction conditions are necessary to generate atomic species.

Milder conditions to halogenate diamond surfaces are employed when halogen atoms are formed in a photochemical reaction [156]. The photodissociation of chlorine gas is rather well known [157, 158]. Miller and Brown prepared chlorinated polycrystalline diamond films [157], single crystals and diamond powders [154] through the irradiation of the samples at $\lambda = 245 \text{ nm}$ up to 24h using a pressure Hg-arc lamp in the presence of Cl_2 gas, as shown in **Figure 1.12** [158].

A different photochemical approach has been used by Nakamura et al. to fluorinate H-terminated diamond surfaces [159]. It is based on the photolysis of perfluoroazooctane, as shown in **Figure 1.13**. During this process, perfluorooctyl radicals abstract a hydrogen atom from the diamond surface. The resulting surface carbon radical reacts with another perfluorooctyl radical to yield a fluorinated surface. A similar approach has been used by

Russels et al. [160], who introduced perfluorobutyl groups at low temperature on a (110) oriented single crystal diamond surface by photolysis of a solution of perfluorobutyl iodide (C_4F_9I) using UV irradiation with a 200W Hg-arc lamp.

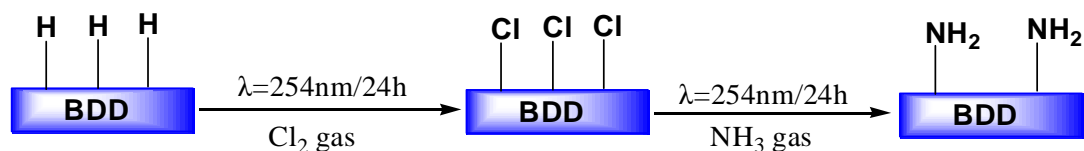


Figure 1.12. Preparation of an amine-terminated BDD surface in a two-step procedure, consisting on the photochemical irradiation of a hydrogenated surface with chlorine followed with ammonia gas.

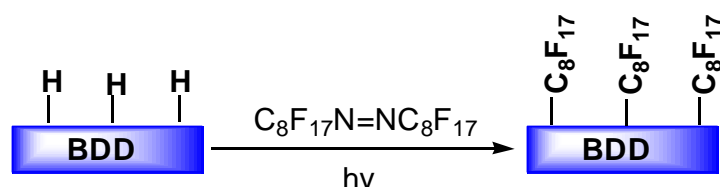


Figure 1.13. Chemical modification on the surface of a diamond film with perfluorooctyl functionality.

There are few reports on halogenation in the liquid phase. Ikeda et al., as shown in **Figure 1.14** [132] attempted chlorination of H-terminated diamond by treatment with sulfuryl chloride (SO_2Cl_2) at $T = 50^\circ C$ under argon atmosphere using 2, 2-azobisisobutyronitrile (AIBN) as a radical initiator. The resulting chlorinated diamonds were further used for the immobilization of thymidine molecules [133].

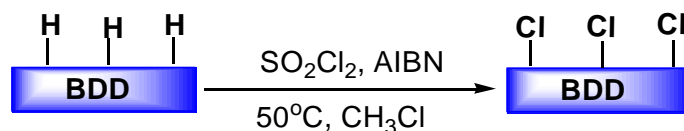


Figure 1.14. Chlorination scheme on diamond surface in the liquid phase.

The stability of the halogenated interfaces depends mainly on the used halogen. Fluorinated diamond surfaces are stable in air and water at room temperature and have been electrochemically characterized [161]. Chlorinated diamond interfaces are reported to form hydroxylates at room temperature in contact with water vapor [162].

1.4.5. Amination of H-terminated diamond surfaces

The chemical reactivity of the chlorinated surface was exploited for the preparation of amine-terminated diamond interfaces. While a thermal treatment up to 450°C in ammonia did not allow surface amination, the reaction of ammonia with chlorinated diamond was markedly different when photochemical conditions were used [154]. The chlorinated sample could be aminated by irradiation of the chlorinated diamond films in NH₃ (g) at room temperature in vacuum for 3-24h [154] or through the reaction with quaternary pyridinium salt [163], as shown in **Figure 1.12**.

Reports on the direct amination of H-terminated diamond in the gas phase have only been reported recently. Radio-frequency plasma was used to promote the direct chemical reaction between the diamond surface and vaporized N-(6-aminohexyl) aminopropyl trimethoxysilane [137]. The relative surface density of primary amines groups (-NH₂) attached to the diamond surface was detected by fluorescence, using fluorescamine in acetone spray as a fluorescence marker. On the other hand, the direct amination of hydrogen-terminated diamond surface using UV irradiation ($\lambda=254\text{nm}$) in an ammonia gas environment was reported recently by the group of Kawarada [164]. The authors have used photolithography to pattern the resulting surface and to immobilize DNA molecules in a controlled fashion. A similar approach was reported by Zhi et al. [165], where an amine functionalized boron-doped diamond surface was prepared by UV irradiation ($\lambda=254\text{nm}$, 6h) of a hydrogen-terminated surface in the presence of allylamine. It is believed that the vinyl groups of allylamine react photochemically with the C-H surface bonds to yield an amine-terminated monolayer covalently bonded to the surface through C-C bonds.

More recently, our group has demonstrated that the use of a cold NH₃ plasma treatment of hydrogenated diamond substrate generates surface terminal amino groups (**Figure 15**) [166].

1.4.6. Reactivity of oxidized diamond surfaces

1.4.6.1 Silanization reactions on oxygen-terminated diamond surfaces

Silanization reaction is a simple way to modify oxygen-terminated diamond surfaces. As silane reagents show no reactivity towards carbonyl or ether groups they can be used to underlie the presence of hydroxyl groups on oxidized diamond. Notsu et al. reacted

electrochemically- and oxygen plasma-oxidized boron-doped diamond (BDD) surfaces with 3-aminopropyltriethoxysilane (APTES) and subsequent characterizations of the modified surface indicate the success of the silanization reaction, as shown in **Figure 1.16** [136, 167, 168]. The modification by APTES is particularly important for possible applications, because the terminal amino group can be used to form a covalent bond with functional molecules such as DNA, enzymes, and immuno-compounds, and highly selective, highly sensitive electrode systems can be created [168].

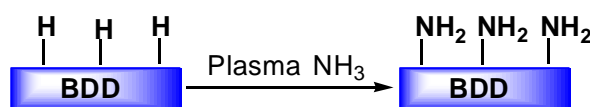


Figure 1.15. Direct amination of hydrogenated boron-doped diamond surfaces using NH_3 plasma.

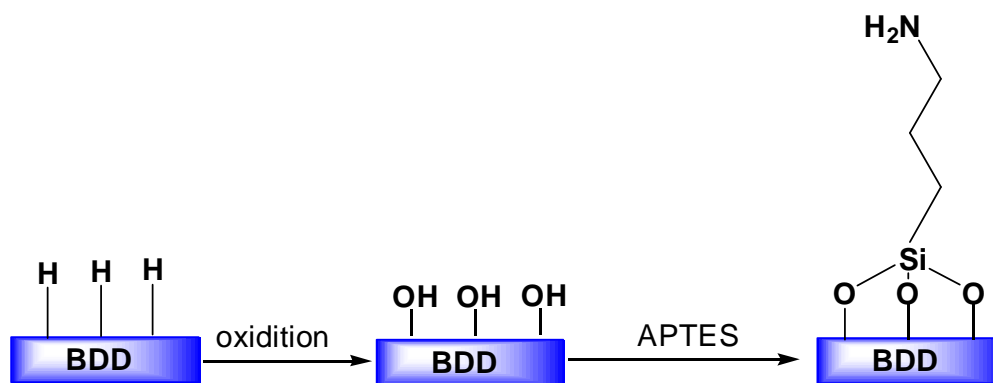


Figure 1.16. Schematic illustration of the silanization reaction of oxidized diamond surface with aminopropyltriethoxysilane.

On the other hand, surface hydroxyl groups on photochemically oxidized diamond surfaces were reacted with perfluorodecyltrichlorosilane [$\text{CF}_3\text{-(CF}_2\text{)}_7\text{-CH}_2\text{-CH}_2\text{-SiCl}_3$] at room temperature (**Figure 1.17**) [138]. The success of the reaction was demonstrated by a significant increase of the contact angle of the modified surface to 109° , as compared to the low value ($< 20^\circ$) of the oxidized BDD surface.

N-(3-trimethoxysilylpropyl) pyrrole (TMPP) linked to oxidized BDD has been reported recently by our group (**Figure 1.18**) [169]. The functional silane layer allowed localized polymer formation to be achieved on the TMPP-modified BDD interface using the direct

mode of a scanning electrochemical microscope (SECM) as well as an electrochemical scanning near-field optical microscope (E-SNOM).

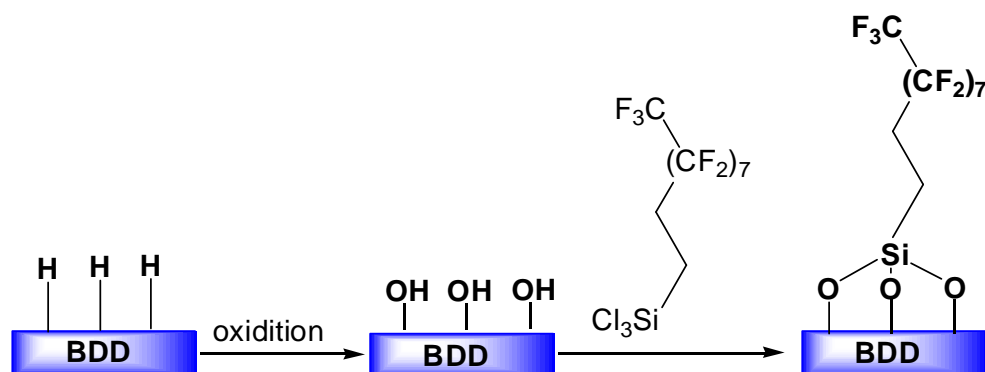


Figure 1.17. Schematic illustration of the silanization reaction of oxidized diamond surface with perfluorodecyl trichlorosilane [138].

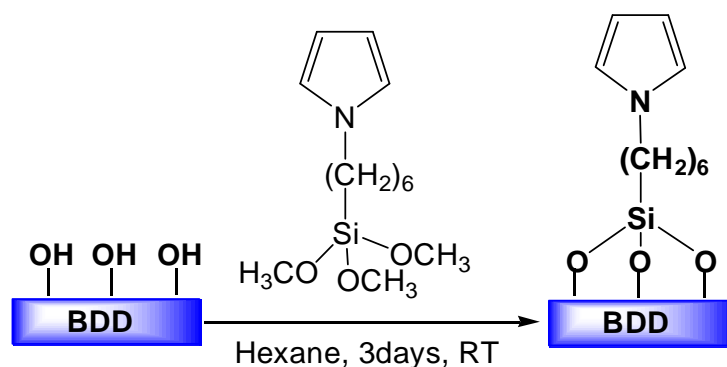


Figure 1.18. Chemical functionalization scheme of oxidized diamond surfaces with *N*-(3-trimethoxysilylpropyl) pyrrole [138].

1.4.6.2 Esterification reactions of oxygen-terminated diamond surfaces

Another possibility of surface modification of oxygen-terminated diamond surface is esterification reaction. The hydroxyl groups of oxidized BDD were successfully tethered to organic molecules through an esterification reaction. Pyrenebutyric acid (**Figure 1.19**) [170], and biotin [133] were covalently linked to oxidized diamond. To reveal the biotin grafting, the authors explored the strong affinity of biotin to fluorescently labeled streptavidin. On the other hand, the photoelectrochemical behavior of a pyrene-terminated BDD surface was studied and cathodic photocurrents have been measured in oxygen saturated electrolyte.

More recently, 3-benzoylbenzoic acid covalently bonded to oxidized diamond was reported by our group (**Figure 1.20**) [171]. Since benzophenone is an efficient photoactivable group,

stable under ambient light and protic solvents [172, 173], the benzophenone terminated BDD surface was successfully used for photochemical immobilization of DNA, peptides and proteins.

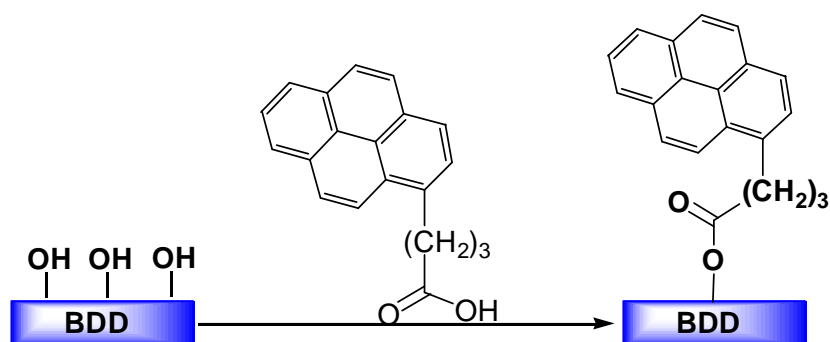


Figure 1.19. Schematic illustration of the esterification reaction of hydroxylated diamond with pyrenebutyric acid [170].

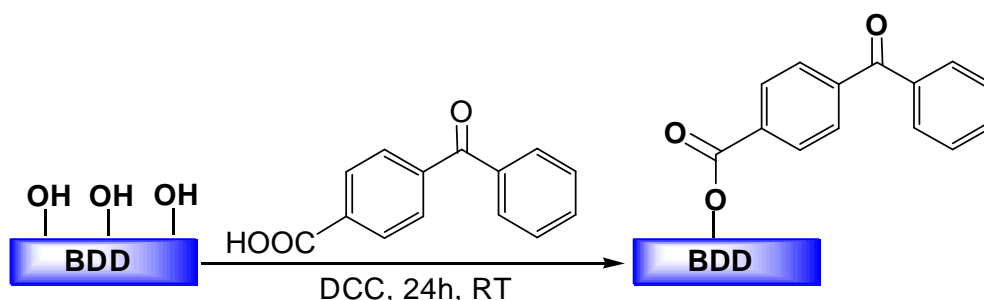


Figure 1.20. Schematic illustration of the esterification reaction of hydroxylated diamond with 3-benzoylbenzoic acid [171].

Zirconium phosphate chemistry has been adapted to oxidized diamond surface [174]. Carboxylic acid layers can be bound to the diamond surface by coordination to zirconium phosphate functionalities. Pyrene was linked in this manner to BDD and a surface coverage of $5 \times 10^{-11} \text{ mol cm}^{-2}$ was determined.

1.4.7. Reactivity of halogenated surfaces

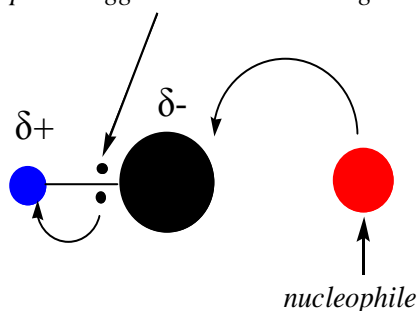
The interest in halogenated interfaces is that they are prone to nucleophilic substitution reactions by breaking the carbon-halogen bond. With the exception of iodine, all of the halogens are more electronegative than carbon (Table 1.1)

Table 1.1. Electronegativity values (Pauling scale)

C	2.5	F	4.0
		Cl	3.0
		Br	2.8
		I	2.5

This means that the electron pair in the carbon-halogen bond will be dragged towards the halogen end, leaving the halogen slightly negative (δ^-) and the carbon slightly positive (δ^+) (**Figure 1.21**), except in the carbon-iodine case.

electron pair dragged towards the halogen end

**Figure 1.21.** The polarity of the carbon-halogen bonds.

The strength of the C-halogen bond is changing drastically as seen in **Table 1.2**.

Table 1.2. The strengths of the carbon-halogen bonds (all values in kJ mol^{-1})

C-H	413	C-F	467
		C-Cl	346
		C-Br	290
		C-I	228

It was demonstrated that the bromo groups in bromopropyl-modified silica nanoparticles can be substituted in a saturated solution of NaN_3 [175]. The exchange of surface bromine of 11-bromo-undecylsiloxane monolayers against azide via nucleophilic substitution with sodium azide in DMF solution was reported by C. Barbot et. al. [176]. Bromine-terminated

silica and glass substrates were immersed in a saturated solution of sodium azide in DMF for 24 h at room temperature to obtain an azide termination [177].

In addition, chlorinated diamond butylated with butyllithium dissolved in THF at 30°C for 4h was reported by Yoshinori Ikeda as shown in **Figure 1.22** [178]. Cl-terminated Si surface was exposed to an alkyllmagnesium halide reagent to prepare alkylated silicon (111) surfaces with $-C_nH_{2n+1}$ ($n = 1$ or 2) or $-C_6H_5CH_2$ groups. Corresponding XPS data indicates that functionalization by the two-step chlorination/alkylation process proceeds cleanly to produce oxide-free Si surfaces terminated with the chosen alkyl group [179]. James R. Heath et. al. fully acetylenylated silicon surface by same way [180]. The resulting Cl-terminated surfaces were exposed to a solution of CH_3MgCl to form methylated Si (111) surface, whereas the Cl-terminated surfaces were exposed to a solution of C_2H_5MgCl to form C_2H_5 -terminated surfaces [181-183].

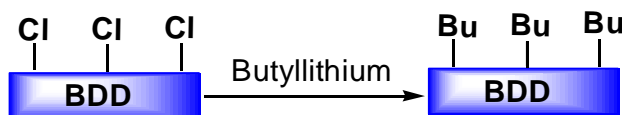


Figure 1.22 Alkylation scheme on chlorinated diamond surface.

1.4.8. Reactivity of aminated diamond surfaces

The aminated diamond surface was further investigated for its ability to bind gold nanoparticles [184] and for the formation of a peptide array [166]. As seen in **Figure 1.23A**, homogeneous and well-distributed gold nanoparticles (AuNPs) were obtained by simple exposure of the amine-terminated BDD surface to an aqueous solution of gold colloid. The Au NPs modified NH_2 -diamond shows interesting catalytic behavior towards oxygen reduction in basic medium, where a significant positive shift of the oxygen reduction peak and an increase in the peak current density upon loading with gold NP is observed.

Linking of glyoxylyl peptides to diamond, based on the formation of a semicarbazide termination on amine-terminated boron-doped diamond (**Figure 1.23A**) was investigated. Two different peptides (peptide 1: FLAG- NH_2 and peptide 2: FLAGCOCHO) were printed in a microarray format on semicarbazide-modified BDD. The fluorescent images (**Figure 23B**), obtained after incubation in the presence of antibody anti-peptide FLAG labeled with

tetramethylrhodamine shows that the fluorescence observed from peptide 2 is more important than with peptide 1. This is consistent with specific covalent ligation of peptide 2 with the semicarbazide surface and the non-covalent interaction of peptide 2 with the semicarbazide surface.

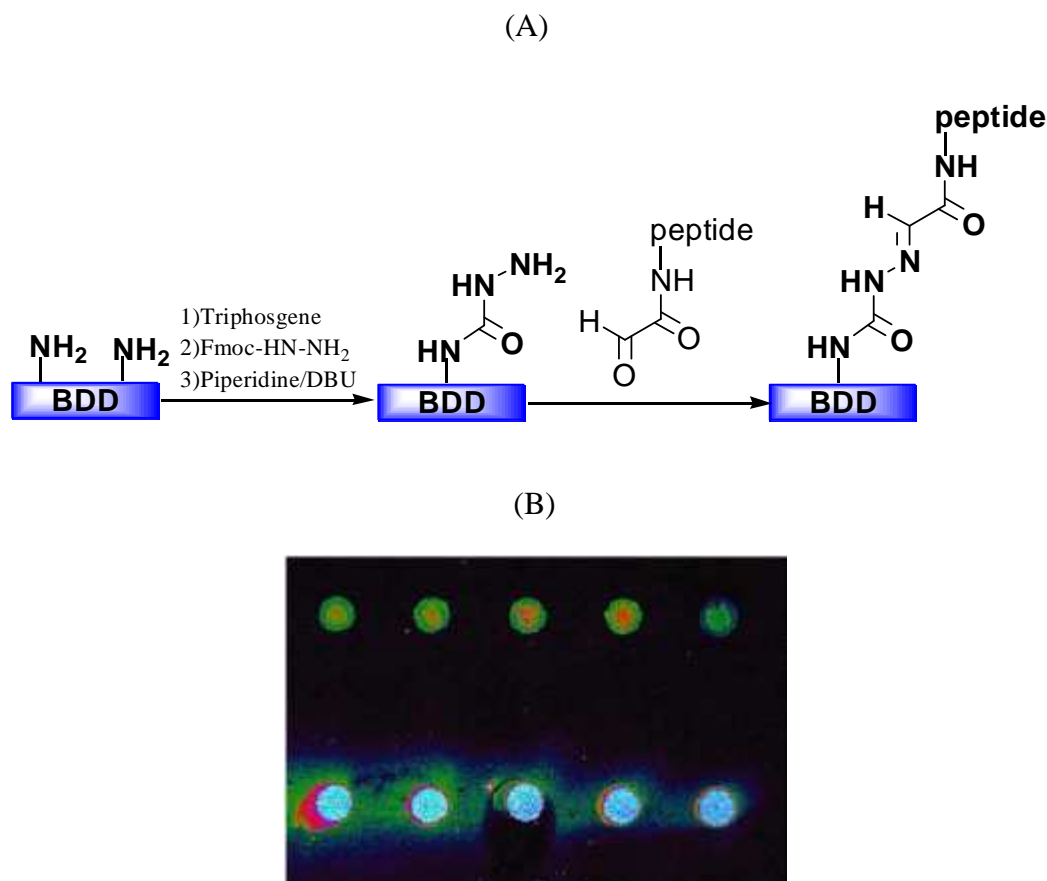


Figure 1.23. A) Formation of a peptide array through site-specific α -oxo semicarbazone ligation on aminated diamond, B) fluorescence image, top (peptide 1: FLAG-NH₂), bottom (peptide 2: FLAG-COCHO).

1.5. Scope of the thesis

Even though diamond surfaces are chemically inert, photochemical, electrochemical and chemical approaches have shown their strength in tethering functional groups to this interface. The opportunities for diamond are wide open. To make it competitive with silicon technology, the core advantages of diamond including the chemical stability, the low electrochemical background current and its wide potential window will have to be optimized. The control of

the surface chemistry of diamond will play a crucial role in this perspective. While these interfaces are nowadays used as analytical devices in different areas, the development of new surface chemistries on diamond has somehow stagnated over the years. The future application of diamond will be in high-throughput systems and biotechnologies. Whether diamond will be the material of choice for biosensing applications will depend on the effort put into the control of its surface.

In this thesis, the initial phase of the study includes the oxidation of boron-doped diamond (BDD) using three different oxidative approaches, and the resulting surfaces were well characterized by X-ray photoelectron spectroscopy (XPS) and Mott-Schottky analysis. A silane coupling agent-3-aminopropyltriethoxysilane (APTES) and a carboxylic acid trifluoroacetic acid (CF_3COOH) were used to verify the difference in terms of grafting density (**Chapter 3**).

In a second phase, “click chemistry” was used as a new strategy to covalently attach acetylene-bearing molecules (thiophene, ferrocene as well as cyclophane) to azide-terminated BDD surfaces. The azide termination was obtained through an esterification reaction between 4-azidobenzoic acid and hydroxyl groups on oxygenated BDD surface. The resulting surfaces were characterized by X-ray photoelectron spectroscopy (XPS), water contact angle and electrochemical measurements (**Chapter 4**).

Ionic liquid (IL): 1-(Methylcarboxylic acid)-3-octylimidazolium-bis (tri fluoromethyl sulfonyl) imide was bonded to oxygenated BDD surface through an esterification reaction as well. The resulting surface was characterized and confirmed by X-ray photoelectron spectroscopy, water contact angle and electrochemical measurements. Anion exchange between $(\text{CF}_3\text{SO}_3)_2\text{N}^-$ and BF_4^- , NO_3^- and PF_6^- on the IL modified BDD surface was investigated subsequently (**Chapter 5**).

A versatile strategy for chemical halogenation of hydrogenated boron-doped diamond (H-BDD) surfaces is discussed. Brominated and chlorinated boron-doped diamond electrodes are prepared in a controlled way through a radical substitution reaction using *N*-halogenosuccinimide in the presence of benzoyl peroxide. The reactivity of the halogenated BDD surfaces was further exploited. The formation of an azide termination by a nucleophilic displacement of the terminal bromo groups with sodium azide was achieved.

Electrochemically active ferrocene moieties were covalently linked to the azide terminated BDD surface using “click” chemistry (**Chapter 6**).

1.6. References

1. M. Chee et al. *Science*. **1996**, 274, 610.
2. E. M. Southern et al. *Nucleic Acids Res.* **1994**, 22, 1368.
3. J. A. Ferguson; T. C. Boles; C. P. Adams; D. R. Walt. *Nature Biotechnol.* **1996**, 14, 1681.
4. M. Schena; D. Shalon; R. W. Davis; P. O. Brown. *Science*. **1995**, 270, 467.
5. V. S. Y. Lin; K. Motesharei; K. P. S. Dancil; M. J. Sailor; M. R. Ghadiri. *Science*. **1997**, 278, 840-843.
6. S. M. Barnard; D. R. Walt. *ibid.* **1991**, 251, 927.
7. P. S. Stayton et al. *Nature*. **1995**, 378, 472.
8. F. J. Rowell. *Biochem. Soc. Trans.* **1991**, 19, 32-35.
9. A. Riklin; E. Katz; I. Willner; A. Stocker; A. F. Buckmann. *Nature*. **1995**, 376, 672.
10. R. V. Parthasarathy; C. R. Martin. *ibid.* **1994**, 369, 298.
11. Y. Shinohara et al. *J. Biochem.* **1995**, 117, 1076.
12. A. Kumar. *The Minerals, Metals & Materials Society*. **2000**, 10, 52.
13. A. S. Dewa; W. H. Ko. *Biosensors. Semiconductor Sensors.* ed. S.M. Sze. *New York: Wiley Interscience*. **1994**, 415.
14. E. A. H. Hall. ed. *Biosensors. New York: Prentice Hall*. **1991**, 201.
15. D. Diamond, ed. *Principles of Chemical and Biological Sensors. New York: John Wiley & Sons*. **1998**, 150, 23.
16. C. R. Lowe. *Biosensors*. **1985**, 1, 4.
17. K. R. Rogers. *Biosens. Bioelectron.* **1995**, 10, 533-541.
18. A. P. F. Turner. *Sens. Actuat.* **1989**, 17, 433-450.
19. N. K. Chaki; K. Vijayamohan. *Biosensors & Bioelectronics*. **2002**, 17, 1-12.
20. J. Xu; M. C. Granger; Q. Chen; J. W. Strojek; T. E. Lister; G. M. Swain. *Anal. Chem.* **1997**, 69, 591A.
21. M. R. Linford; P. Fenter; P. M. Eisenberger; C. E. D. Chidsey. *J. Am. Chem. Soc.* **1995**,

- 117, 3145.
22. T. Strother; W. Cai; X. Zhao; R. J. Hamers; L. M. Smith. *J. Am. Chem. Soc.* **2000**, 122, 1205.
 23. T. Strother; R. J. Hamers; L. M. Smith. *Nucleic Acids Res.* **2000**, 28, 3535.
 24. Z. Lin; T. Strother; W. Cai; X. Cao; L. M. Smith; R. J. Hamers. *Langmuir* **2002**, 18, 788-796.
 25. T. Strother; T. Knickerbocker; J. N. Russell; J. E. Butler; L. M. Smith; R. J. Hamers. *Langmuir*. **2002**, 18, 968-971.
 26. G. M. Swain; A. B. Anderson; J. C. Angus. *MRS Bulletin*. **1998**, 7, 56.
 27. M. Fryda; L. Schäfer; I. Tröster. *Recent Res. Devel. Electrochem.* **2000**, 4, 85.
 28. Y. V. Pleskov. *Advances in Electrochemical Science and Engineering*. Editors R.C. Alkire; D. M. Kolb. *Wiley-VCH*. **2002**, 8, 209.
 29. R. G. Compton; J. S. Foord; F. Marken. *Electroanal.* **2003**, 15, 1349.
 30. W. Haenni; P. Rychen; M. Fryda; C. Comninellis. *Thin-Film Diamond Part B*. Editor. Ch. Nebel. *Semiconductors and Semimetals series. Elsevier*. **2004**, 149.
 31. M. Panizza; G. Cerisola. *Electrochim. Acta.* **2005**, 51, 191.
 32. O. Chailapakul; W. Siangproh; D.A. Tryk. *Sensor Lett.* **2006**, 4, 99.
 33. M. A. Q. Alfaro; S. Ferro; C. A. Martínez-Huitle; Y. M. Vong. *J. Braz. Chem. Soc.* **2006**, 17, 227.
 34. A. Kraft. *Int. J. Electrochem. Sci.* **2007**, 2, 355-385.
 35. A. Fujishima; Y. Einaga; T. N. Rao; D.A. Tryk. *Diamond Electrochemistry. Elsevier B.V. Amsterdam.* **2005**.
 36. G. M. Swain; M. Ramesham. *Anal. Chem.* **1993**, 65, 345.
 37. H. Kawai; Y. Araki; T. Sakai; T. Ogawa; H. Umezawa. *Phys. Stat. Sol. A.* **2001**, 185, 79.
 38. T. Vo-Dinh; J. P. Alarie; N. Isola; D. Landis; A. L. Wintenberg; M. N. Ericson. *Anal. Chem.* **1999**, 71, 358.
 39. Q. Y. Chen; M. C. Granger; T. E. Lister; G. M. Swain. *J. Electrochem. Soc.* **1997**, 144, 3806.
 40. F. Z. Cui; D. J. Li. *Surf. Coat. Technol.* **2000**, 131, 481.

41. M. Nesladek. *Semicond. Sci. Technol.* **2005**, 20, R19.
42. W. Wesner; M. Kotschan; R. Hermann; W. Staber; M. Schelch. *International patent application. WO2004*, 00558.
43. A. Ciecwiwa; R. Wüthrich; C. Comminellis. *Electrochem. Commun.* **2006**, 8,375.
44. K. Gruber. *International patent application. WO2005*, 116302.
45. Y. V. Pleskov; M. D. Krotova; V. G. Ralchenko; A. V. Khomich; R. A. Khmelnitskiy. *Electrochim. Acta.* **2003**, 49, 1171.
46. Y. V. Pleskov; M. D. Krotova; V. V. Elkin; V. G. Ralchenko; A. V. Khomich; R. A. Khmelnitskiy. *Electrochim. Acta.* **2005**, 50, 1149.
47. I. M. Landstrass; K. V. Ravi. *Appl. Phys. Lett.* **1989**, 55, 975.
48. M. Fryda; T. Matthee; S. Mulcahy; A. Hampel; L. Schäfer; I. Tröster. *Diam. Relat. Mater.* **2003**, 12, 1950.
49. L. Schäfer; M. Höfer; R. Kröger. *Thin Solid Films.* **2006**, 515, 1017.
50. T. Yano; D. A. Tryk; K. Hashimoto; A. Fujishima. *J. Electrochem. Soc.* **1998**, 145, 1870.
51. W. Haenni; A. Perret; P. Rychen. *International patent application. WO 2002*, 061181.
52. C. H. Goeting; F. Jones; J. S. Foord; J. C. Eklund; F. Marken; R. G. Compton; P. R. Chalker ; C. Johnston. *J. Electroanal. Chem.* **1998**, 442, 207.
53. H. B. Martin; A. Argoitia; J. C. Angus; U. Landau. *J. Electrochem. Soc.* **1999**, 146, 2959.
54. J. van de Lagemaat; D. Vanmaekelbergh; J. J. Kelly. *J. Electroanal. Chem.* **1999**, 475, 139.
55. Q. Chen; D. M. Gruen; A. R. Krauss; T. D. Corrigan; M. Witek; G. M. Swain. *J. Electrochem. Soc.* **2001**, 148, E44.
56. S. C. Eaton; A. B. Anderson; J. C. Angus; Y. E. Evstefeeva; Y. V. Pleskov. *Electrochem. Solid-State Lett.* **2002**, 5, G65.
57. S. Vaddiraju; S. Eaton-Magana; J. A. Chaney; M. K. Sunkara. *Electrochem. Solid-State Lett.* **2004**, 7, G331.
58. J. J. Mares; M. Nesladek; P. Hubik; D. Kindl; J. Kristofik. *Diam. Relat. Mater.* **2007**, 16, 1.
59. Y. V. Pleskov; A. Y. Sakharova; M. D. Krotova; L. L. Builov; B. V. Spitsyn. *J. Electroanal. Chem.* **1987**, 228, 19.

60. H. B. Martin; A. Argoitia; U. Landau; A. B. Anderson; J. C. Angus. *J. Electrochem. Soc.* **1996**, 143, L133.
61. N. Katsui; E. Takahashi; M. Toyoda; T. Kurosu; M. Iida; S. Wakita; Y. Nishiki ; T. Shimamume. *J. Electrochem. Soc.* **1998**, 145, 2358.
62. F. Beck; H. Krohn; W. Kaiser; M. Fryda; C. P. Klages; L. Schäfer. *Electrochim. Acta.* **1998**, 44, 525.
63. F. Beck; W. Kaiser; H. Krohn. *Electrochim. Acta.* **2000**, 45, 4691.
64. N. Vinokur; B. Miller; Y. Avyigal; R. Kalish. *J. Electrochem. Soc.* **1996**, 143, L238.
65. A. Ciecwiwa; R. Wüthrich; C. Comninellis. *Electrochem. Commun.* **2006**, 8, 375.
66. A. Chatterjee; R. G. Compton; J. S. Foord; M. Hiramatsu; F. Marken. *Phys. Stat. Sol. (a).* **2003**, 199, 49.
67. M. C. Granger; M. Witek; J. Xu; J. Wang; M. Hupert; A. Hanks; M. D. Koppang; J. E. Butler; G. Lucazeau; M. Mermoux; J. W. Strojek; G. M. Swain. *Anal. Chem.* **2000**, 72, 3793.
68. S. Ferro; A. De Battisti. *Electrochim. Acta.* **2002**, 47, 1641.
69. D. Becker; K. Jüttner. *Electrochim. Acta.* **2003**, 49, 29.
70. D. Becker; K. Jüttner. *J. Appl. Electrochem.* **2003**, 33, 659.
71. J. A. Bennett; J. Wang; Y. Show; G. M. Swain. *J. Electrochem. Soc.* **2004**, 151, E306.
72. Y. V. Pleskov; Y. E. Evstefeeva; M. D. Krotova; P. Y. Lim; H. C. Shih; V. P. Varnin; I. G. Teremetskaya; I. I. Vlasov; V. G. Ralchenko. *J. Appl. Electrochem.* **2005**, 35, 857.
73. K. Jüttner; D. Becker. *J. Appl. Electrochem.* **2007**, 37, 27.
74. Y. Maeda; K. Sato; R. Ramaraj; T. N. Rao; D. A. Tryk; A. Fujishima. *Electrochim. Acta.* **1999**, 44, 3441.
75. S. Ferro; A. De Battisti. *Phys. Chem. Chem. Phys.* **2002**, 1, 1915.
76. S. Ferro; A. De Battisti. *J. Electroanal. Chem.* **2002**, 533, 177.
77. A. Y. Sakharova; Y. V. Pleskov; F. Di Quarto; S. Piazza; C. Sunseri; I. G. Teremetskaya; V. P. Varnin. *J. Electrochem. Soc.* **1995**, 142, 2704.
78. L. Boonma; T. Yano; D. A. Tryk; K. Hashimoto; A. Fujishima. *J. Electrochem. Soc.* **1997**, 144, L142.
79. T. N. Rao; D. A. Tryk; K. Hashimoto; A. Fujishima. *J. Electrochem. Soc.* **1999**, 146, 680.

80. M. Panizza; G. Sine; I. Duo; L. Ouattara; C. Comninellis. *Electrochem. Solid-State Lett.* **2003**, 6, D17.
81. C. Comninellis. Electrochemical stability of BDD electrodes in acid medium. Proc. 7th Workshop Diamond Electrodes. *Interlaken* 19.10.2004.
82. L. Schäfer; S. Arndt; D. Herrmann; M. Höfer; D. Becker; K. Jüttner. Diamond electrodes under high current density. Proc. 7th Workshop Diamond Electrodes. *Interlaken* 19.10.2004.
83. X. Chen; G. Chen. *J. Electrochem. Soc.* **2004**, 151, B214.
84. J. M. Halpern; S. Xie; G. P. Sutton; B. T. Higashikubo; C. A. Chestek; H. Lu; H. J. Chiel; H. B. Martin. *Diam. Relat. Mater.* **2006**, 15, 183.
85. S. Xie; G. Shafer; C. G. Wilson; H. B. Martin. *Diam. Relat. Mater.* **2006**, 15, 225.
86. Y. L. Zhou; J. F. Zhi. *Electrochem. Commun.* **2006**, 8, 1811.
87. A. Härtl; E. Schmich; J. A. Garrido; J. Hernando; S. R. Catharino; S. Walter; P. Feulner; A. Kromka; D. Steinmüller; M. Stutzmann. *Nature Mater.* **2004**, 3, 702.
88. W. Yang; J. E. Butler; J. N. Russell; R. J. Hamers. *Langmuir* **2004**, 20, 6778.
89. K. Stolarczyk; E. Nazaruk; J. Rogalski; R. Bilewicz. *Electrochem. Commun.* **2007**, 9, 115.
90. A. A. Rouse; J. B. Bernhard; E. D. Sosa; D. E. Golden. *Appl Phys Lett.* **1999**, 75, 3417.
91. R. J. Hamers; J. E. Butler; T. Lassetera ; B. M. Nicholasa ; J. N. Russell ; K. Y. Tsea ; W. Yanga. *Diam. Relat. Mater.* **2005**, 14, 661–668.
92. T. Knickerbocker; T. Strother; M. P. Schwartz; J. N. Russell; J. Butler; L. M. Smith; R. J. Hamers. *Langmuir* **2003**, 19, 1938–1942.
93. B. Sun; S. E. Baker; J. E. Butler; H. Kim; J. N. Russell; L. Shang; K. Y. Tse; W. Yang; R. J. Hamers. *Diam. Relat. Mater.* **2007**, 16, 1608.
94. T. L. Lasseter; B. H. Clare; N. L. Abbott; R. J. Hamers. *J. Am. Chem. Soc.* **2004**, 126, 10220-10221.
95. W. Yang; J. E. Butler; J. N. Russell; R. J. Hamers. *Analyst.* **2007**, 132, 296.
96. B. Rezek; D. Shin; Y. Nakamura; C. E. Nebel. *J. Am. Chem. Soc.* **2006**, 128, 3884.
97. N. Yang; H. Uetsuka; H. Watanabe; T. Nakamura; C.E. Nebel. *Chem. Mater.* **2007**, 19, 2852.

98. P. Christiaens; V. Vermeeren; S. Wenmackers; M. Daenen; K. Haenen; M. Nesladek; M. VandeVen; M. Ameloot; L. Michiels; P. Wagner. *Biosens. Bioelectron.* **2006**, 22, 170.
99. C. E. Nebel; D. Shin; D. Takeuchi; T. Yamamoto; H. Watanabe; T. Nakamura. *Diam. Relat. Mater.* **2006**, 15, 1107.
100. J. R. Retama; J. Hernando; B. L. Ruiz; A. Hartl; D. Stinmuller; M. Stutzmann; E. L. Cabarcos; J. A. Garrido. *Langmuir.* **2006**, 22, 5837.
101. Y. L. Zhong; K. F. Chong; P. W. May; Z. K. Chen; K. P. Loh. *Langmuir.* **2007**, 23, 5824.
102. W. Yang; O. Auciello; J. E. Butler; W. Cai; J. A. Carlisle; J. E. Gerbi; D. M. Gruen; T. L. Knickerbocker; T. L. Lassetter; J. N. Russell; L. M. Smith; R. J. Hamers. *Nature Mat.* **2002**, 253-257.
103. M. C. Lu; T. Knickerbocker; W. Cai; W. S. Yang; R. J. Hamers; L. M. Smith. *Biopolymers.* **2004**, 73, 606.
104. A. Hartl; E. Schmich; J. A. Garrido; J. Hernanod; S. C. R. Catharino; S. Walter; P. Feulber; A. Kromka; D. Steinmuller; M. Stutzmann. *Nature Mat.* **2004**, 1-7.
105. B. M. Nichols; J. E. Butler; J. N. Russell; R. J. Hamers. *J. Phys. Chem. B.* **2005**, 109, 20938.
106. B. M. Nichols; K. M. Metz; K. Y. Tse; J. E. Butler; J. N. Russell; R. J. Hamers. *J. Phys. Chem B.* **2006**, 110, 16535.
107. T. C. Kuo; R. L. McCreery; G. M. Swain. *Electrochem. Solid-State Lett.* **1999**, 2, 288-290.
108. J. Wang; J. A. Carlisle. *Diam. Rel. Mater.* **2006**, 15, 279.
109. P. Allongue; M. Delamar; B. Desbat; O. Fagebaume; R. Hitmi; J. Pinson; J. M. Serveant. *J. Am. Chem. Soc.* **1997**, 119, 201.
110. W. Yang; S. E. Baker; J. E. Butler; C. S. Lee; J. N. Russell; L. Shang; B. Sun; R. J. Hamers. *Chem. Mater.* **2005**, 17, 938-940.
111. G. Shul; P. Actis; B. Marcus; M. Opallo; R. Boukherroub; S. Szunerits. *Diam. Rel. Mater.* **2008**, 17, 1394-1398.
112. J. Pinson; F. Podvorica. *Chem. Soc. Rev.* **2005**, 34, 429.
113. F. Anariba; S. H. DuVall; R. L. McCreery. *Anal. Chem.* **2003**, 75, 3837-3844.
114. Y. L. Zhou; J. F. Zhi. *Electrochem. Commun.* **2006**, 8, 1811.

- 115.B. Rezek; D. Shin; C. E. Nebel. *Langmuir*. **2007**, 23, 7626.
- 116.H. Uetsuka; D. Shin; N Tokuda; K. Saeki; C. E. Nebel. *Langmuir*. **2007**, 23, 3466.
- 117.J. S. Foord; W. Hao; S. Hurst. *Diam. Relat. Mater*. **2007**, 16, 877.
- 118.T. Tsubota; K. Urabe; S. Egawa; H. Takagi; K. Kusakabe; S. Morooka; H. Meada. *Diam Relat Mater*. **2000**, 9, 219.
- 119.T. Tsubota; O. Hirabayashi; S. Ida; S. Nagaoka; M. Nagata; Y. Matsumoto. *Diam Relat Mater*. **2002**, 11, 1360-1365.
- 120.T. Tsubota; O. Hirabayashi; S. Ida; S. Nagaoka; M. Nagata; Y. Matsumoto. *J. Cer. Soc. Jpn*. **2002**, 110, 669-675.
- 121.T. Tsubota; O. Hirabayashi; S. Ida; S. Nagaoka; M. Nagata; Y. Matsumoto. *Phys Chem Chem Phys*. **2002**, 4, 806-811
- 122.T. Tsubota; O. Hirabayashi; S. Ida; S. Nagaoka; M. Nagata; Y. Matsumoto. *Diam Relat Mater*. **2002**, 11, 1374-1378.
- 123.T. Tsubota; S. Ida; O. Hirabayashi; S. Nagaoka; M. Nagata; Y. Matsumoto. *Phys. Chem. Chem. Phys*. **2002**, 4, 3881-3886.
- 124.T. Tsubota; S. Tanii; S. Ida; S. Nagaoka; Y Matsumoto. *PhysChem Chem Phys*. **2003**, 5,1474-1480
- 125.T. Tsubota; S. Tanii; S. Ida; M. Nagata; Y. Matsumoto. *DiamRelat Mater*. **2004**, 13, 1093-1097.
- 126.S. Ida; T. Tsubota; O Hirabayashi; M. Nagata; Y. Matsumoto; A. Fujishima. *Diam Relat Mater*. **2003**, 12, 601-605.
- 127.S. Ida; T. Tsubota; S. Tanii; M. Nagata; Y Matsumoto. *Langmuir*. **2003**, 19, 9693-9698.
- 128.T. Ando; K. Yamamoto; M. Ishii; M. Kamo; Y. Sato. *J. Chem. Soc*. **1993**, 89, 3635.
- 129.P. E. Pehrsson; T. W. Mercer. *Surf. Sci*. **2000**, 460, 49.
- 130.P. John; N. Polwart; C. E. Troupe; J. I. B. Wilson. *J. Am. Chem. Soc*. **2003**, 125, 6600.
- 131.H. Notsu; I. Yagi; T. Tatsuma; D. A. Tryk; A. Fujishima. *Electrochem.Solid-State Lett*. **1999**, 2, 522.
- 132.Y. Ikeda; T. Saito; K. Kusakabe; S. Morooka; H. Maeda; Y. Taniguchi; Y. Fujiwara. *Diam. Relat. Mater*. **1998**, 7, 830-838.
- 133.D. Delabouglise; B. Marcus; M. Mermoux; P. Bouvier; J. Chane-Tune; J. P. Petit; P.

- Mailley; T. Livache. *Chem. Comm.* **2003**, 2698-2699.
- 134.C. H. Goeting; F. Marken; A. Gutiérrez-Sosa; R. C. Compton. *Diam. Relat. Mat.* **2000**, 9, 390.
- 135.H. Notsu; I. Yagi; T. Tatsuma; D. A. Tryk; A. Fujishima. *J. Electroanal. Chem.* **2000**, 492, 31.
- 136.E. Popa; H. Notsu; T. Miwa; D. A. Tryk; A. Fujishima. *Electrochem. Solid State Lett.* **1999**, 2, 49.
- 137.R. Ohta; N. Saito; Y. Inoue; H. Sugimura; O. Takai. *J. Vac. Sci. Technol. A.* **2004**, 22, 2005.
- 138.R. Boukherroub; X. Wallart; S. Szunerits; B. Marcus; P. Bouvier; M. Mermoux. *Electrochem. Comm.* **2005**, 7, 937.
- 139.H. Kanazawa; K-S. Song; T. Sakai; Y. Nakamura; H. Umezawa; M. Tachiki; H. Kawarada. *Diam. Relat. Mater.* **2003**, 12, 618.
- 140.M. Riedel; J. Ristein; L. Ley. *Diam. Relat. Mater.* **2004**, 13, 746.
- 141.S. Foord; C. H. Lau; M. Hiramatsu; R. B. Jackman; C. E. Nebel; P. Bergonzo. *Diam. Relat. Mater.* **2002**, 11, 856
- 142.J. Shirafuji; T. Sugino. *Diam. Relat. Mater.* **1996**, 5, 706.
- 143.J. I. B. Wilson; J. S. Walton; G. Beamson. *J. Electron Spectrosc. Relat. Phenom.* **2001**, 121, 183.
- 144.T. Yamada; T. Yokoyama; A. Sawabe. *Diam. Relat. Mater.* **2002**, 11, 780.
- 145.C. Saby; P. Muret. *Diam. Relat. Mater.* **2005**, 11, 851.
- 146.H. Notsu; T. Tatsuma; A. Fujishima. *Characterization of oxygenated diamond electrodes.* **2004**. 10, 1.
- 147.D. A. Teyk; K. Tsunozaki; T. N. Rao; A. Fujishima. *Diam. Relat. Mater.* **2001**,10, 1804.
- 148.E. Popa; Y. Kubota; D. A. Tryk; A. Fujishima. *Anal. Chem.* **2000**, 72, 1724.
- 149.H. Notsu; T. Fukasawa; T. Tatsuma; D. A. Tryk; A. Fujishima. *Electrochem. Solid-State Lett.* **2001**, 4, H1-H3
- 150.K. Hayashi; S. Yamanaka; H. Watanabe. *J. Appl. Phys.* **1997**, 81,744.
- 151.T. Yamada; T. J. Chuang; H. Seki; Y. Mitsuda. *Mol. Phys.* **1991**, 76, 887.
- 152.A. Freedman; C. D. Stinespring. *AppL. Phys. Lett.* **1990**, 57, 1194.

- 153.R. Sappok; H. P. Boehm. *Carbon*.**1968**, 6, 283.
- 154.J .B. Miller; D. W. Brown. *Langmuir*. **1996**, 12, 5809.
- 155.Y. Liu; G. Zhenning; J. L. Margrave; V. N. Khabashesku. *Chem. Mat.* **2004**, 16, 3924-3930.
- 156.T. Ando; M. N. Gamo; R. E. Rawles; K. Yamamoto; M. Kamo; Y. Sato. *Diam. Relat. Mat.* **1996**, 5, 1136.
- 157.J. B. Miller; D. W. Brown. *Diam. Relat. Mater.* **1995**, 4, 435.
- 158.J. B. Miller. *Surf. Sci.* **1999**, 439, 21.
- 159.T. Nakamura; K. Tsugawa; M. Ishihara; T. Ohana; A. Tanaka; Y. Koga. *Diam. Relat. Mat.* **2004**, 13, 1084.
- 160.C. S. Kim; R. C. Mowrey; J. E. Butler; J. N. Russell. *J. Phys. Chem. B.* 1998, 102, 9290-9296.
- 161.A. Freedman. *J. Appl. Phys.* **1994**, 75, 3112.
- 162.T. Ando; K. Yamamoto; M. Matsuzawa; Y. Takamatsu; S. Kawasaki; F. Okino; H. Touhara; M. Kamo; Y. Sato. *Diam. Relat. Mat.* **1996**, 5, 1021-1026.
- 163.B. Ohtani; Y. H. Kim; T. Yano; K. Hashimoto; A. Fujishima; K. Uosaki. *Chem Lett.* **1998**, 1, 953-954.
- 164.G. J. Zhang; K. S. Song; Y. Nakamura; T. Ueno; T. Funatsu; I. Ohdomari; H. Kawarada. *Langmuir*. **2006**, 22, 3728-3734.
- 165.R. H. Tian; T. N. Rao; Y. Einaga; J. F. Zhi. *Chem Mater.* **2006**, 18, 939.
- 166.Y. Coffinier; S. Szunerits; C. Jama; R. Desmet; O. Melnyk; B. Marcus; L. Gengembre; E. Payen; D. Delabouglise; R. Boukherroub. *Langmuir*. **2007**, 23, 4494-4497.
- 167.Y. Coffinier; S. Szunerits; B. Marcus; R. Desmet; O. Melnyk; L. Gengembre; E. Payen; D. Delabouglise; R. Boukherroub. *Diam. Relat. Mater.* **2007**, 16, 892-898.
- 168.T. Kondo; K. Honda; D. A. Tryk; A. Fujishima. *J. Electrochem. Soc.* **2005**, 152, E18.
- 169.P. Actis; M. Manesse; C. Nunes-Kirchner; G. Wittstock; Y. Coffinier; R. Boukherroub; S. Szunerits. *Phys. Chem. Chem. Phys.* **2006**, 8, 4924-31.
- 170.P. Bouvier; D. Delabouglise; A. Denoyell; B. Marcus; M. Mermoux; J-P Petit. *Electrochem. Solid-State Lett.* **2005**, 8, E57.
- 171.S. Szunerits, N. Shirahata; P. Actis; J. Nakanishir; R. Boukherroub. *Chem. Commun.* **2007**,

2793.

- 172.E. Delamarche; G. Sundarababu; H. Biebuyck; B. Michel; C. Gerber; H. Sigrist; H. Wolf ; H. Rigsdorf; N. Xanthopoulos; H. J. Mathieu. *Langmuir*. **1997**, 12, 1997.
- 173.G. Dorman; G. D. Prestwich. *Biochem*. **1994**, 33, 5661.
- 174.M. Mazur; P. Krysinski; G. J. Blanchard. *Langmuir*. **2005**, 21, 8802.
- 175.R. Ranjan; W. J. Brittain. *Macromol. Rapid Commun*. **2008**, 29, 1104-1110.
- 176.C. Barbot; O. Bouloussa; W. Szymczak; M. Plaschke; G. Buckau; J. P. Durand; J. Pieri; J. I. Kim; F. Goudard. *Coll. Surf. A: Physicochem. Eng. Aspects*. **2007**, 297, 221-239.
- 177.C. Haensch; S. Hoepfener; U. S. Schubert. *Nanotechnology*. **2008**, 19, 035703.
- 178.Y. Ikeda; T. Saito; K. Kusakabe; S. Morooka; H. Maeda; Y. Taniguchi; Y. Fujiwara. *Diamond Relat. Mater*. **1998**, 7, 830-834.
- 179.L. J. Webb; E. J. Nemanick; J. S. Biteen; D. W. Knapp; D. J. Michalak; M. C. Traub; A. S. Y. Chan; B. S. Brunshwig; N. S. Lewis. *J. Phys. Chem. B*. **2005**, 109, 3930-3937.
- 180.R. D. Rohde; H. D. Agnew; W. S. Yeo; R. C. Bailey; J. R. Heath. *J. Am. Chem. Soc*. **2006**, 128, 9518-9525.
- 181.L. J. Webb; N. S. Lewis. *J. Phys. Chem. B*. **2003**, 107, 5404.
- 182.A. Bansal; X. Li; S. I. Yi; W. H. Weinberg; N. S. Lewis. *J. Phys. Chem. B*. **2001**, 105, 10266.
- 183.H. Yu; L. J. Webb; J. R. Heath; N. S. Lewis. *Appl. Phys. Lett*. **2006**, 88, 252111.
- 184.S. Szunerits; M. Manesse; G. Denault; B. Marcus; C. Jama; R. Boukherroub. *Electrochem. Solid-State Lett*. **2007**, 10, G43-G46.

CHAPTER 2

MATERIAL AND METHODS

2.1. Materials and reagents

2.1.1. Chemicals

Silicon wafers were purchased from Siltronics. All cleaning and etching reagents were clean room grade. 96% Sulfuric acid (H_2SO_4), 30% hydrogen peroxide (H_2O_2), and hydrofluoric acid 50% (HF) were supplied by Amplex. 3-Aminopropyltrimethoxysilane (APTMS), Cerium sulfate hydrate (CeSO_4), Potassium hexacyanoferricyanide ($\text{Fe}(\text{CN})_6^{4-}$), Potassium chloride (KCl), *N, N'*-Decyclohexylcarbodiimide (DCC), Anhydrous dimethyl sulfoxide (DMSO), 4-Dimethylaminopyridine (DMAP), Anhydrous dichloromethane (DCM), 3-Aminopropyltriethoxysilane (APTES), Trifluoroacetic acid (CF_3COOH 99.5%), Ethynyl thiophene, Thiophene, Ethynyl ferrocene, (+)-Sodium L-ascorbate, 99.999% Copper(II) sulfate pentahydrate ($\text{CuSO}_4 \cdot 5\text{H}_2\text{O}$), Anhydrous 99.8% *N, N*-Dimethylformamide (DMF), 99.9% Anhydrous tetrahydrofuran (THF), 4-Pentynoic acid, Ammonium hexafluorophosphate (NH_4PF_6), Anhydrous acetonitrile (CH_3CN), Potassium hexacyanoferricyanide ($\text{Fe}(\text{CN})_6^{4-}$), Tetraethyl ammonium hexafluorophosphate (TEAPF_6), Tetrabutylammonium tetrafluoroborate (Bu_4NBF_4), Bis (trifluoromethanesulphonyl) imide lithium salt ($\text{C}_2\text{F}_6\text{LiNO}_4\text{S}_2$), Sodium fluoroborate (NaBF_4), Sodium hexafluorophosphate (NaPF_6), Sodium Nitrate, Benzoyl peroxide, *N*-Bromosuccinimide (NBS), *N*-Chlorosuccinimide (NCS), and Decylmagnesium bromide ($\text{CH}_3(\text{CH}_2)_9\text{MgBr}$) 1.0M solution in diethyl ether were available from Aldrich. 4-Azidobenzoic acid was obtained from TCI Europe. Sodium azide (NaN_3) was obtained from Fluka. Anhydrous carbon tetrachloride (CCl_4) was purchased from Riedel-de Haën Co.. All of above chemicals were used without further purification. Other chemicals were reagent grade or higher and were used as received unless otherwise specified. Alcohol **1** [1], Bipyridium salt **4**[2] and **5**[3] were obtained following the procedures described in the literature. Solvents were purified and dried by the literature methods.

2.1.2. Deionized water

The water used throughout the experiments in this thesis was purified with a milli-Q system from Millipore Co. (resistivity = 18M Ω .cm).

2.1.3. Glassware and containers

All glassware or PTFE (Polytetrafluoroethene) containers were cleaned with a piranha (H₂SO₄: H₂O₂=3:1 mixture) solution for 10-20min, followed by copious rinsing with deionized water until the water pH becomes neutral, then dried under a nitrogen stream. Before using, all containers were dried in an oven at 120°C more than 1 hour.

2.1.4. Safety considerations

The mixture H₂SO₄/H₂O₂ (piranha) solution is a strong oxidant. It reacts violently with organic materials. It can cause severe skin burns. It must be handled with extreme care in a well-ventilated fume hood while wearing appropriate chemical safety protection.

HF is a hazardous acid which can result in serious tissue damage if burns were not appropriately treated. Etching of silicon should be performed in a well-ventilated fume hood with appropriate safety considerations: face shield and double layered nitrile gloves.

2.2. Synthesis of alkyne-functionalized cyclophane **6**

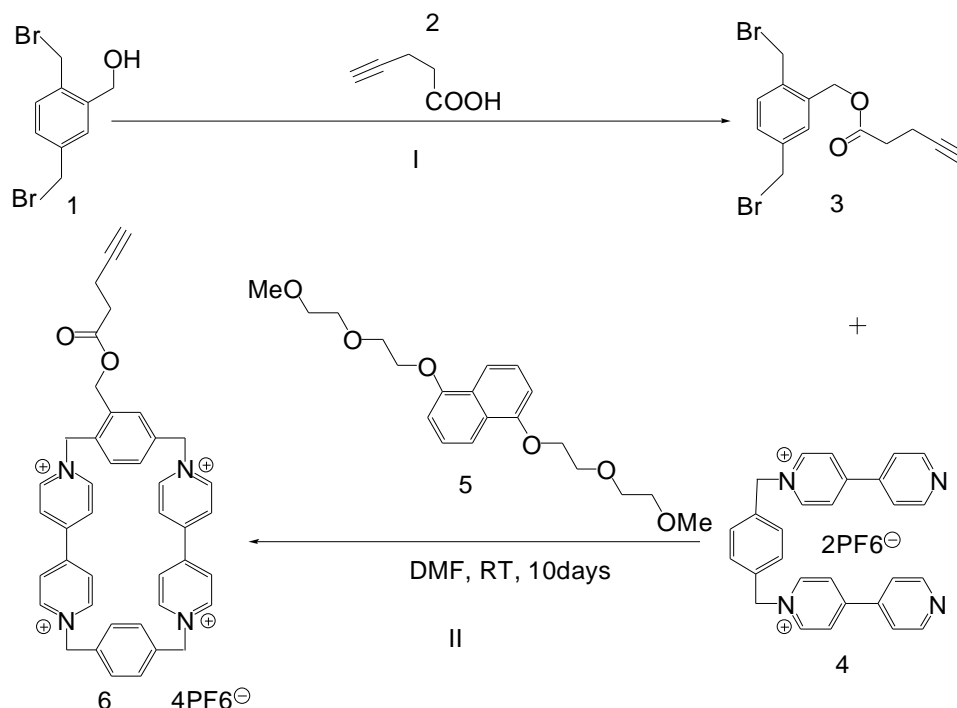
2.2.1. Synthesis of solid **3**

A solution of the alcohol **1** (1 g, 3.40 mmol), 4-pentynoic acid **2** (0.33 g, 3.40 mmol), *N,N'*-decyclohexylcarbodiimide (0.70 g, 3.40 mmol), and 4-dimethylaminopyridine (catalytic amount) in dichloromethane (CH₂Cl₂) (40 mL) was stirred under N₂ for 6h at room temperature. The resulting suspension was filtered, and the filtrate was evaporated and subjected to column chromatography (SiO₂: petroleum ether/ethanol, 2:18) to furnish **3** as a white solid, as shown in **Scheme 2.1. (I)**.

2.2.2. Synthesis of alkyne-functionalized cyclophane **6**

A solution of bipyridium salt **4** (0.76g, 1.1mmol), **3** (0.4g, 1.1mmol), and **5** (1.17g, 3.2 mmol) in dry DMF (30 mL) was stirred under N₂ at room temperature for 10 days. The solvent was removed under vacuum and the residue was subjected to a liquid-liquid extraction (CHCl₃/H₂O). The aqueous layer was concentrated and the residue was purified using column chromatography (SiO₂: MeOH/NH₄Cl (2M)/MeNO₂, 4:4:2). The fractions containing the product were combined and concentrated under vacuum. The residue was dissolved in hot water and an aqueous NH₄PF₆ solution was added. The precipitate was

collected by filtration, washed with water and Et₂O, and finally dried under vacuum, yielding a white solid **6**, as shown in **Scheme 2.1. (II)**.



Scheme 2.1. Different steps for the synthesis of cyclophane **6**.

2.3. Preparation of the substrates

2.3.1. Hydrogen terminated boron-doped diamond samples

Polycrystalline diamond layers were synthesized on a high purity p-type silicon wafer using microwave plasma-enhanced chemical vapor deposition (PECVD) technique in a conventional reactor [4,5]. The growth conditions used were as follows: substrate temperature 700–900°C, total gas flow of a mixture of 0.7% methane in hydrogen 100sccm; total pressure in the reactor 20Torr (30mbar); microwave power 700W. The dopant source was boron oxide set in a Pt crucible placed on the substrate holder near the silicon substrate. Before commencing the diamond growth, the silicon substrates were ultrasonically damaged with diamond powder in ethanol in order to improve the nucleation density. After deposition, the methane flow was stopped and the films were kept under hydrogen plasma for an additional 30 min. For 24 h of deposition, the film thickness reached 8μm. The dopant concentration in the diamond layers, as estimated from Raman spectroscopy measurements is in the range 10¹⁹–10²⁰B cm⁻³. The film resistivity was ≤ 0.1Ωcm as measured with a four-point probe. The as-deposited samples were further treated for half an hour with hydrogen plasma under the

following conditions: 100sccm of hydrogen flux, 25Torr reactor pressure with a 600W microwave power leading to a sample surface temperature of about 700°C. At the end of the plasma treatment, the microwave power was switched off and the samples were allowed to cool down under the hydrogen flux.

Figure 2.1 displays a scanning electron microscopy (SEM) image of a typical as-grown diamond film. The polycrystalline diamond film consists of randomly oriented crystallites of few microns size and with predominantly cubic (100) and triangular (111) faces.

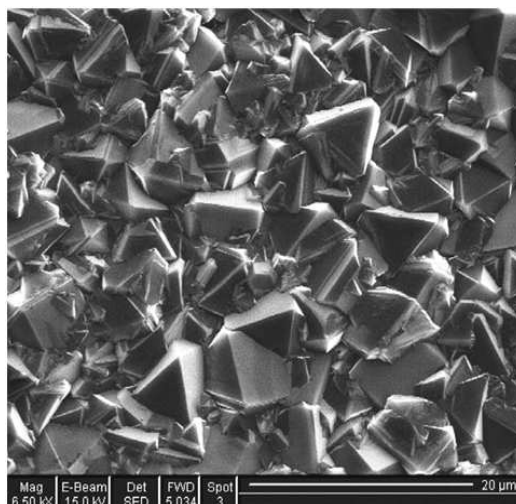


Figure 2.1. Scanning electron microscopy (SEM) image of as-grown boron-doped polycrystalline diamond surface [5].

Figure 2.2 displays an X-ray photoelectron survey (XPS) spectrum of the as-deposited boron-doped diamond surface showing signals due to C 1s at 284eV. A small signal due to O 1s at 531eV was present in the spectrum. However, it is difficult to assign precisely the origin of the peak whether it is due to surface contamination during sample handling or to interstitial incorporation within the C–C backbonds during sample growth.

2.3.2. Hydrogen-terminated free-standing boron-doped diamond films

Polycrystalline boron-doped free-standing diamond films were purchased from Windsor Scientific (Slough Berkshire, U.K.). Briefly, highly boron-doped polycrystalline CVD diamond layers were grown to a thickness greater than 500 μ m by adding diborane to the methane and hydrogen source gases supplied to a microwave CVD reactor. The samples were polished on both the nucleation and growth sides to a mirror finish. The final BDD electrodes had a thickness of about 500 μ m. The electrodes were supplied as 5 x 5mm square plates. The resulting samples had a bulk electrical resistance of about 0.75 Ω m. The average solid-state boron concentration of this material was reported by the manufacturer to be about 5 x

10^{20}cm^{-3} as determined by secondary ion mass spectroscopy (SIMS). Prior to use, samples were cleaned in 3:1 (v/v) concentrated $\text{H}_2\text{SO}_4/\text{H}_2\text{O}_2$ (30%) for 15min, rinsed copiously with Milli-Q water, and then slightly polished using diamond paste ($0.3\mu\text{m}$) to obtain a smooth particle-free surface. Experiments were carried out on different samples with similar results.

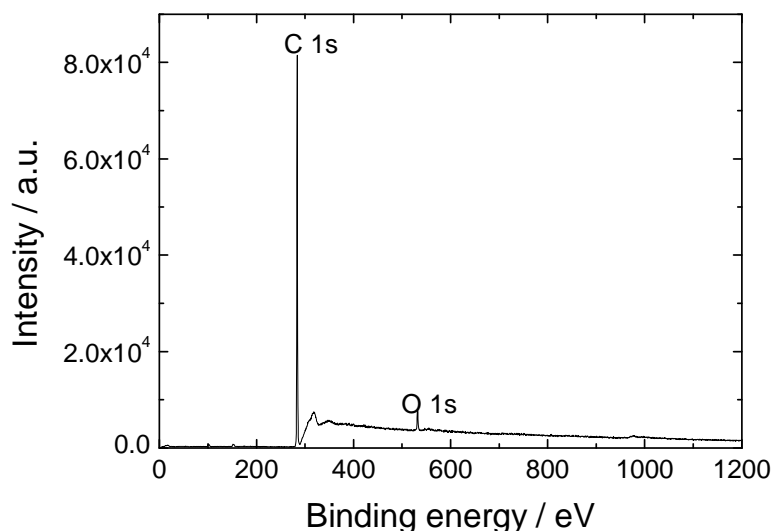


Figure 2.2. X-ray photoelectron spectroscopy (XPS) survey of a hydrogen-terminated boron-doped diamond surface.

Figure 2.3 shows a typical topographic tapping-mode AFM image of an oxidized polished BDD interface. The high quality of the polishing is demonstrated by the low root-mean-square roughness of approximately 1 nm. Nevertheless, it is still possible to differentiate some surface features in the topographic image. From the AFM image, some grain boundaries can be distinguished. A reason that the AFM image displays these features could be that different surface facets polish at different rates; therefore, there are small height differences on the sample. Finally, the particle observed in the lower part of the AFM image in **Figure 2.3** corresponds to an impurity on the surface. Indeed, it was observed that the oxygen-terminated BDD electrode readily adsorbed impurities onto its surface, most likely because of its hydrophilic character.

Hydrogenation of the surface of these samples was performed in an Ultra High Vacuum UHV CVD chamber using the hot-filament chemical vapor deposition mode (HF CVD) elsewhere described [7]. The conditions were the followings: 100sccm H_2 for 10 minutes, $P = 15\text{mbar}$ with tungsten filaments (two pairs of tungsten filaments placed 5mm and 10mm above the substrate, respectively) at 180W (around 2450K). The surface of the substrate was

heated on the rear side by an infrared heater in order to keep a constant temperature of 973K. Following this treatment the sample was cooled to room temperature with hydrogen.

2.3.3. Hydrogen-terminated porous silicon substrates

Double-side polished Si(100) oriented p-type silicon wafers (boron-doped, 1-15 Ω -cm resistivity) were first cleaned in 3:1 concentrated H₂SO₄/30% H₂O₂ for 20min at 80°C and then sonicated in Milli-Q water for 10 min. The clean wafers were immersed in 50% HF aqueous solution for 1 min at room temperature to remove the native oxide. The hydrogen-terminated surfaces were electrochemically etched in a 1:1 (v/v) solution of pure ethanol and 50% HF for 5 min at a current density of 10mA/cm². After etching, the samples were rinsed with pure ethanol and were dried under a stream of dry nitrogen prior to use [8].

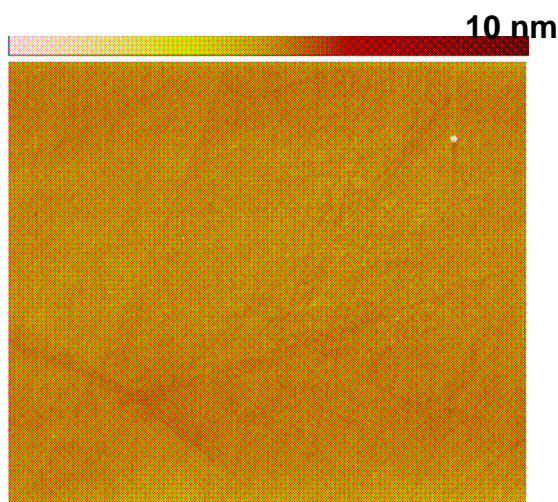


Figure 2.3. Tapping-mode AFM image of an oxygen-terminated polished polycrystalline BDD surface (scan size: 14 μ m \times 14 μ m) [6].

2.4. Functionalization of the substrates

The cleaning procedure is an essential step to start with a very clean substrate. Impurities at the surface would result in inhomogeneous immobilization of recognition molecules and insufficient reproducibility.

The standard cleaning methods of a hydrogen terminated boron-doped diamond surface is, in general, sonication in isopropanol and water for 5minutes each (2times) and blow-drying with nitrogen. Whereas, for the cleaning of functionalized boron-doped diamond surface consists on stirring the substrate in a proper solvent on the orbital platform shaker, and if necessary, an additional sonication step for 2min is used.

All the experiments were performed in a clean room.

2.4.1. Functionalization of oxygen-terminated boron-doped diamond

2.4.1.1. Oxidation of hydrogen-terminated boron-doped diamond

2.4.1.1.1. Electrochemical oxidation

Galvanostatic conditions were used to electrochemically oxidize hydrogen-terminated BDD in H₂SO₄ (0.5M). The electrochemical conditions used were: $j = 0.1 \text{ mA cm}^{-2}$, $t = 40 \text{ min}$.

2.4.1.1.2. Photochemical Oxidation

A low pressure mercury arc lamp (UVO cleaner, Nr. 42-220, Jelight, USA) was used to photochemically oxidize BDD samples in the presence of O₂ and H₂O. Light power is 1.6mW/cm².

2.4.1.1.3. Oxygen-plasma

The hydrogenated BDD samples were oxidized with oxygen plasma for 1.5 min using a Plasmalab 80 Plus (Oxford Instruments) instrument using the following conditions: oxygen flow: 20sccm; power: 100W; gas pressure: 100mT.

2.4.1.2. Modification of three kinds of oxygen terminated boron-doped diamond

2.4.1.2.1. Silanization

The oxidized diamond surfaces were silanized in a solution of 3% 3-aminopropyltriethoxysilane (APTES) in methanol/water: 95/5 (v:v) for 30min under sonication. The resulting surfaces were then washed with methanol, water (two times), and methanol, then dried under a nitrogen stream and finally annealed at 110°C for 15min.

2.4.1.2.2. Esterification

The oxidized diamond surfaces were immersed in a solution of trifluoroacetic acid (CF₃COOH) (2mmol) and *N, N'*-dicyclohexylcarbodiimide (DCC) (2.2mmol) in dry DMSO (10 ml), and 4-Dimethylaminopyridine (DMAP) (45mg) was added. Reaction was kept at room temperature for 24h under nitrogen atmosphere. The resulting surfaces were washed with dichloromethane (5min, 2times), ethanol (5min, 2times) and water, and then dried under a stream of nitrogen.

2.4.1.3. Click chemistry

2.4.1.3.1. Azide termination

4-Azidobenzoic acid (2mmol), *N, N'*-Dicyclohexylcarbodiimide (2.2mmol) and 45mg of 4-Dimethylaminopyridine (DMAP) were dissolved in 20ml dry tetrahydrofuran (THF). The oxidized BDD (oxidation time is 55min, other conditions are same to **2.4.1.1.2**) was immersed in the solution and left at room temperature for 24h under a nitrogen atmosphere. The sample

was removed from the solution, washed with THF (5min, twice), dichloromethane (5min, twice), ethanol (5min, twice) and finally with water, and then dried under a nitrogen stream.

2.4.1.3.2. “Clicking” ferrocene on azide-terminated BDD surface

The azide-terminated BDD surface was immersed in 15 ml ethanol–water (1:2) solution of ethynyl ferrocene (2mM), CuSO₄·5H₂O (100μM) and sodium ascorbate (150μM) and kept for 24h at room temperature. The resulting surface was washed with ethanol and water, and dried under a stream of nitrogen.

2.4.1.3.3. “Clicking” thiophene on azide-terminated BDD surface

The azide-terminated BDD surface was immersed in 15ml ethanol/water (v/v=1/2) solution of ethynyl thiophene (5mM), CuSO₄·5H₂O (100μM) and sodium ascorbate (150μM) and kept for 24h at room temperature. The resulting surface was washed with ethanol and water, and dried under a stream of nitrogen.

2.4.1.3.4. “Clicking” cyclophane on azide-terminated BDD surface

The azide-terminated BDD surface was immersed in a solution of **6** (0.05g, 0.04mmol) in DMF (10mL) at room temperature. Then CuI (0.8mg, 0.004mmol, 10mol %) was added. The solution was kept for 48h in the dark in a glove box and the solvent was carefully removed under high vacuum. DMF was added to remove unreacted starting materials. The resulting surfaces were washed with THF and dried under a stream of nitrogen.

2.4.1.4 Esterification between hydroxyl groups of oxygenated boron doped diamond (HO-BDD) and ionic liquid (IL)

Ionic liquid (IL):1-(Methylcarboxylacid)-3-octylimidazolium-bis (trifluoromethyl sulfonyl) imide) (2mmol) and *N, N'*-Decyclohexylcarbodiimide (DCC) (2.2 mmol) were dissolved in dry DMSO (10 ml) as well as 4-Dimethylaminopyridine (DMAP) (45mg). Oxidized boron doped diamond (oxidation time is 55min, other conditions are same to **2.4.1.1.2**) was immersed in the solution and left at room temperature for 24 h under nitrogen atmosphere.

The samples were washed with dichloromethane (5 min, 2 times), ethanol (5 min, 2 times) and water, and then dried under a stream of nitrogen.

To verify for unspecific absorption of the IL, the same experiment was carried out without the addition of DCC and DMAP.

2.4.1.4.1 Anion exchange reactions

1-(Methylcarboxylacid)-3-octylimidazolium-bis(trifluoromethyl sulfonyl) imide) modified BDD surfaces were kept in 200mM solution of NaBF₄ in water with constant shaking. After 48hours, samples were washed thoroughly with copious amount of water and dried under nitrogen stream.

The resulting surfaces were exchanged back by immersing in a solution of $C_2F_6LiNO_4S_2$ in water (200mM) with constant shaking. 48hours, then samples were washed as above. And another three times were repeated alternatively by same way. 1-(Methylcarboxylic acid)-3-octylimidazolium-bis (trifluoromethyl sulfonyl) imide modified BDD surfaces were also exchanged with other anions, such as NO_3^- and PF_6^- . Samples were kept in 200mM solution of $NaNO_3$ and $NaPF_6$ in water 48hours respectively, and then washed as above.

2.4.2. Halogenation of hydrogen terminated boron-doped diamond

Cleaned H-BDD was immersed in flask with a solution of benzoyl peroxide (0.1mmol) (benzoyl peroxide was employed as a radical initiator) and either N-bromosuccinimide (NBS, 2mmol) or N-chlorosuccinimide (NCS, 2mmol) in 20mL anhydrous CCl_4 , which had been fully degazed with N_2 for 20minutes. The resulting mixture was heated to $80^\circ C$ to activate the radical initiator, and then kept for 3hours under nitrogen atmosphere using standard preparative Schlenk-line procedures. The samples were subsequently washed with CCl_4 (2min, 2times), ethanol (2min, 2times) and deionized water (2min, 2times) under agitation and dried under a nitrogen stream.

2.4.2.1. Reaction halogenated boron-doped diamond surfaces with Grignard reagents

The chemical reactivity of the halogenated boron-doped diamond surfaces (Br-BDD) was further investigated by exposing the brominated boron-doped diamond surface to a Grignard reagent. A similar strategy has been reported for the alkylation of chlorinated diamond [9] and Si surfaces [10]. The Br-BDD was immersed in an anhydrous THF (20ml) and 10ml of 1M $C_{10}H_{21}MgBr$ in diethyl ether. The mixture was heated under reflux for 72h in a constant temperature bath set at $80^\circ C$ under a nitrogen stream using standard preparative Schlenkline procedures. The resulting surface was rinsed at room temperature with 1% CF_3COOH solution in THF (2min, 2times), deionized water (2min, 2times) under agitation, and sonicated in methanol (2min, 2times) and dried under a stream of nitrogen.

2.4.2.2. Reaction of the brominated boron-doped diamond (Br-BDD) with sodium azide

Brominated boron-doped diamond (Br-BDD) and a saturated solution of NaN_3 in 20mL anhydrous dimethylformamide (DMF) were placed into a flask under N_2 atmosphere using standard preparative Schlenk-line procedures. This solution was kept at $80^\circ C$ over night. The sample was removed from the solution, copiously rinsed with anhydrous DMF (2min, 2times), deionized water (2min, 2times) under agitation, followed by drying under a nitrogen stream.

2.4.2.3. Azide-alkyne Huisgen cycloaddition reaction between ethynyl ferrocene and azide-terminated boron-doped diamond (N₃-BDD)

The “click” reaction between the azide-terminated boron-doped diamond (N₃-BDD) surface with ethynyl ferrocene was carried out in ethanol/water (5mL/10mL) solution containing 5mM of ethynyl ferrocene, 150μM of sodium ascorbate and 100μM of CuSO₄·5H₂O (to generate a catalytically active Cu(I) species). The reaction was run for 24h under inert atmosphere at 50 °C. The surface was removed from the reaction mixture and washed in de-ionized water and ethanol under agitation conditions (2times for 5min each) and blow-dried under nitrogen stream.

2.4.3. Functionalization of porous silicon surfaces with thiophene groups

2.4.3.1. Amine termination

The hydrogen-terminated porous silicon (PSi) surfaces were first oxidized in the following sequence: UV/ozone treatment for 40min followed by immersion in a piranha solution for 30 min. Surface amination was performed by reaction of the oxidized PSi surface with 3% aminopropyltrimethoxysilane (APTMS) in methanol/water: 95/5 (v/v) for 60 min under gentle shaking. The resulting surfaces were then washed with methanol, water (two times), and methanol and finally annealed at 120°C for 20min.

2.4.3.2. Azide termination

4-Azidobenzoic acid (2mmol) and *N, N*-Decyclohexylcarbodiimide (2.2mmol) were dissolved in dry DMSO (10ml). The aminated PSi surface was immersed in the solution and left at room temperature for 24 h under nitrogen atmosphere. The sample was then washed with dichloromethane (5min, 2times), ethanol (5min, 2times) and finally with water, and dried under a stream of nitrogen.

2.4.3.3. “Clicking” thiophene on azide-terminated PSi surface

The azide-terminated PSi surface was immersed in 15ml ethanol/water (1/2: v/v) solution of ethynyl thiophene (5mM), CuSO₄·5H₂O (100μM) and sodium ascorbate (150μM) and kept for 24 h at room temperature. The resulting surface was washed with ethanol and water, and dried under a stream of nitrogen.

2.4.3.4. Polymerization of the surface linked thiophene units

Galvanostatic electrochemical polymerization of the thiophene-modified PSi was performed in dry CH₃CN/0.1M Bu₄NBF₄ solutions with and without addition of 0.1M thiophene by applying a constant current of 1 mA cm⁻² for 40 min. The resulting

polythiophene films were characterized using cyclic voltammetry in $\text{CH}_3\text{CN}/0.1\text{M Bu}_4\text{NBF}_4$ at 20mVs^{-1} .

2.5. Surface characterization

2.5.1. Contact angle measurements

We used a remote-computer controlled goniometer system (DIGIDROP by GBX, France) for measuring the contact angles. Contact angles were measured from sessile drops by lowering a $1\mu\text{L}$ drop suspended from a fine, blunt syringe needle onto the surface, using an optical subsystem to capture the profile of a pure liquid on a solid substrate (**Figure 2.4A**). Both sides of the drop were measured (**Figure 2.4B**). This was repeated three times and averaged to obtain contact angle for the surface. The accuracy is $\pm 2^\circ$. All measurements were made under ambient atmosphere at room temperature, and the water used for contact angles measurement was deionized and filtered through a Millipore-Q system.

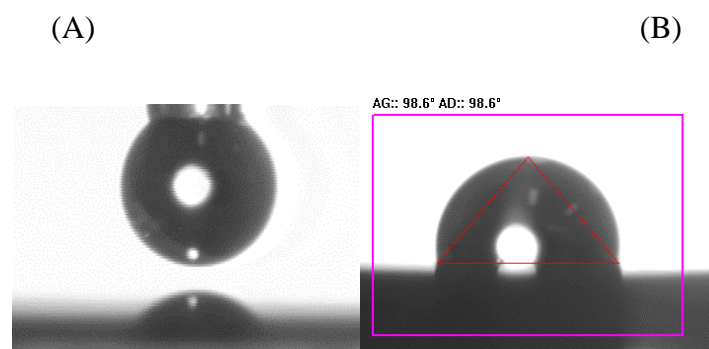


Figure 2.4. Lower a drop on a solid substrate (A) and measure contact angle (B)

2.5.2. X-ray photoelectron spectroscopy (XPS)

Before transfer to the XPS analyzer, the samples were rinsed in deionized water for 30s, and then handled under a water drop protection before dried under an argon steam. XPS measurements were carried out on a VG 220i XL system, with a base pressure of 5×10^{-10} torr and using the $\text{AlK}\alpha$ (1486.5eV) X-ray monochromatized radiation with a pass energy of 20 or 8eV (resolution 0.2eV). Energy levels of XPS were calibrated with Au single crystal. The spectra were processed using the VG Eclipse Data system.

2.5.3. Electrochemistry

All electrochemical experiments were performed using an Autolab potentiostat 30 (Eco Chemie, Utrecht, The Netherlands). The sample was mounted in a PTFE holder with a copper contact. Electrochemical experiments were performed using a classical three-electrode device with a platinum wire was used as counter electrode and BDD as working electrode.

2.5.3.1. Electrochemistry conditions used in Chapter.3

Capacitance-voltage ($C-V$) measurements have been carried out in H_2SO_4 (0.5M) using a Fabelle-CNRS potentiostat, and a lock-in amplifier (EG and G5208). The frequency was set at 1107Hz. Cyclic voltammetry ($I-V$) measurements were performed with two redox couples: $Ce^{4+/3+}$ (10mM) and $[Fe(CN)_6]^{3-/4-}$ (10mM) in 0.5M H_2SO_4 . A mercury sulfate electrode (MSE, $E^\circ = 0.4$ vs. SCE) was used as reference.

2.5.3.2. Electrochemistry conditions used in Chapter.4

Measurement for azide terminated BDD was exploited in an aqueous solution of $Fe(CN)_6^{4-}$ (10 mM) and KCl (0.1M) in dry acetonitrile, ferrocene terminated BDD was studied in an electrolyte solution (0.1M) prepared from tetraethyl ammonium hexafluorophosphate ($TEAPF_6$) and dry DMF, while investigation for cyclophane terminated BDD was in dry acetonitrile (0.1 M Bu_4NPF_6). Electrochemical thiophene polymerization was carried out in an acetonitrile/ 0.1 M $LiClO_4$ electrolyte solution with or without the presence of thiophene monomer (0.2 M) by sweeping the potential between -0.2 V and +2.0 V vs. Ag/AgCl at a scan rate of 100 mV s^{-1} .

An Ag/AgCl reference electrode was used. The solution was purged with nitrogen prior to recording the electrochemical data, and all measurements were recorded under a nitrogen atmosphere.

2.5.3.3. Electrochemistry conditions used in Chapter.5

All potentials were relative to the 0.01M Ag^+/Ag system in acetonitrile (+ 0.29V vs. saturated calomel electrode). Cyclic voltammetry ($I-V$) measurements were performed in an aqueous solution of 10mM $Fe(CN)_6^{4-}$ in 0.1M KCl. Electroactive windows of BDD electrodes were checked in KCl (0.1M) water solution before and after functionalization.

2.5.3.4. Electrochemistry conditions used in Chapter.6

We studied the electrochemical properties of the halogenated BDD surfaces using $[Fe(CN)_6]^{3-/4-}$ as the redox couple in solution. $I-E$ curves recorded on H-BDD, Br-BDD and Cl-BDD electrodes were studied in an aqueous solution of 10mM $Fe(CN)_6^{4-}$, 0.1M KCl in deionized water. Electroactive windows of BDD electrodes were checked in KCl (0.1M) water solution before and after halogenation. Electrochemical properties of ferrocene terminated BDD were investigated in a solution of 0.1M tetraethyl ammonium

hexafluorophosphate (TEAPF₆) in DMF. An Ag/AgCl reference electrode was used.

2.5.4. Scanning electron microscopy (SEM) imaging

SEM images were obtained using an electron microscope ULTRA 55 (Zeiss, France) equipped with a thermal field emission emitter and three different detectors (EsB detector with filter grid, high efficiency In-lens SE detector, Everhart-Thornley secondary electron detector).

2.5.5. Atomic force microscopy (AFM) imaging

The samples were imaged with a Dimension 3100 model AFM (Veeco, Santa Barbara, CA) equipped with a Nanoscope IV controller (Digital Instruments) with a C-AFM apparatus. Platinum/iridium cantilevers (CONTPt-20 tapping mode point probe, Nanoworld) with force constants of $\sim 0.2 \text{ N m}^{-1}$ and resonant frequencies of $\sim 13 \text{ kHz}$ were used (tapping mode). A bias voltage was applied to the sample from the AFM controller, and the tip was at virtual ground. Current voltage curves were recorded using a separate DAQ card (DT 306, Data Translations) and software. No current-limiting resistor was added to the circuit.

2.6. References

1. G. Cooke.; P. Woisel.; M. Bria.; F. Delattre.; J. F.Garety; S. G.Hewage; G. Rabani; G. M. Rosair *Org. Lett.* **2006**, 8, 1423-1426.
2. P. L. Anelli; P. R Ashton.; R. Ballardini; V. Balzani; M. Delgado; M. T. Gandolfi; T. T. Goodnow; A. E. Kaifer; D. Philp; M. Pietraszkiewicz; L. Prodi; M. V. Reddington; M. V. Slawin; A. M. Z. Spencer; J. F. Stoddart; C. Vicent; D. J. Williams. *J. Am. Chem. Soc.* **1992**, 114, 193-218.
3. M. Asakawa; W. Dehaen; G. L'Abbe; S. Menzer; J. Nouwen; F. M.Raymo; J. F.Stoddart; D. J.Williams. *J. Org. Chem.* **1996**, 61, 9591-9595.
4. M. Mermoux; L. Fayette; B. Marcus; N. Rosman; L. Abello ; G. Lucazeau. *Diam. Relat. Mater.* **1995**, 4, 745.
5. R. Boukherroub; X. Wallart; S. Szunerits; B. Marcus; P. Bouvier; M. Mermoux, *Electrochem. Commun.* **2005**, 7, 937.
6. S. Szunerits; M. Mermoux; A. Crisci; B. Marcus; P. Bouvier; D. Delabouglise; J.-P. Petit; S. Janel; R. Boukherroub; L. Tay. *J. Phys. Chem. B* **2006**, 110, 23888-23897.
7. J. C. Arnault; L. Demuynck; C. Speisser ; F. Le Normand. *Eur. Phys. J. B.* **1999**, 11, 327-343.

8. R. Boukherroub; S. Szunerits. *Book title: Electrochemistry at the Nanoscale by Patrik Schmuki and Sannakaisa Virtanen (Editors). Springer-Verlag New York. 2008, Series: Nanostructure Science and Technology Series.183-248.*
9. Y. Ikeda; T. Saito; K. Kusakabe; S. Morooka; H. Maeda; Y. Taniguchi; Y. Fujiwara. *Diam. Relat. Mater. 1998, 7, 830.*
10. A. Bansal; X. Li; I. Lauermaun; N. S. Lewis. *J. Am. Chem. Soc. 1996, 118, 7225.*

CHAPTER 3

OXIDATION OF HYDROGEN TERMINATED BORON DOPED DIAMOND ELECTRODES

3.1. Introduction

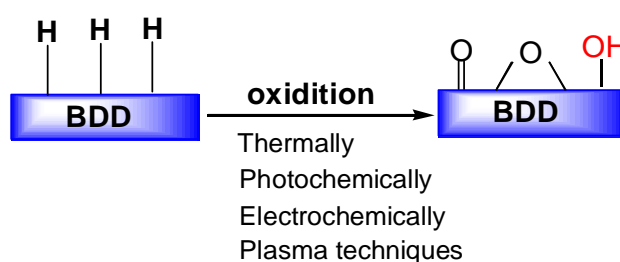
For a long time, the surface of diamond was considered as chemically inert to most reagents, posing difficulties to its chemical functionalization. The last fifteen years, however, have seen a substantial progress in the development of specific chemical, photochemical and electrochemical surface modification methods for the introduction of different functional groups [1]. This was facilitated by protocols that oxidize a diamond surface to obtain an OH-termination without forming graphite and losing the superior properties of diamond. As the simplest and most effective surface structure modification, surface oxidation treatment makes great interest since the resulting oxidized surface is highly stable and can be recovered only by hydrogen plasma treatment at elevated temperatures [1]. Furthermore, the presence of oxygen on the diamond surface has a significant influence on the chemical reactivity [2, 3], electrical conductivity [4, 5], field emission [6, 7] and Schottky barrier heights [8].

Various conditions for the oxidation reaction of hydrogen-terminated diamond surface were reported in the literature including thermal [9-11], plasma [8, 12], electrochemical techniques [14, 15], singlet oxygen [16] and ozone treatment [13, 14, 16] (**Scheme 3.1**). There is only one report using photochemical conditions for surface oxidation [14]. It consists on the irradiation of hydrogen-terminated polycrystalline diamond with vacuum ultraviolet light (VUV) at $\lambda = 172\text{nm}$ for 3h in the presence of O_2 and H_2O . The generated surface hydroxyl groups were coupled with p-aminophenyltrimethoxysilane to yield an organic layer terminated with amino groups.

It was demonstrated that the chemical composition of the oxidized diamond depends strongly on the method used for surface oxidation of the initial hydrogen-terminated diamond surface. For example, thermal oxidation of hydrogen-terminated diamond under various conditions showed a surface composition dominated by ether (C-O-C) and carbonyl (C=O) groups. On the other hand, electrochemical anodization or plasma treatment of diamond

surface generates surface termination composed of ether (C-O-C), carbonyl (C=O), and hydroxyl (OH) groups. The presence of the surface hydroxyl species was demonstrated by further coupling of the oxidized surface with alkyltrichlorosilanes [21] and biotinylated esters [22].

Recently, our group has reported on the photochemical oxidation of hydrogen-terminated boron-doped diamond (BDD) surfaces in ambient air using a low pressure mercury arc lamp [14]. The Technique is easy to carry out and offers the possibility for surface chemical patterning [23]. The resulting surface was characterized using X-ray photoelectron spectroscopy (XPS) and cyclic voltammetry. XPS analysis suggested the presence of ether (C-O-C), carbonyl (C=O), and hydroxyl (OH) groups. The oxidized surface served as a starting point for the preparation of biomolecular interfaces with high stability and excellent biomolecular recognition properties [23, 24]. Furthermore, the formation of self-assembled monolayers (SAM) is possible similarly to the well-known procedures on oxide surfaces [14, 25, 26].



Scheme 3.1. Schematic illustration of the oxidation reaction of hydrogen-terminated boron-doped diamond surface using different means.

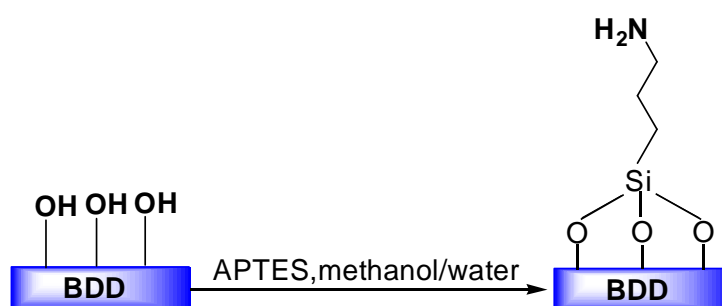
No real attempt has been made in the literature until now to compare different oxidative approaches adequately. The formation of hydroxyl groups is for the most part desired, as well known chemical routes can be used to link functional groups to -OH units. However, the different oxidative methods proposed give no recommendation in terms of the amount of hydroxyl groups formed on the surface.

3.2. Objectives

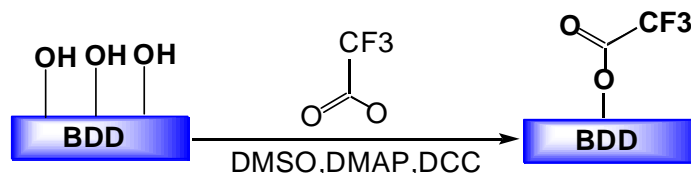
This chapter is to compare the surface properties and give qualitative and quantitative information about the different surface functions formed on moderately boron doped diamond interfaces oxidized using three different approaches: (i) electrochemical oxidation through anodical polarization, (ii) photochemical oxidation with a UV/ozone lamp and (iii) oxidation

using oxygen plasma.

X-ray photoelectron spectroscopy (XPS) and Mott-Schottky analysis were used to characterize the differently oxidized interfaces. In the study, assuming the existence of hydroxyl groups on oxygen terminated diamond electrode surfaces, we have sought to modify the three different interfaces chemically with a silane coupling agent-3-aminopropyltriethoxysilane (APTES) (as shown in **Scheme 3.2**) and trifluoroacetic acid (CF_3COOH) (as shown in **Scheme 3.3**) to verify the difference in terms of grafting density, which is linked to the presence of C-OH groups and not reactive with carbonyl, carboxyl, or ether groups.



Scheme 3.2. Schematic illustration of the silanization reaction of oxygen-terminated boron-doped diamond surface using APTES.

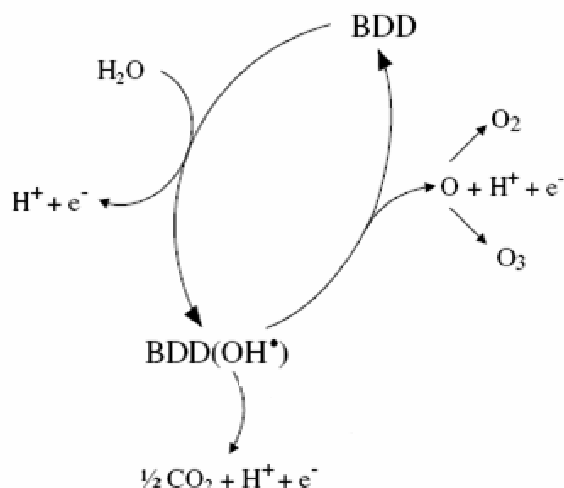


Scheme 3.3. Schematic illustration of the esterification reaction of oxygen-terminated boron-doped diamond surface using trifluoroacetic acid.

3.3. Results and discussion

3.3.1 Electrochemical Oxidation

For electrochemical oxidation in H_2SO_4 (0.5M), a model was proposed by Ch. Comninellis et al. [27] (as shown in **Scheme 3.4**)



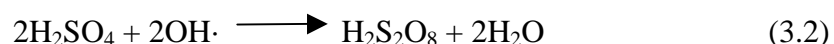
Scheme 3.4. A proposed model for electrochemical oxidation in H₂SO₄ (0.5M)

According to this model, the first step is water discharge on BDD with the formation of hydroxyl radicals (**equation 3.1**):



The electrogenerated hydroxyl radicals can be involved in three parallel reactions:

(i) Oxidation of supporting electrolyte: In the case of H₂SO₄ supporting electrolyte, electrogenerated hydroxyl radicals react with sulfuric acid giving peroxodisulfuric acid (**equation 3.2**):



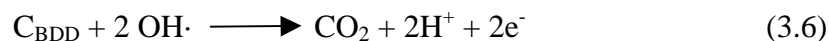
(ii) O₃ production: A further possible reaction of OH• is oxidation to atomic oxygen (**equation 3.3**) followed by formation of ozone (**equation 3.4**) or evolution of oxygen (**equation 3.5**):



A similar mechanism involving adsorbed hydroxyl radicals was proposed by Babak et al. [28] for ozone evolution on PbO₂ electrode. The fact that boron doped diamond gives a current efficiency for ozone evolution lower than PbO₂ can be explained by the different adsorption properties of BDD and PbO₂ electrode surfaces. In fact, ozone evolution is favoured by the adsorption of hydroxyl radicals on the anode surface, as occurs on the

hydrated surface of lead dioxide, while on boron-doped diamond, which is well known to have an inert surface, OH• radicals are very weakly adsorbed.

(iii) BDD corrosion: Another possible reaction pathway for the electrogenerated hydroxyl radicals is the combustion of BDD to CO₂ (**equation 3.6**) during the anodic polarisation at high current density [29].



The effect of anodic and cathodic treatments on the charge transfer rate of boron doped diamond electrodes have been shown recently by the group of Simon and Etcheberry [30-32]. They demonstrated using XPS analysis that as-deposited highly-doped (10²⁰cm⁻³) BDD electrodes contain a small amount of oxygen (4-5%), which strongly increased (20%) after mild anodic treatment in H₂SO₄. High-resolution XPS of the C1s spectral region showed that after electrochemical oxidation, next to the bulk diamond component at 284.4 eV, oxygenated carbon species appear at 3.2 to 5eV higher energies and were attributed to C=O (8%), as well as at 1.6 to 2eV higher energies linked to C-O (12%) groups. From *C-V* measurements, where a displacement of the flat band potential to more positive values was obtained, it could be concluded, that the increase in oxygen functionalities is mainly due to C-O functionalities like hydroxyl or ether groups rather than C=O groups (carbonyl or carboxylic) [32].

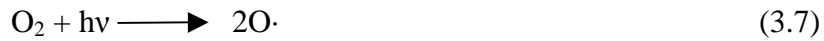
Previous works have shown that moderately doped electrodes are the most affected by the elimination of hydrogen and thus the removing of the C-H superficial conductive layer [33] which is a crucial point for BDD physicochemical properties. However, the use of electrochemical oxidative methods is limited to the use moderately to highly doped diamond interfaces. A more general approach for the oxidation of diamond is based on photochemical or plasma based techniques. Both techniques are interesting as they allow the patterning of diamond interfaces as demonstrated by us and others [24, 34-35]. The present work investigates quantitatively and qualitatively the formed surface functions using photochemical and oxygen plasma oxidation and compares it with the electrochemical technique. The focus will be mainly on the formation of hydroxyl groups for the use in further chemical approaches

3.3.2 Investigation of photochemical oxidized diamond

Principle of UV/ozone has been depicted in appendix. According to it, we can deduced that after hydrogen terminated boron doped diamond electrodes were placed on the sample stage, some reactions in reaction chamber for the formation of hydroxyl terminated BDD were carried out as follows (**equation 3.7-3.11**):

3.3.2.1 Contact angle measurements

Among the macroscopic surface parameters which can be sensitive to surface chemistry, wettability is particular interesting. The nature of diamond surface termination can be revealed by its hydrophobic or hydrophilic character. Hydrogen-terminated diamond is hydrophobic with a contact angle $91\pm 2^\circ$ (**Figure 3.1**); while oxygen-terminated diamond is know to be hydrophilic. The formation of oxygen functionalities on H-BDD can be thus revealed by a modification of the surface wettability. **Figure 3.1** shows the change in water contact angle when moderately doped H-BDD was photochemical oxidized with a UV/ozone lamp with a power output of $P=1.6\text{mW cm}^{-2}$. The first 15minutes show a progressive decrease of the water contact angle θ and points towards an evolution of the surface properties of H-BDD. Thereafter, water contact angle remains almost constant at $32\pm 3^\circ$ for the next 10 minutes, before it decreases further to a contact angle of $6\pm 2^\circ$. The evolution of the surface's wettability is generally linked to a change in either the chemical or morphological properties. In general, it is claimed that the contact angles are greater on rough surfaces than on smooth surfaces [36, 37].



To exclude any morphological changes, SEM measurements were performed on BDD before and after photochemical oxidation. **Figure 3.2** shows that photochemical oxidation for 55 min have no significant effect on the surface morphology of diamond, both the two types of BDD surfaces have complete crystal grains and clear grain boundaries.

Atomic force microscopy (AFM) images represented in **Figure 3.3** directly provide the surface morphology, which qualitatively show the stability in surface roughness with photochemical oxidation for 5min, 10min, 15min, and 55min in agreement with *in situ* SEM measurements.

In order to overcome the coincidence caused by small scan size, more detailed roughness characterization was performed, as shown in **Table 3.1**, the data for the root-mean-square (Rms) roughness as well as average roughness (Ra) depend significantly on the scanning

range and the surface features. Oxygen terminated electrode surface roughness is a little larger than the hydrogen terminated one, which could be attributed to the action of etching non-diamond phase at the grain boundaries. As a whole, there is little variation in morphologies of the different surfaces, under same scan size, both of Rms and Ra are stable, especially while AFM scan size is $5\mu\text{m}$. Consequently, the wettability evolution can be only attributed to a chemical evolution of the surface.

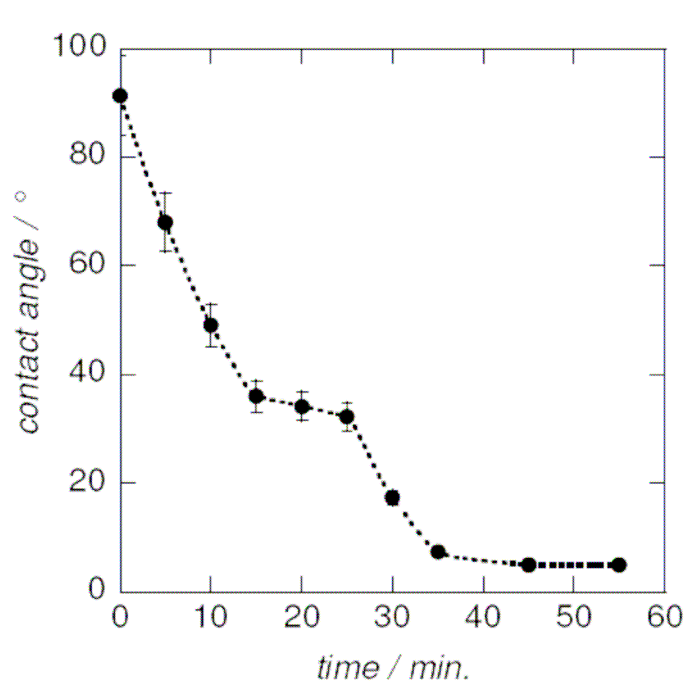


Figure 3.1. Change of water contact angle on BDD surface as a function of successive photochemical oxidation with a UV/ozone lamp at 1.6 mW cm^{-2} .

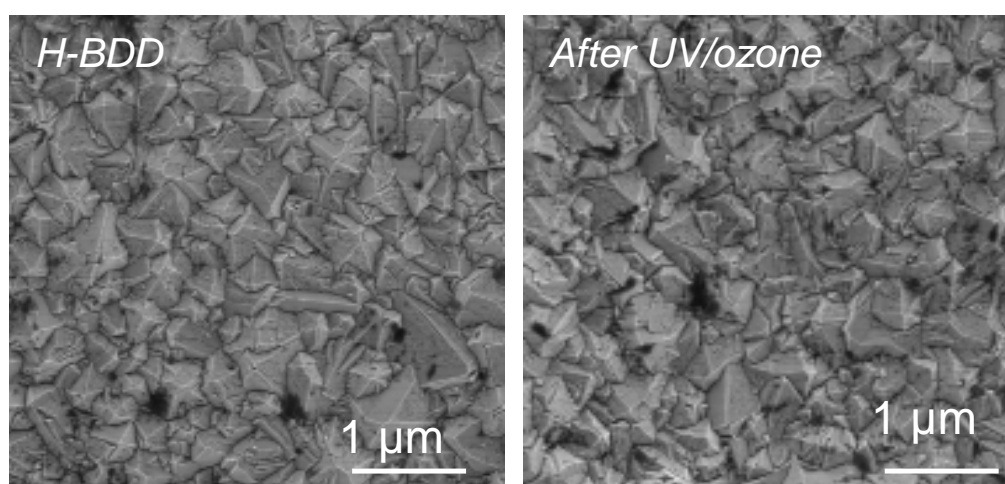


Figure 3.2. SEM images of H-BDD and after 55 min oxidation with UV/ozone.

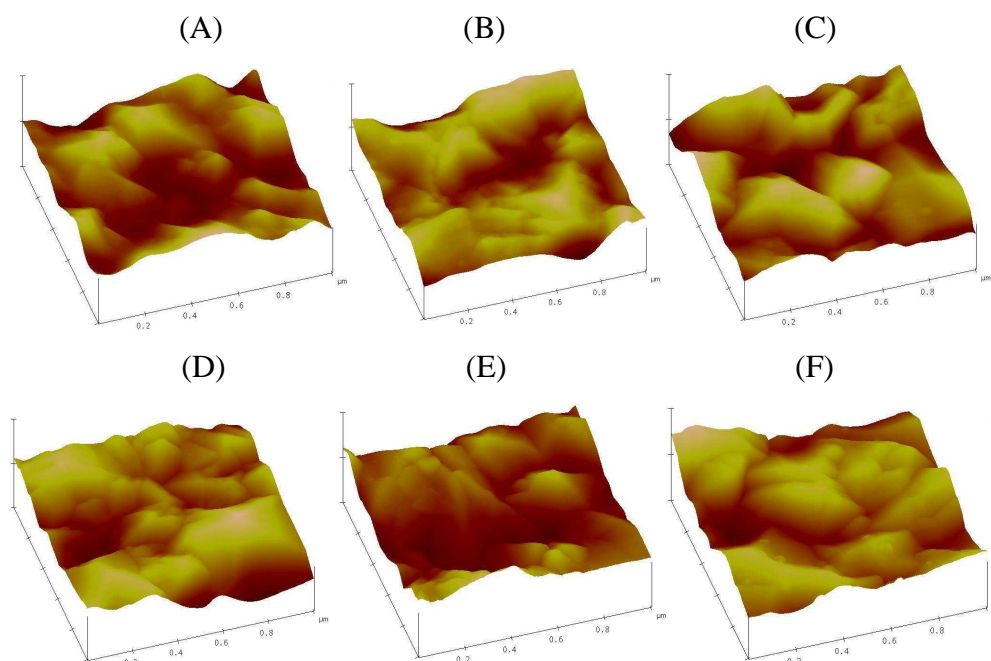


Figure 3.3. AFM images characterizing the surface roughness and morphology. Z-axis is 250nm/div, X-axis and Y-axis both are 0.2 μ m/div. (A) H-BDD (B)HO-BDD after photochemical oxidation 5min (C) HO-BDD after photochemical oxidation 10min(D) HO-BDD after photochemical oxidation 15min (E) HO-BDD after photochemical oxidation 55min (F) HO-BDD after plasma oxidation 1.5min.

Table 3.1. Characterization of surface roughness, AFM scan size in brackets.

<i>sample</i>	<i>Rms(Rq)(nm)</i>	<i>Ra(nm)</i>
H-BDD	27.548(1 μ m)	22.482(1 μ m)
	40.239(2 μ m)	31.542(2 μ m)
	62.919(5 μ m)	50.556(5 μ m)
O-BDD-5	27.553(1 μ m)	22.061(1 μ m)
	43.900(2 μ m)	35.342(2 μ m)
	64.528(5 μ m)	52.290(5 μ m)
O-BDD-10	32.669(1 μ m)	26.621(1 μ m)
	50.794(2 μ m)	39.286(2 μ m)
	61.128(5 μ m)	49.456(5 μ m)
O-BDD-15	35.702(1 μ m)	28.323(1 μ m)
	47.492(2 μ m)	39.964(2 μ m)
	58.889(5 μ m)	48.599(5 μ m)
O-BDD-55	38.121(1 μ m)	30.924(1 μ m)
	46.784(2 μ m)	37.998(2 μ m)
	58.630(5 μ m)	48.40(5 μ m)
O-BDD-plasma	40.293(1 μ m)	32.082(1 μ m)
	45.144(1 μ m)	35.926(1 μ m)
	61.022(1 μ m)	49.809(1 μ m)

3.3.2.2 Electrochemical Characterization

The electrochemical window of a substrate is the voltage range between which the substrate doesn't get oxidized nor reduced. This range is important for the efficiency of an electrode, out of this range, water gets electrolysed, spoiling the electrical energy that is intended for another electrochemical reaction. **Figure 3.4** shows electroactive windows of H-BDD and photochemical oxidized 55min oxygenated BDD. There is an obvious change after photochemical oxidation, oxygenated BDD has wider electroactive window, which is in agreement with the results published by A. Fujishima et.al. [38].

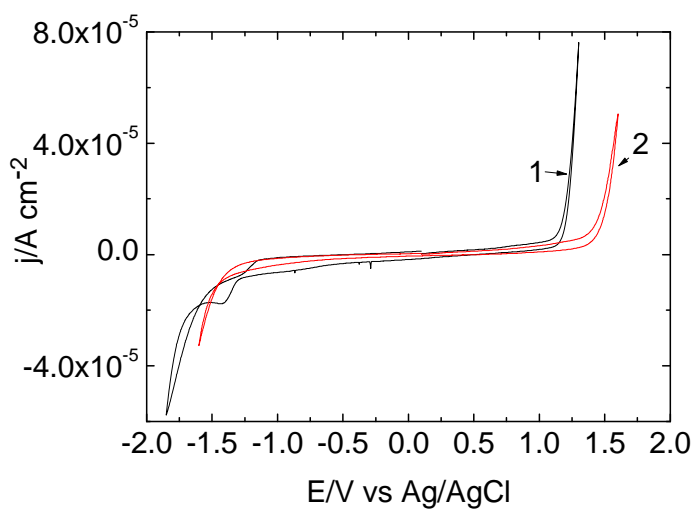


Figure 3.4. Cyclic voltammograms of BDD electrodes in an aqueous solution of KCl (0.1 M): H-BDD (curve 1), UV/ozone treatment for 55 min oxidised-BDD (curve 2); scan rate: 50 mV s⁻¹.

$C-V$ measurements are like contact angle measurements linked to the electrode/liquid properties. **Figure 3.5A** shows Mott-Schottky plots of H-BDD over a potential range of 1.2 V in 0.5 M H₂SO₄. The linear $C^{-2}-V$ measurements performed on H-BDD are very reproducible and indicate the apparent space charge density (N_A) and the apparent flat band potential (E_{FB}) values, which are approximately $E_{FB}=1.2\pm 0.1\text{V/MSE}$ and $N_A=(3.35\pm 2.5)\times 10^{19}\text{cm}^{-3}$. Photochemical oxidized BDD interfaces show the same Mott-Schottky behaviour as H-BDD without significant change in the slope and thus the apparent space charge density. **Figure 3.5B** shows representative Mott-Schottky plots for H-BDD and after photochemical oxidation for 15min and **Table 3.2** summarizes the determined E_{FB} and N_A after the successive oxidative treatments. As discussed by Simon et al, a positive shift in E_{FB} is characteristic to the formation of C-O functions on the surface of BDD rather than C=O [26]. Short photochemical oxidation (15min) shows anodically shifted E_{FB} and is indicative for the formation of mainly C-O. After 55min is the potential cathodically shifted and indicates the formation of other functionalities.

To complete the electrochemical characterizations, I - V curves have been also performed on the different interfaces using two different redox mediators, $Ce^{4+/3+}$ and $[Fe(CN)_6]^{3-/4-}$ (Figure 3.6).

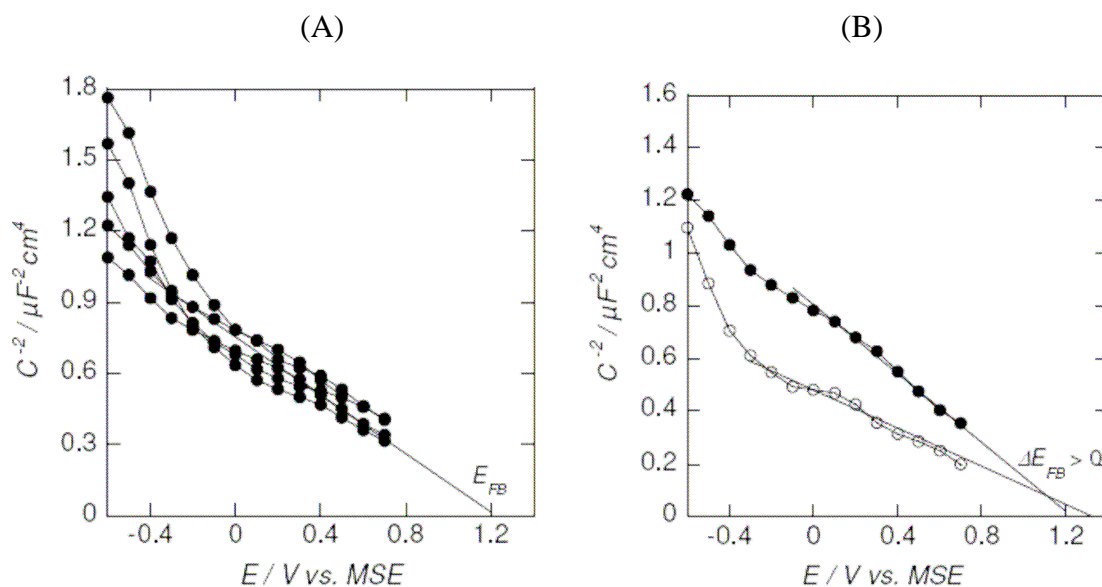


Figure 3.5. Mott-Schottky representation $C^{-2} = f(E)$ in H_2SO_4 (0.5M) at five different moderately doped H-BDD interfaces (A) and after UV/ozone treatment (\circ) of one H-BDD (\bullet) interface for 15min (B)

Table 3.2. Determined flat band potential (E_{FB}) and apparent space charge density (N_A) for H-BDD, electrochemically (O-BDD-EC), photochemically (O-BDD-x, x = 5, 10, 15, 55) and oxygen plasma oxidized BDD (O-BDD-plasma)* difficult to measure

sample	oxidation time / min	$\tilde{\theta}$	$E_{FB}/V/MSE$	$N_A/cm^{-3} \times 10^{19}$	$\Delta E_p [Ce^{4+/3+}] / V$	$\Delta E_p [Fe(CN)_6^{3-/4-}] / V$
H-BDD	-	90	1.20±0.05	3.35±2	0.67	0.60
O-BDD-EC	40	15	2.4±0.05	3.35±2	2.9*	4*
O-BDD-5	5	68	1.33±0.05	3.35±2.5	1.16	1.42
O-BDD-10	10	49	1.30±0.05	3.35±3	0.74	0.21
O-BDD-15	15	37	1.30±0.05	3.35±2	0.81	0.27
O-BDD-55	55	5	0.94±0.05	3.35±2	1.51*	1.15*
O-BDD-plasma	1.5	10	1.56±0.05	3.35±2	3.26	2.69

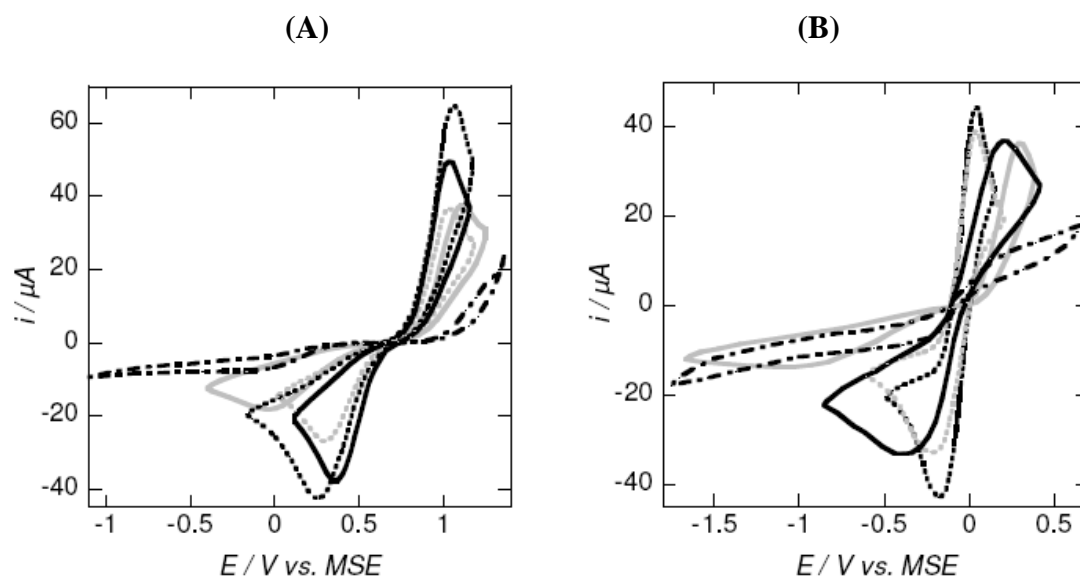


Figure 3.6. Experimental voltammetric i - V curves for as-deposited BDD (black) and photochemically oxidized diamond at different times: 5 min (grey), 10 min (grey dotted), 15min (black dotted), 55 min (black dash-dot): (A) $\text{Ce}^{4+/3+}$ (10mM) in 0.5M H_2SO_4 and (B) solution: $\text{Fe}(\text{CN})_6^{4-}$ (10mM) in KCl (0.1M)/water, scan rate = 0.1V s^{-1} , geometric area = 0.1cm^2

The $\text{Ce}^{4+/3+}$ redox couple has a high redox potential ($E^0 = 1\text{V/MSE}$) close to the anodic limit of the diamond window and is known to be a good electrochemical probe to study the consequences of the superficial layer modifications of BDD electrodes. The electron kinetics of the inner-sphere redox mediator $[\text{Fe}(\text{CN})_6]^{3-/4-}$ is highly sensitive to the diamond termination as the reaction appears to proceed through a specific surface site. In both cases, a strong decrease of the charge transfer is observed after treatment of H-BDD for 5min with UV/ozone (**Table 3.2**). After 10-15min the charge transfer kinetics is however largely enhanced. This behaviour can be linked to the elimination of C=O and/or to an amelioration of the p^+ conductivity character of the superficial C-H layer. Overall, this indicates that there are still C-H presents on the surface after 15min oxidation. After 55min has the electrochemical behaviour finally changed drastically. Completely irreversible electrochemical behaviour is observed with both mediators. This indicates that the superficial surface conductivity has completely disappeared. The low contact angle of 5° is coherent with fully oxidation of the BDD interface.

3.3.2.3 XPS analysis

To get a qualitative and quantitative idea about the formed oxygen functionalities XPS was performed on the different BDD interfaces. **Figure 3.7** shows XPS spectra of the C1s spectral region for as-grown diamond and for photochemical oxidized BDD for 55min.

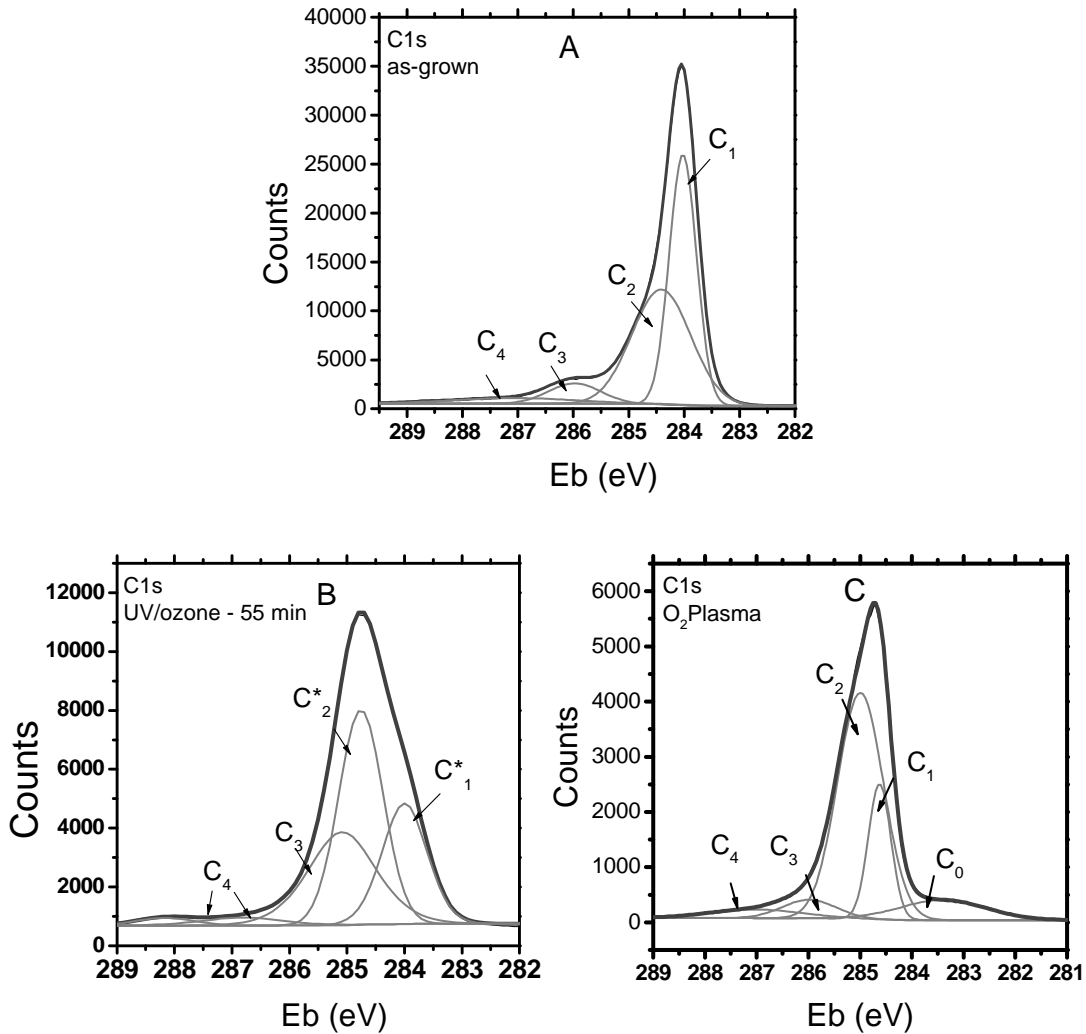


Figure 3.7. C1s XPS spectra of H-BDD before (A) after photochemical oxidation 55 min (B) and after O₂ plasma (C).

The XPS spectrum of as-grown BDD (**Figure 3.7A**) is in accordance with XPS results performed of H-terminated moderately doped microcrystalline diamond [39]. The C1s peak exhibits two main components at 283.8eV (C-1) and 284.5eV (C-2) attributed respectively to hydrogenated and non-hydrogenated diamond surface. Due to air exposure, the XPS spectrum of diamond exhibits additional components at higher energies. The peak at ~ 286eV (C-3) is assigned to hydroxyl (-OH) or ether (O-C-O) groups, while peaks at higher energy (~287 to 288eV, C-4) are attributed to carbonyl, carboxylic or ester carbon species (C=O).

Table 3.3 resumes the O/C+O atomic concentrations ratios calculated from well defined C1s and O1s core level spectra, respectively at 284.5eV and 532.5eV. The initial O/C+O ratio is 9 % for the as-grown sample. After 5min photochemical oxidation the O/(C+O) ratio has increased to 15%, with mainly an increase of the C-O contribution and keeping the C=O

content constant. The increase of C-O functions is in accordance with the anodic displacement of the flat band potential and the decrease in contact angle (**Table 3.2**).

Continuing photochemical oxidation results in a decrease of the overall oxygen content due to a decrease in the C=O surface together with a minor increased in the C-O amount and of component C-1. The increase of C-1, linked to an increase of the p^+ conductivity character of the superficial C-H layer, might be also responsible for the highly accelerated charge transfer kinetics on these surfaces (**Table 3.2**).

Table 3.3. Proportions of each C1s contributions obtained by peak fitting for H-BDD, electrochemically (O-BDD-EC), photochemically (O-BDD-x, x = 5, 10, 15, 55) and oxygen plasma oxidized BDD (O-BDD-plasma)

<i>Sample</i>	<i>C-0</i>	<i>C-1</i>	<i>C-2</i>	<i>C-3</i>	<i>C-4</i>	<i>O/(C+O)</i>
	%					
<i>H-BDD</i>	-	45	45	7	4	9
<i>O-BDD-EC</i>	-	10	71	14	5	18
<i>O-BDD-5</i>	-	64	21	10	5	14.7
<i>O-BDD-10</i>	-	56	32	11	1	10
<i>O-BDD-15</i>	-	65	21	13	1	13
<i>O-BDD-55</i>	-	23	43	29	5	23
<i>O-BDD-plasma</i>	9	18	61	6	5	12

Photochemical oxidation for 55 min results in a very different C1s spectrum, being much broader and shifted to lower energies (**Figure 3.7B**). The O/(C+O) ratio is largely increased which is coherent with the low contact angle of 5°. This indicates that the superficial hydrogenated layer is mainly destroyed as indicated by *I-V* measurements with redox couples and seen in a decrease of the C-1 component. As the atomic ratio of O/C+O (23%) is to a much smaller than the ratio $[C-3_{(C-O)}+C-4_{(C=O)}]/C_{total}$ (34 %) it can be concluded that O-C-O groups rather than C-OH groups are formed by this oxidation process. In a comparison, electrochemical oxidized diamond showed a O/C+O of 18% and a $[C-3_{(C-O)}+C-4_{(C=O)}]/C_{total}$ of 19 %, pointing towards preferential formation of C-OH over O-C-O (**Table 3.3**).

3.3.3 Investigation of oxygen plasma oxidized diamond

According to the chapter 2, formation of hydroxyl terminated BDD can be depict by **equation 3.12-3.14**. As-deposited BDD samples were oxidized with oxygen plasma for 1.5min. The water contact angle determined was 10° after this treatment. The plasma oxidized interface showed a significant change in its electrochemical behaviour.

Figure 3.8 shows Mott-Schottky and I - V plots of oxygen plasma treated BDD. The slope has significantly increased with a flat band potential positively displaced by 0.460V. This behaviour is in agreement with the formation of C-O functions. The electrochemical charge transfer rate is decreased as observed for photochemical oxidized BDD interface for 55min. XPS analysis shows however rather different characteristics. The increase of oxygen functions is rather low after oxygen plasma treatment with an O/(C+O) ratio of ~12%, much lower than after electrochemical and photochemical oxidation. In addition, a new carbon component at low energy, 283.4 (C-O) is observed (**Figure 3.7C**). This component is related to the formation of sp² carbon and indicates that oxygen plasma treatment results in partly graphitization of the surface.



3.3.4 Silanization of the three interfaces

The amount of formed hydroxyl groups on diamond is important for consecutive surface functionalization based on C-OH chemistry. The oxidized diamond interfaces were reacted with 3-aminopropyltriethoxysilane (APTES) and characterized by XPS (**Figure 3.9**).

Survey of the hydrogen terminated BDD surface showing signals due to C 1s at 285 eV and O1s at 532.6 eV, respectively. The origin of the oxygen peak is not clear. It could be assigned to surface contamination or to interstitial incorporation within the C-C backbonds during sample growth (originating from boron oxide used for doping) or to surface partial oxidation. After photochemical oxidation in air, an increase of the signal of O1s was observed, consistent with surface oxidation (**Figure 3.9b**). Additional peaks due to N1s and Si2p (absent in the oxidized BDD surface XPS survey) and a relative increase of O1s signal were observed when the oxidized BDD surface was reacted with APTES (**Figure 3.9c**). The increase of the O1s signal was not expected since the reaction of the oxidized BDD surface with APTES should take place without any oxygen incorporation according to **Scheme 3.2**.

Figure 3.10A displays the high-resolution XPS spectrum (carbon C1s peak) of the hydrogenated BDD surface. The C1s spectrum displays an asymmetric peak with a tail between 286 and 287eV, which is a good indication of the presence of C-O groups and/or amorphous carbon at the grain boundaries. After photochemical oxidation 55min, the XPS spectrum displays three signals due to C1s from the bulk and from the surface C-O features at

285, 286.4 and 288.5eV, respectively (**Figure 3.10B**). Based on the diamond structure, it is expected that the sp^3 C-H bonds on the (111) facets will be terminated with hydroxyl groups while the CH_2 groups on the (100) facets will be transformed to carbonyl and ether functional groups. The signals from the surface hydroxyl and ether groups are undistinguishable. An additional peak at 284eV due to C-Si was observed after coupling of the surface hydroxyl groups with aminopropylsilane molecules. Moreover, a net increase of the signal at 286.4eV was observed, which results most likely from C-N incorporation on the surface and is in agreement with the chemical composition of the layer (**Figure 3.10C**).

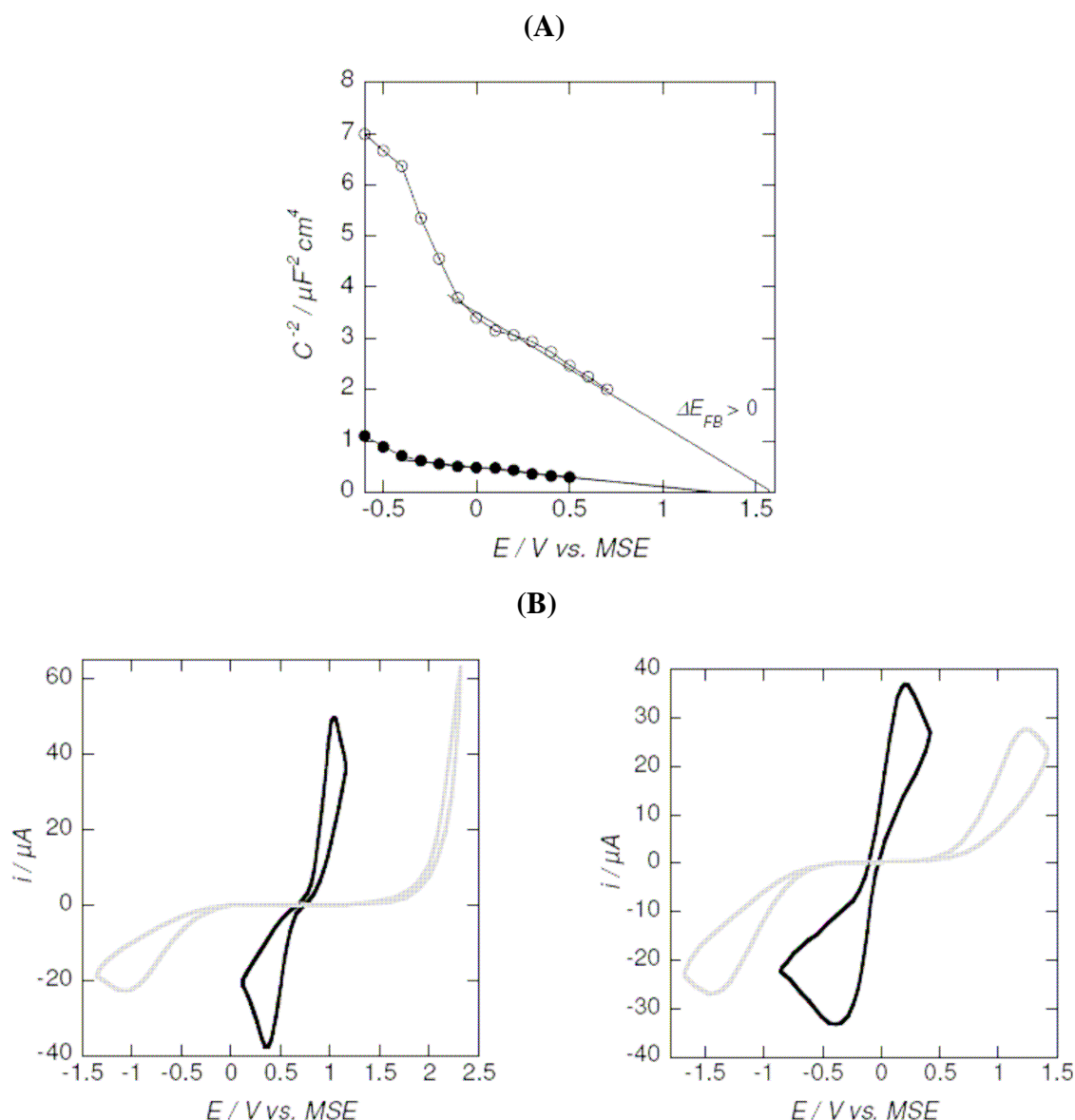


Figure 3.8. (A) Mott-Schottky representation $C^{-2} = f(E)$ in H_2SO_4 (0.5 M) at moderately doped H-BDD before (\bullet) and after oxygen plasma oxidation (\circ); (B) Experimental voltammetric i - E curves for H-BDD (black) and after oxygen plasma oxidation (grey); (B-left) $Ce^{4+/3+}$ (10 mM) in 0.5 M H_2SO_4 and (B-right) solution: $Fe(CN)_6^{4-}$ (10 mM) in KCl (0.1 M)/water, scan rate = $0.1 V s^{-1}$, geometric area = $0.1 cm^2$

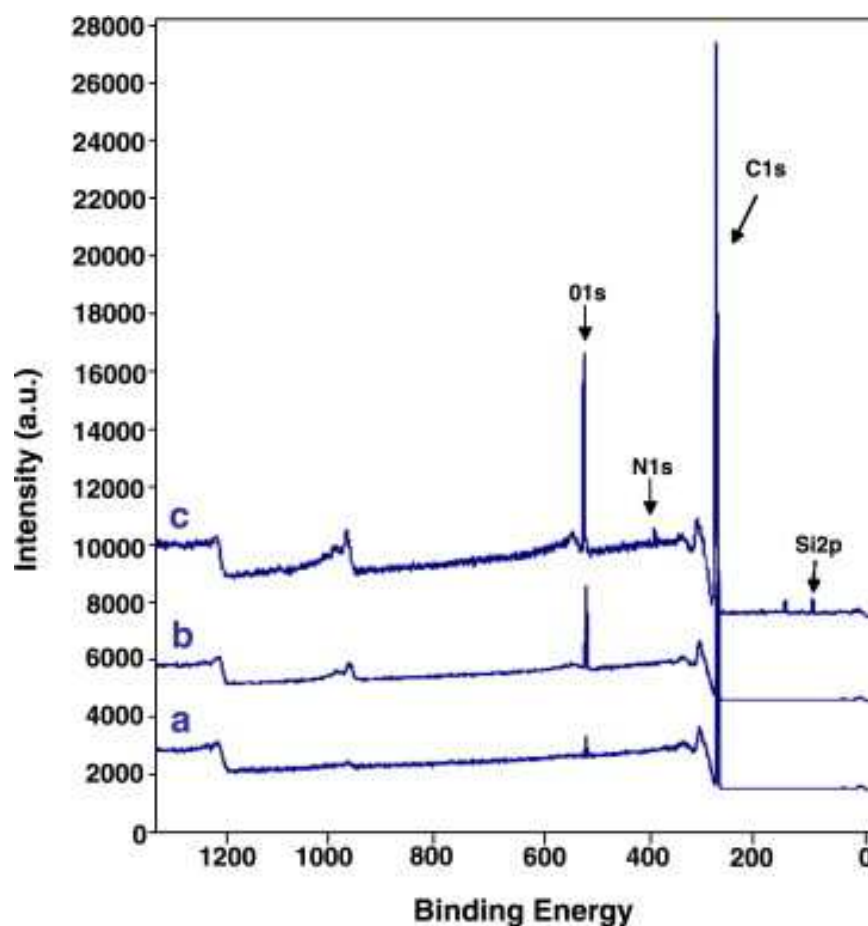


Figure 3.9. XPS survey of hydrogen-terminated boron-doped diamond surface before (a) and after photochemical oxidation 55min in air (b); surface (b) after chemical reaction with aminopropyltriethoxysilane (APTES) (c).

The O/N and Si/ N ratios are reported in **Table 3.4**. In all cases is the obtained Si/N ratio of 1.2 slightly higher than the expected ratio of 1.0 for a formed monolayer and indicates that some dimerization or even polymerization has taken place. However, the Si/N ratio is comparable on all samples. The concentrations of N measured after the silanization of the different oxidized samples are given in **Table 3.4**. As the [N] value is linked to the amount of grafted molecules on BDD surface, it could be noticed that the photochemical treatment (5min) and the electrochemical anodization give the best results, while oxygen plasma appears to be the less competent method. The increase between the lowest [N] value (2.4% for oxygen plasma) and the largest recorded (3.5% for 5min photochemical) is ~ 1.5 times.

The N/O ratio is also worthy of interest as it shows the “efficiency” of the silanization reaction. It varies from 0.18 for the anodised sample to 0.28 for the sample photochemically oxidized during 5min, indicating that the UV method is the more adapted for surface functionalization. However as the treatment time of the photochemical oxidation increases, one notices a decrease of the N/O ratio which indicates that even though the contact angle is

decreasing the amount of hydroxyl group is not improved, but rather replaces by C-O-C groups. After oxygen plasma treatment the rather low O/(C+O) ratio results in a lower N/O ratio indicating that this method is less adapted for the formation of oxygen and also hydroxyl functions. The increase between the lowest N/O ratio (oxygen plasma and electrochemical oxidised one) the largest recorded (5min photochemical) is ~ 1.5 times.

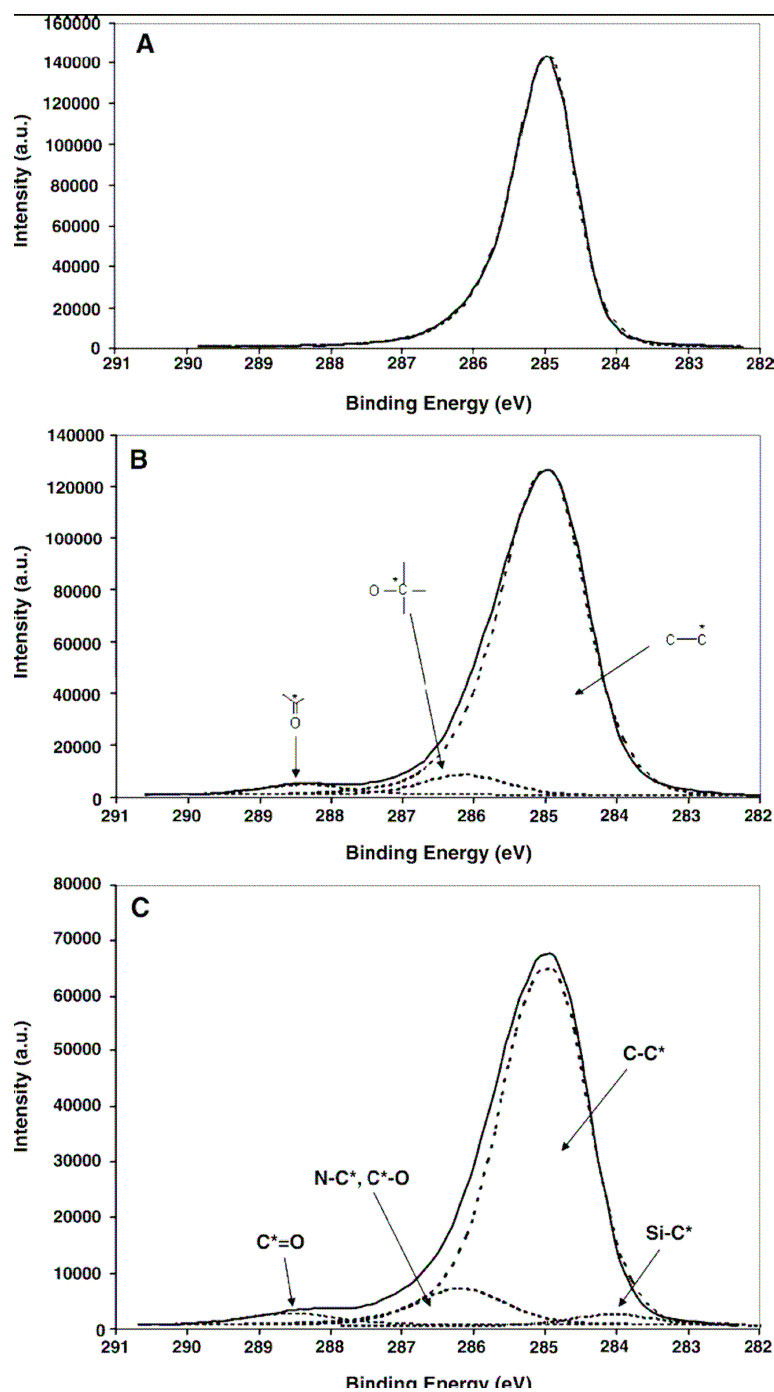


Figure 3.10. High-resolution XPS spectra of C1s of hydrogen-terminated boron-doped diamond surface before (A) and after photochemical oxidation in air (B); surface (B) after chemical reaction with aminopropyltriethoxysilane (APTES) (C).

Table 3.4. Quantitative results from XPS analysis of differently oxidized interfaces.

<i>sample</i>	$C_{1s} / \%$	$O_{1s} / \%$	$N_{1s} / \%$	$Si_{2p} / \%$	N/O	Si/N
<i>O-BDD-EC</i>	75	18	3.2	3.8	0.18	1.18
<i>O-BDD-5</i>	80.2	12.4	3.5	3.9	0.28	1.11
<i>O-BDD-10</i>	81.92	11.48	2.87	3.73	0.25	1.29
<i>O-BDD-15</i>	79.28	13.52	3.10	4.10	0.23	1.32
<i>O-BDD-55</i>	79.52	14.06	2.81	3.61	0.20	1.28
<i>O-BDD-plasma</i>	82.0	12.3	2.40	2.90	0.19	1.21

3.3.5 Esterification of the oxidized interfaces

For further investigation of hydroxyl groups on the differently oxidized surfaces, an esterification reaction with CF_3COOH was performed. The resulting surfaces were characterized by XPS and the XPS analysis of differently oxidized interfaces after esterification is shown in **Table 3.5**. F1s peaks located at $\sim 688eV$ (absent in the H-BDD surface XPS analysis) were observed on all oxidized surfaces attributed to successfully covalent linking of CF_3COOH on BDD surfaces. Further more, as the treatment time of the photochemical oxidation increases, an increase of the F1s signal which indicates that the amount of hydroxyl group is improved in accord with treatment time in disagreement with the results above. An increase of the signal of O 1s observed in all cases due to surface oxidation and covalent linking of CF_3COOH can be readily understood. At. % of O1s of photochemical oxidized BDD surfaces varies from 7.65% (oxidized for 5min) to 9.57% (oxidized for 55min), while there is a big leap from treated 10min to 55min. This indicates that the longer photochemical oxidation time, the bigger amount oxygen on CF_3COOH modified BDD surfaces, consistent with the results above.

Table 3.5. Quantitative results from XPS analysis of H-BDD and differently oxidized BDD interfaces after coupling with CF_3COOH .

H-BDD						
Nam	Start	Peak		FWHM		SF
e	BE	BE	End BE	eV	At. %	Al
						Scof
C1s	291.00	284.20	275.00	2.52	94.16	1.00
O1s	537.11	532.85	527.00	3.28	3.09	2.93
Cl2p	205.00	200.33	194.00	1.88	1.59	2.29

Si2p	105.00	101.68	97.00	4.03	0.32	0.82
N1s	403.09	399.88	397.00	1.70	0.80	1.80
Ag3d	376.18	368.29	366.00	1.67	0.03	18.04

BDD - 5 min

Nam	Start	Peak		FWHM		SF	Al
e	BE	BE	End BE	eV	At. %	Scof	
C1s	290.00	284.22	276.00	1.55	88.26	1.00	
O1s	536.00	532.06	528.00	2.92	7.65	2.93	
Cl2p	203.00	199.09	196.00	3.46	0.19	2.29	
Si2p	106.95	101.87	96.00	2.79	3.56	0.82	
N1s	402.86	402.00	401.19	1.00	0.04	1.80	
Ag3d	378.00	368.17	365.00	2.51	0.21	18.04	
F1s	691.00	687.99	685.00	2.99	0.09	4.43	

BDD - 10 min

Nam	Start	Peak		FWHM		SF	Al
e	BE	BE	End BE	eV	At. %	Scof	
C1s	290.00	284.24	275.12	1.53	89.33	1.00	
O1s	538.00	532.04	528.00	2.98	7.58	2.93	
Cl					0.00		
Si2p	106.33	101.83	95.41	2.66	2.53	0.82	
N1s	402.00	399.59	397.00	3.08	0.38	1.80	
Ag3d	376.00	368.42	366.00	1.48	0.08	18.04	
F1s	690.00	688.10	686.00	2.44	0.11	4.43	

BDD - 55 min

Nam	Start	Peak		FWHM		SF	Al
e	BE	BE	End BE	eV	At. %	Scof	
C1s	291.00	285.07	275.00	2.67	88.32	1.00	
O1s	537.00	532.04	527.00	3.12	9.57	2.93	

C12p	202.14	198.20	194.00	4.37	0.10	2.29
Si2p	105.59	102.39	100.00	3.00	0.31	0.82
N1s	404.00	400.07	397.00	4.12	0.60	1.80
Ag3d	376.00	367.98	365.00	2.52	0.08	18.04
F1s	693.00	688.44	685.00	1.82	0.29	4.43
Se2p	168.00	163.41	159.00	3.78	0.72	1.00

BDD – EC

Nam	Start	Peak		FWHM		SF	Al
e	BE	BE	End BE	eV	At. %	Scof	
C1s	290.00	285.01	275.00	2.83	81.59	1.00	
O1s	537.00	531.99	526.00	3.21	11.24	2.93	
C12p	205.00	199.95	196.00	3.25	0.42	2.29	
Si2p	105.00	101.26	98.06	2.83	1.16	0.82	
N1s	404.00	399.89	391.65	3.93	2.11	1.80	
F1s	692.00	687.97	683.00	2.99	3.02	4.43	
Se3p	172.00	168.14	161.00	3.08	0.45	4.53	

Electrochemical oxidized surface shows the biggest oxygen amount, further more, At. % of F1s is also the biggest one, suggesting most hydroxyl group formation on BDD. Therefore, we can conclude that electrochemical oxidation is a most efficient oxidation method to some extent.

In addition, C12p, Si2p, Ag3d and Se2p were observed widely, which are not expected since the reaction of the oxidized BDD surface with CF₃COOH should take place without any of their incorporation according to **Scheme 3.3**.

3.4 Conclusion

Three different methods for the oxidation of as-deposited moderately doped diamond interfaces have been compared in terms of electrochemical behaviour and surface properties investigated by water contact angle measurements and XPS analysis.

Table 3.6 tries to summaries the advantages and disadvantages of each approach. In general, it is can be concluded that diamond interfaces exhibiting better grafting efficiency

also show a more positive flat band position. This behaviour suggest strongly that a positive shift of the flat band potential is related to the formation of C-OH bonds rather than C-O-C groups, which completes previous results reported by us in reference [26]. Taking this into account, the electrochemical oxidation is one of the preferred methods, forming the highest amount of C-OH groups without graphitizing the diamond interface as observed in the case of oxygen plasma. However, photochemical oxidation for short times (5 to 15min) results in high N/O ratios together with an increase in electron transfer kinetics (for 15min of treatment) and is an alternative for un-doped diamond samples.

3.5 Perspectives

Since electrochemical oxidation is limited to conductive surface and more difficult to perform compared to photochemical oxidation and oxygen plasma, we prefer to develop a series of methods to introduce as more as possible hydroxyl group(which can be linked with many groups we need) on BDD by latter two ways. Even though, termination groups of the oxidized BDD after oxidation including photochemical oxidation and oxygen plasma oxidation still can not be controlled as wished. In the future, we will figure this out.

Table 3.6. Comparison of different oxidative methods.

<i>Oxidative method</i>	<i>Advantages</i>	<i>Disadvantages</i>
Electrochemical	1. Formation of mainly C-OH groups 2. No change of the surface morphology	1. Need of conductive interface
UV/ozone	1. Easy to perform 2. After 5 min formation of mainly C-OH groups 3. Photolithographic methods possible 4. Can be used on diamond interface with and without dopant	1. after 55 min strong decrease of electrochemical activity 2. Formation of mainly C-O-C groups rather than C-OH
Oxygen plasma	1. Fast 2. Photolithographic methods possible 3. Can be used on diamond interface with and without dopant	1. Less adapted for the formation of oxygen functionalities 2. Graphitization of the diamond surface

3.6 References

1. S. Szunerits; R. Boukherroub. *J. Solid-State Electrochem.* **2008**, 12, 1205-1218.
2. J. S. Foord; L. C. Hian; R. B. Jackman. *Diam. Relat. Mater.* **2001**, 10, 710-714.
3. H. Notsu; I. Yagi; T. Tatsuma; D.A. Tryk; A. Fujishima. *J. Electroanal. Chem.* **2000**, 492, 31-37.
4. J. Shirafuji; T. Sugino. *Diam. Relat. Mater.* **1996**, 5, 706-713.
5. J. S. Foord; C. H. Lau; M. Hiramatsu; R. B. Jackman; C. E. Nebel; P. Bergonzo. *Diam. Relat. Mater.* **2002**, 11, 856-860.
6. T. Yamada; T. Yokoyama; A. Sawabe. *Diam. Relat. Mater.* **2002**, 11, 780-783.
7. J. I. B. Wilson; J. S. Walton; G. Beamson. *J. Electron. Spectrosc. Relat. Phenom.* **2001**, 121, 183-201.
8. C. Saby; P. Muret. *Diam. Relat. Mater.* **2002**, 11, 851 - 855.
9. T. Ando; K. Yamamoto; M. Ishii; M. Kamo; Y. Sato. *J. Chem. Soc. Faraday Trans.* **1993**, 89, 3635.
10. , P. E. Pehrsson; T. W. Mercer. *Surf. Sci.* **2000**, 460, 49.
11. P. John; N. Polwart; C. E. Troupe; J. I. B. Wilson. *J. Am. Chem. Soc.* **2003**, 125, 6600.
12. H. Notsu; I. Yagi; T. Tatsuma; D. A. Tryk; A. Fujishima. *Electrochem. Solid-State Lett.* **1999**, 2, 522.
13. I. Yagi; H. Notsu; T. Kondo; D. A. Tryk; A. Fujishima. *J. Electroanal. Chem* **1999**, 473, 173.
14. R. Boukherroub; X. Wallart; S. Szunerits; B. Marcus; P. Bouvier; M. Mermoux. *Electrochem. Comm.* **2005**, 7, 937.
15. H. Kanazawa; K. S. Song; T. Sakai; Y. Nakamura; H. Umezawa; M. Tachiki; H. Kawarada. *Diam. Relat. Mater.* **2003**, 12, 618.
16. M. Riedel.; J. Ristein; L. Ley. *Diam. Relat. Mater.* **2004**, 13, 746.
17. D. Delabouglise; B. Marcus; M. Mermoux; P. Bouvier; J. Chane-Tune; J. P. Petit; P. Mailley; T. Livache. *Chem. Comm.* **2003**, 2698-2699.
18. C. H. Goeting; F. Marken; A. Gutiérrez-Sosa; R. C. Compton. *Diam. Relat. Mat.* **2000**, 9, 390.
19. H. Notsu; I. Yagi; T. Tatsuma; A. D. Tryk; A. Fujishima *J. Electroanal. Chem.* **2000**, 492, 31-37.

20. E. Popa; H. Notsu; T. Miwa; D. Tryk A.; A. Fujishima. *Electrochem. Solid State Lett.* **1999**, 2, 49-51.
21. H. Notsu; T. Fukazawa; T. Tatsuma; D.A. Tryk; Y. Fujiwara. *Electrochem. Solid-State Lett.* **2001**, 4, H1–H3.
22. D. Delabouglise; B. Marcus; M. Mermoux; P. Bouvier; J. Chane-Tune; J.-P. Petit; P. Mailley; T. Livache. *Chem. Commun.* **2003**, 2698–2699.
23. S. Szunerits; N. Shirahata; P. Actis; J. Nakanishir; R. Boukherroub. *Chem. Commun.* **2007**, 2793-2795.
24. Y. Coffinier; S. Szunerits; B. Marcus; R. Desmet; O. Melnyk; L. Gengembre; E. Payen; D. Delabouglise; R. Boukherroub. *Diam. Relat. Mater.* **2007**, 16, 892–898.
25. S. Szunerits; M. Manesse; P. Actis; C. Nunes-Kirchner; G. Wittstock; B. Marcus; Y. Coffinier; R. Boukherroub. *Phys.Chem.Chem.Phys.* **2006**, 8, 4924–4931.
26. S. E Pust; S. Szunerits; R. Boukherroub; G.Wittstock. *Nanotechnology.* **2009**, 20(075302), 1-12.
27. P. A. Michaud; M. Panizza; L. Ouattara; T. Diaco; G. Foti; Ch. Comninellis. *J. Appl. Electrochem.* **2003**, 33,151.
28. A. A. Babak; R. Amadeli; A. De. Battisti; V. N. Fateev. *Electrochim. Acta.* **1994**, 9, 597.
29. N. Katsuki; E. Takashashi; M. Toyoda; T. Kurosu; M. Iida; S. Wakita; T. Nishiki; T. Shimamune. *J. Electrochem. Soc.* **1998**, 145, 2358.
30. H. A.Girard; N. Simon; D. Ballutaud; M. Herlem; A. Etcheberry. *Diam. Relat. Mater.* **2007**, 16, 316.
31. H. A. Girard; N. Simon; D. Ballutaud; E. Rochefoucauld; A. Etcheberry. *Diam. Relat. Mater.* **2007**, 16, 888.
32. H. A. Girard; N. Simon; D. Ballutaud; A. Etcheberry. *C. R. Chimie.* **2008**, 11,1010.
33. N. Simon; H. Girard; D. Ballutaud; M. Herlem; A. Etcheberry. *Diam. Relat. Mater.* **2005**, 44, 1179
34. S. zunerits; N. Shirahata; P. Actis; J. Nakanishir; R. Boukherroub. *Chem. Commun.* **2007**, 2793.
35. G. J. Zhang; K. S. Song; Y. Nakamura; T. Ueno; T. Funatsu; I. Ohdomari; H. Kawarada. *Langmuir.* **2006**, 22, 3728-3734.
36. R. H. Dettre; R. E. Johnson. *Adv. Chem.Ser.* **1964**, 43, 136.
37. B. Muller; M. R. R. Michel; S. M. De. Paul; R. Hofer; D. Heger; D. Grutzmacher. *J. Vac. Sci.Technol.B.* **2001**, 19, 5.

38. H. Nostu; T. Tatsuma; A. Fujishima. *Characterization of oxygenated diamond electrodes*. **2004**. 10, 1.
39. D. Ballutaud; N. Simon; H. Girard; E. R. Bouchet-Fabre. *Diam. Relat. Mater.* **2006**, 15, 716.

CHAPTER 4

“CLICKING” ORGANIC MOLECULES BEARING ACETYLENE GROUP TO AZIDE-TERMINATED BORON-DOPED DIAMOND SURFACES

4.1. Introduction

“Click” chemistry in general [1], and the Cu(I)-catalyzed Huisgen 1,3-dipolar cycloaddition of alkynes and azides in particular [2], is generating enormous excitement for surface modification, because it just may be a strategy for quantitative coupling of chemical species to a surface, thus allowing complex molecular architectures to be prepared on a surface in a well-controlled manner.

Independently reported in 2002 by Sharpless [3] and Meldal [4], and intended to represent a chemically simple conjugation approach with a wide scope, copper (I)-catalyzed azide-alkyne cycloaddition reactions have since then found numerous applications in fields as diverse as drug discovery and material sciences [5,6]. Examples of these so named “click” reactions on polymer and solid surfaces have been recently reviewed [7,8], and numerous strategies to exploit this reaction to benefit from its high selectivity, high yields and remarkable tolerance to reaction conditions are now available to surface scientists [9,10]. Azides and alkynes are highly energetic functional groups with particularly narrow distributions of reactivity. Thanks to their weak acid-base properties, they are nearly inert toward biological molecules and the reaction conditions found inside living cells. At the same time, azide and alkyne groups are easy to introduce into organic compounds by both nucleophilic and electrophilic processes. One may therefore envision their incorporation into biological molecules by organic synthesis and chemical conjugation (or via biosynthetic pathways using designed precursors) to create unique points of addressable reactivity in large and complex targets.

1, 2, 3-Triazole-based polymers generated from the Cu (I)-catalyzed cycloaddition between multivalent azides and acetylenes are effective adhesive materials for surfaces. The addition of Cu catalyst was found to be important for the synthesis of stronger adhesive polymers when cured at room temperature. Heating also accelerated curing rates, but the maximum

adhesive strengths achieved at both room and high temperatures were the same, suggesting that cross-linking reaches the same advanced point in all cases. Polytriazoles also form adhesives to aluminum, but copper is bound more effectively, presumably because active Cu (I) ions may be leached from the surface to promote cross-linking and adhesion.

However, the detailed reaction mechanism of this Cu (I)-catalyzed cycloadditions has not been completely understood, a popular proposed reaction mechanism was published by Sharpless et al. [11]. **Figure 4.1** gives an overview of the proposed reaction mechanism: conversion of the alkyne **1** to the acetylide **2** is well known to be involved in many C-C bond forming reactions in which Cu acetylide species are bona fide intermediates. In the next step, the azide replaces one of the ligands and binds to the copper atom via the nitrogen proximal to carbon, forming intermediate **3**. This is effectively a starting point for the stepwise sequence schematically. After that, the distal nitrogen of the azide in **3** attacks the C-2 carbon of the acetylide, forming the unusual six-membered copper (III) metallacycle **4**. From **4**, the barrier for ring contraction, which forms the triazolyl-copper derivative **5**, is very low. Proteolysis of **5** releases the triazole product, thereby completing the catalytic cycle.

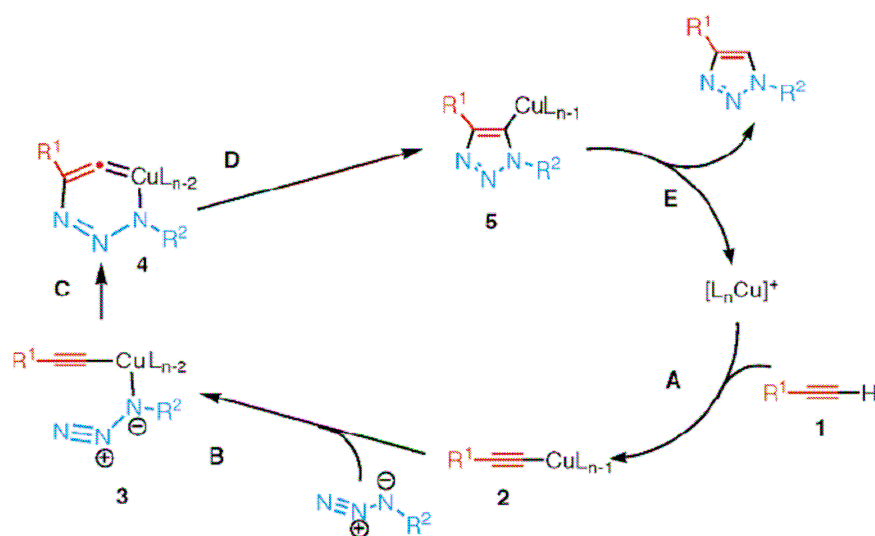


Figure 4.1. Proposed reaction mechanism by Sharpless et al. [11].

The numerous advantages of click chemistry and its previous applications to surface modification represent important assets to design an efficient and versatile strategy for the incorporation of functional groups on solid substrates. Chidsey and Choi reported near quantitative coupling yields on gold surfaces using Cu(I)-catalyzed alkyne-azide cycloaddition reactions[12-15] Since click chemistry has been successfully used to

functionalize gold nanoparticles[16], single-walled carbon nanotubes[17], powdered silica[18,19], metal nanoparticles[20], and flat silicon wafers[21-23] and porous silicon[24].

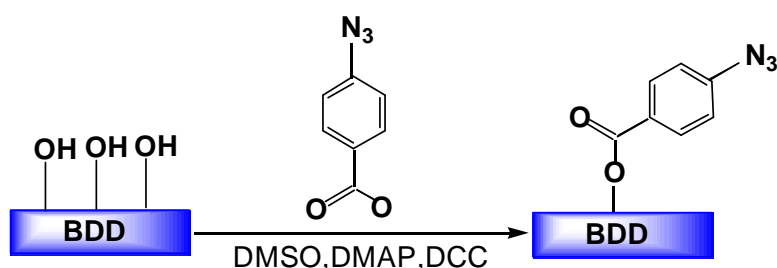
In chapter 3, we have discussed in details the different methods for the oxidation of boron-doped diamond surfaces. Photochemical oxidation of hydrogenated BDD with UV/ozone and electrochemical oxidation can provide hydroxyl groups (-OH) on boron-doped diamond surface. The formation of hydroxyl groups is for the most part desired, as well known chemical routes can be used to link functional groups to -OH units. Esterification reactions are the simplest and most often performed among organic transformations. It is the general name for a chemical reaction in which two reactants (typically an alcohol and an acid) form an ester as the reaction product. Therefore through an esterification reaction, carboxylic acid and its derivatives can be covalently linked to the hydroxyl groups of oxidized boron-doped diamond. The esterification reaction has already been successfully employed on oxidized boron-doped diamond using pyrene alkylcarboxylic acid [25], acid-terminated biotin [26], and more recently 3-benzoylbenzoic acid [27]. However, any derivatives of carboxylic acid with useful functionalities can be attached onto electrode surfaces via the esterification reaction.

In the search for new strategies to derivatize BDD surfaces, we adopted the “click” chemistry, the Huisgen 1, 3-dipolar cycloaddition of terminal acetylenes with azides [28, 29]. The advantage of using 4-azidobenzoic acid, a commercially available molecule, for the introduction of an azide group on the BDD surface is the fact that this molecule can be easily coupled to any -OH, -NH₂ or -SH terminated surface. This class of chemical reactions found countless applications in different fields. A wide range of useful molecules with ethynyl group such as ethynyl ferrocene, ethynyl thiophene, etc. can be attached onto diamond surfaces via “click chemistry”.

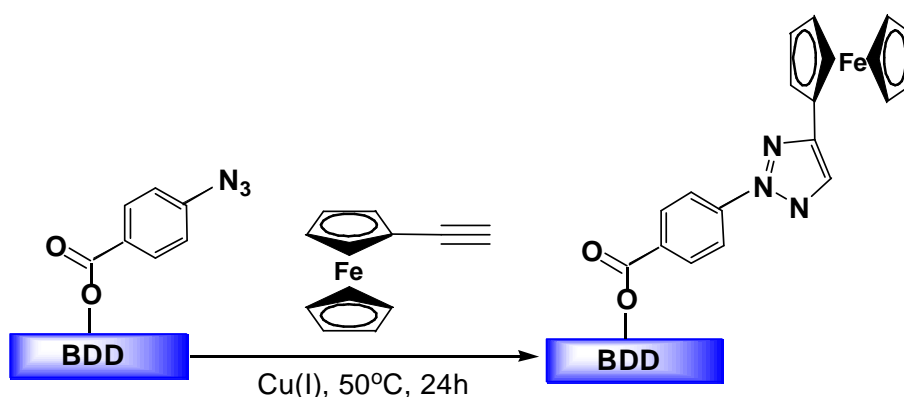
4.2. Objectives

In this chapter, boron-doped diamond was photochemically oxidized using UV/ozone. Azide termination was obtained by esterification reaction of surface hydroxyl groups of the oxidized BDD with 4-azidobenzoic acid at room temperature, as shown in **Scheme 4.1**. The resulting surfaces were further reacted with ethynyl ferrocene, ethynyl thiophene (thiophene terminated BDD was further electropolymerized) as well as ethynyl cyclophane using “click” chemistry (**Scheme (4.2, 4.3, and 4.4)**).

In addition, according to the principle of Fourier Transform Infrared Spectroscopy (FTIR) (as shown in **Annex 8**), polycrystalline diamond layers, which were deposited on silicon wafer, are impossible to be characterized by FTIR. However, as a material with a high surface area, porous silicon (P-Si) surface can be characterized by FTIR in transmission mode. And generally, for surface functionalization, BDD and P-Si have a lot in common, thus we got optimization conditions from clicking thiophene groups on the azide-terminated porous silicon surface and the FTIR characterizations.



Scheme 4.1. Esterification reaction scheme on diamond surface using 4-azidobenzoic acid.



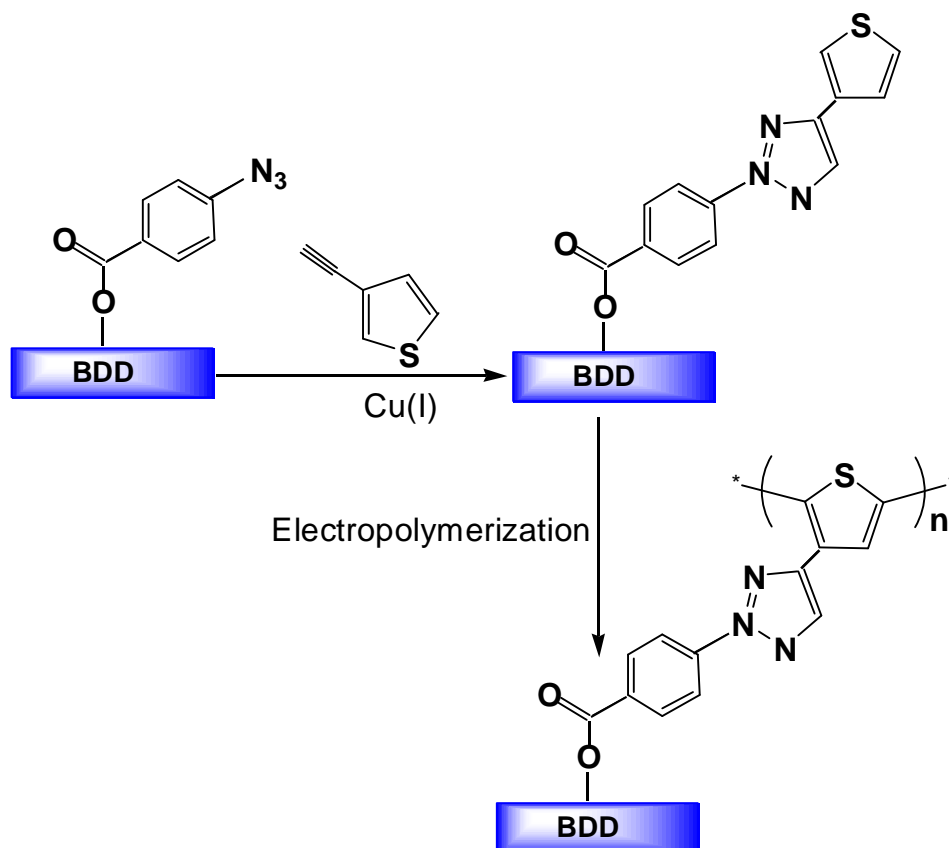
Scheme 4.2. Scheme of clicking ethynyl ferrocen to azide-terminated diamond surface.

4.3. Results and discussion

4.3.1. Characterization of azide-terminated BDD surfaces

Water contact angle measurements were used to examine the macroscopic evolution in the wetting properties of the boron-doped diamond electrode before and after functionalization (**Table 4.1**). The as-prepared BDD is hydrogen-terminated. This termination confers a hydrophobic character to the surface with a water contact angle $\theta = 94 \pm 2^\circ$. Photochemical oxidation (UV-ozone for 2h) of the BDD substrate yields a surface termination with a hydrophilic character. The contact angle value decreased significantly to $\theta = 8^\circ$. Chemical

esterification of the terminal hydroxyl groups with 4-azidobenzoic acid led to an increase in contact angle. A value of $53 \pm 2^\circ$ was measured for the azide-terminated BDD surface.



Scheme 4.3. Scheme of clicking ethynyl thiophene to azide-terminated diamond surface and its electropolymerization.

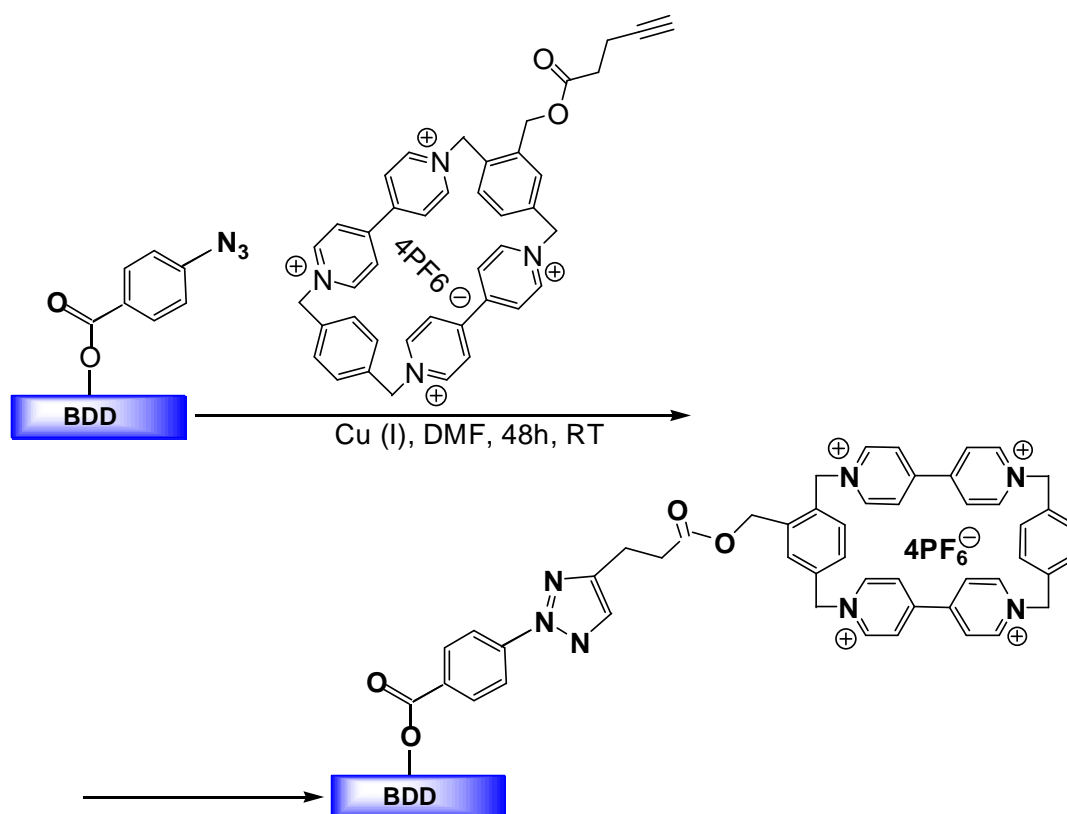
4.3.1.1. X-ray photoelectron spectroscopy (XPS) analysis

Figure 4.2 displays the XPS survey spectrum of the azide terminated BDD surface. It shows a main peak at 285eV due to C 1s and a peak at 532eV due to O 1s. An additional peak at ~400eV, characteristic of nitrogen (N1s) is also observed. High resolution XPS investigation of the N1s was performed (**Figure 4.3**). Careful analysis showed two peaks at 401 and 406eV, suggesting the presence of two nitrogen species in the azide-terminated monolayer, and reflects the differently charged nitrogen atoms in the azide group [30-32]. This indicates the success of the esterification reaction.

4.3.1.2. Electrochemistry measurement

Cyclic voltammetry (CV) was used to characterize the different diamond surfaces. **Figure 4.4** shows the *i-E* curves for an aqueous solution of $10\text{mM Fe(CN)}_6^{4-}$ in 0.1M KCl at a hydrogen-terminated, an oxidized and an azide-terminated BDD interface. While the

hydrogenated diamond shows a well defined redox wave and the oxidized diamond inhibited electrode kinetics, as reported previously [33], the azide-terminated BDD shows the characteristics of a partially blocked electrode. From the shape of the CV (peaks rather than sigmoidal shape), it can be further deduced that the blocking is rather weak.



Scheme 4.4 Scheme of clicking ethynyl cyclophane to azide-terminated diamond surface.

Table 4.1. Water contact angle (CA) for boron doped diamond surfaces with different terminations.

Surface	Contact angle(°)
H-BDD	94±2
HO-BDD	8±2
N ₃ -BDD	53±2
Ferrocene-BDD	14±2
Thiophene-BDD	50±2
Cyclophane-BDD	20±2

4.3.2 Characterization of ferrocene-terminated BDD surfaces

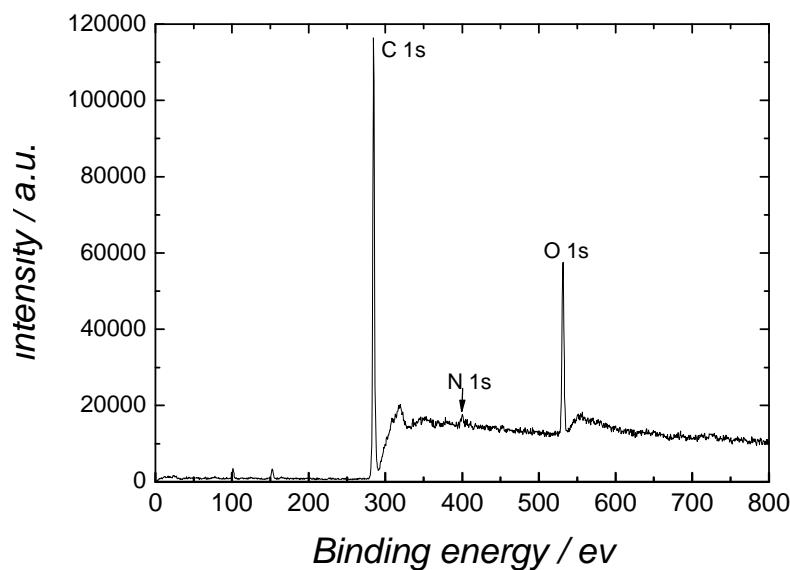


Figure 4.2. XPS survey spectrum of the azide-terminated BDD surface.

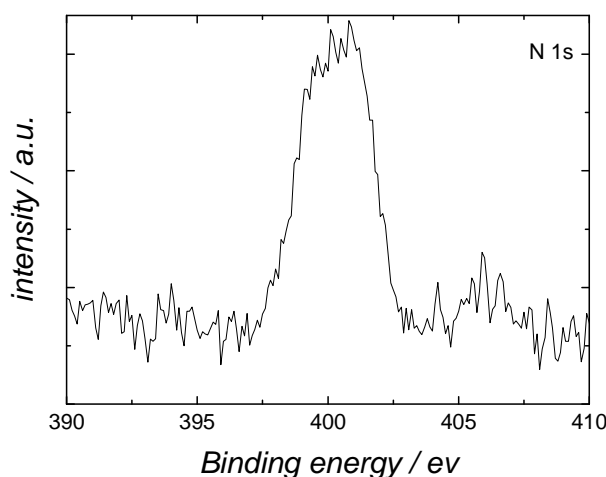


Figure 4.3. High-resolution XPS spectrum of the N 1s peak of the azide-terminated BDD surface.

Ferrocene and its numerous derivatives have no large-scale applications, but are ideal to be characterized by XPS and electrochemical means. In this chapter, we developed a versatile strategy on the covalent linking of ethynyl ferrocene to azide-terminated BDD electrodes using click chemistry. The course of the reaction was followed by X-ray photoelectron spectroscopy (XPS), water contact angle and electrochemical measurements. Cyclic voltammetry (CV) showed unambiguously the presence of surface ferrocene groups.

After clicking ferrocene groups to the azide terminal groups, the contact angle dropped significantly to $\theta = 14 \pm 2^\circ$, demonstrating that ferrocene terminated BDD surface is very hydrophilic (**Table 4.1**).

X-ray photoelectron spectroscopy is a valuable tool to evaluate the changes in the surface chemical composition and bonding occurred during surface derivatization. **Figure 4.5a** displays the XPS survey spectrum of an oxidized BDD surface. It shows a main peak at 285eV due to C1s from the bulk and a peak at 532eV due to O1s. After chemical coupling of the terminal hydroxyl groups with 4-azidobenzoic acid, an additional peak at ~ 400eV was observed, in agreement with the chemical composition of the molecule.

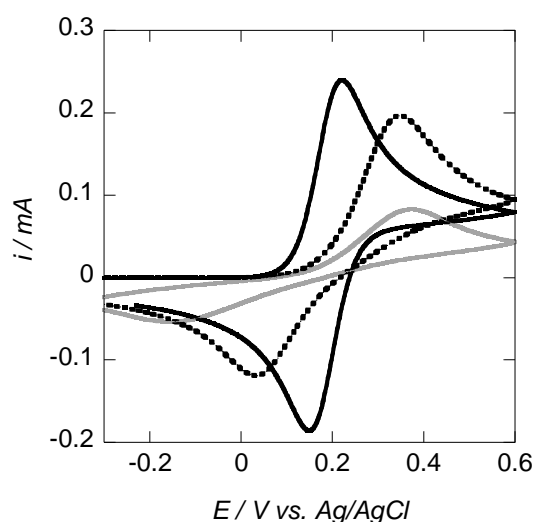


Figure 4.4. Cyclic voltammograms of BDD electrodes in an aqueous solution of $\text{Fe}(\text{CN})_6^{4-}$ (10 mM) in KCl (0.1 M): H-BDD (black), N_3 -BDD (grey), HO-BDD (black dotted), scan rate: 0.05V/s

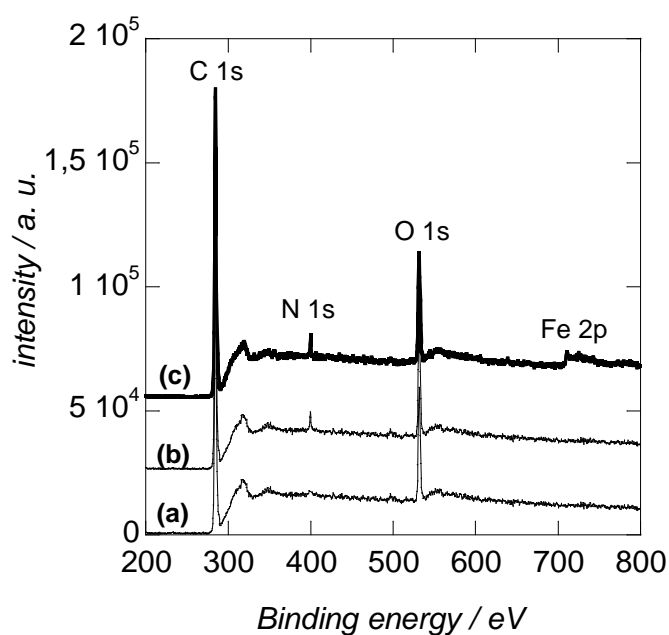


Figure 4.5. XPS survey spectra of the photochemically oxidized BDD surface (a), the azide-terminated BDD surface before (b) and after (c) coupling of ethynyl ferrocene via click chemistry.

Subsequent reaction of the terminal azido groups with ethynyl ferrocene in the presence of Cu(I) catalyst led to the appearance of a new peak in the XPS survey spectrum at $\sim 710\text{eV}$ due to Fe2p (**Figure 4.5**). After clicking ferrocene groups onto the azide-terminated BDD surface, the peak at 406eV disappears almost completely and the peak at 400eV broadens (FWHM = 5.7eV). This can be taken as evidence for the transformation of the azide group into 1, 2, 3-triazole unit bound to the terminal ferrocene head *via* “click chemistry”. In addition, high resolution XPS scan of the Fe2p region demonstrates the presence of the ferrocene moieties onto the BDD surface (**Figure 4.6**). The Fe2p_{3/2} and 2p_{1/2} peaks occur at 711.7 and 725.6eV , respectively. This clearly indicates that the Fe moiety exists mainly in its (III) oxidation state, in agreement with previously reported results on ferrocene groups anchored onto hydrogen-terminated silicon surfaces [34-36]. Integration of the peak area of N1s and Fe2p gave N1s/Fe2p ratio of 6.4, higher than the theoretical value of 3. This corresponds to a conversion of approximately 47% of the azide groups to the triazole rings.

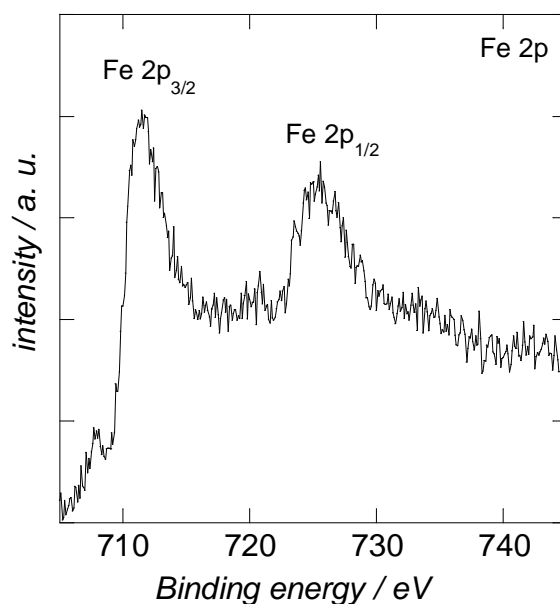


Figure 4.6. High-resolution XPS spectrum of the Fe 2p after clicking an azide-terminated BDD surface with ethynyl ferrocene.

The ferrocene modified BDD surface was probed by CV in a solution of 0.1 M tetraethyl ammonium hexafluorophosphate (TEAPF_6) in DMF (**Figure 4.7A**). The redox peak with a $E_0 \sim -0.63\text{V}$ vs. Ag/AgCl and a peak separation of $\Delta E = 296\text{mV}$ evidence the presence of ferrocene units on BDD. The bound ferrocene moiety shows a high redox potential, as compared to other ferrocene modified electrodes such as on gold ($E_0 \sim -0.33\text{--}0.46\text{V}$ vs. Ag/AgCl)[37] and crystalline silicon ($E_0 \sim -0.15\text{V}$ vs. Ag/AgCl) [38]. The cathodically shifted

E_0 of the ferrocene moiety on crystalline silicon as compared to gold is surprising. In control experiments, CVs of an oxidized and an azide-terminated BDD electrodes were recorded in a DMF solution containing 0.1M tetraethyl ammonium hexafluorophosphate (TEAPF₆) and ethynyl ferrocene (5mM). A $E_0=0.61\text{V}$ vs. Ag/AgCl was determined, in agreement with the redox potential of the ferrocene modified BDD interface ($E_0\sim 0.63\text{V}$ vs. Ag/AgCl). At this stage, the origin of this anodic potential shift is not clear.

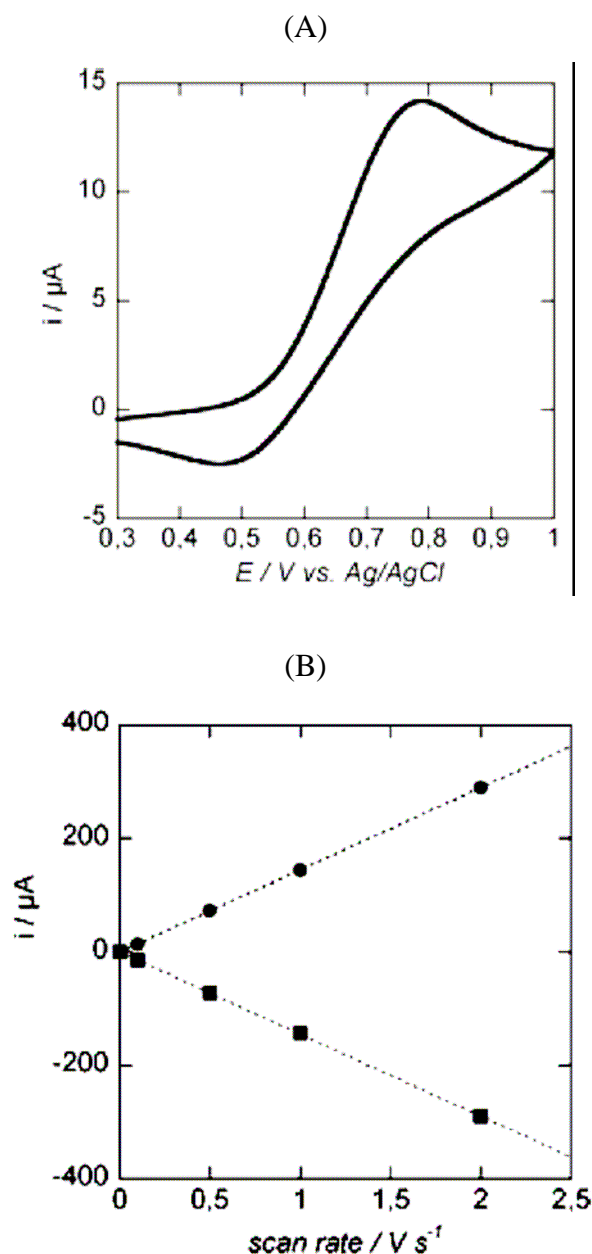


Figure 4.7. (A) Cyclic voltammograms of ferrocene-terminated BDD surface in TEAPF₆ (0.1 M/DMF), scan rate: 0.1V s^{-1} . (B) peak current as a function of scan rate for anodic (●) and cathodic (■) peak currents.

An analysis of the change in peak currents as a function of scan rate allows assessing that the ferrocene moieties are surface bound rather than absorbed. **Figure 4.7B** indicates that the anodic and cathodic peak currents scale linearly with the scan rate v rather than with $v^{1/2}$, suggesting a surface redox process. A similar behavior was observed on single-crystal Si(111) surfaces modified with ferrocene carboxylic acid[38], and on gold modified with ferrocene-based alkanethiol layers.[39] On the ferrocene-terminated BDD electrode, the ferrocene signal shows a quasi-reversible redox behavior like observed by Heath et al[38] on n-type crystalline silicon. The quasi-reversible redox behavior might be linked to the p-type semiconducting characteristic of boron doped diamond.

The ferrocene coverage on the surface was calculated by integrating the anodic peak area according to $\Gamma = Q_a/nFA$, where F is the Faraday constant, n is the number of electrons exchanged ($n=1$) and A is the surface area ($A=0.38\text{cm}^2$). A surface coverage of $\Gamma = (3.46 \pm 0.5) \times 10^{14}$ molecules cm^{-2} is obtained. This is higher than the reported $\Gamma = 0.39 \times 10^{14}$ molecules cm^{-2} on Si (111) and $\Gamma = 0.78 \times 10^{14}$ molecules cm^{-2} on gold, also using a click chemistry approach [37].

4.3.3 Clicking thiophene to the azide-terminated BDD

Coating of different materials with conducting electroactive polymers such as polyaniline, polypyrrole, polythiophene, and their derivatives is subject to intense investigation for practical applications in various fields such as metallization of dielectrics, batteries, antistatic coatings, shielding of electromagnetic interferences, sensors, nonlinear optical and electroluminescent devices[40,41] Furthermore, their use as thin films on metal and semiconductor surfaces has attracted considerable attention in recent years. For applicability on electrical devices, good adherence and stability of the resulting structures are required.

Since the covalent attachment of organic layers on semiconductor surfaces is a commonly used concept [42,43], here we propose a new strategy to covalently link thiophene units onto an azide-terminated BDD electrode surface using “click” chemistry. Coupling of the azide terminated electrode surface with thiophene bearing an acetylene terminal group allowed the covalent linking of a polymerizable thiophene unit to the diamond surface. Cycloaddition of ethynyl thiophene to the azide-terminated BDD surface led to a slight decrease of the contact angle ($50 \pm 2^\circ$) (**Table 4.1**).

Figure 4.8 displays the XPS survey spectra of the different interfaces in the process of thiophene termination. Photochemically oxidized BDD shows a main peak at 285eV due to C 1s from the bulk and a peak at 532eV due to O 1s. After chemical coupling of the terminal

hydroxyl groups with 4-azidobenzoic acid, an additional peak at $\sim 400\text{eV}$ was observed, in agreement with the chemical composition of the molecule. Subsequent reaction of the terminal azido groups with ethynyl thiophene in the presence of Cu(I) catalyst led to the appearance of a new peak in the XPS survey spectrum at 165eV due to sulfur signal corresponding to S 2p (**Figure 4.8c**). The high resolution XPS spectrum of this band is seen in **Figure 4.9**. The XPS spectrum of the S2p of the thiophene-terminated BDD can be deconvoluted into a doublet, consisting of two components: S2p_{1/2} and S2p_{3/2} located at binding energies of 164.5 and 167.5eV, respectively. The separation of S2p_{1/2} and S2p_{3/2} peaks ($\sim 3.0\text{eV}$) and the ratio of their area (~ 0.5) are in close agreement with the theoretical values determined from the spin orbit splitting effect [44-46]. Moreover, the positions of these two peaks are in accordance with earlier reported values for thiophene linked to self-assembled monolayers [46-49]. This result confirmed the above conclusion that the thiophene group had been linked onto the BDD surface rather than physisorbed. Additional evidence of the 1, 2, 3-triazole formation on the azide-terminated monolayer was derived from additional XPS investigations of the N 1s spectral region. A single peak at $\sim 400\text{eV}$ is observed, thus confirming the conversion of the azide functions (**Figure 4.10**).

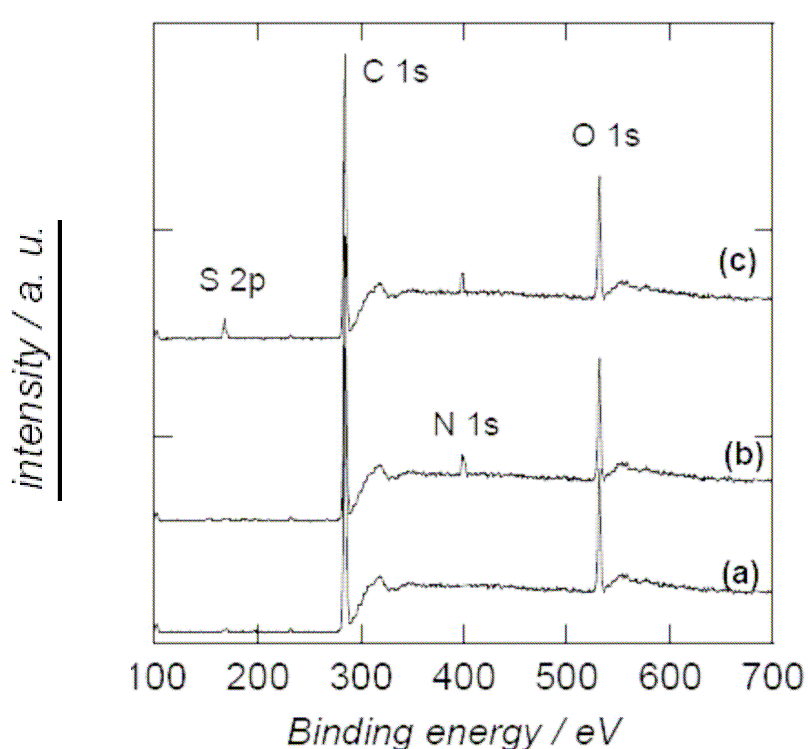


Figure 4.8. XPS survey spectra of the photochemically oxidized BDD surface (a), the azide-terminated BDD surface before (b) and after (c) coupling of ethynyl thiophene via click chemistry.

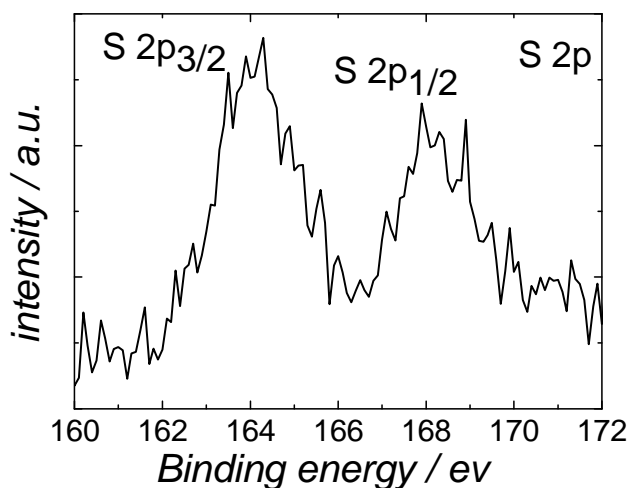


Figure 4.9. High-resolution XPS spectrum of the S 2p band of the thiophene terminated BDD surface.

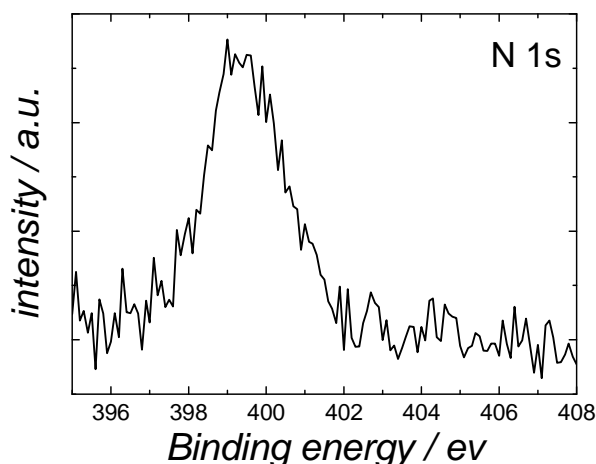


Figure 4.10. High-resolution XPS spectrum of the N 1s band of the thiophene terminated BDD surface.

Figure 4.11 shows the voltammetric behavior of thiophene modified BDD in dry acetonitrile/ 0.1M LiClO₄). In the first scan an irreversible shoulder is observed at ~1.27V (vs. Ag/AgCl: 0.01M) with an intense increase in current at potentials higher than ~1.3V. Indeed, the oxidation of thiophene units to its radical cation occurs at potentials of ~2.0V vs. SCE [50]. The shoulder at ~1.27V could be due to the oxidation of the thiophene dimer, 2, 2'-bithiophene [50]. In a consecutive second the oxidation current is decreased and no oxidative shoulders are observed after the third scan. This indicates that most of the aromatic rings have reacted. As the formed radical cations are highly reactive species, the most likely reaction path is the coupling with neighboring radical cations to form oligomeric and polymeric structures on the BDD interface. The surface coverage of the electroactive species

can be estimated from the current intensity of the anodic shoulder observed at 1.27V presented in **Figure 4.11**. Using the voltammetric response of unmodified BDD as the background current, the surface coverage Γ can be estimated using equation **4.1**:

$$i_{pa} = \frac{(1-\alpha)nn_a F^2 A \nu \Gamma}{2.718RT} \quad (4.1)$$

where i_{pa} is the anodic peak current, α the charge transfer coefficient (assumed to be 0.5), n the total number of electrons, n_a the number of electrons involved in the rate determining step, F the Faraday constant and ν the scan rate. Assuming $n=n_a=2$ electrons a surface coverage of $1.38 \times 10^{-10} \text{ mol cm}^{-2}$ is obtained.

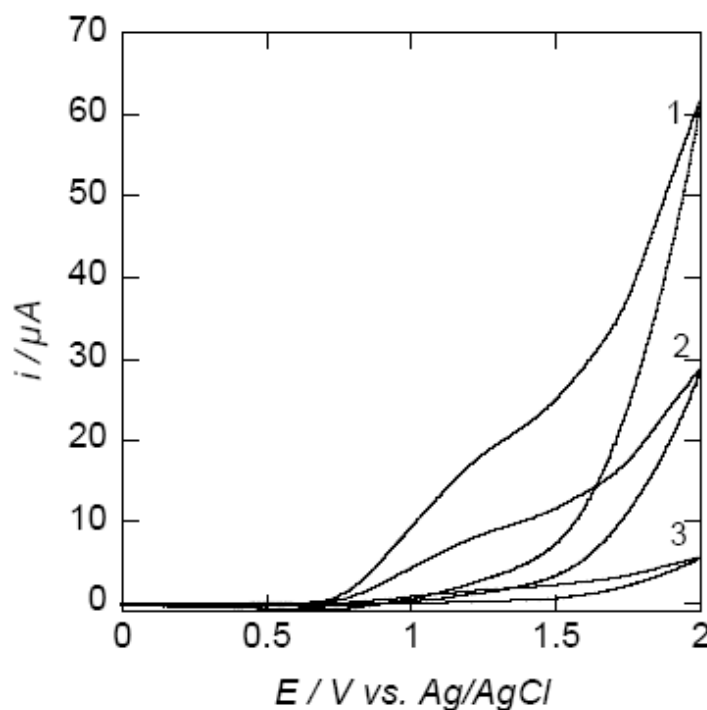


Figure 4.11. Subsequent cyclic voltammetric i - E curves for thiophene modified BDD: solution: LiClO_4 (0.1 M)/acetonitrile, $A=0.35\text{cm}^2$, scan rate = 0.1V s^{-1} .

To obtain higher coverage of conducting polymer material, the thiophene-modified BDD interface was furthermore electrochemically oxidized in the presence of thiophene monomers. Electrochemical polymerization of thiophene monomers can be carried out by using potentiostatic, galvanostatic and cyclic potential sweep techniques. In the present study, a cyclic potential sweep technique was employed. Although this technique requires longer reaction times to obtain the polymer film as compared to potentiostatic and galvanostatic methods, it is advantageous as the electrochemical characteristics of the growing polymers

can be monitored during the polymerization process. **Figure 4.12** shows typical cyclic voltammograms of the electrochemical polymerization of thiophene on thiophene-modified BDD in a 0.1M LiClO₄ acetonitrile solution. The anodic peak at 1.17V and cathodic peak at 0.78V appearing after the third scan correspond to the oxidation of polythiophene. As the polymerization process proceeds, the peak current increases in the successive cycles, indicating the growth of the polymer on the surface of the BDD interface. The anodic peak shifts gradually to higher values as the thickness of the polymer film increases and could be attributed to a decrease of the film conductivity [51].

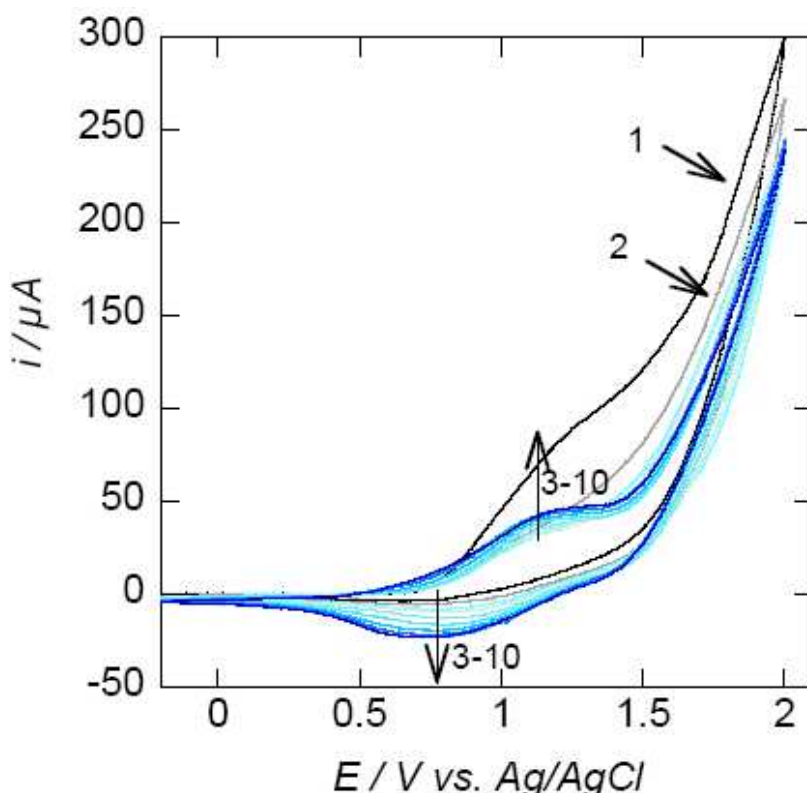


Figure 4.12. Subsequent cyclic voltammetric i - E curves for electrochemical polymerization of thiophene on thiophene-modified BDD: solution: LiClO₄ (0.1M)/acetonitrile/ thiophene (0.1M), $A = 0.35\text{cm}^2$, scan rate = 0.1V s^{-1} .

Cyclic voltammograms of the polythiophene films resulting from the above polymerizations were measured in monomer free LiClO₄/acetonitrile solution (**Figure 4.13A**). The redox process of the polymer is chemically reversible as the amount of cathode charge is essentially the same as the anodic charge. Both, anodic and cathodic peaks are quite broad, which is probably caused by the slow diffusion of the dopant anions (ClO₄⁻ in our case) in and out of the film. The peak-to-peak separation ΔE_p is $\sim 39\text{mV}$ as expected for surface confined redox species. A linear relationship was observed between the anodic peak current and the

scan rate (**Figure 4.13B**) characteristic of an electroactive polymer film grafted on an electrode where the current is not diffusion controlled [52].

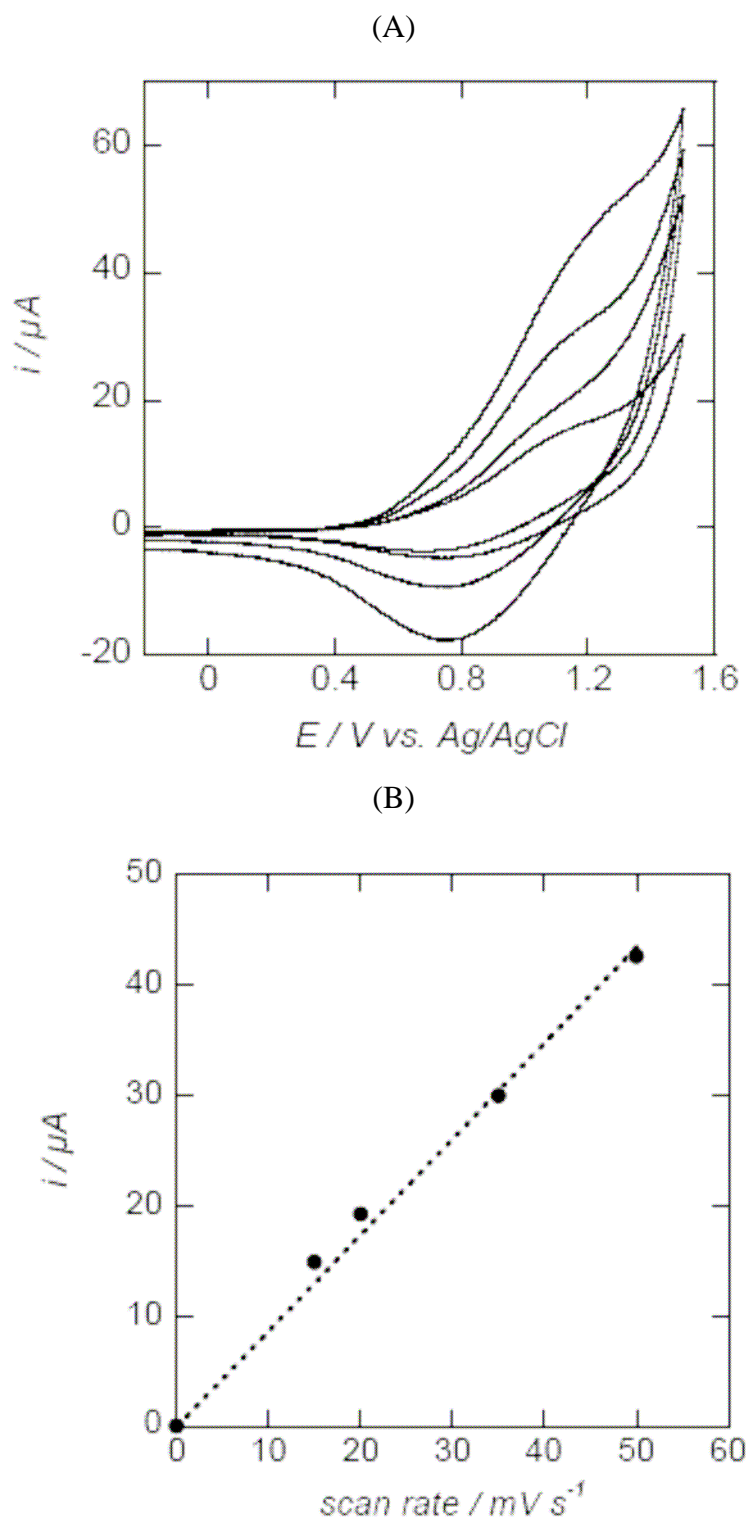


Figure 4.13. (A) Cyclic voltammograms of polythiophene measured in monomer free acetonitrile/0.1 M LiClO_4 solution at various scan rates (15, 20, 35, 50 mV s^{-1}) (B) Dependence of the anodic peak current on the scan rate for the polymer film.

4.3.4. Clicking of cyclophane to azide terminated BDD surfaces

Recently, this ‘click’ methodology has been extended to feature interlocked structures (e.g., rotaxanes and catenanes) [53-60]. This methodology is particularly attractive for the synthesis of systems of this type, as it offers advantages over more traditional methods in terms of improved yields and increased sophistication of the resulting structures. Here, we extend this methodology to a new alkyne-functionalized cyclophane conveniently ‘clicked’ onto an azide-functionalized boron doped diamond surface.

The synthesis of the alkyne-functionalized cyclophane **6** is shown in **Scheme 2.1**. Derivative **3** is conveniently prepared from 1-pentynoic acid **2** and alcohol **1**, and proved to be a versatile building block for the construction of cyclophane **6**. Cyclophane **6** was synthesized from compounds **3** and **4** using a template-directed clipping methodology using **5** [45].

The course of the reaction was followed by X-ray photoelectron spectroscopy (XPS), water contact angle and electrochemical measurements. After clicking cyclophane groups to the azide terminated BDD surface, the contact angle dropped to $20\pm 2^\circ$, as compared to $60\pm 2^\circ$ for the azide termination surface (**Table 4.1**), indicating that the cyclophane groups display a hydrophilic character.

To investigate the changes in the surface composition after the introduction of the cyclophane functionality on the azide-terminated BDD surface, cyclophane-terminated BDD surface was analyzed by XPS (**Figure 4.14**). XPS survey spectrum is shown in **Figure 4.14A**. When compared with the XPS survey spectrum of the azide-terminated BDD surface (**Figure 4.2**), a new peak at 688eV ascribed to F1s appeared after clicking cyclophane groups onto the azide-terminated BDD surface. The high resolution XPS spectrum of F1s is displayed in **Figure 4.14B**. It consists of a single peak at 688 eV. However, an expected peak at 124-136eV due to phosphorus atom was absent as expected for the cyclophane moieties. **Figure 4.14C** displays the high resolution XPS spectrum of N1s of the cyclophane modified BDD surface, showing two peaks at 399.4eV and 401.6eV corresponding to nitrogen in the form of 1, 2, 3-triazole and in the aromatic ring, respectively. All above indicates that cyclophane has been successfully clicked on the azide-terminated BDD surface.

We have further exploited the electrochemical signature of the electroactive cyclophane moiety to investigate whether the cyclophane is grafted onto the BDD surface using click chemistry. The cyclic voltammogram of the cyclophane-terminated BDD surface recorded in acetonitrile (0.1M Bu₄NPF₆) (**Figure 4.15**) reveals the formation of two redox waves (absent in the azide terminated surface), presumably corresponding to the sequential

formation of the diradical dication and fully reduced states of the cyclophane, respectively [61, 62]. However, significant attenuation of the current was observed, which is consistent with surface inhibition due to the presence of either an overall low density surface grafting and/or the presence of defect domains. For further understanding, cyclic voltammograms of cyclophane solution on an azide modified BDD surface as well as on gold surface were investigated under the same conditions (**Figure 4.15**). Since two excellent redox waves were observed on gold surface, much lower current on the former surface indicates a more blocked surface. As a whole, cyclophane covalently linked on BDD surface was further confirmed.

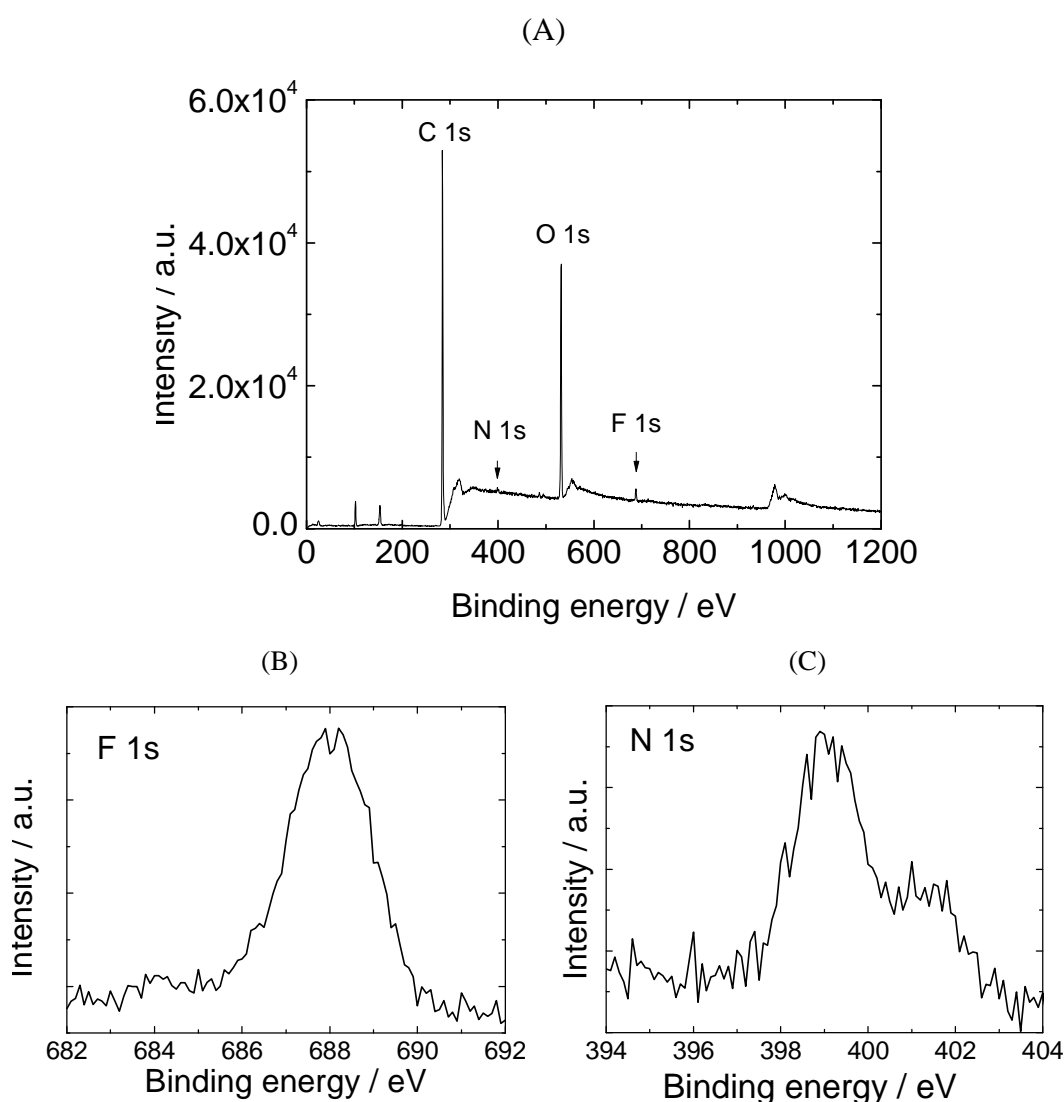


Figure 4.14. XPS survey spectra of cyclophane terminated BDD surface (A) high-resolution XPS spectrum of F1s (B) high-resolution XPS spectrum of N1s (C).

4.4. Functionalization of porous silicon surfaces with thiophene groups

4.4.1. Grafting of ethynyl thiophene on porous silicon

Scheme 4.5 shows the two-step procedure to get an amine termination on the PSi surface. First, the freshly prepared PSi surface was oxidized using UV/ozone and piranha and aminated through silanization with APTMS. Next, the amine terminal groups were reacted with 4-azidobenzoic acid in dry DMSO to produce N₃-terminated PSi. Covalent linking of thiophene units was carried out using “click” chemistry between the N₃- groups terminating the PSi surface and the ethynyl group of the functionalized thiophene in the presence of a copper(I) catalyst. Finally, polymerize thiophene-terminated PSi surface through electropolymerization, as shown in **Scheme 4.6**.

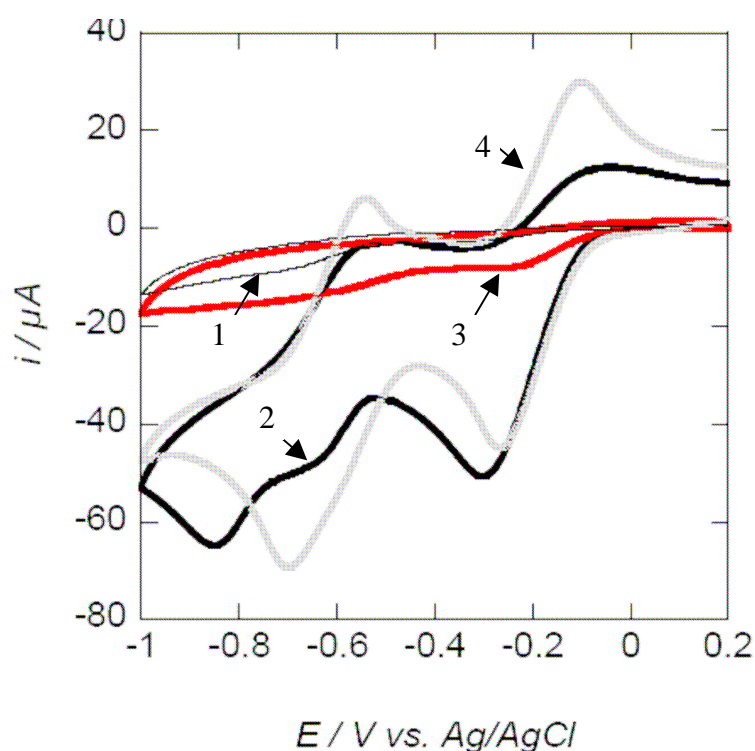
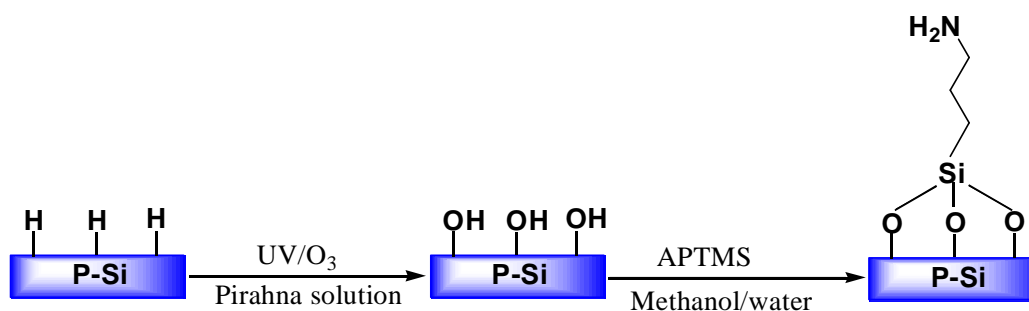
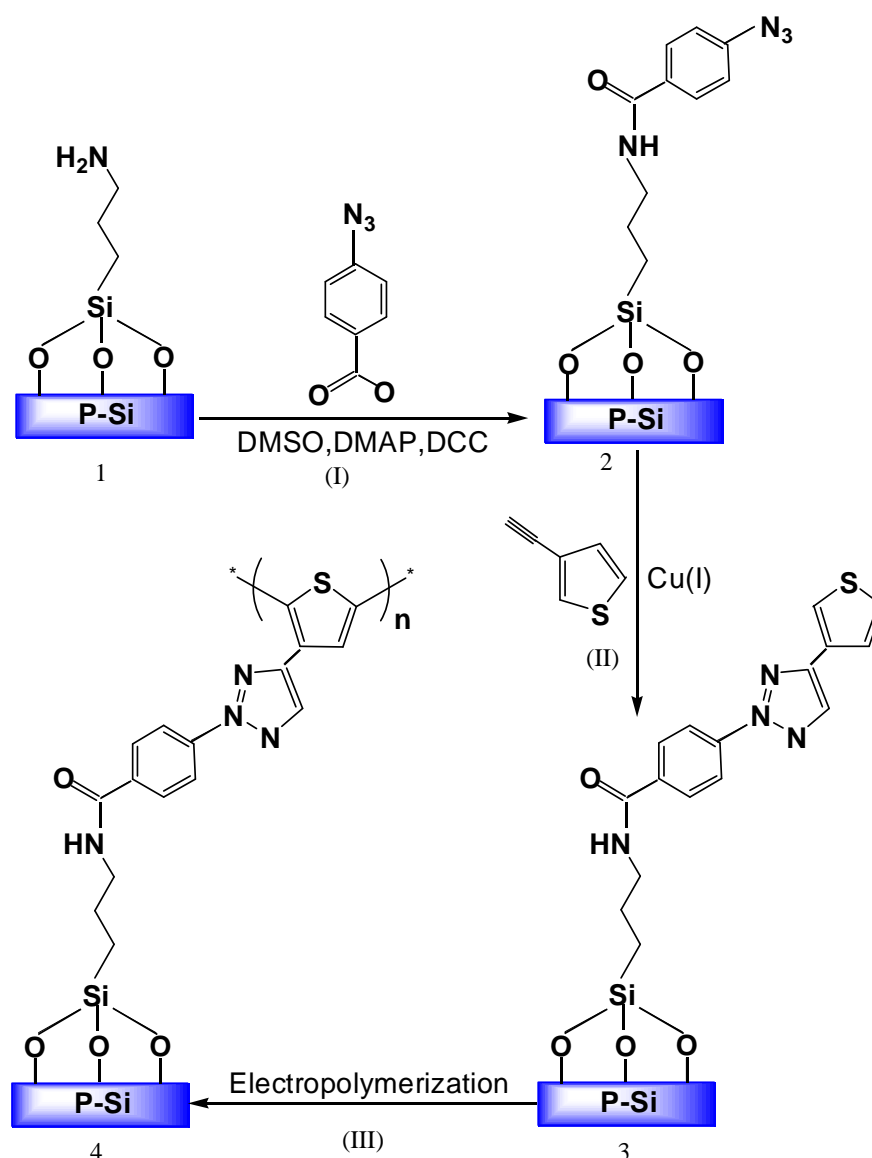


Figure 4.15. Cyclic voltammogram of azide modified BDD surface (curve 1), cyclophane solution on azide modified BDD surface (curve 2), cyclophane clicked BDD surface (curve 3), cyclophane solution on gold surface (curve 4) in acetonitrile (0.1 M Bu₄NPF₆) solution. Scan rate: 0.1V/s⁻¹.



Scheme 4.5. Amination scheme on porous silicon surface using APTMS



Scheme 4.6. Schematic illustration of the chemical derivatization and electropolymerization of porous silicon substrates with thiophene.

4.4.2. Surface characterization

Water contact angle measurements were used to follow the changes in the wetting properties of the freshly-prepared P-Si surface before and after functionalization (**Table 4.2**). The as-prepared, hydrogen-terminated P-Si surface, displays a hydrophobic character with a water contact angle $\sim 104^\circ$. The surface became completely hydrophilic after oxidation. A water contact angle of 4° was measured for such a surface, in agreement with a fully oxidized, hydroxyl-rich surface. Surface silanization with APTMS induced a slight increase of the contact angle to 15° . After coupling of 4-azidobenzoic acid with the aminated P-Si surface, a significant increase of the contact angle was observed (65°). Cycloaddition of ethynyl thiophene to the azide-terminated P-Si surface led to a slight decrease of the contact angle

(58°). No significant change of the contact angle was observed after electropolymerization (63°).

Table 4.2. Water contact angle (CA) for porous silicon surfaces with different terminations

Surface	Contact angle(°)
P-Si	104±2
HO-P-Si	4±2
H ₂ N-P-Si	15±2
N ₃ -P-Si	65±2
thiophene-P-Si	58±2
polythiophene-P-Si	63±2

As a control surface, functionalized P-Si interfaces were characterized by FT-IR measurement. **Figure.4.16** shows the FT-IR spectra of the different stages leading to azide linking. The oxidized P-Si interface shows a strong Si-O vibration band at 1055cm⁻¹ and a broad absorption at around 3400cm⁻¹ most likely due to OH vibration and adsorbed water molecules (**Figure.4.16a**). After coupling of APTMS, the band at ~3400 cm⁻¹ is reduced while C-H stretching peaks appear at 2951 and 2874cm⁻¹ due to asymmetric and symmetric vibrations, respectively. NH stretching band is observed at 3400-3300cm⁻¹, presenting a very large peak (**Figure. 4.16b**). After treating the aminated P-Si surface with 4-azidobenzoic acid in the presence of DCC, DMAP, the appearance of an intense peak at 2100cm⁻¹, characteristic of $\nu_{as}(N_3)$ stretching is observed. The absorption peaks at 1650cm⁻¹ and 1550cm⁻¹ can be respectively assigned to the C=O and NH deformation band of amide group (**Figure. 4.16c**). This clearly indicates the successful grafting of 4-azidobenzoic acid on the P-Si surface. Considering the similarity of hydroxyl and amine during esterification reaction, we can conclude that covalent linking between hydroxyl and carboxylic acid also performed. The azide-terminated P-Si surface was reacted with ethynyl thiophene with a Cu (I) catalyst present. **Figure. 4.16d** shows the complete disappearance of $\nu_{as}(N_3)$. These spectral changes are a clear indication of a reaction of the azide group with ethynyl thiophene. There was an obvious absorption peak at ~1000cm⁻¹, which is the characteristic of the formed 1, 2, 3-triazole. A sharp band at 690cm⁻¹, characteristic of the C-S stretching of the thiophene rings, appeared in the thiophene grafted P-Si surface spectrum. The IR bands assigned to the =C-H stretching of attached thiophene are situated between 3000 and 3200cm⁻¹[63] but it is overlaid by the strong NH stretching band. This result indicated that the thiophene group

had been introduced to the P-Si surface, from which we can optimistically deduce that cycloaddition of ethynyl thiophene to the azide-terminated BDD surface may be also achieve.

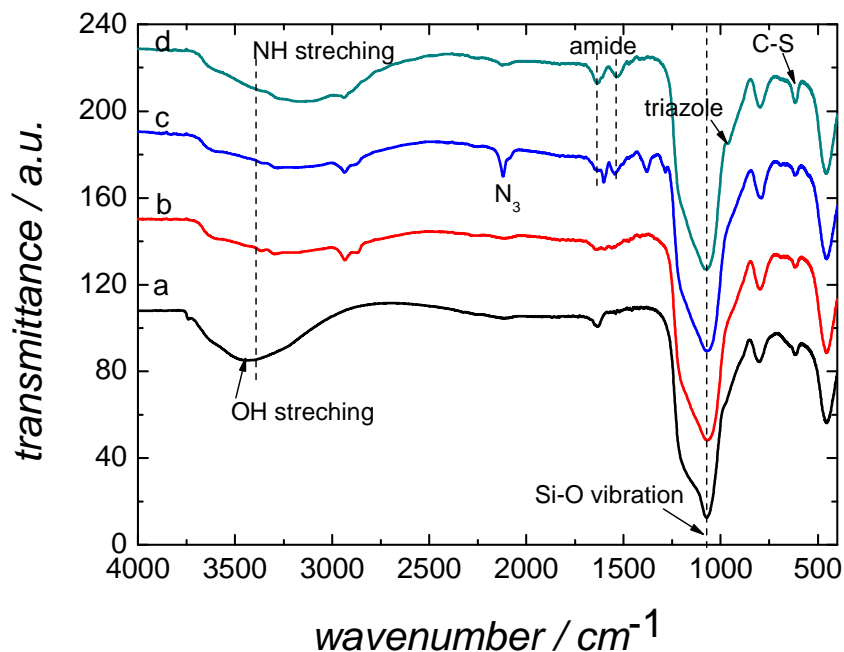


Figure.4.16. Transmission FTIR spectra of oxidized P-Si (a), aminated P-Si (b), azide-terminated P-Si (c) and after “clicking” ethynyl thiophene (d).

4.4.3. Electrochemical polymerization

Figure 4.17 shows the voltammetric behavior of a P-Si substrate modified with thiophene *via* “click” chemistry in dry $\text{CH}_3\text{CN}/0.1\text{M Bu}_4\text{NBF}_4$. In the first scan a weak irreversible shoulder is observed at $\sim 1.1\text{V}$ (vs. Ag/AgCl : 0.01M), which can be ascribed to the oxidation of thiophene unit to its radical cation. In the following cycle, the shoulder is not present indicating that all of the electrochemically generated radical cations have reacted. As these intermediates are highly reactive species the most likely reaction path is the coupling with neighboring radical cations to form oligomeric and polymeric structures on the P-Si interface. The large currents observed for potentials higher than $\sim 1.3\text{V}$ correspond mainly to the oxidation and/or dissolution of underlying silicon [64].

The surface coverage of the electroactive species can be estimated from the current intensity of the anodic shoulder observed at 1.16V of the linear sweep voltammograms presented in **Figure 4.17**. Using the voltammetric response of unmodified P-Si as the background current, the surface coverage Γ can be estimated using **equation 4.1**. Assuming $n=n_a=2$ electrons a surface coverage of $3.47 \times 10^{-10} \text{mol cm}^{-2}$ is obtained. This corresponds well

to surface coverage reported by Fabre et al. on Si(111) surface with thiophene-modified alkyl monolayers (4.7×10^{-10} mol cm⁻²)[60].

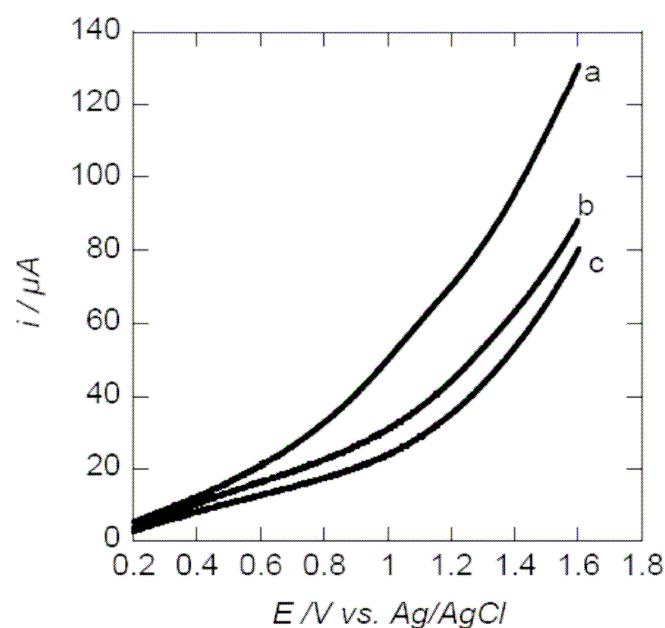


Figure 4.17. Linear sweep voltammograms in CH₃CN/Bu₄NBF₄ at 0.02V s⁻¹ of thiophene-modified PSi (a) first scan, (b) second scan, (c) unmodified PSi surface.

4.4.4. Formation of polythiophene films on thiophene-modified PSi

To reach higher surface coverage of the conducting material, the thiophene-modified PSi was immersed in the electrolyte containing 0.1M thiophene and the monomer was electrochemically oxidized by applying a current density of 1mA cm⁻² for 40min. As seen in **Figure 4.18A**, the onset of the thiophene oxidation occurs at 0.9V [65]. The crossing of forward and backward scans in the region of thiophene oxidation is characteristic for the polymerization and deposition of conducting polymers [66]. Following the potential evolution during the electrochemical synthesis of polythiophene as a function of time under galvanostatic conditions allows the observation of three different stages during the polymerization. Within the first seconds, the potential rises corresponding to polymer nucleation presumably at the pore bottom (**Figure 4.18B, section I**). The second step corresponds to polymer growth inside the porous layer (**section II**) and finally, the polymer film is formed on top of the PSi surface (**section III**).

The sequential p-doping and undoping of the electrochemically synthesized polymer is illustrated in the cyclic voltammogram in **Figure 4.19A**. Polythiophene deposited on thiophene-modified PSi exhibits a broad redox system between -0.50 and -0.15V, characteristic for polythiophene. The results are corroborated by FTIR analysis.

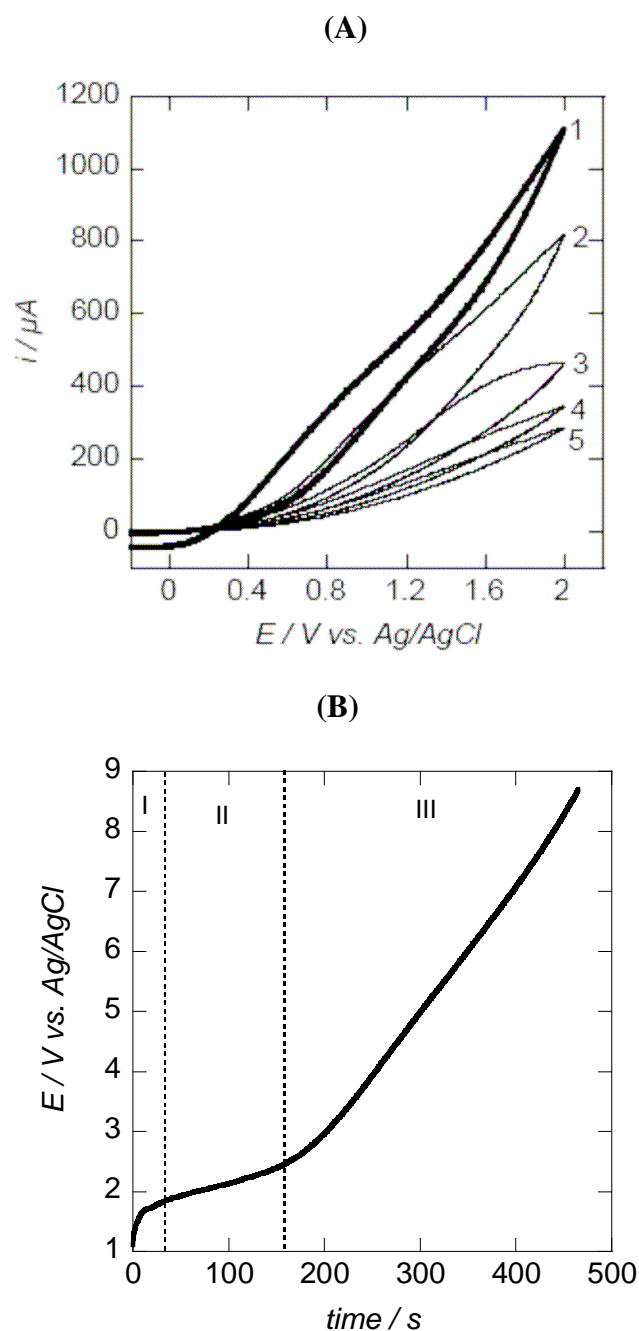


Figure 4.18. (A) Cyclic voltammograms corresponding to the anodic electropolymerization of thiophene monomer on thiophene-terminated P*Si* and (B) characteristic chronoamperogram of the electrochemical synthesis of polythiophene under galvanostatic conditions (1mA cm^{-2})

Figure 4.19B exhibits the transmission FTIR spectrum of the P*Si*/polythiophene hybrid structure. The C=C stretching of polythiophene ring is seen at 1401cm^{-1} and 1509cm^{-1} , and the C-H stretching at 3259cm^{-1} . The wetting properties of the P*Si*/polythiophene structure (49°) are comparable to that of the thiophene-terminated P*Si* surface (46°), as expected for surfaces with similar terminations (**Table 4.2**).

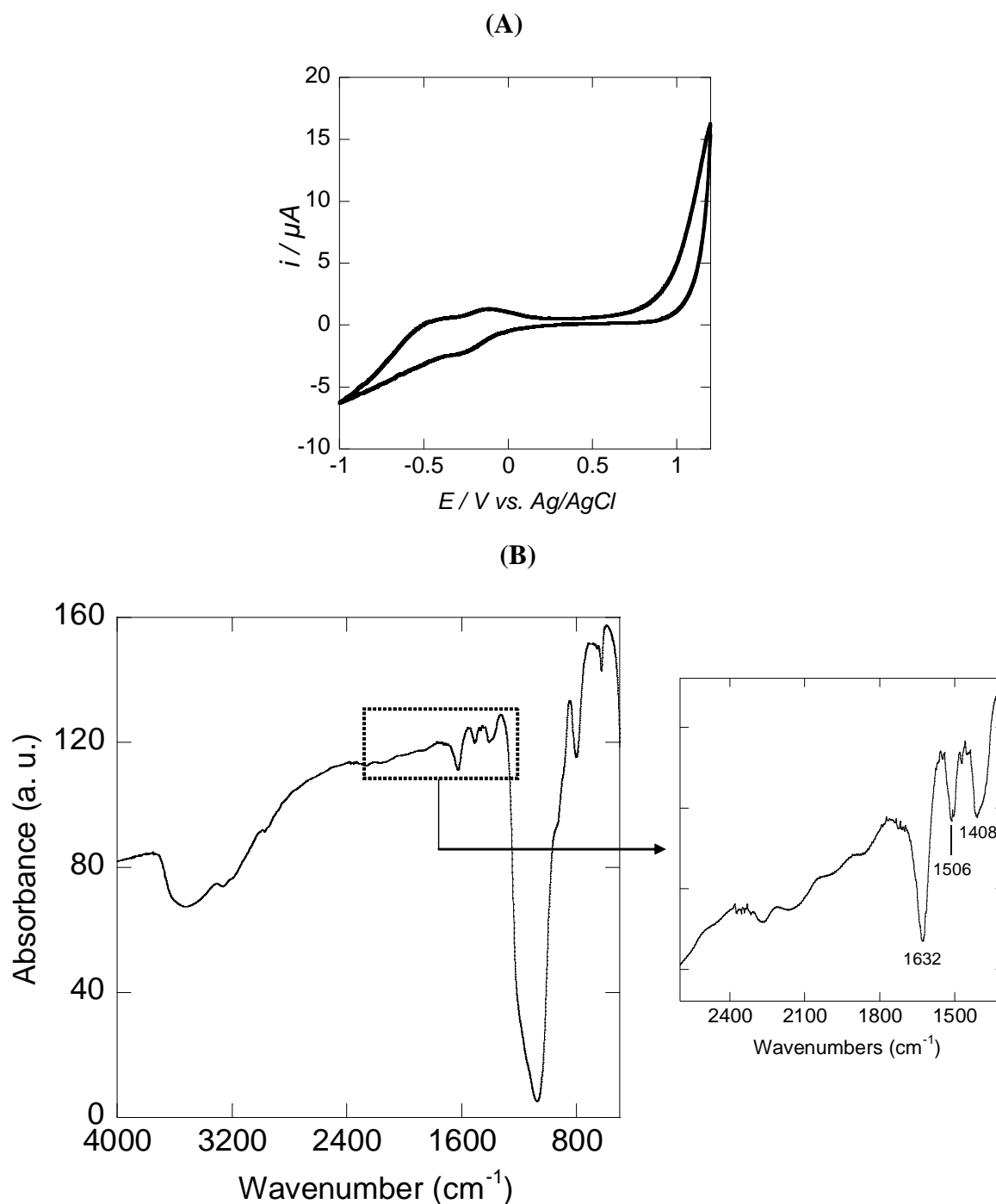


Figure 4.19. (A) Cyclic voltammogram of the BF_4 -doped polythiophene film formed galvanostatically (0.05 mA cm^{-2} ; $t = 40 \text{ min}$): electrolyte solution: $\text{CH}_3\text{CN}/0.1 \text{ M Bu}_4\text{NBF}_4$, scan rate: 0.02 V s^{-1} ; (B) transmission FT-IR of PSi/polythiophene hybrid structure.

Figure 4.20A displays the SEM images of a freshly prepared PSi substrate. The porous layer displays an average pore diameter of approximately 5 nm and a thickness of 1.25 μm . After galvanostatic formation of polythiophene, a smooth and compact of $\sim 20 \text{ nm}$ thick film is observed **Figure 4.20B**. The absence of visible pores in the SEM image agrees well with a polymerization reaction inside the pores and on the top surface.

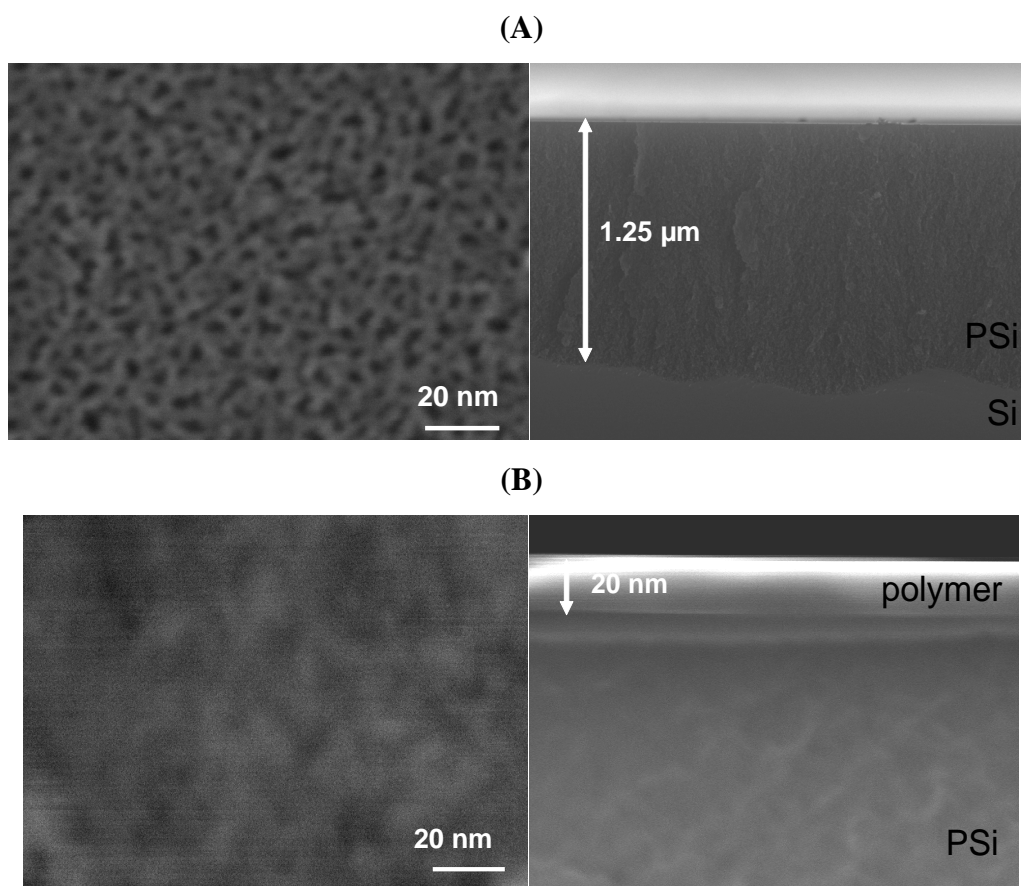


Figure 4.20. SEM micrographs of the as-prepared PSi surface (A) and PSi/polythiophene hybrid structure formed galvanostatically (0.05 mA cm^{-2} ; $t = 40 \text{ min}$) (B): cross-sectional (left) and top (right) views.

SEM-EDX analysis of the polythiophene-covered interface shows the presence of sulfur (0.34 norm.at.%), carbon (3.92 norm.at.%) and Si substrate (35.97 norm.at.%). The polymer is covering the surface evenly as exhibited via EDX-imaging (**Figure 4.21**).

4.5 Conclusion

Azide termination was obtained by the chemical reaction of hydroxyl-terminated BDD surface with 4-azidobenzoic acid under mild conditions.

The attachment of an electroactive ferrocene moiety on the azide-terminated BDD surface was achieved in high selectivity and yield using click chemistry.

Furthermore, the applicability of the azide-alkyne [3+2] cycloaddition was successfully demonstrated with ethynyl thiophene on BDD surface and PSi surface. Electrochemical polymerization of terminal “thiophene” units with thiophene monomer in solution led to the formation of a polythiophene film covalently linked to the BDD and PSi surface.

Synthesized alkyne-functionalized cyclophane also undergoes click chemistry to conveniently attach these units onto a preformed azide-functionalized BDD surface.

In conclusion, we have demonstrated that “click” chemistry can be successfully applied for coupling functional molecules bearing a terminal acetylene group to azide-terminated BDD surfaces. Because of the gentle nature of the procedure, the strategy developed in this work can be used as a general platform to prepare functionalized surfaces for various applications.

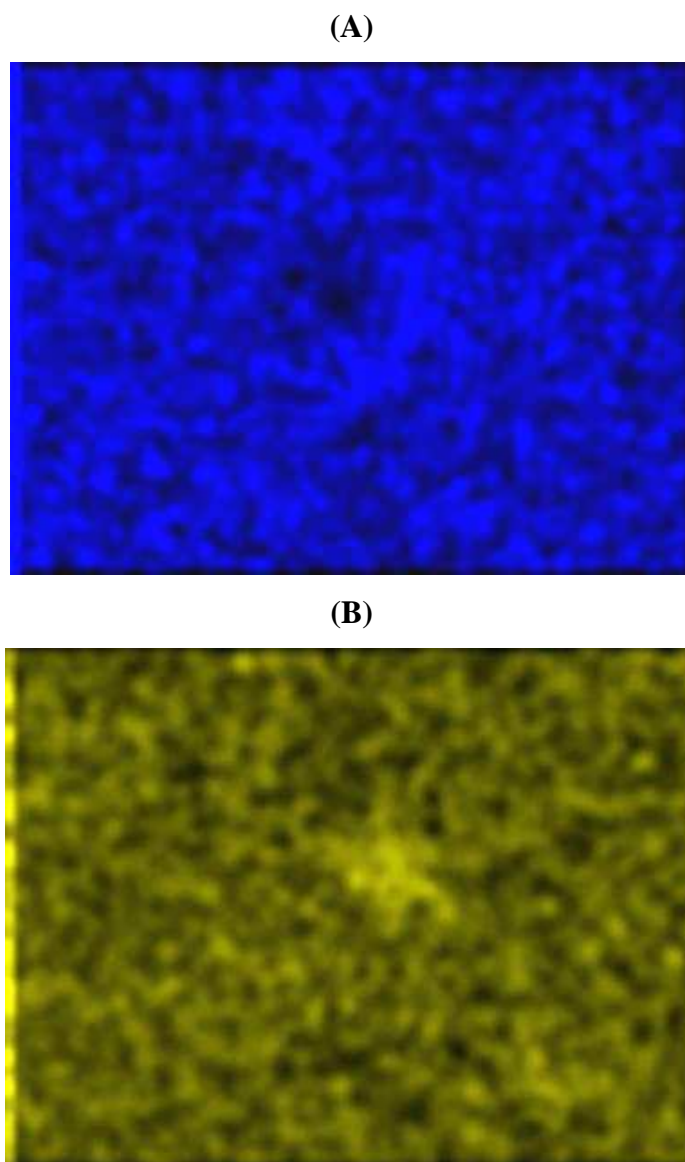


Figure 4.21. Energy Dispersive X-ray (EDX) images of polythiophene electrochemically deposited on thiophene-terminated PSi surface: C (A) and S (B).

4.6 Perspectives

The resulting polythiophene-terminated BDD will be studied further for applications in

various fields, including light emitting diodes and sensors. The optical and electrical properties of the polymer/BDD junction are currently under investigation in our laboratory.

Based on the successful linking of cyclophane to the azide-terminated BDD surface, we are currently exploiting the covalent coupling of the corresponding rotaxane and catenane onto azide terminated BDD surfaces using click chemistry.

In summary, the applicability of this reaction scheme for coupling alkyne-terminated carbohydrates and other alkyne-functionalized molecules to flat supports is currently under investigation in our laboratory.

4.7 References

1. H. C. Kolb; M. G. Finn; K. B. Sharpless. *Angew. Chem. Int. Ed.* **2001**, 40, 2004.
2. R. Huisgen; *Pure Appl. Chem.* **1989**, 61, 613.
3. V. V. Rostovtsev; L. G. Green; V. V. Fokin; K. B. Sharpless. *Angew. Chem. Int. Ed.* **2002**, 41, 2596.
4. C. V. Tornøe; C. Christensen; M. Meldal. *J. Org. Chem.* **2002**, 67, 3057.
5. H. C. Kolb; K. B. Sharpless. *Drug Discovery Today.* **2003**, 8, 1128.
6. W. H. Binder; R. Sachsenhofer; *Macromol. Rapid Commun.* **2007**, 28, 15.
7. J. F. Lutz. *Angew. Chem. Int. Ed.* **2007**, 46, 1018.
8. N. K. Devaraj; J. P. Collman. *QSAR Comb. Sci.* **2007**, 26, 1253.
9. S. Ciampi; T. Böcking, K. A. Kilian; M. James; J. B. Harper; J. J. Gooding. *Langmuir.* **2007**, 23, 9320.
10. A. G. Marrani; E. A. Dalchiele; R. Zanoni; F. Decker; F. Cattaruzza; D. Bonifazi; M. Prato. *Electrochim. Acta.* **2008**, 53, 3903.
11. F. Himo; T. Lovell; R. Hilgraf; V. V. Rostovtsev; L. Noodleman; K. B. Sharpless; V. V. Fokin. *J. Am. Chem. Soc.* **2005**, 127, 210.
12. J. P. Collman; N. K. Devaraj; C. E. D. Chidsey. *Langmuir.* **2004**, 20, 1051-1053.
13. J. K. Lee; Y. S. Chi; I. S. Choi. *Langmuir.* **2004**, 20, 3844-3847.
14. N. K. Devaraj; R. A. Decreau; W. Ebina; J. P. Collman; C. E. D. Chidsey. *J. Phys. Chem. B.* **2006**, 110, 15955-15962.
15. J. P. Collman; N. K. Devaraj; T. P. A. Eberspacher; C. E. D. Chidsey. *Langmuir.* **2006**, 22, 2457-2464.
16. D. A. Fleming; C. J. Thode; M. E. Williams. *Chem. Mater.* **2006**, 18, 2327-2334.
17. H. Li; F. Cheng; A. M. Duft; A. Adronov. *J. Am. Chem. Soc.* **2005**, 127, 14518-14524.

18. T. Lummerstorfer; H. Hoffmann. *J. Phys. Chem. B.* **2004**, 18, 3963-3966.
19. M. Ortega-Muñoz; J. Lopez-Jaramillo; F. Hernandez-Mateo; F. Santoyo-Gonzalez. *Adv. Synth. Catal.* **2006**, 348, 2410-2420.
20. M. A. White; J. A. Johnson; J. T. Koberstein; N. J. Turro. *J. Am. Chem. Soc.* **2006**, 128, 11356-11357.
21. S. Ciampi; T. Böcking; K. A. Kilian; M. James; J. B. Harper; J. J. Gooding. *Langmuir.* **2007**, 23, 9320-9329.
22. A. G. Marrani; E. A. Dalchiele; R. Zanoni; F. Decker; F. Cattaruzza; D. Bonifazi; M. Prato. *Electrochimica Acta.* **2008**, 53, 3903-3909.
23. R. V. Ostaci, D. Damiron, S. Capponi, G. Vignaud, Léger, Y. Grohens, E. Drockenmuller, *Langmuir*, **2008**, 24, 2732-2739.
24. S. Ciampi; T. Böcking; K. A. Kilian; J. B. Harper; J. J. Gooding. *Langmuir.* **2008**, 24, 5888-5892.
25. P. Bouvier; D. Delabouglise; A. Denoyell; B. Marcus; M. Mermoux; J. P. Petit. *Electrochem. Solid-State Lett.* **2005**, 8, E57.
26. D. Delabouglise; B. Marcus; M. Mermoux; P. Bouvier; J. Chane-Tune; J. P. Petit; P. Mailley; T. Livache. *Chem. Comm.* **2003**, 2698.
27. S. Szunerits; N. Shirahata; P. Actis; J. Naknishir; R. Boukherroub. *Chem. Commun.* **2007**, 2793.
28. H. C. Kolb; M. G. Finn; K. B. Sharpless. *Angew. Chem. Int. Ed.* **2001**, 40, 2004-2021.
29. V. V. Rostovtsev; L. G. Green; V. V. Fokin; K. B. Sharpless. *Angew. Chem. Int. Ed.* **2002**, 41, 2596.
30. M. T. Lee; G. S. Ferguson. *Langmuir* **2001**, 17, 762.
31. S. A. AlBataineh; L. G. Britcher; H. J. Griesser. *Surf. Sci.* **2006**, 600, 952.
32. C. Haensch; S. Hoeppe; U. S. Schubert. *Nanotechnology.* **2008**, 19, 035703-035710.
33. R. Boukherroub; X. Wallart; S. Szunerits; B. Marcus; P. Bouvier; M. Mermoux. *Electrochem. Comm.* **2005**, 7, 937.
34. E. A. Dalchiele; A. Aurora; G. Bernardini; F. Cattaruzza; A. Flamini; P. Pallavicini; R. Zanoni; F. Decker. *J. Electroanal. Chem.* **2005**, 579, 133-142.
35. R. Zanoni; F. Cattaruzza; C. Coluzza; E. A. Dalchiele; F. Decker; G. Di Santo; A. Flamini; L. Funari; A. G. Marrani. *Surf. Sci.* **2005**, 575, 260-272.
36. R. D. Rohde; H. D. Agnew; W.S. Yeo; R. C. Bailey; J. R. Heath. *J. Am. Chem. Soc.* **2006**, 128, 9518-9525.
37. J. P. Collman; N.K. Devaraj; C. E. D. Chidsey. *Langmuir.* **2004**, 20, 1051-1053.

38. R. D. Rohde; H. D. Agnew; W. S. Yeo; R. C. Bailey; J. R. Heath. *J. Am. Chem. Soc.* **2006**, 128, 9518-9525.
39. A. M. Napper; H. Haiying Liu; D. H. Waldeck. *J. Phys. Chem. B.* **2001**, 105, 7699-7707.
40. J. Zyss; J. F. Nicoud. *Curr. Opin. Solid-State Mater. Sci.* **1996**, 1, 533-546.
41. A. Malinauskas. *Polymer* **2001**, 42, 3957-3972.
42. J. M. Buriak. *Chem. Rev.* **2002**, 102, 1272.
43. R. Boukherroub. *Curr. Opin. Solid-State Mater. Sci.* **2005**, 9, 66-72.
44. D. G. Castner; K. Hinds; D. W. Grainger. *Langmuir.* **1996**, 12, 5083-5086.
45. T. Ishida; M. Hara; I. Kojima; S. Tsuneda; N. Nishida; H. Sasabe; W. Knoll. *Langmuir.* **1998**, 14, 2092-2096.
46. B. Fabre; G. P. Lopinski; D. D. M. Wayner. *J. Phys. Chem. B.* **2003**, 107, 14326-14335.
47. B. Liedberg; Z. Yang; I. Engquist; M. Wirde; U. Gelius; G. Gotz; P. Bäuerle; R. M. Rummel; Ch. Ziegler; W. Gopel. *J. Phys. Chem. B.* **1997**, 101, 5951-5962.
48. G. Tourillon; Y. Jugnet. *J. Chem. Phys.* **1988**, 89, 1905-1913.
49. P. Dannetun; M. Boman; S. Stafstrom; W. R. Salaneck; R. Lazzaroni; C. Fredriksson; J. L. Bredas; R. Zamboni; C. Taliani. *J. Chem. Phys.* **1993**, 99, 664-672.
50. Y. Wei; C. C. Chan; J. Tian; G. W. Jang; K. F. Hsueh. *Chem. Mater.* **1991**, 3, 888.
51. A. Yassar; J. Roncali; F. Garnier. *Macromolecules.* **1989**, 22, 804.
52. E. W. Tsai; S. Basak; J. P. Ruiz; J. R. Reynolds; K. Rajeshwar. *J. Electrochem. Soc.* **1989**, 136, 3683.
53. O. S. Miljanic; W. R. Dichtel; S. Mortezaei; J. F. Stoddart. *Org. Lett.* **2006**, 8, 4835-4838.
54. W. R. Dichtel; O. S. Miljanic ; J. M. Spruell; J. R. Heath; J. F. Stoddart. *J. Am. Chem. Soc.* **2006**, 128, 10388-10390.
55. P. Mobian; J. P. Collin; J. P. Sauvage. *Tetrahedron Lett.* **2006**, 47, 4907-4909.
56. V. Aucagne; K. D. Haenni; D. A. Leigh; P. J. Lusby; D. B. Walker. *J. Am. Chem. Soc.* **2006**, 128, 2186-2187.
57. D. Tuncel; J. H. G. Steinke. *Macromolecules.* **2004**, 37, 288-302.
58. A. I. prahamian; W. R. Dichtel; T. Ikeda; J. R. Heath; J. F. Stoddart. *Org. Lett.* **2007**, 9, 1287-1290.
59. A. B. Braunschweig; W. R. Dichtel; O. S. Miljanic; M. A. Olson; J. M. Spruell; S. I. Khan; J. R. Heath; J. F. Stoddart. *Chem. Asian J.* **2007**, 2, 634.
60. J. M. Spruell; M. R. Dichtel; J. R. Heath; J. F. Stoddart. *Chem. Eur. J.* **2008**, 14, 4168-4177.
61. M. Bria; Julien Bigot; G. Cooke ;J. Lyskawa; G. Rabani; V. M. Rotello ; P. Woisel.

- Tetrahedron*. **2009**, 65, 400-407.
62. P. L. Anelli; P. R. Ashton; R. Ballardini; V. Balzani; M. Delgado; M. T. Gandolfi; T. T. Goodnow; A. E. Kaifer; D. Philp; M. Pietraszkiewicz; L. Prodi; M. V. Reddington; M. V. Slawin; A. M. Z. Spencer; J. F. Stoddart; C. Vicent; D. J. Williams. *J. Am. Chem. Soc.* **1992**, 114, 193-218.
63. B. Fabre; G. P. Lopinski; D. D. M. Wayner. *J. Phys. Chem. B.* **2003**, 107, 14326.
64. B. Fabre; D. D. M. Wayner. *J. Electroanal. Chem.* **2004**, 567, 289.
65. M. Can; K. Pekmez; N. Pekmez; A. Yildiz. *Synth. Met.* **1999**, 104, 9.
66. G. Zotti; S. Cattarin; N. Comisso. *J. Electroanal. Chem.* **1987**, 235, 259.

CHAPTER 5

FUNCTIONALIZATION OF OXYGENATED BORON-DOPED DIAMOND SURFACE WITH AN IONIC LIQUID

5.1. Introduction

Ionic liquids are composed entirely of ions. For example, molten sodium chloride is an ionic liquid; in contrast, a solution of sodium chloride in water (a molecular solvent) is an ionic solution. The most widely used ionic liquids are probably imidazolium based salts.

Room-temperature ionic liquids (ILs) are widely used as clean solvents and catalysts for green chemistry [1-6]. Their properties such as hydrophobicity, hydrophilicity, and viscosity can be tuned by controlling the nature of the counter anion or the alkyl chain on the cation. The chemical stability and toxicity of the ionic liquid also depends on the anion used. While the widely used counter anions such as PF_6^- and BF_4^- can hydrolyze to HF when heated in the presence of water, methyl sulfate anions have been shown to be more biodegradable[5,6]. This drawback has prompted some companies to introduce alternate anions, though many of these are still fluorinated materials. In these ILs, the fluorine of the anion is bonded to carbon, the C-F bond being inert to hydrolysis. Thus, ILs based upon CF_3SO_3^- , $(\text{CF}_3\text{SO}_3)_2\text{N}^-$ and related anions are being marketed [7].

This new class of salts displays, along with low vapour pressure, thermal stability, high ionic conductivity, and remarkable solubility. These properties have been exploited for the functionalization of carbon materials. Indeed, the use of conventional ionic liquids (ILs) to exfoliate and functionalize single-walled carbon nanotubes with aryldiazonium salts was reported by Tour et al. [8]. The chemical reaction was conducted at room temperature in the presence of ILs and K_2CO_3 . Independently, Liang et al. have synthesized a new class of stable, conductive, and hydrophobic room-temperature ILs based on diazonium salts. The liquid

nature of the diazonium IL was exploited for the modification of carbon substrates by either thermal decomposition or electrochemical reduction of the diazonium ion [9].

Recently, we have combined the environmentally benign properties of ionic liquids with the high reactivity of aryldiazonium salts for the green chemical derivatization of hydrogen-terminated boron-doped diamond [10] and glassy carbon (GC) electrodes[11]. Reaction of the BDD or glassy carbon substrates with 4-nitroazobenzene (NAB) in conventional ionic liquids takes place under mild conditions. The reaction was performed at room temperature for 1h in 1-butyl-3-methylimidazolium methyl sulphate (hydrophilic) and in 1-butyl-3-methylimidazolium hexafluorophosphate (hydrophobic) to yield organic layers covalently attached to the surface through C-C bonds.

The wetting properties of the IL can be easily varied by changing the alkyl chain length of the IL cations. The longer the alkyl chain lengths of the IL cations are, the more hydrophobic are the ionic liquid (IL) cations and more difficult to be transported into aqueous phases *via* ion exchange [12]. Accordingly, the ion-exchange process is another unique property of IL-based extractions involving charged species, and the more hydrophobic anions give rise to not only greater distribution coefficients but also the less losses of ionic liquids (ILs).

5.2. Objectives

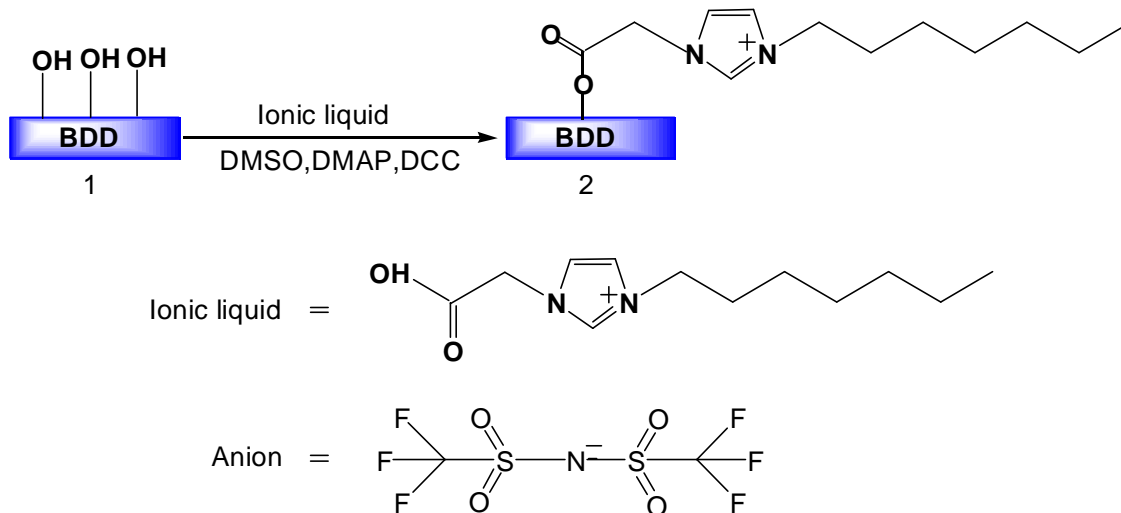
In this chapter, we have performed esterification reaction of hydroxyl-terminated boron-doped diamond with an ionic liquid (IL): 1-(Methyl carboxylic acid) -3-octylimidazolium-bis (trifluoromethyl sulfonyl) imide), as shown in **Scheme 5.1**. The effect on the wetting properties by exchanging chemically the counter ion of the covalently linked IL was investigated.

5.3. Results and discussion

5.3.1. XPS characterization

Figure 5.1 shows the XPS survey spectrum of ionic liquid (IL) functionalized BDD surface. It displays peaks at 285eV due to C1s and a peak at 532eV due to O1s as in the initial

oxidized BDD sample. Additional peaks at 689eV, characteristic peak of F 1s, at ~ 402eV due to nitrogen (N1s) and at 168eV due to S2p clearly indicate the successful covalent linking of the ionic liquid to the hydroxyl-terminated boron-doped diamond. The presence of N1s (7.98%), F1s (16.4%) and S2p (5.09%) next to C1s (53.11%) and O1s (15.11%) is in agreement with the grafting of the IL onto the diamond surface. Some Si (2.31%) was in addition detected, which can be assigned to the underlying interface onto which diamond had been deposited. The ratio of N/F = 0.49 and S/F=0.31 are comparable to the theoretical values being N/F = 0.50 and S/F=0.33. High resolution XPS investigation of C1s, N1s, F1s and S2p were explored for further analysis.



Scheme 5.1. Schematic illustration of the chemical functionalization of oxidized BDD surface with 1-(Methylcarboxylic acid)-3-octylimidazolium-bis (trifluoromethylsulfonyl)imide).

The XPS high resolution spectrum of C1s of the ionic liquid terminated BDD surface could be resolved into five component peaks: a hydrocarbon (C-C) peak located at 284.0eV, a peak due to ether (C-O-C) groups at 287.2eV, a peak due to amide (N-C) at 286.5eV, a C=O peak at 289eV and a C-F peak at 292.6eV (**Figure 5.2**). The N-C and C-F peaks can be unambiguously assigned to the ionic liquid.

Figure 5.3 displays the high resolution XPS spectrum of the N1s of the ionic liquid derivatized BDD surface. Contributions from S-N (399eV) and N-C (402eV) with a proportion of ~1/2 can be clearly observed. The peak at 399eV can be attributed to the nitrogen bonded to the sulfonyl groups. However, the major component associated with a high

binding energy (402eV) is due to the imine group in the form of imidazolic ring, according to the literature [13-17].

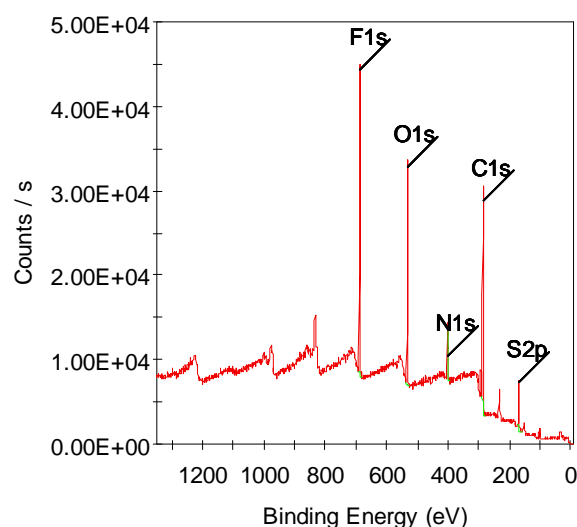


Figure 5.1. XPS survey spectrum of 1-(methylcarboxylacid)-3-octylimidazolium-bis (trifluoromethyl sulfonyl) imide) modified BDD surface.

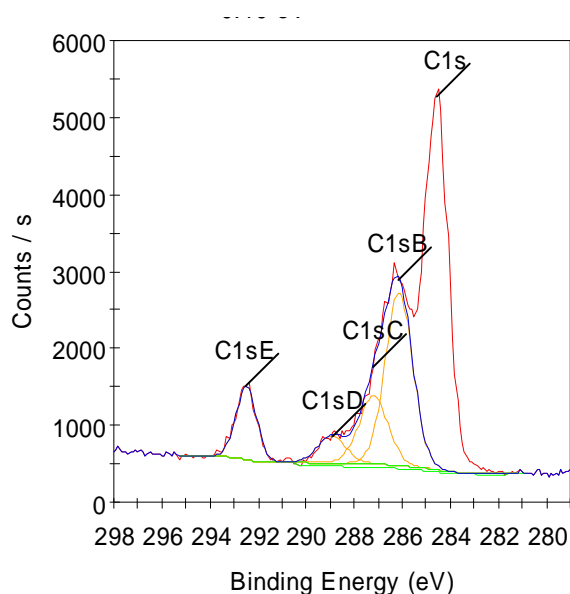


Figure 5.2. High-resolution XPS spectrum of the C1s band of 1-(methyl carboxylic acid) -3-octylimidazolium-bis (trifluoromethyl sulfonyl) imide) terminated BDD surface.

Figure 5.4A shows the high-resolution XPS spectrum of the F 1s peak centered at 688.9eV, which can be related to the fluorine in CF₃ groups of the IL anion. The high-resolution XPS of the S2p can be decomposed into two components S2p_{3/2} and S2p_{1/2} located at 168.5 and

169.8eV, respectively (**Figure 5.4B**). The ratio of these two bands clearly indicates that the S species exists mainly in its $2p_{3/2}$ state and can be related to sulfur in sulfonyl configuration.

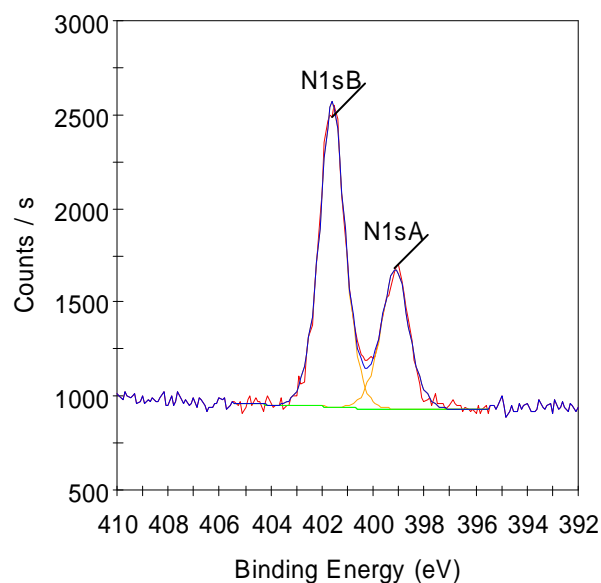


Figure 5.3. High-resolution XPS spectrum of the N1s band of 1-(methylcarboxylacid) -3-octylimidazolium-bis (trifluoromethyl sulfonyl)imide)modified BDD surface.

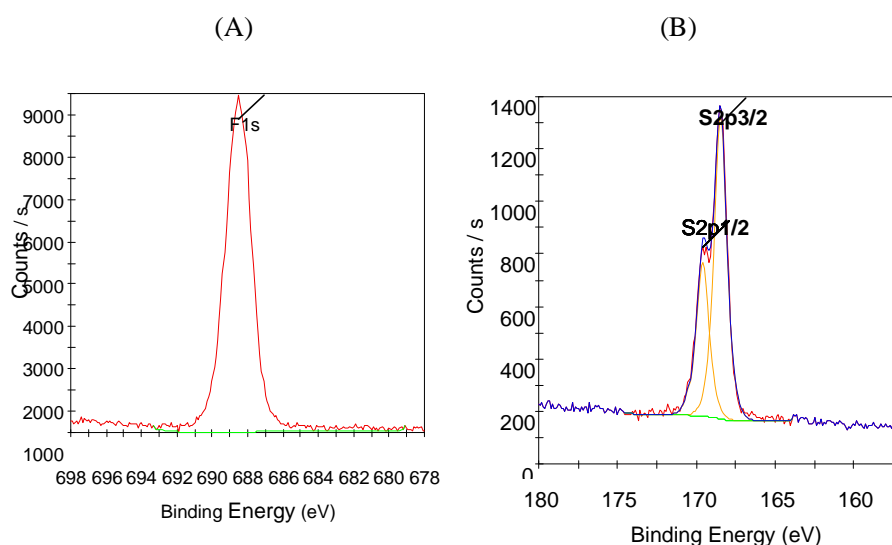


Figure 5.4. High-resolution XPS spectrum of the F1s (A) and S2p bands of the ionic liquid-terminated BDD surface.

To confirm the covalent linking of the IL onto the oxidized BDD surface, the reaction was carried out in the absence of the coupling agent and catalyst (DCC and DMAP) (**Scheme 5.1**).

Figure 5.5 displays the XPS survey spectrum of the oxidized BDD surface immersed in the

IL without DCC and DMAP. It exhibits peaks due to C1s and O1s, in agreement with the absence of covalent linking of the IL. From the high-resolution XPS spectrum of the C1s (**Figure 5.6**), it can be seen that C-O (20%) and C=O (4.7%) bands are formed, while the peaks due to N-C and C-F (characteristic peaks of the IL) did not appear as before. The result suggests that the coupling agent (DCC) and the catalyst (DMAP) are required for coupling the IL to the terminal hydroxyl groups of the oxidized BDD surface.

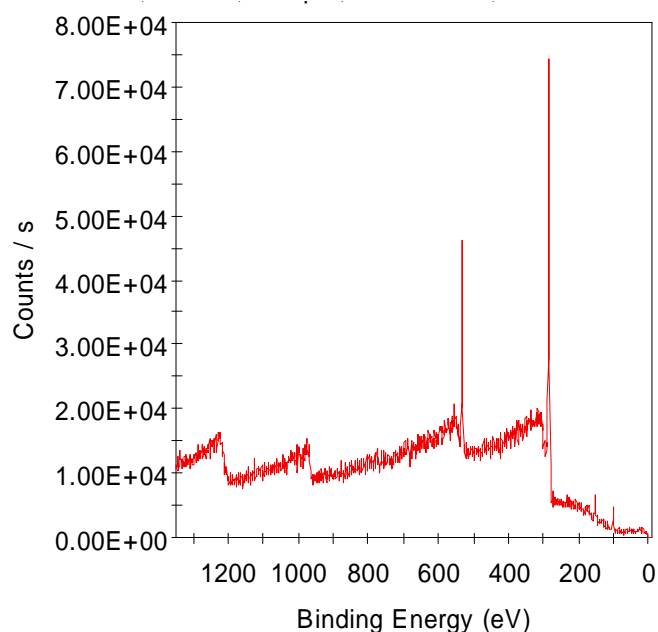


Figure 5.5. XPS survey spectrum of oxidized BDD surface modified with 1-(methyl carboxylic acid)-3-octylimidazolium-bis (trifluoromethyl sulfonyl) imide) in absence of the coupling agent (DCC) and catalyst (DMAP).

5.3.2. Electrochemical investigation

Due the high boron content of the diamond, this interface can also investigated using cyclic voltammetry (**Figure 5.7**). **Figure 5.7A** shows the electroactive window of the oxidized (**curve 1**) in comparison of the IL modified BDD (**curve 2**). The presence of the covalently attached IL reduces the electroactive window slightly. However, it seems the oxidation/reduction is highly catalyzed as seen in the broad wave at $E = -1\text{V}/\text{Ag}/\text{AgCl}$. **Figure 5.7B** displays the i - E curves for an aqueous solution of $10\text{ mM Fe}(\text{CN})_6^{4-}$ in 0.1M KCl at an oxidized diamond and at an IL modified BDD surface. The oxidized diamond inhibits electrode kinetics, as reported previously by us and others [18, 19]. The presence of the IL

shows only a slight attenuation of the peak current but an increase in irreversibility. This indicates that the IL is not blocking electron transfer to the underlying diamond interface. This could be due to the positively charged amine group of the imidazole ring, showing electrostatic interaction with the negatively charged $\text{Fe}(\text{CN})_6^{4-}$ mediator.

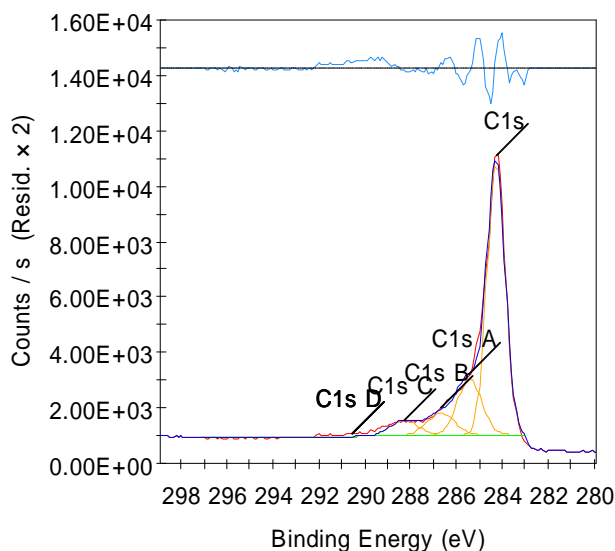


Figure 5.6. High resolution XPS spectrum of the C1s of oxidized BDD surface modified with 1-(methyl carboxylic acid)-3-octylimidazolium-bis (trifluoromethyl sulfonyl) imide) in absence of the coupling agent (DCC) and catalyst (DMAP).

5.3.3. Water contact angle measurements

Water contact angle measurements were used to follow the changes in the wetting properties of the boron-doped diamond electrode before and after functionalization. As-grown diamond surface exhibits a water contact angle of $\sim 94 \pm 2^\circ$ (**Figure 5.8 (a)**). The hydrophobic character of the surface is assigned to the hydrophobic nature of the C-H bonds terminating the hydrogen-terminated surface. After oxidation with UV/ozone, the water contact angle decreased to $8 \pm 2^\circ$ (**Figure 5.8 (b)**).

After treatment with 1-(methylcarboxylic acid)-3-octylimidazolium-bis (trifluoromethyl sulfonyl) imide), the contact angle of the IL-terminated BDD surface shows a significant increase to $72 \pm 2^\circ$, which is a good indication for IL covalent bonding on the BDD surface (**Figure 5.1 (c)**).

5.4. Anion exchange reactions

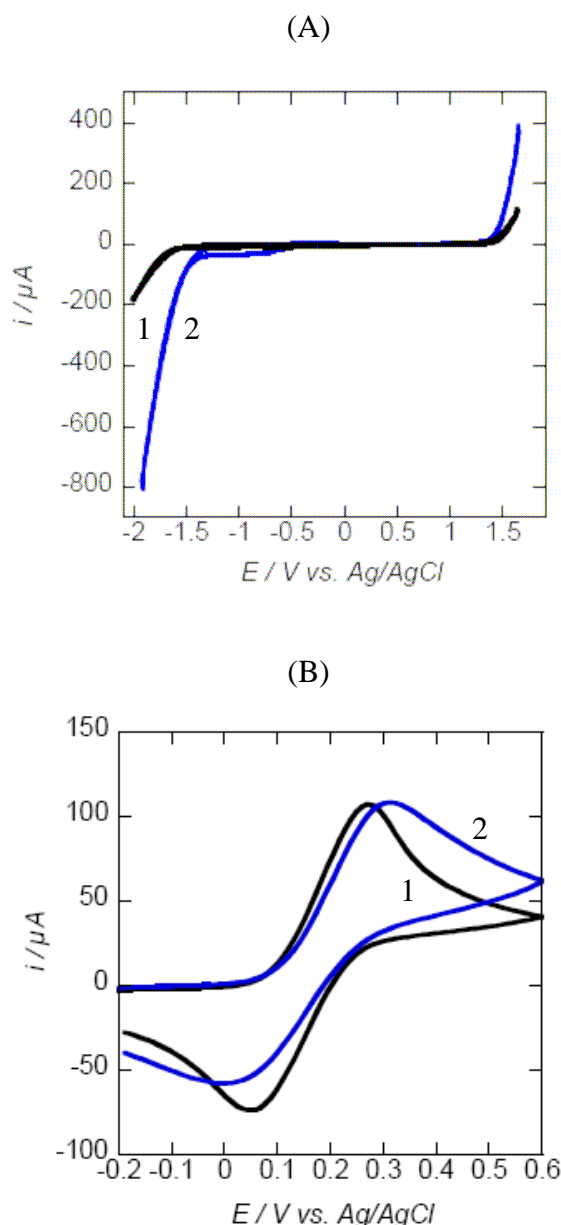


Figure 5.7. Cyclic voltammogram of oxidized (curve 1) BDD and IL modified one (curve 2). Scan rate: 50 mV s^{-1} , electrolytes: (A) KCl (0.1 M/water), (B) $\text{Fe}(\text{CN})_6^{4-}$ (10 mM)/KCl (0.1M/water).

IL-terminated BDD surface was subjected to anion exchange between $(\text{CF}_3\text{SO}_3)_2\text{N}^-$ and BF_4^- for several times. After a first exchange with BF_4^- anion, the contact angle of the BDD surface dropped to $22 \pm 2^\circ$ (**Figure 5.9 (2)**), displaying a more hydrophilic character. The contact angle increased back to $70 \pm 2^\circ$ (**Figure 5.9 (3)**) after immersion in $(\text{CF}_3\text{SO}_3)_2\text{N}^-$ aqueous solution for 24h at room temperature. Comparing **Figure 5.9 (3)** with **Figure 5.9 (1)**, there is a very slight contact angle decrease, which can be attributed to reaction efficiency due to reaction equilibrium. Based on this result, it is also easy to understand that after a second

exchange with BF_4^- anion, the contact angle decreased to $33\pm 2^\circ$, but not to $22\pm 2^\circ$ (**Figure 5.9 (4)**). As well a value of $46\pm 2^\circ$ (not $72\pm 2^\circ$) (**Figure 5.9 (5)**) was measured for contact angle of a BDD surface after a second exchange back to $(\text{CF}_3\text{SO}_3)_2\text{N}^-$ anion. After a third exchange with BF_4^- anion, the surface contact angle measured was $35\pm 2^\circ$.

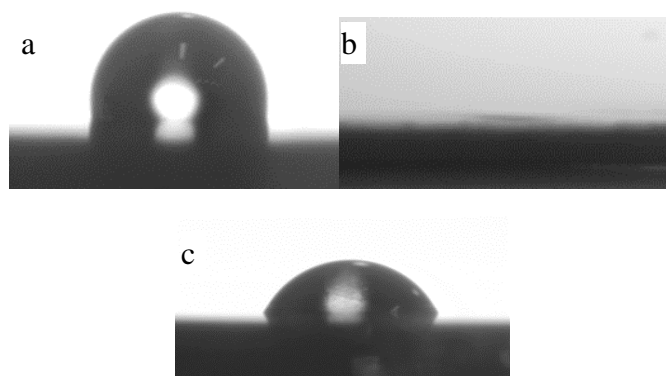


Figure 5.8. Contact angle of a hydrogen-terminated BDD surface before (a) and after UV/ozone oxidation (b), and surface after modification with IL (c).

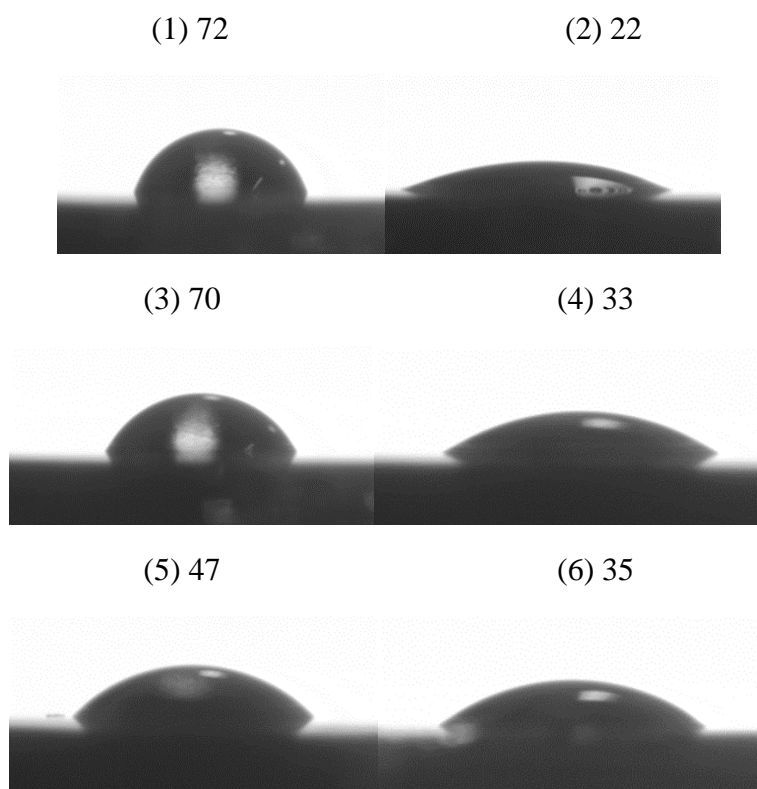


Figure 5.9. Contact angle of 1-(methylcarboxylacid)-3-octylimidazolium-bis(trifluoromethyl sulfonyl)imide modified BDD surface (1), after first exchange with BF_4^- anion (2), after exchanging back to $(\text{CF}_3\text{SO}_3)_2\text{N}^-$ anion (3), after second exchange with BF_4^- anion (4), after exchanging back to $(\text{CF}_3\text{SO}_3)_2\text{N}^-$ anion (5) and after third exchange with BF_4^- anion(6).

The variation of the contact angle of the BDD surface was further displayed in **Figure 5.10**. The first alternation cycle shows excellent regeneration of $(\text{CF}_3\text{SO}_3)_2\text{N}^-$ anion (**Figure 5.10** ($x=3$)). However, an obvious contact angle increase from **Figure 5.10** ($x=2$) to **Figure 5.10** ($x=4$) was observed, while subsequent regeneration of $(\text{CF}_3\text{SO}_3)_2\text{N}^-$ anion led to a much smaller contact angle (**Figure 5.10** ($x=5$)). Finally, **Figure 5.10** ($x=6$) shows no significant change, as compared to **Figure 5.10** ($x=4$). As discussed above, the reaction efficiency results in contact angle variation.

Anyway, the contact angle of the IL modified BDD varied alternatively in the whole process of anion exchange reactions between $(\text{CF}_3\text{SO}_3)_2\text{N}^-$ and BF_4^- anions. Optimization of the anion exchange conditions is currently under investigation in our laboratory.

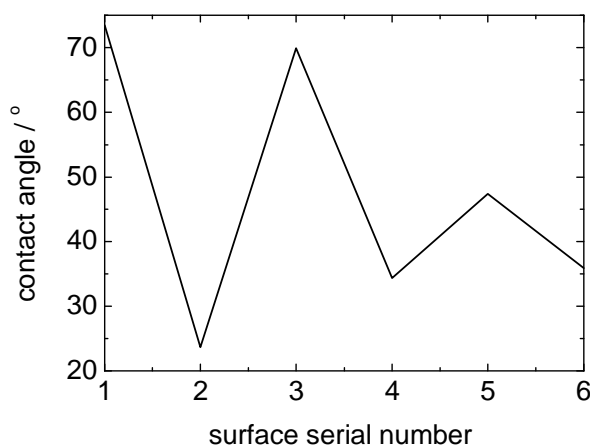


Figure 5.10. Change of water contact angle of a BDD surface after several anion exchange between $(\text{CF}_3\text{SO}_3)_2\text{N}^-$ and BF_4^- (axis $x=1, 2, 3, 4, 5, 6$ in this graph are corresponding to the serial number of **Figure 5.9**)

Finally, the anion exchange of $(\text{CF}_3\text{SO}_3)_2\text{N}^-$ anion of the IL modified BDD surface with NO_3^- and PF_6^- anions was also investigated. The contact angle values of the resulting IL modified BDD surfaces are shown in **Table 5.1**. After exchanging $(\text{CF}_3\text{SO}_3)_2\text{N}^-$ with NO_3^- anion, a value of $50 \pm 2^\circ$ was measured, while exchanging with PF_6^- anion yielded a hydrophilic character and the contact angle significantly dropped to $20 \pm 2^\circ$.

5.5. Conclusion

In summary, we have demonstrated that the esterification reaction can be successfully applied for coupling an ionic liquid bearing a carboxylic acid group to hydroxyl-terminated BDD electrodes. The covalent attachment of 1-(methylcarboxylacid)-3-octylimidazolium-bis(trifluoromethyl sulfonyl) imide) was achieved in high selectivity and yield. Anion exchange reactions between $(\text{CF}_3\text{SO}_3)_2\text{N}^-$ and BF_4^- anion were carried readily even though the exchanging efficiency on BDD surface decreased gradually in the course of the reactions. This technique opens up new opportunities for chemical functionalization of diamond surfaces with ionic liquids for fundamental studies of electrochemical process at the modified electrodes and for potential applications in the field of tribology.

Table 5.1. Contact angle of different ILs modified BDD surface

Anion	Contact angle (°)
$(\text{CF}_3\text{SO}_3)_2\text{N}^-$	72±2
NO_3^-	50±2
PF_6^-	20±2

5.6. Perspectives

BF_4^- anion exchange conditions are under optimization to get higher yields. Other anions will be exploited in the same way in order to broaden the ionic liquid structure and the resulting electrochemical characteristics.

5.7. References

1. M. C. Buzzeo; R. G. Evans; R. G. Compton. *Chem. Phys. Chem.* **2004**, 5, 1107.
2. R. D. Roger; K. R. Seddon. Ionic Liquids: industrial applications for green chemistry: ACS Symposium. *American Chemical Society: Washington DC.* **2002**.
3. B. Ohtani; Y. H. Kim; T. Yano; K. Hashimoto; A. Fujishima; K. Uosaki. *Chem. Lett.* **1998**, 953, 954.

4. P. Wasserscheid; T. Welton. *Ionic Liquids in Synthesis*. Wiley-VCH: Weinheim, **2003**.
5. J. Ranke; S. Stolte; R. Stormann; J. Arning; B. Jastorff. *Chem. Rev.* **2007**, 107, 2183-2206.
6. M. Matzke; S. Stolte; K. Thiele; T. Juffernholz; J. Arning; J. Ranke; U. Welz-Biermann; B. Jastorff. *Green Chem.* **2007**, 9, 760.
7. J. H. Davis; P. A. Fox. *Chem. Commun.* **2003**, 1209-1222.
8. B. K. Price; J. L. Hudson; J. M. Tour. *J. Am. Chem. Soc.* **2005**, 127, 14867.
9. C. Liang; J. F. Huang; Z. Li; H. Luo; S. Dai. *J. Org. Chem.* **2006**, 586.
10. G. Shula; P. Actis; B. Marcus; M. Opallo; R. Boukherroub; S. Szunerits. *Diam. Relat. Mater.* **2008**, 17, 1394-1398.
11. P. Actis; G. Caulliez; G. Shul; M. Opallo; M. Mermoux; B. Marcus; R. Boukherroub; S. Szunerits. *Langmuir.* **2008**, 24, 6327-6333.
12. H. Luo; S. Dai; P. V. Bonnesen. *Symposia Papers Presented Before the Division of Environmental Chemistry American Chemical Society*. Anaheim, CA. March 28-April 1, **2004**.
13. R. Foerch; N. S. Mc Intyre; D. H. Hunter. *J. Polym. Sci.: Part A.* **1990**, 28, 803.
14. R. Foerch; N. S. Mc Intyre; R. N. S. Sodhi; D. H. Hunter. *J. Appl. Polym. Sci.* **1990**, 40, 1903.
15. H. Yasuda; H. C. March; S. Brandt; C. N. Reilly. *J. Polymer Sci.: Polym. Chem. Ed.* **1977**, 15, 991.
16. R. W. Paynter *Surf. Interface Anal.* **1998**, 26, 674.
17. J. Grimblot; B. Mutel; V. Moineau; T. Colson; O. Dessaux; P. Goudmand. *Surf. Interface Anal.* **2000**, 30, 415-419.
18. S. Szunerits; R. Boukherroub. *J. Solid State Electrochem.* **2008**, 12, 1205-1218.
19. M. Wang; M. R. Das; V. G. Praig; F. LeNormand; M. S. Li; R. Boukherroub; S. Szunerits. *Chem. Commun.* **2008**, 6294-6296.

CHAPTER 6

PREPARATION OF HALOGENATED BORON-DOPED DIAMOND ELECTRODES AND THEIR REACTIVITY

6.1. Introduction

Halogenation in the gas phase was one of the first surface modifications investigated on diamond surfaces. Fluorine and chlorine atoms directly react with diamond and allow surface halogenation[1-3] The conditions necessary to generate atomic species are rather vigorous and corrosive (e.g. $\text{Cl}_2/400\text{-}500^\circ\text{C}$; $\text{F}_2/470^\circ\text{C}$)[2,3]. Milder conditions can be used during photochemically initiated gas phase halogenation [4,5]. To date, the only report on the halogenation of diamond in the liquid phase has been reported by Ikeda et al. in 1998[7], who chlorinated diamond powder with sulfuryl chloride (SO_2Cl_2) aided by the radical initiator 2, 2-azobisisobutyronitrile (AIBN) at 50°C and also brominated diamond powder using Br_2 at 50°C in chloroform. The development of simple and controllable solution-based procedures for halogenation of continuous diamond films is thus still sought after.

A halogen such as bromine when reacted with an alkene causes the π -bond to break, resulting in the formation a haloalkane. This makes the hydrocarbon more reactive since bromine is a good leaving group and commonly used for further chemical reactions such as nucleophilic substitution reactions. One of the numerous substitution reactions concerns the replacement of $-\text{Br}$ by azido ($-\text{N}_3$) groups. This is of particular interest, because azide termination offers the possibility for “clicking” molecules bearing an acetylene terminal group.

The “click” chemistry on polymer and solid surfaces have been recently reviewed [8,9], and various strategies to exploit this reaction to benefit from its high selectivity, high yields and remarkable tolerance to reaction conditions are now available to surface scientists [10,11].

J. P. Collman has demonstrated successful “click” chemistry to covalently attach acetylene-bearing molecules to azide-terminated self-assembled monolayers on gold [12]. Similar report on silicon wafers was published by T. Lummerstorfer [13] (detailed in **Chapter 4**).

6.2. Objectives

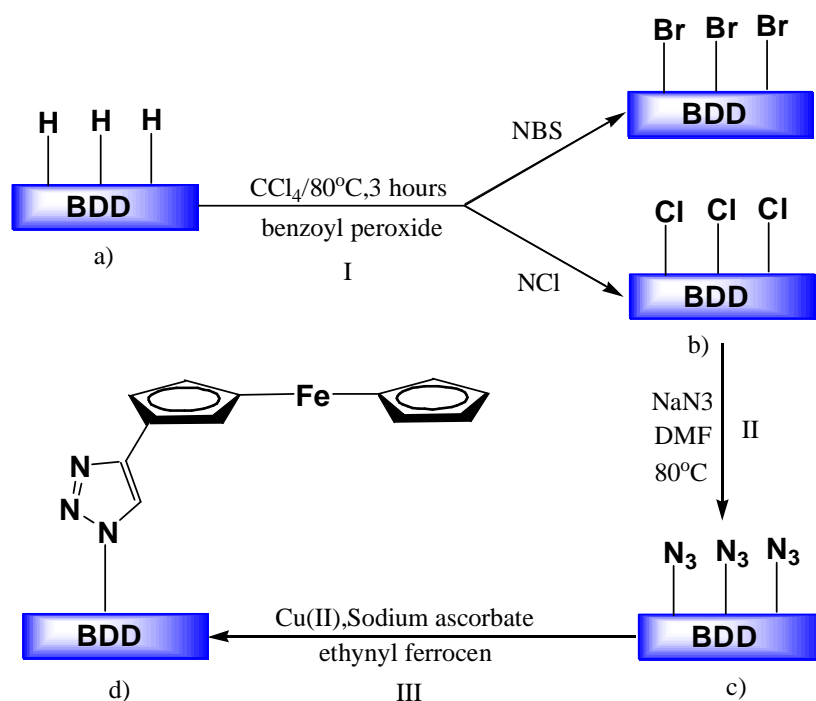
In this chapter, we describe a versatile strategy for brominating and chlorinating hydrogenated boron-doped diamond (H-BDD) interfaces using *N*-bromo- and *N*-chlorosuccinimide (NBS and NCS), respectively as shown in **Scheme 6.1(I)**. The chemical reactivity of the halogenated boron-doped diamond surfaces (Br-BDD) with Grignard reagents was further investigated (**Scheme 6.2**). The halogenated interfaces were also reacted with sodium azide through a nucleophilic substitution reaction. The resulting azide terminated diamond surfaces (N₃-BDD) were used to trigger the “click” reaction (**Scheme 6.1(II)**). Because of the attractive electrochemical properties of ferrocene-containing molecules, such as fast electron-transfer rates, reversible redox activities and favorable redox potentials, we show here that ferrocene derivatives can be grafted onto non-oxidized diamond surfaces by “click chemistry”, as shown in **Scheme 6.1(III)**. These redox-active ferrocene-containing layers on a boron-doped diamond (BDD) surface, because of their ability to store and release charges reversibly, have the potential to be used as hybrid molecular /semiconductor memory devices.

6.3. Results and discussion

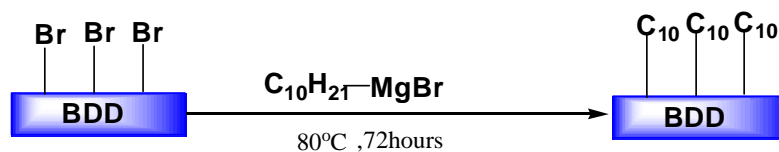
6.3.1. Contact angle

Contact angle measurements were used to follow the changes in surface wetting properties after each functionalization step. The water contact angle of diamond surfaces with different terminations and chemical compositions were investigated (**Table 6.1**). Hydrogen-terminated BDD surface showed a water contact angle of $93 \pm 2^\circ$, as expected for a surface terminated with hydrophobic C-H bonds. Chemical grafting of electron withdrawing groups to the

diamond interface does not influence significantly the wetting properties. Contact angles of $87 \pm 2^\circ$ and $85 \pm 2^\circ$ are obtained for the brominated diamond (Br-BDD) and chlorinated diamond (Cl-BDD) interfaces, respectively. The values are comparable to those reported in the literature for diamond surfaces halogenated using plasma treatment [14]. The high contact angles give a first indication that oxidation has not taken place preferentially under such reaction conditions, as this would result in contact angles $<10^\circ$.



Scheme 6.1. Halogenation of H-BDD through radical substitution reaction using NBS and NCS and its reactivity.



Scheme 6.2. Alkylation of a brominated BDD surface using $C_{10}H_{21}MgBr$.

Table 6.1. Contact angle of boron-doped diamond (BDD) surfaces with different terminations

	H-BDD	Br-BDD	Cl-BDD	$C_{10}H_{21}$ -BDD	N_3 -BDD	Ferrocene-BDD
Contact angle	$93 \pm 2^\circ$	$87 \pm 2^\circ$	$85 \pm 2^\circ$	$100 \pm 2^\circ$	$70 \pm 2^\circ$	$20 \pm 2^\circ$

The stability of the interfaces was determined by following the change of contact angle over time. After 14 days exposure to ambient conditions, the contact angles determined remained unchanged within the error range, indicating that both interfaces are fairly stable in air. When immersed in water for 2 days, the contact angles decreased to $83 \pm 2^\circ$ for the brominated diamond (Br-BDD) and to $81 \pm 2^\circ$ for the chlorinated diamond (Cl-BDD). Furthermore, brominated and chlorinated diamonds were immersed in water for more than one month, contact angles were checked from time to time. **Figure 6.1** displays the change of the water contact angle over time. We can see that after one month, both chlorinated and brominated diamond surfaces were completely oxidized

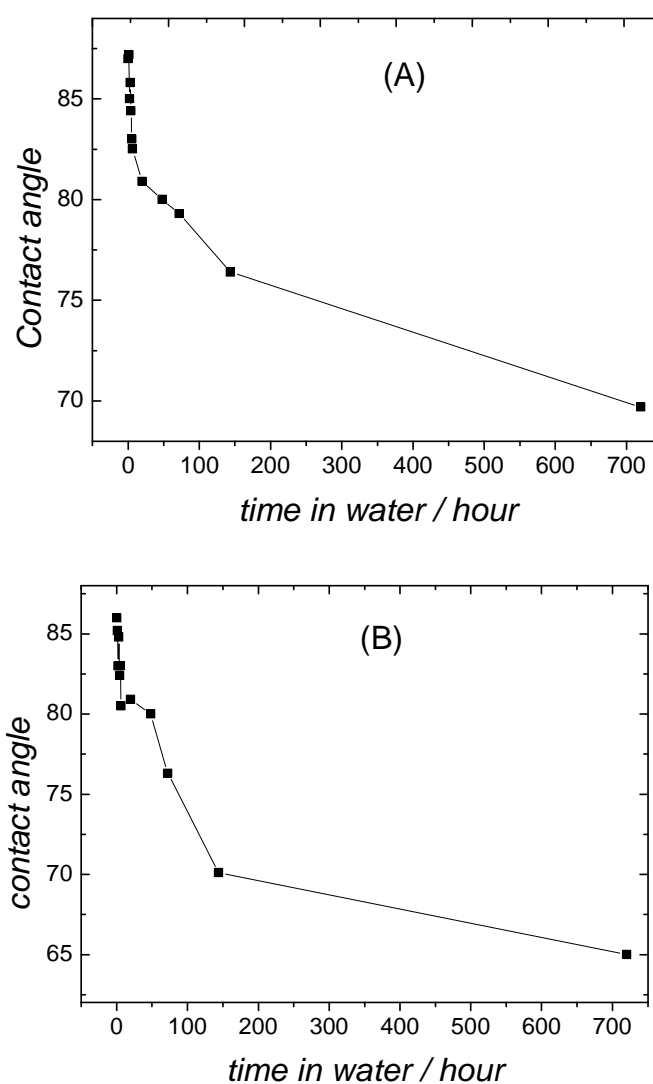


Figure 6.1. Change of water contact angle on (A) Br-BDD (B) Cl-BDD diamond surfaces.

The chemical reactivity of the halogenated BDD surfaces was further investigated by exposing the brominated BDD surface to a Grignard reagent. A similar strategy has been reported for the alkylation of chlorinated diamond [7] and Si surfaces [15]. The Br-BDD was immersed in an anhydrous THF (20ml) and 10 ml of 1M $C_{10}H_{21}MgBr$ in diethyl ether. The mixture was heated for 72h in a constant temperature bath set at 80°C. The resulting surface was rinsed at room temperature with 1% CF_3COOH solution in THF, Milli-Q water, sonicated in methanol and dried under a stream of nitrogen [16]. The contact angle of the decyl-terminated diamond ($C_{10}H_{21}$ -BDD) surface increased to $100\pm 2^\circ$, due to the hydrophobic character of the long alkyl chain. The value is in agreement with contact angles between 100 - 108° reported for chemically modified silicon and perfluorodecyl silane modified polycrystalline diamond surfaces [17].

Finally, nucleophilic displacement of the terminal halogen groups of the Br-BDD surface with sodium azide led to contact angle decrease. A value of $70\pm 2^\circ$ was measured for the azide-terminated diamond (N_3 -BDD) surface. After clicking ferrocene moieties to the azide terminal groups, the contact angle dropped to $20\pm 2^\circ$, as depicted in **Table 6.1**.

6.3.2 Electrochemical characterisation

We studied the electrochemical properties of the modified BDD surfaces using $[Fe(CN)_6]^{3-/4-}$ as the redox couple in solution. **Figure 6.2A** shows the $i-E$ curves in an aqueous solution of 10mM $Fe(CN)_6^{4-}$ in 0.1M KCl aqueous solution recorded on H-BDD, Br-BDD and Cl-BDD electrodes.

A significant decrease of the apparent rate constant is observed for the halogenated BDD electrodes, being similar to that of UV/ozone oxidized interfaces [17]. In the case of Cl-BDD, the standard electrochemical potential shifted to more anodic values. In contrast to F-BDD, where a window of ideal polarisability of 5V could be recorded [56,57], Cl-BDD and Br-BDD surfaces show electroactive windows similar to that of H-BDD (**Figure 6.2B**).

The decyl-terminated BDD ($C_{10}H_{21}$ -BDD) surface was further characterized by cyclic voltammetry using $Fe(CN)_6^{4-}$ as the redox couple in solution (**Figure 6.3**). Attenuation of the current is observed, which is consistent with surface inhibition due to the presence of a long alkyl chain on the surface, comparable to perfluorodecyl-terminated BDD [18]. The current

signal is however rather intense suggesting that the electrode is not fully blocked. This points towards either an overall low-density surface grafting and/or the presence of defect domains.

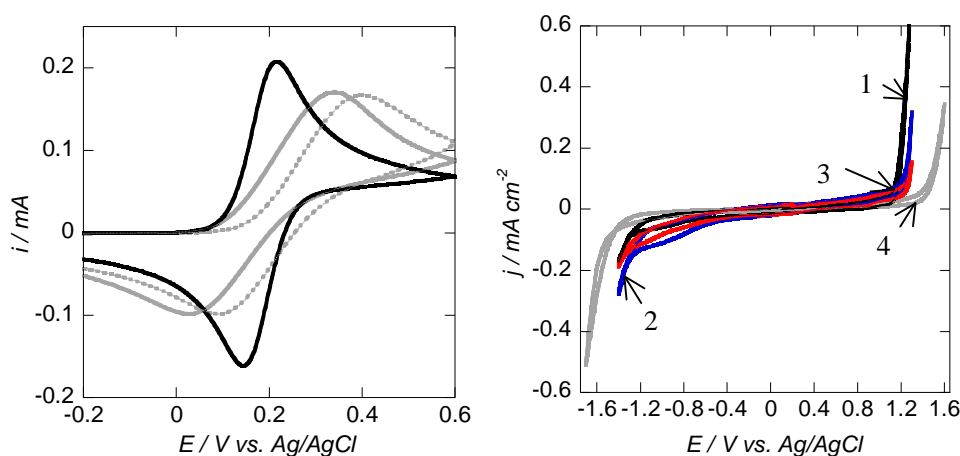


Figure 6.2. Cyclic voltammograms of BDD electrodes in an aqueous solution of (A) $\text{Fe}(\text{CN})_6^{4-}$ (10mM) in KCl (0.1 M): H-BDD (black), Br-BDD (grey), Cl-BDD (grey dotted); (B) KCl (0.1 M): H-BDD (curve 1), Br-BDD (curve 2), Cl-BDD (curve 3), UV/ozone oxidised-BDD (curve 4); scan rate: 50mV s^{-1} .

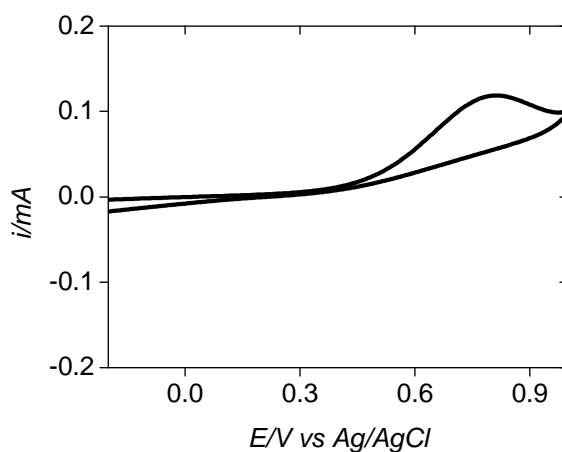


Figure 6.3. Cyclic voltammogram of $\text{C}_{10}\text{H}_{21}$ -BDD electrode in an aqueous solution of $\text{Fe}(\text{CN})_6^{4-}$ (10 mM) in KCl (0.1 M) aqueous solution; scan rate: 50 mV s^{-1} .

Figure 6.4 (curve 1) shows a i - E curve for a ferrocene modified BDD surface in 0.1M tetraethyl ammonium hexafluorophosphate (TEAPF_6) in DMF. The signal at $\sim 1.0\text{V}$ vs. Ag/AgCl is due to the ferrocene termination. In order to confirm the ferrocene-terminated BDD (after “click chemistry” on the azide- terminated surface), a cyclic voltammogram (CV) of alkynylferrocene in solution was recorded on a azide terminated BDD surface and both

compared; the i - E curve obtained is shown as **Figure 6.4 (curve 2)**.

For alkynylferrocene in solution (**curve 2**) typical redox peaks at 0.51 V and 0.88 V are shown. The signal at ~ 1.0 V (**curve 1**) is due to the alkynylferrocene termination. The reduction peak is however suppressed, possibly due to a low density grafting, molecular orientation and/or the presence of defect domains on the surface. The small shoulder, located at 0.81 V, is also due to ferrocene as substituted ferrocene can show a more complex redox behavior. Compared to alkynyl ferrocene in solution, the oxidation peak is shifted to higher potential for the surface bound species.

A similar behavior of ferrocene was observed on single-crystal Si (111) surfaces modified with ferrocene carboxylic acid [19], and on gold modified by ferrocene-based alkanethiol layers [20]. On basis of this, we can conclude the presence of ferrocene units on BDD surface.

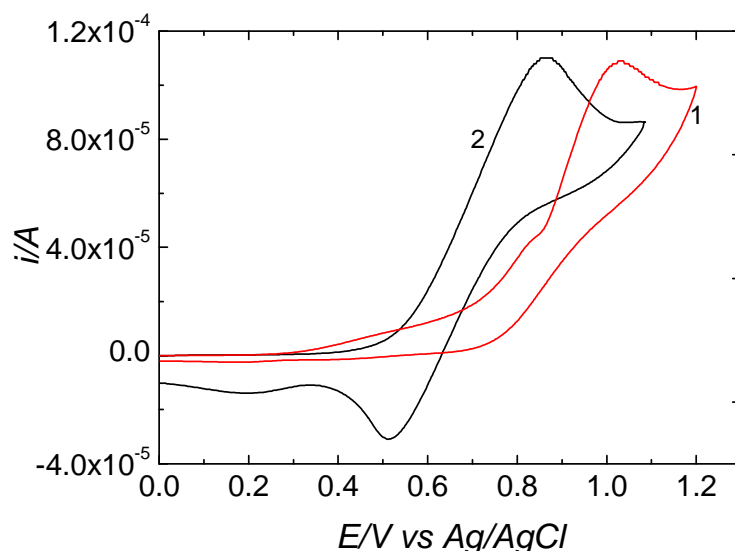


Figure 6.4. Cyclic voltammograms of alkynylferrocene in solution on an azide terminated BDD interface (curve 2) and on a ferrocene-terminated (curve 1) BDD surface in TEAPF_6 (0.1M/DMF), scan rate: 0.1 V s^{-1} .

6.3.3. X-ray photoelectron spectroscopy (XPS) analysis

X-ray photoelectron spectroscopy is a valuable tool to evaluate the changes in the surface chemical composition and to monitor covalent bonds formed during surface derivatization. The XPS survey of as-deposited BDD displays a main peak for C1s at 285.08eV and a small peak at 532eV for O1s with a O/C ratio of 0.30. The presence of oxygen is most likely due to partial oxidation of the BDD surface during its handling and transferring. After reaction with

NBS and NCS, additional peaks at 183.9eV and 190.5eV due to Br3p and at 199.8eV and 201.3eV due to Cl2p are observed (**Figure 6.5**). The atomic concentration ratio Br/C and Cl/C are estimated to be 0.18 and 0.15 respectively. The values are comparable to those reported by Kondo et al. [14]. The O/C ratio after halogenation increased to 0.98 for Br-BDD and 1.01 for Cl-BDD, indicating that some oxidation is taking place during halogenation. High-resolution XPS (**Figure 6.5C**) of the C1s band indicates the formation of C=O groups (288.6eV). The shoulder at \sim 286.3eV is due to the formation of C-X (X = Br, Cl) and C-O bonds.

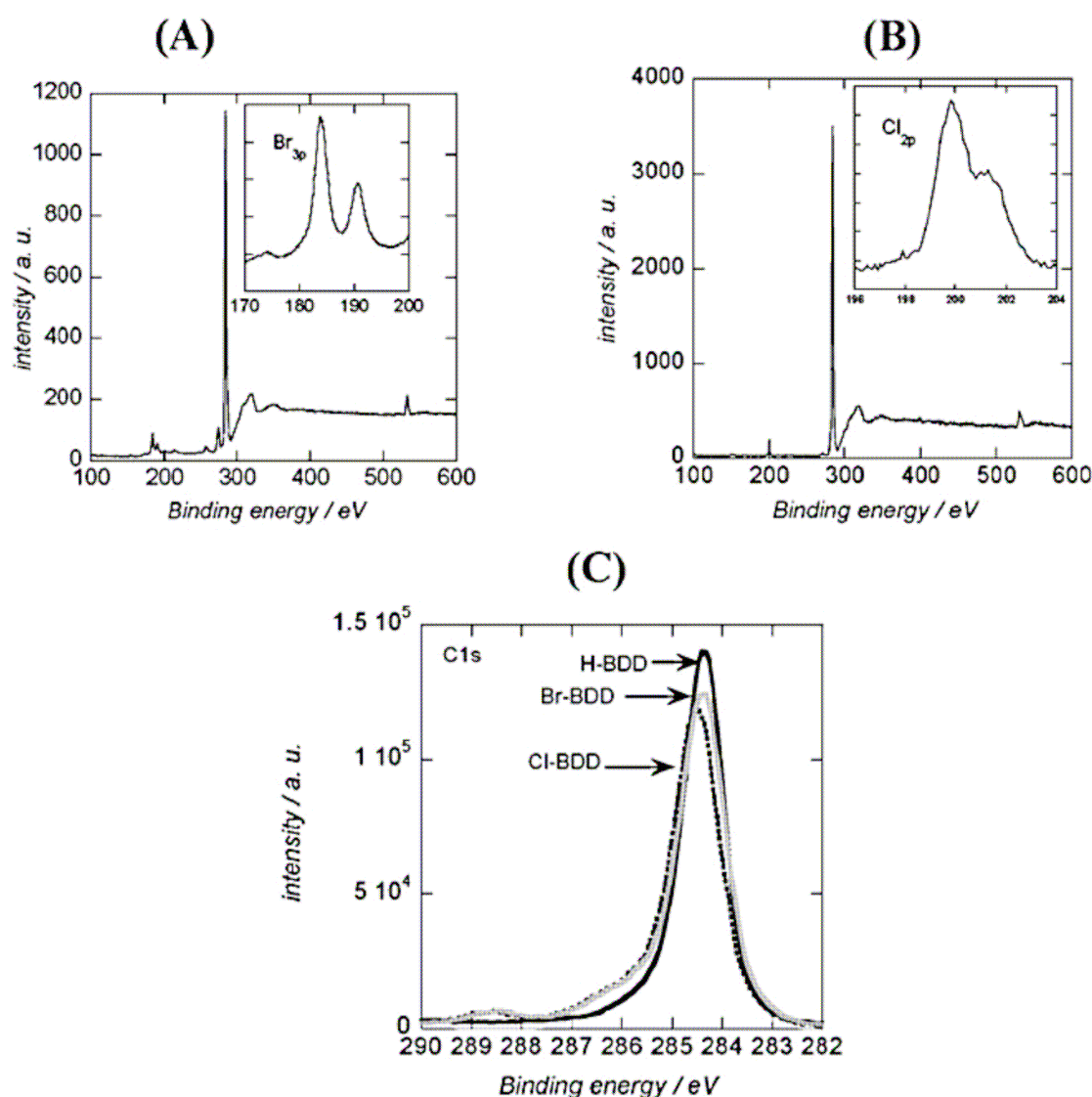


Figure 6.5. XPS survey of (A) brominated and (B) chlorinated diamond surfaces. The insets correspond to the high-resolution XPS of Br3p and Cl2p; (C) high-resolution XPS of the C1s band of as-deposited BDD (black), Br-BDD (grey) and Cl-BDD (black dotted).

Chemical conversion of bromine into azide termination led to the complete disappearance of

the Br3p signal (183.9eV and 190.5eV) (**Figure 6.6B**), indicating the substitution of the bromine functions of the monolayer. The substitution reaction of bromine with azide groups resulted in the appearance of a signal in the N1s region of the XPS spectrum (**Figure 6.6C**).

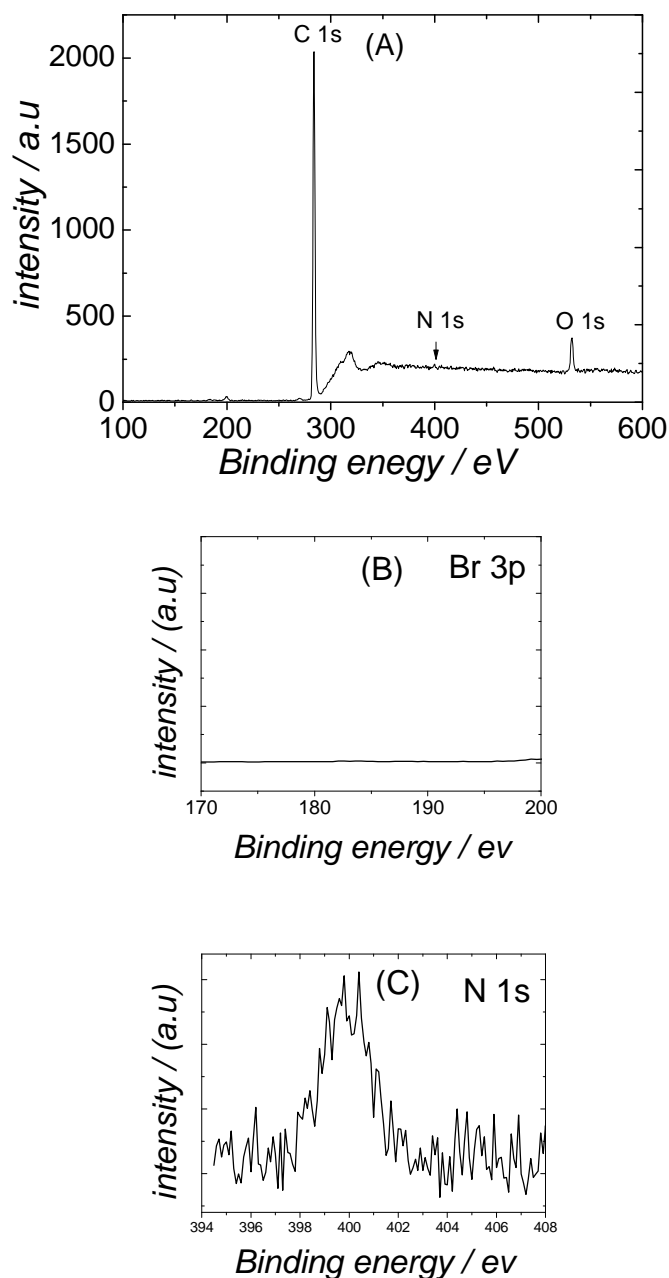


Figure 6.6. (A) XPS survey spectrum of azide terminated diamond surfaces (N_3 -BDD), (B) High-resolution XPS spectrum of Br3p, (C) The high-resolution XPS spectrum of N1s.

Careful analysis showed the presence of a split peak at 401 and 405eV (**Figure 6.6C**), the high- and low-binding energy peaks are, respectively, assigned to the central, electron-deficient N atom in the azide group, and to the two nearly equivalent azide N atoms,

in a region which did not show any signal for the brominated boron-doped diamond (Br-BDD) electrodes. This peak splitting indicated the presence of two nitrogen species present in the azide-terminated monolayer, and reflects the differently charged nitrogen atoms in the azide group, suggesting the presence of chemically different nitrogen atoms consistent with the chemical composition of the monolayer [21].

Moreover, the complete disappearance of the bromine peak (**Figure 6.6C**) that was observed in the brominated diamond surface suggests a complete conversion of the bromine functions to azide (>95%) or to a competitive oxidation reaction. Such functionalized azide-terminated monolayers now represent a substrate that could be employed in 1, 3-dipolar cycloaddition reactions if reacted with terminal acetylene substituted molecules. To demonstrate this possibility, ethynyl ferrocene was used for “clicking” with the azide terminated diamond surface.

Reaction of the terminal azido groups with ethynyl ferrocene in the presence of Cu(I) catalyst led to the appearance of a new peak in the XPS survey spectrum at ~ 710eV due to Fe2p (**Figure 6.7A**).

After clicking ferrocene groups onto the azide-terminated BDD surface, the peak at 405eV disappears and the one at 400eV doesn't show any obvious change (**Figure 6.7C**). This can be taken as an evidence for the transformation of the azide group to the 1, 2, 3-triazole unit bound to the terminal ferrocene head *via* “click chemistry”. Furthermore, a huge increase of the O1s peak was observed due to a competitive oxidation reaction during the “clicking” step.

In addition, the scan of the Fe2p region demonstrates the presence of ferrocene moieties onto the BDD surface (**Figure 6.7B**). The Fe2p_{3/2} and 2p_{1/2} have been, respectively, found at 711.7 and 725.6eV with a 2:1 peak area ratio, this clearly indicates that the Fe species exists mainly in its (III) oxidation state, in agreement with previously reported results on ferrocene moieties anchored to hydrogen-terminated silicon [19] and azide-terminated BDD [21] surfaces. The corresponding binding energy and full width at half maximum (FWHM) values are close to the data previously reported on ferrocene derivatives anchored onto Si(100) and BDD surfaces [19,21].

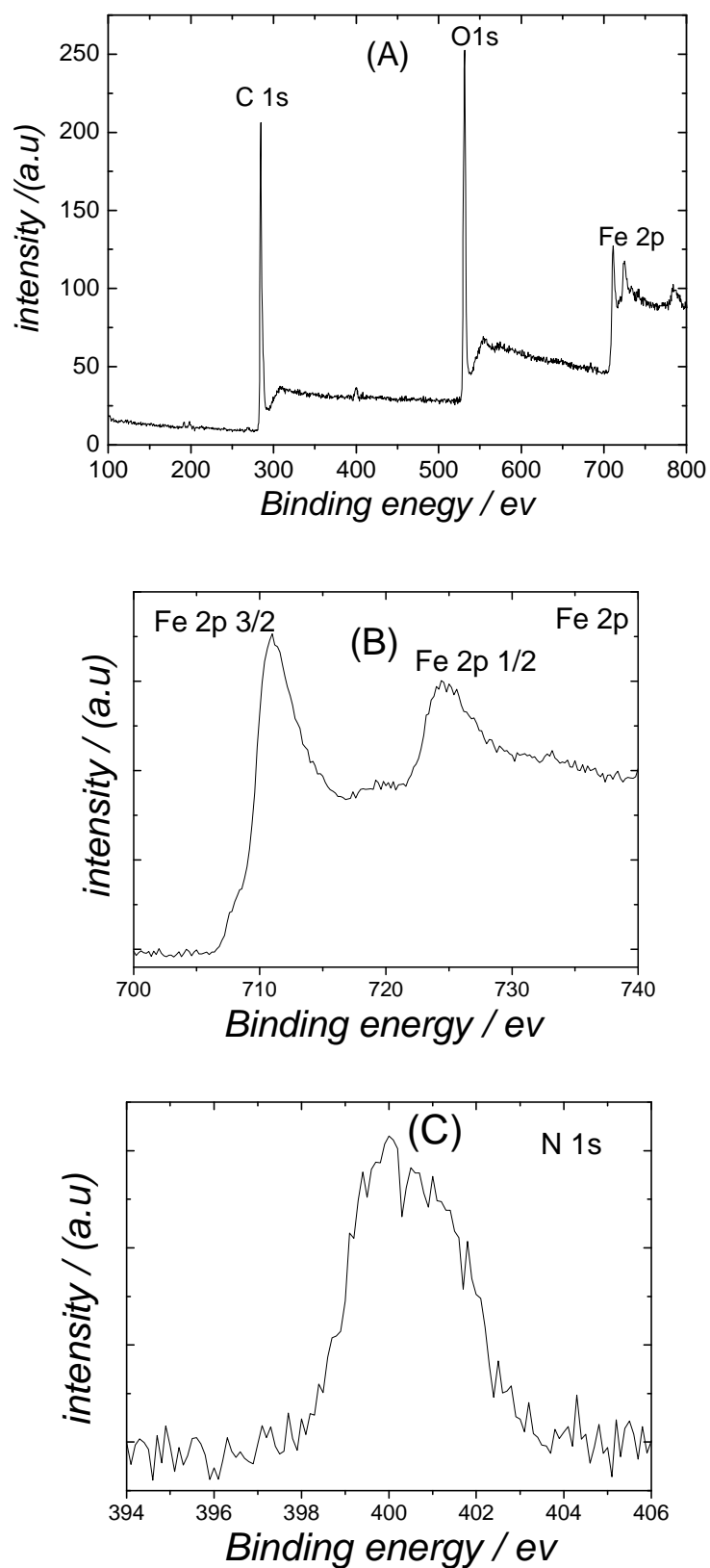


Figure 6.7. (A) XPS survey of the azide-terminated BDD surface after “clicking” with ethynyl ferrocene (B) The high-resolution XPS of the Fe 2p (C) The high-resolution XPS of the N1s.

6.4. Reaction mechanism

6.4.1. Halogenation reaction

Among various radical initiators, benzoyl peroxide was found to be the most effective in abstracting hydrogen on the surface. Due to its low dissociation energy, the O-O bond in these peroxides breaks easily, generating radicals [22-24]. When benzoyl peroxide is thus heated up to temperatures of about $T = 60-80^{\circ}\text{C}$, it decomposes into benzoyl radicals. In the presence of a H-terminated diamond surface in CCl_4 (under N_2 atmosphere, at $T = 80^{\circ}\text{C}$ for $t = 3\text{h}$), the benzoyl radicals formed can abstract a hydrogen atom on the diamond surface, then halogen atoms were introduced from *N*-halogenosuccinimide (*N*-bromosuccinimide or *N*-chlorosuccinimide), accompanied with succinimide radicals generation (**Figure 6.8**). The succinimide radicals continue abstracting hydrogen atoms from the surface, and succinimide radicals propagate simultaneously. A succinimide radical, once formed, rapidly reacts with whatever is available. In reality if more than one hydrogen is present, the starting material would keep reacting till there is no succinimide radical any more, it is termination.

6.4.2. Nucleophilic substitution

The bromine terminal group can be easily substituted by azide group through a nucleophilic substitution reaction with sodium azide, where the nucleophile is the N_3^- and the leaving group is Br^- . During the substitution reaction of halogenated hydrocarbons using sodium azide (**Figure 6.9**), the lone-pair electrons on the N_3^- ion will be strongly attracted to the δ^+ carbon, and will move towards it, beginning to make a co-ordinate (dative covalent) bond. In the process, the electrons in the C-Br bond will be pushed even closer towards the bromine, making it increasingly negative. There is obviously a point in which the N_3^- is half attached to the carbon and the C-Br bond is half way to being broken. This is called a transition state. It isn't an intermediate. It can't be isolated-even for a very short time. It's just the mid-point of a smooth attack by one group and the departure of another. The movement goes on until the N_3^- is firmly attached to the carbon, and the bromine has been expelled as a Br^- ion. The solvent is important. If water is present it tends to get substitution by OH^- instead of N_3^- .

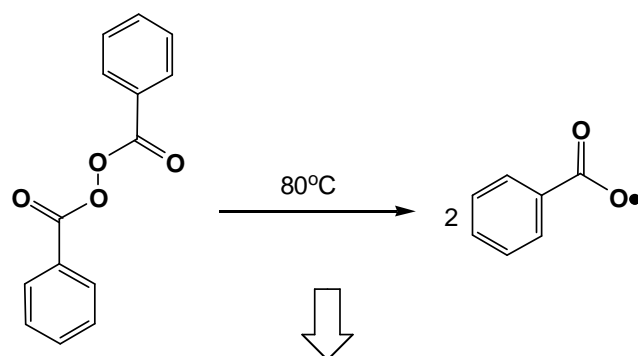
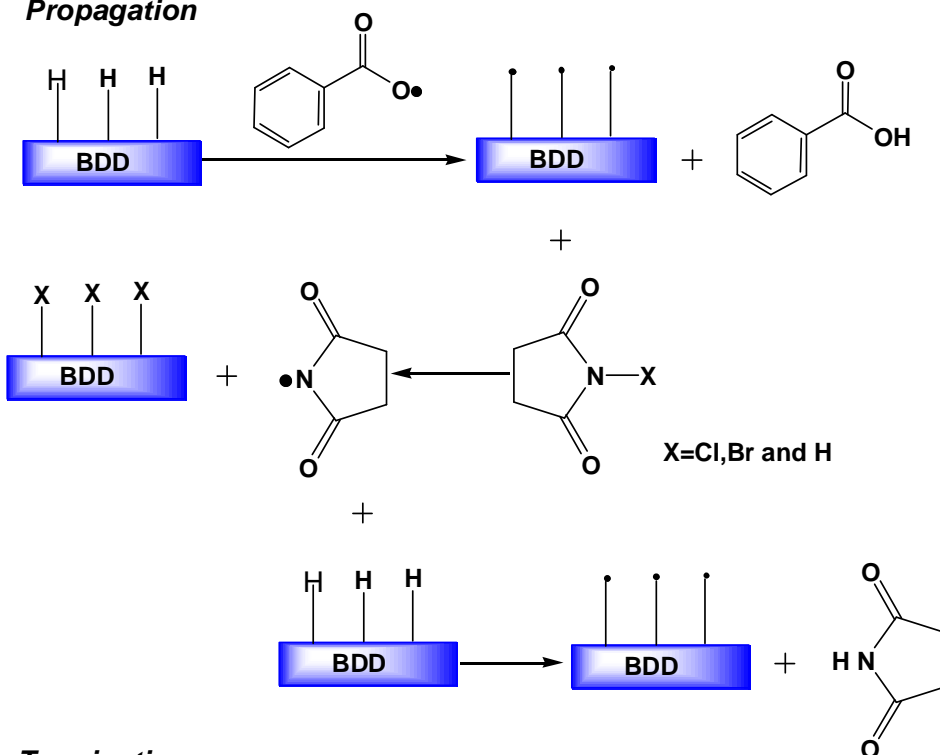
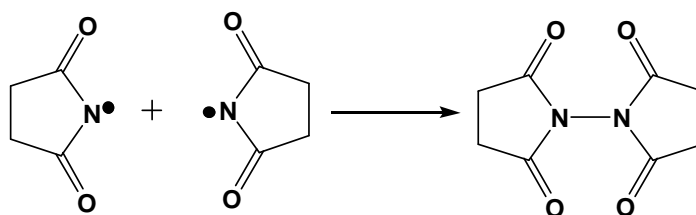
Initiation

Propagation

Termination


Figure 6.8. Mechanism of the halogenation reaction of hydrogenated diamond surfaces using a radical initiator.

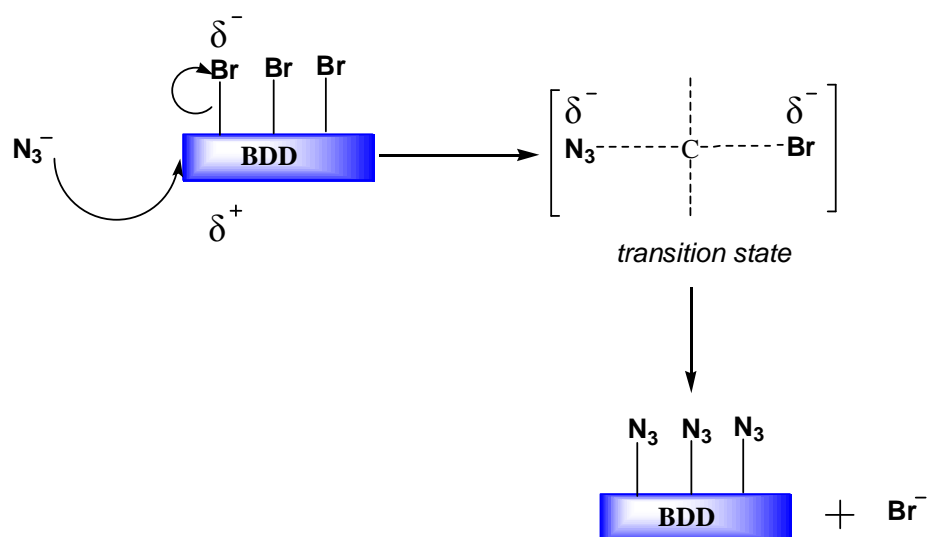


Figure 6.9. Mechanism of nucleophilic substitution of Br moieties by azide groups.

6.4.3. Click reaction

Clicking ethynyl ferrocene with azide terminated diamond surface is a typical Cu (I)-catalyzed cycloaddition (**Figure 6.10**). The reaction mechanism was discussed in details in the **Chapter 4**. Cu (II) and sodium ascorbate were used to generate a catalytically active Cu (I) species and the reaction was carried out in the most commonly used solvent: water/ethanol at 50°C (for the sake of higher reaction rate).

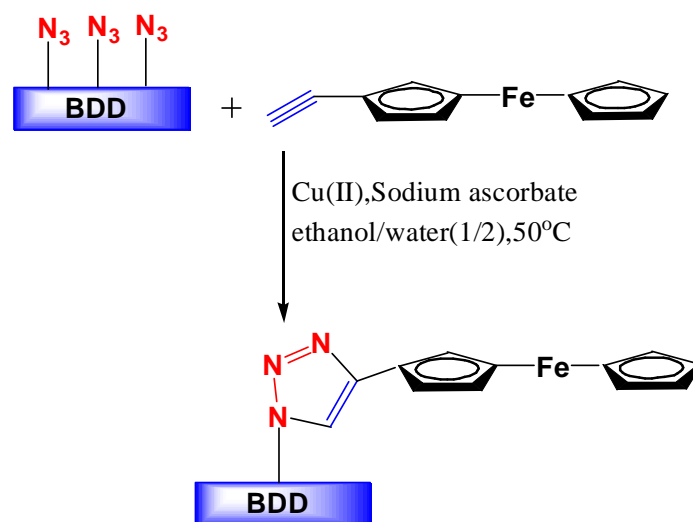


Figure 6.11. Click reaction between ethynyl ferrocene and azide-terminated BDD surface.

6.5. Conclusion

In summary, the results presented here demonstrate an easy-to-perform and controllable formation of Br-BDD and Cl-BDD on a diamond film. The interest of halogen-functionalised BDD is in the high reactivity of the surface-bound halogens that can be utilised for the introduction of other surface functionalities. This was demonstrated by exposing Br-BDD to alkyl-Grignard reagents. Azide termination on diamond surfaces (N₃-BDD) can be obtained by a nucleophilic substitution reaction with sodium azide. Finally, the azide termination was exploited for “clicking” ethynyl ferrocene to the BDD electrodes. The attachment of an electroactive ferrocene moiety was achieved in high selectivity and yield. Because of the gentle nature of the procedure, the strategy developed in this work can be used as a general platform to prepare functionalized surfaces for various applications.

6.6. Perspectives

From the XPS analysis, it was clear that the nucleophilic substitution of -Br by -N₃ groups was accompanied by a partial oxidation of the surface. Surface oxidation is known to influence the electrochemical properties of the BDD surface. This aspect has to be optimized in order to reduce surface oxidation during Br displacement.

Furthemore, in order to prepare functional surfaces for biosensing applications, biomolecules bearing an acetylene group should be immobilized on the azide-terminated BDD surface using “click” chemistry.

6.7. References

1. J. B. Miller; D. W. Brown. *Langmuir*. **1996**, 12, 5809-5817.
2. A. Freedman. *J. Appl. Phys.* **1994**, 75, 3112-3120.
3. Y. Liu; G. Zhenning; J. L. Margrave; V. N. Khabashesku. *Chem. Mater.* **2004**, 16, 3924-3930.
4. T. Ando; R. E. Rawles; K. Yamamoto; M. Kamo; Y. Sato. *Diam. Relat. Mater.* **1996**, 5, 1136-1142.
5. J. B. Miller; D. W. Brown. *Diam. Relat. Mater.* **1995**, 4, 435-440.

6. J. B. Miller. *Surf. Sci.* **1999**, 439, 21.
7. Y. Ikeda; T. Saito; K. Kusakabe; S. Morooka; H. Maeda; Y. Taniguchi; Y. Fujiwara. *Diam. Relat. Mater.* **1998**, 7, 830-834.
8. J. F. Lutz. *Angew. Chem. Int. Ed.* **2007**, 46, 1018.
9. N. K. Devaraj; J. P. Collman. *QSAR Comb. Sci.* **2007**, 26, 1253.
10. S. Ciampi; T. Böcking, K. A. Kilian; M. James; J. B. Harper; J. J. Gooding. *Langmuir.* **2007**, 23, 9320.
11. A. G. Marrani; E. A. Dalchiele; R. Zanoni; F. Decker; F. Cattaruzza; D. Bonifazi; M. Prato. *Electrochim. Acta.* **2008**, 53, 3903.
12. J. P. Collman; N. K. Devaraj; C. E. D. Chidsey. *Langmuir.* **2004**, 20, 1051.
13. T. Lummerstorfer; H. Hoffmann. *J. Phys. Chem. B.* **2004**, 108, 3963.
14. T. Kondo; H. Ito; K. Kusakaba; K. Ohkawa; Y. Einaga; A. Fujishima; T. Kawai. *Electrochim. Acta.* **2007**, 52, 3841.
15. A. Bansal; X. Li; I. Lauermann; N. S. Lewis. *J. Am. Chem. Soc.* **1996**, 118, 7225-7226.
16. R. Boukherroub; S. Morin; F. Bensebaa; d D. D. M. Wayner. *Langmuir.* **1999**, 15, 3831-3835.
17. R. Boukherroub; X. Wallart; S. Szunerits; B. Marcus; P. Bouvier; M. Mermoux. *Electrochem. Commun.* **2005**, 7, 937
18. J. B. Miller; D. W. Brown. *Langmuir.* **1996**, 12, 5809.
19. R. D. Rohde; H. D. Agnew; W. Yeo; R. C. Bailey; J. R. Heath. *J. Am. Chem. Soc.* **2006**, 128, 9518.
20. A. M. Napper; H. H. Liu; D. H. Waldeck. *J. Phys. Chem. B.* **2001**, 105, 7699.
21. M. R. Das; M. Wang; S. Szunerits; L. Gengembre; R. Boukherroub. *Chem. Commun.* **2009**, 1-4.
22. T. Tsubota; O. Hirabayashi; S. Ida; S. Nagaoka; M. Nagata; Y. Matsumoto. *Diam. Relat. Mater.* **2002**, 11, 1360.
23. Y. Ikeda; T. Saito; K. Kusakabe; S. Morooka; H. Maeda; Y. Taniguchi; Y. Fujiwara. *Diam. Relat. Mater.* **1998**, 7, 830.
24. T. Nakamura; M. Suzuki; M. Ishihara; T. Ohana; A. Tanaka; Y. Koga. *Langmuir.* **2004**, 20, 5846.

CHAPTER 7

CONCLUSION AND PERSPECTIVES

For many years, diamond surfaces were considered as chemically inert, which restricts their use in various aspects of life sciences and biotechnology. In the last ten years, there has been a huge progress in the development of strategies for derivatization of diamond surfaces. These techniques are based on photochemical, electrochemical and chemical approaches, and have shown their strength in tethering functional groups to the diamond surface.

To make it competitive with silicon technology, the core advantages of diamond, including the chemical stability, the low electrochemical background current and its wide potential window will have to be optimized. The control of the surface chemistry of diamond will play a crucial role in this perspective. While these interfaces are nowadays used as analytical devices in different areas, the development of new surface chemistries on diamond has somehow stagnated over the years. Two approaches to functionalize diamond interfaces have been mainly used: photochemical linking of functional alkenes and diazonium-based chemistry. The difficulty in controlling the formation of a monolayer using diazonium-based chemistry and the immobilization of long functionalized alkene chains hindering largely electron transfer opens the search for new functionalization pathways. Some interesting approaches have been recently proposed through the direct amination of H-terminated diamond. The possibility to pattern the surface makes diamond an adapted platform for the generation of microarrays. Indeed, the future application of diamond will be in high-throughput systems and biotechnology. Whether diamond will be the material of choice for biosensing applications will depend on the effort put into the control of its surface chemistry.

In contrast to other semiconductors, linking organic molecules onto diamond surfaces does not require carbon-carbon (C-C) bond formation. Given the high chemical stability of C-O, C-N, C-S, C-P,...bonds, the functionalization of hydrogenated, oxidized, aminated,.. diamond surfaces will lead to the formation of stable organic monolayers.

This study provided quantitative methods for the functionalization of boron-doped diamond surfaces. Coupling biological species onto the functionalized diamond surfaces in a controlled fashion will allow not only the construction of biosensing devices, but may be of interest for

fundamental studies of living cell morphology in contact with surface structures.

This thesis aimed at the chemical modification of boron-doped hydrogen-terminated surfaces (BDD) for potential applications in biosciences. Several new strategies for surface derivatization of the diamond surface have been developed.

7.1. Functionalization of oxygen-terminated diamond surfaces

In spite of the high stability of diamond, oxidation of the hydrogenated surface is relatively easy to perform. Three different oxidation methods: (i) electrochemical oxidation through anodic polarization, (ii) photochemical oxidation using UV/ozone and (iii) oxidation using oxygen plasma of as-deposited moderately boron-doped diamond interfaces have been compared in terms of electrochemical behaviour and their surface properties were investigated using water contact angle measurements and X-ray photoelectron spectroscopy (XPS) analysis. It is demonstrated that diamond interfaces exhibiting better APTES grafting efficiency also show a more positive flat band position. This behaviour suggests strongly that a positive shift of the flat band potential is related to the formation of C-OH bonds rather than C-O-C groups. Based on this result, the electrochemical oxidation is one of the preferred methods, leading to the formation of the highest amount of C-OH groups without graphitizing the diamond interface, as observed in the case of oxygen plasma treatment. However, for APTES modified BDD surface, photochemical oxidation for short times (5 to 15 min) results in high N/O ratios together with an increase in electron transfer kinetics (for 15 min of treatment) and is an alternative for undoped diamond samples.

7.1.1. “Clicking” organic and biological molecules bearing acetylene group to azide terminated boron-doped diamond surfaces

We have demonstrated that “click” chemistry can be successfully applied for coupling organic molecules bearing a terminal alkyne group to azide-terminated BDD surfaces. Electroactive moieties such as thiophene, ferrocene and cyclophane were introduced on an azide-terminated BDD surface by using “click” chemistry in the presence of a copper(I) catalyst. The resulting surfaces were characterized using XPS, water contact angle and electrochemical measurements. As a result, 1) the attachment of an electroactive ferrocene moiety on azide-terminated BDD surface was achieved in high selectivity and yield, 2) the applicability of azide-alkyne [3+2] cycloaddition was successfully demonstrated with ethynyl thiophene and further electrochemical polymerization of the terminal “thiophene” units with

thiophene monomers in solution led to the formation of a polythiophene film covalently linked to the BDD surface, 3) alkyne-functionalized cyclophane can undergo click chemistry to conveniently attach these units onto a preformed azide-functionalized BDD surface. Azide termination was obtained through a simple esterification reaction between hydroxyl terminated BDD surface and 4-azidobenzoic acid in the presence of DCC and DMAP in dark at room temperature.

In summary, due to the gentle nature of the procedure, the strategy developed in this work can be used as a general platform to prepare functionalized surfaces for various applications.

7.1.2. Chemical functionalization of oxygenated boron-doped diamond using ionic liquids

Ionic liquid-----1-(Methylcarboxylacid)-3-octylimidazolium-bis(trifluoromethyl sulfonyl) imide was covalently grafted to the BDD surface through an esterification reaction between the carboxyl groups of the ionic liquid and the terminal hydroxyl groups of an oxidized BDD surface. The resulting surface was characterized and confirmed by XPS, water contact angle and electrochemical measurements. Anion exchange reaction between $(\text{CF}_3\text{SO}_3)_2\text{N}^-$ and BF_4^- anions was also exploited. Contact angles of IL-modified BDD varied alternatively in the process of anion exchange reaction between $(\text{CF}_3\text{SO}_3)_2\text{N}^-$ and BF_4^- anions, suggesting the successful anion exchange.

This technique opens up new opportunities for chemical functionalization of diamond surfaces towards applications in analytical field and for studying fundamental electrochemical processes at hybrid electrodes.

7.2. Functionalization of hydrogen-terminated diamond surfaces

Brominated and chlorinated surfaces are obtained via a radical substitution reaction of C-H groups on diamond with bromine and chlorine radicals. The conditions for the halogenation involve refluxing in anhydrous CCl_4 in the presence of a radical initiator, such as benzoyl peroxide to result in Br-BDD and Cl-BDD interfaces. This versatile strategy was developed for chemically functionalizing hydrogenated boron-doped diamond (H-BDD) surfaces in a manner that stabilizes the underlying diamond against oxidation and allows for both chemical and electrochemical functionalization of the surface. The chemical reactivity of the halogenated BDD surfaces was confirmed by exposing the brominated BDD surface to a Grignard reagent. Subsequently, azide termination was obtained by a nucleophilic substitution

reaction with sodium azide. The resulting azide-terminated BDD surface was covalently coupled to ethynyl ferrocene using “clicking chemistry”. These redox-active ferrocene-containing layers on a boron-doped diamond (BDD) surface, because of their ability to store and release charges reversibly, have the potential to be used as hybrid molecular/ semiconductor memory devices.

7.3. Perspectives

Despite the rapid progress made in the past ten years in the science and technology behind diamond films prepared by chemical vapour deposition (CVD), the commercialization of this amazing material is still in its infancy. Researchers and industry are concentrating their efforts on the development of methods to scale up the CVD process and reduce production costs to the level at which it becomes economically viable to use diamond as the material of choice. The material is far from being the “ultimate engineering material” even though some devices are already on the marketplace, such as diamond heat spreaders, windows, cutting tools and surface acoustic waves (SAW) filters. In the next future, we expect to see diamond films in many more applications, especially in electronics and bioelectronics.

The field of chemical functionalization and assembly of organic monolayers on diamond surfaces will remain very active for the coming years. This will be mainly driven by potential applications of such hybrid structures in different fields ranging from molecular electronics to biosensors, biological microelectromechanical systems (bioMEMS) and nanotechnology. There is a huge progress in the elaboration of new grafting techniques under mild conditions and steps towards understanding the reaction mechanism involved during the grafting process. However, there are some limitations to overcome before reaching stable, reproducible and reusable devices based on organic monolayer/diamond hybrids. The main drawback for using diamond/organic monolayer as a biochip substrate and fluorescence for the detection scheme of biomolecular interactions on the surface is the possible fluorescence quenching in the close vicinity of the semiconductor. Finally, the improvement of the monolayers quality to resist biofouling is a real challenge to design selective and sensitive devices for monitoring biomolecular interactions.

The extension of the functionalization strategies developed on diamond surfaces to diamond-like carbon (DLC) films and diamond nanoparticles will open new opportunities for potential applications of thin carbon-based films in biomaterials, drug delivery, biosensors and bioimaging.

APPENDIX

Appendix 1. Ultrasonic bath

Ultrasonic cleaning is the most up-to-date cleaning process for removing particles from the substrate surfaces, for supporting amphiphile dissolution and for periodic cleaning of containers and glassware. Its special advantages include the most thorough cleaning of the components to be cleaned, in the shortest time, without additional manual work and without damaging the items to be cleaned. The ultrasonic treatment will remove even the most stubborn dirt from inside drillings and cavities in seconds. The object to be cleaned is placed in a chamber containing a suitable ultrasound conducting fluid (an aqueous or organic solvent, depending on the application). An ultrasound generating transducer built into the chamber, or lowered into the fluid, produces ultrasonic waves in the fluid by changing size in concert with an electrical signal oscillating at ultrasonic frequency.

In this thesis work, sonication was performed in an Ultrasonic bath (BRANSON 2500) using water as the transmitter.

Appendix 2. Orbital platform shaker

Heidolph Rotamax 120 orbital platform shaker was used for cleaning and some chemical reaction agitation.

Appendix 3. UV-ozone

An easy method for oxidizing substrate surfaces is the treatment in UV-ozone [1]. **Figure 1** illustrates an example of an ultraviolet ozone oxidation system which combines ultraviolet radiation, ozone, and heat to gently and effectively remove organic contaminants from a variety of substrates [2].

The UV-ozone oxidation system includes a source of ozone in this case which is provided by feeding dry oxygen through a particulate filter and feeding the dry particulate free oxygen through an ozone generator (**equations 1, 2**). The ozone then flows into a reaction chamber of the ultraviolet ozone oxidation system. The reaction chamber includes a UV lamp positioned

above a heated sample stage. The exhaust from the reaction chamber may be passed through an optional ozone killer such an ozone decomposition catalyst unit where unreacted ozone is destroyed before entering the atmosphere (**equation 4**).

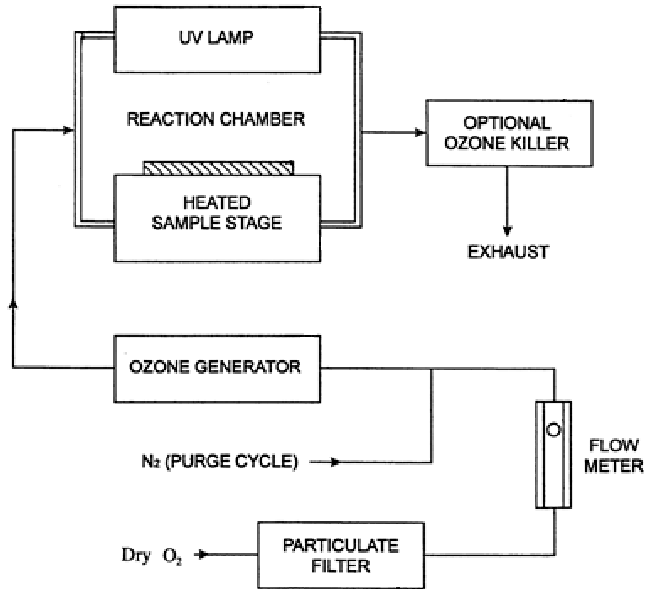
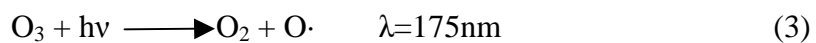
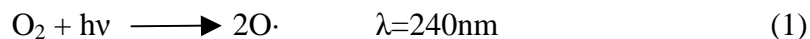


Figure 1. Schematic view of ultraviolet-ozone oxidation system [2].

In use, ozone flows into the reaction chamber and is uniformly distributed over the sample by the membrane diffuser. The UV lamp provides uniform UV radiation of the sample. Some of the ozone decomposes into oxygen molecules and atomic oxygen when exposed to the UV radiation (**equation 3**) and then sample surface is oxidized by bonding with atomic oxygen due to its high reactivity. Simultaneously, organic material such as photoresist, solvent residues, human skin oils, and pump oil are excited or disassociated by the short wavelength UV radiation. The atomic oxygen oxidizes the excited organic molecules to form simpler, harmless products such as carbon dioxide and water. This process cleans or removes organic contaminants from the sample which are then exhausted from the reaction chamber.



In this work, UVO cleaner (Nr. 42-220, Jelight, USA) was used. Singlet oxygen, ozone

and/or high energy UV-light irradiation oxidize hydrogen terminated boron doped diamond surface.

Appendix 4. Oxygen plasma

Oxygen plasma has been used for oxidizing surfaces in a vacuum. **Figure 2** shows a schematic view of our plasma instrument system (Plasmalab 80 Plus, Oxford Instruments). The oxidizing process takes place while the chamber is at 0.6 Torr in rough pumping mode and is of a short duration (1 - 10 minutes). The plasma oxidation is activated by operator command when needed. When activated the chamber is vented first to partial vacuum and then evacuation recommenced.

At the correct pressure oxygen is bled into the plasma source and then plasma is ignited to create activated oxygen radicals for oxidizing (**equations 5, 6**). After a short time the plasma and oxygen leak are turned off and the system is pumped down to remove the residual oxidation products.

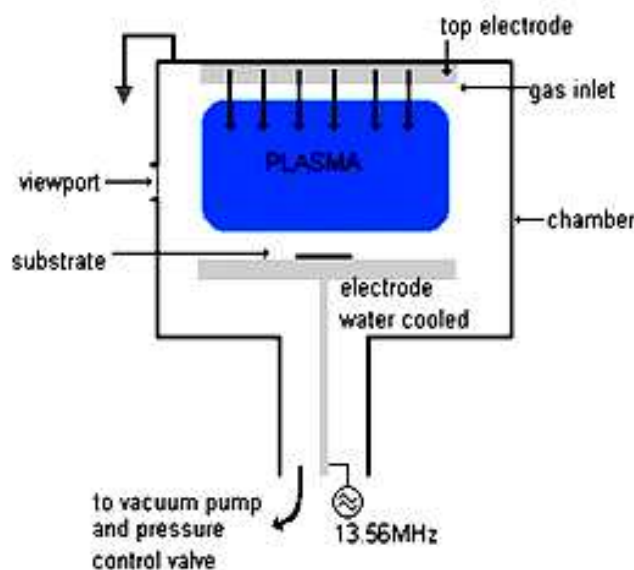


Figure 2. Schematic view of plasma system [3].



Oxygen ions and radicals are very effective cleaning agents. The oxidizing process involves the oxygen gas ions and radicals reacting with the hydrocarbons inside the chamber. These reactions yield H_2O , CO and CO_2 that are then removed from the system by the vacuum

pumps.

Appendix 5. Contact angle

The contact angle is the angle at which a liquid/vapor interface meets the solid surface. The contact angle is specific for any given system and is determined by the interactions across the three interfaces. Most often the concept is illustrated with a small liquid droplet resting on a flat horizontal solid surface. The shape of the droplet is determined by the Young relation. Water contact angles are known to depend on both surface morphology and surface chemical composition. The wetting property of a surface is defined according to the angle θ , which forms a liquid droplet on the three phase contact line (interface of three media - **Figure 3a**). A surface is regarded as wetting when the contact angle, which forms a drop with this one, is lower than 90° (**Figure 3a**). In the opposite case (the contact angle is higher than 90°), the surface is non wetting (**Figure 3b**). For water, the terms “hydrophilic” and “hydrophobic” are commonly used for wetting and non wetting surfaces, respectively. Superhydrophobic surfaces display water contact angles as high as 150° or even nearly 180° (as shown in **Figure 3b**).

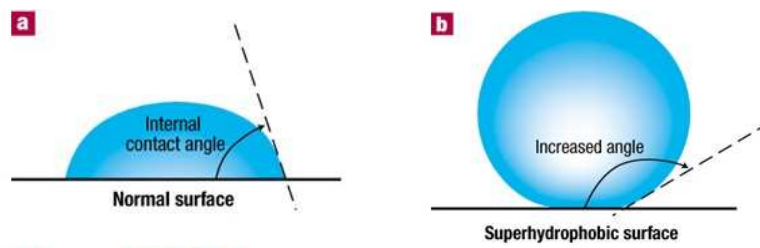


Figure 3. Contact angles of normal surface (a) and superhydrophobic surface (b) [4]

The contact angle of a liquid on a surface according to the surface tension is given by the relation of Young (1). The surface tension, noted γ is the tension which exists at the interface of two systems (solid/liquid, liquid/liquid, and solid/gas). It is expressed in energy per unit of area ($\text{mJ}\cdot\text{m}^{-2}$), but can also be regarded as a force per unit of length ($\text{mN}\cdot\text{m}^{-1}$). From this definition, it is possible to identify three forces acting on the three phase contact line: γ_{LG} (liquid surface stress/gas), γ_{LS} (liquid/solid surface stress) and γ_{SG} (solid surface stress/gas). The three forces are represented in **Figure 4**.

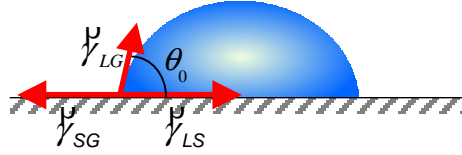


Figure 4. Surface forces acting on the three phase contact line of a liquid droplet deposited on a substrate.

At the equilibrium state:

$$\gamma_{LS} + \gamma + \gamma_{SG} = 0 \quad (7)$$

By projection on the solid, the relation of Young [5] is obtained:

$$\gamma_{LS} = \gamma_{SG} - \gamma \cos \theta_0 \quad (8)$$

It is also possible to establish the equation (8) by calculus of the surface energy variation related to a displacement dx of the three phase contact line:

$$dE = (\gamma_{LS} - \gamma_{SG})dx + \gamma dx \cos \theta \quad (9)$$

At the equilibrium state, using energy minimization ($dE = 0$), the Young relation (8) is found.

Appendix 6. Scanning electron microscopy (SEM)

The SEM is a microscope that uses electrons instead of light to form an image. Since their development in the early 1950's, scanning electron microscopes have developed new areas of study in the medical and physical science communities. The SEM has allowed researchers to examine a much bigger variety of specimens.

The scanning electron microscope has many advantages over traditional microscopes. The SEM has a large depth of field, which allows more of a specimen to be in focus at one time. The SEM also has much higher resolution, so closely spaced specimens can be magnified at much higher levels. Because the SEM uses electromagnets rather than lenses, the researcher has much more control in the degree of magnification. All of these advantages, as well as the actual strikingly clear images, make the scanning electron microscope one of the most useful instruments in research today. The SEM uses an electron beam to acquire knowledge about the sample morphology (shown as **Figure 5**). This method requires a conductive sample. In the case of non-conductive materials an ultra-thin layer of metal e.g.

gold or platinum is deposited on top of the sample. The primary electron beam is produced at a cathode, placed at the top of column, named gun. There are two main types of electron guns, a hot filament gun, where electrons are extracted from a heated tungsten wire through thermionic emission, or the field emission gun (FEG) where the electrons are extracted from a needle shape cathode by the application of a strong electric field. The extracted electrons are accelerated from a few hundred to tens of thousands of electron volts. The primary electron beam is focused by a magnetic lens and apertures onto the sample surface. To limit electron scattering in the column a high vacuum is needed. This also prevents sample oxidation. Next, a set of scan coils deflect the beam in a scanning pattern over the sample surface. When the examined material is struck by the electron beam several types of signals are formed. Secondary electrons are produced by the interactions between the primary electrons and the weakly bonded conduction-band electrons in metals or the valence electrons of insulators and semiconductors. They have low energy, and thus come from a very shallow region at the sample surface. On this basis information about sample topography can be elucidated. Backscattered electrons are created by electron beam interaction with the positive charged nucleus *via* elastic collisions. They have high energy. This allows getting knowledge about morphology and average surface composition [6, 7].

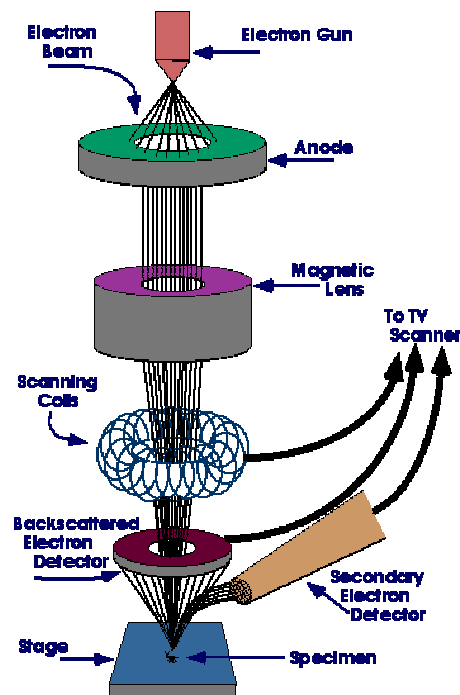


Figure 5. Schematic view of SEM [8]

I have used the scanning electron microscope ULTRA 55 Zeiss, Electron Gun is FEG (field effect gun) to image the diamond surfaces. Its features are shown as follow:

- Acceleration Voltage 200 V -30 kV
- Resolutions 1.7 nm at 1 kV and 1 nm at 15 kV
- Magnification 20x to 900 000x
- 2 Secondary detectors: INLENS and External
- 2 backscattered detectors: QBSD and EsB
- stage 130 mm x 130 mm

Appendix 7. Atomic force microscopy (AFM)

Scanning probe microscopes (SPM) are a set of tools with very small parts that help scientists to image objects at the nanometer. Each type of scanning probe microscope involves a very fine probe tip that scans back and forth over a surface. The first SPM was the scanning tunneling microscope (STM). STM is limited to surfaces that are electrically conductive. Later, Atomic Force Microscopy (AFM) was invented, which could scan any surface, conductive or not. The AFM has the advantage of imaging almost any type of surface, including polymers, ceramics, composites, glass, and biological samples. Binnig, Quate, and Gerber invented the Atomic Force Microscope in 1985. Their original AFM consisted of a diamond shard attached to a strip of gold foil. The diamond tip contacted the surface directly, with the interatomic van der Waals forces providing the interaction mechanism. Detection of the cantilever's vertical movement was done with a second tip - an STM placed above the cantilever.

AFM probe deflection: most AFMs instruments use a laser beam deflection system, introduced by Meyer and Amer, where a laser is reflected from the back of the reflective AFM lever and onto a position-sensitive detector. AFM tips and cantilevers are microfabricated from Si or Si₃N₄. Typical tip radius is from a few to tens of nm (**Figure 6**).

In the experiments presented in this thesis dimension 3100 AFM was used, and the tapping mode was employed (as shown in **Figure 7**). The Dimension 3100 AFM is an instrument capable of imaging specimens with a horizontal and vertical resolution down to a fraction of a nanometer. The instrument works by measuring the deflection produced by a sharp tip on micron-sized cantilever as it scans across the surface of the specimen. Sample sizes that can be handled by the instrument range from small pieces to 150mm diameter wafers.

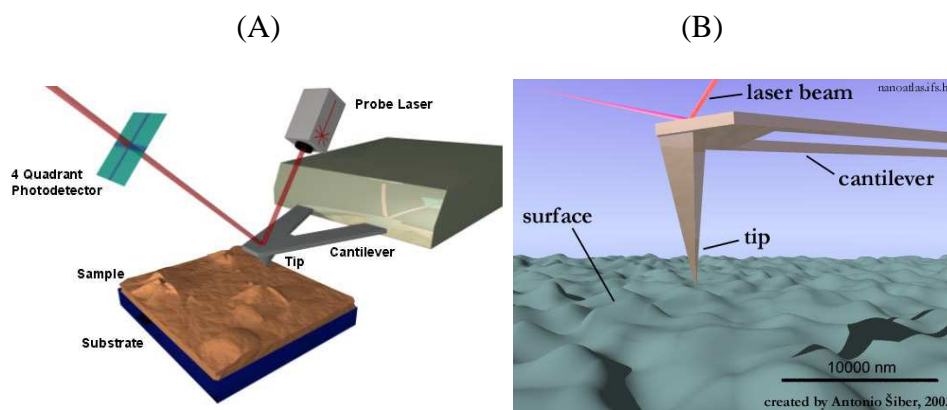


Figure 6. A schematic 3D description of basic principle of atomic force microscope (AFM) (A) and its amplified representation (B) [9]

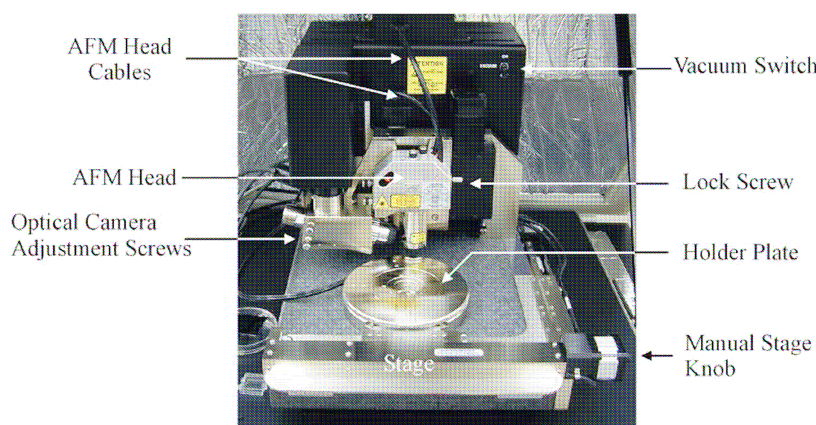


Figure 7. Overall dimension 3100 AFM view

Appendix 8. Fourier-Transform Infrared Spectroscopy (FTIR)

Infrared spectroscopy provides information about chemical compounds structure. This is due to the interaction between the infrared (IR) radiations with matter. The photon energy in this range is not enough to excite electrons but induces vibrational excitation of covalently bounded atoms and groups. The atoms in a molecule are constantly oscillating around average positions changing the bonds length (stretching vibrations) and angles (bending vibrations) between them. Atoms in a given molecule absorb a unique set of IR radiation frequencies matching the frequencies of the molecular oscillations and the spectrum with bands corresponding to functional groups can be recorded [10]. In principle the absorption of IR radiation is possible, if the vibrations cause a change in the dipole moment of the molecule.

In the experiments of this thesis the transmittance spectra of porous silicon surfaces were recorded. The FTIR spectra were measured by detection of attenuated light after its passage

through the sample. To acquire detailed information about species adsorbed on metal support the reflectance technique was used [11]. This non-destructive method allows studying very thin films and to determine the orientation of molecules. The IR radiation is directed onto the surface of the sample at an angle of incidence (I) which is equal to the angle of the reflection (R) (**Figure 8**). The choice of the angle of incidence depends on the adsorbed film thickness and for very thin coatings it equals about 80° .

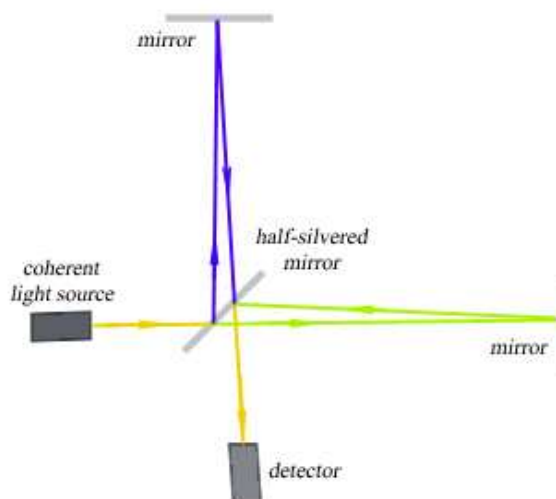


Figure 8. Schematic illustration of IR

Appendix 9. Cyclic voltammetry

Cyclic voltammetry provides considerable information on the thermodynamics of redox processes, for example redox potential, and the kinetics of heterogeneous electron-transfer reactions and coupled chemical reactions or adsorption processes. For that reason the technique was chosen in this work to obtain qualitative information about electrochemical reactions. In this method the potential is swept between two values E_i and E_e at a fixed rate in forward scan and is then reversed and in backward scan swept back to E_i , forming a triangular potential waveform (**Figure 9a**).

During the potential sweep the potentiostat measures the current resulting from the applied potential. The current vs. potential plot is used for the analysis (**Figure 9b**). When the bulk solution initially contains only a reduced form (Red) of the redox couple at the initial potential (lower than the redox potential) no conversion of Red to Ox occurs. As the applied potential approaches the redox potential, the anodic current increases until a peak is reached

$I_{p,a}$ (forward scan). At this point the potential is sufficiently positive that any Red reaching electrode surface is converted to Ox (**equation 10**):



The characteristic peak is formed because of the initial increase of Red concentration gradient and further depletion of Red form. At this point the current depends upon the rate of mass transfer to the electrode surface. During the reverse scan (backward scan), the previously generated Ox form accumulated near the electrode surface is reduced to Red form. This reaction results in increasing of the cathodic current which in reversible process produces a peak shape response (**equation 11**):



When the reversible redox system remains in equilibrium throughout the potential scan the peak current for the Red-Ox couple at 25°C can be described by the Randles-Sevcik **equation 12**[12]:

$$i_p = (2.69 \cdot 10^5) \cdot n^{2/3} \cdot A \cdot C \cdot D^{1/2} \cdot v^{1/2} \quad (12)$$

Where: n – number of the electrons transferred

A – Electrode area (cm^2)

D – Diffusion coefficient ($\text{cm}^2 \text{s}^{-1}$)

C – Redox probe concentration (mol cm^{-3})

v – The scan rate (V s^{-1})

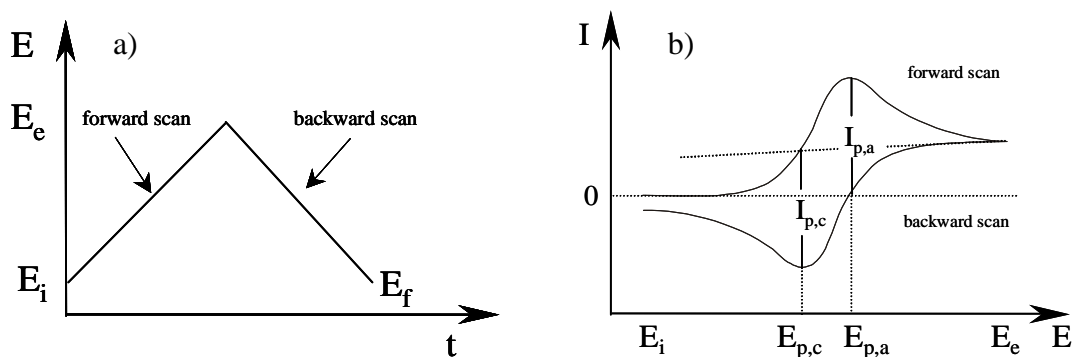


Figure 9. a) Cyclic potential sweep b) resulting cyclic voltammogram.

Moreover, the equilibrium requires the surface concentration to be maintained according to Nernst equation. Under these conditions the cyclic voltammogram is characterised by the following properties:

- the formal potential is centred between $E_{p,a}$ and $E_{p,c}$; $E^0 = (E_{p,a} + E_{p,c})/2$
- the separation between the peak potentials is equal $59/n$ mV at 25°C for all scan rates, where n is the number of the transferred electrons; $E_p = (E_{p,a} - E_{p,c})$
- the peak width is equal to $28.5/n$ mV at 25°C for all scan rates; $E_{p/2} = E_{1/2}$
- the peak current ratio ($i_{p,a}/i_{p,c}$) is equal to unity for all scan rates
- the peak current is linearly dependent on the concentration of the redox probe
- the peak current increases linearly with the square root of the scan rate

For the irreversible and quasi-reversible systems, when the chemical reaction is coupled to the redox process or adsorption of either reactants or products occur the individual peaks are reduced and widely separated. The peak current at 25°C in such a system is described by the following **equation 13** [12]:

$$i_p = (2.99 \cdot 10^5) \cdot n \cdot \alpha^{1/2} \cdot A \cdot C \cdot D^{1/2} \cdot \nu^{1/2} \quad (13)$$

Where: α - transfer coefficient

During the electrochemical reaction both the Red and Ox form can be involved in an adsorption-desorption process. When both forms adsorb on the electrode surface this interfacial behaviour satisfy the Nernstian equation and exhibits symmetrical cyclic voltammetric peaks ($\Delta E_p = 0$) and a peak half width of $90.6/n$ mV at 25°C . The peak current is linearly dependent on the surface coverage (Γ) and the potential scan rate (**equation 14**) [12]:

$$i_p = \frac{n^2 \cdot F^2 \cdot \Gamma \cdot A \cdot \nu}{4 \cdot R \cdot T} \quad (14)$$

where: F is the Faraday constant (C mol^{-1})

Γ is the surface coverage (mol m^{-2})

R is the gas constant ($\text{J mol}^{-1} \text{K}^{-1}$)

T is the temperature (K)

The surface coverage can be determined by the quantity of charge consumed by the surface process (**equation 15**):

$$Q = n \cdot F \cdot A \cdot \Gamma \quad (15)$$

The prepeak or postpeak is observed on the voltammogram when either the Ox or the Red form is observed at a potential more positive or negative than the diffusion-controlled peak, respectively[12].

In the thesis, electrochemical experiments were performed using an Autolab potentiostat 30 (Eco Chemie, Utrecht, The Netherlands). The electrochemical cells were fabricated from white cylinders of PTFE. The diamond sample that was to be used as a working electrode (WE) was laid horizontally and sandwiched between two PTFE cylinders (**Figure 10**). A platinum wire was used as counter electrode and all potential were relative to the 0.01M Ag^+/Ag system.

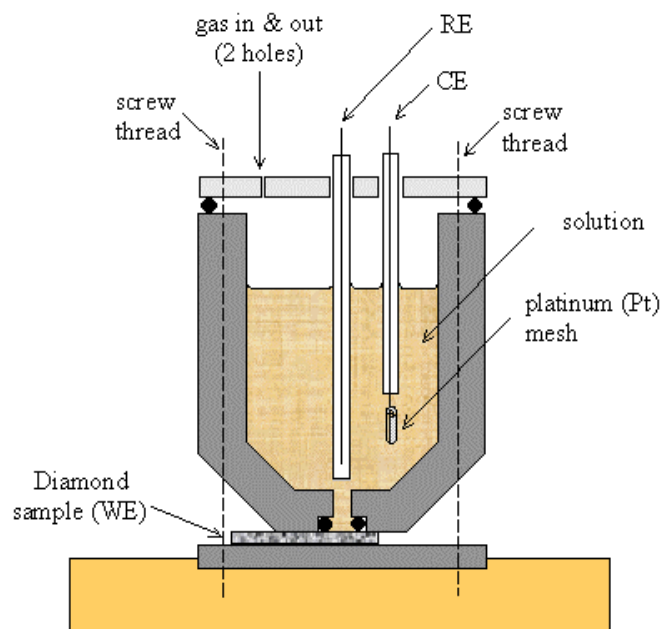


Figure 10. A schematic diagram of an electrochemistry cell

Appendix 10. X-ray Photoelectron Spectroscopy (XPS)

XPS instruments consist of an x-ray source, an energy analyzer for the photoelectrons, and an electron detector. The analysis and detection of photoelectrons requires that the sample be placed in a high-vacuum chamber. Since the photoelectron energy depends on X-ray energy, the excitation source must be monochromatic. The energy of the photoelectrons is analyzed by an electrostatic analyzer, and the photoelectrons are detected by an electron multiplier tube or a multichannel detector such as a microchannel plate (as shown in **Figure 11**).

X-ray photoelectron spectroscopy (XPS), also called electron spectroscopy for chemical analysis (ESCA) is an electron spectroscopic method that uses X-rays to eject electrons from inner-shell orbitals. The principle is represented in **Figure 12**. Each atom in the surface has a core electron with the characteristic binding energy that is conceptually, not strictly, equal to the ionization energy of that electron. When an X-ray beam directs to the sample surface, the energy of the X-ray photon is adsorbed completely by the core electron of an atom. If the photon energy, $h\nu$, is large enough, the core electron will then escape from the atom and emit out of the surface. The emitted electron with the kinetic energy of E_{kin} is referred to as the photoelectron. The binding energy of the core electron is give by the Einstein relationship (**equation 16**) [14, 15].

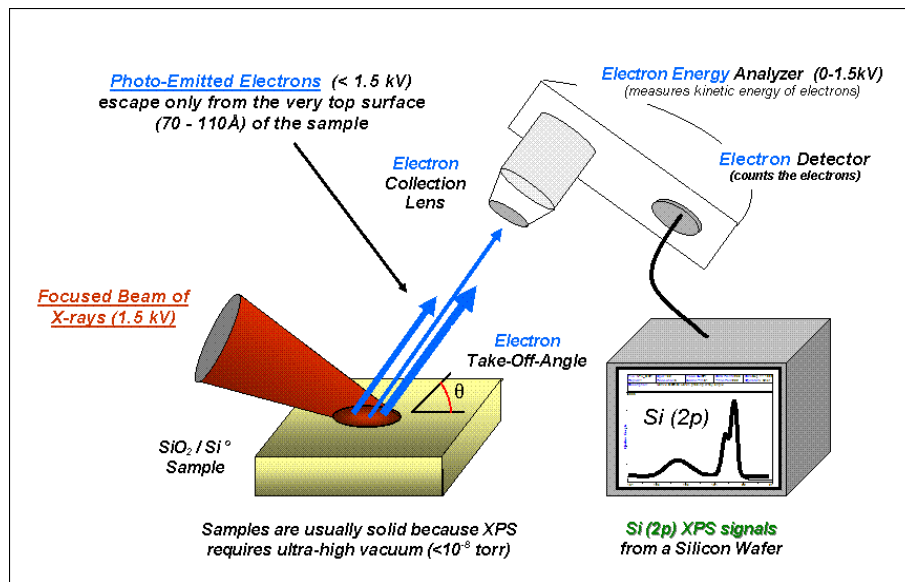


Figure 11. Basic components of an XPS system [13]

$$E_b = h\nu - E_{kin} - W_f \quad (16)$$

Where $h\nu$ is the X-ray photon energy (for monochromatic Al K α , $h\nu = 1486.6\text{eV}$); E_{kin} is the kinetic energy of photoelectron, which can be measured by the energy analyzer; and W_f is the work function induced by the analyzer, about 4~5eV. Since the work function, W_f can be compensated artificially. It is eliminated, giving the binding energy as follows (**equation 17**):

$$E_b = h\nu - E_{kin} \quad (17)$$

Where W_f is the work function of the spectrometer.

The experiments of this thesis were carried out on a VG 220i XL system. The VG 220i XL

system is an extremely versatile XPS system. It is equipped with two types of X-ray sources, the twin-anode and the twin crystal monochromated source. XPS can identify all elements, since the binding energy of the peaks is characteristic of each element with a 0.1 atomic percent sensitivity, with the exception of H and He present in the outer 10nm of a sample. XPS can also provide information on chemical bonding. Other capabilities of the system include depth profiles, line scans, and angle resolved XPS and ion scattering (1keV He⁺). Technical specifications are shown as follows:

- Small area XPS (<20 μm)
- Imaging XPS ($\sim 2\ \mu\text{m}$)
- Typically 0.1 at. % (1000ppm) detection sensitivity
- 0.5 eV energy resolution

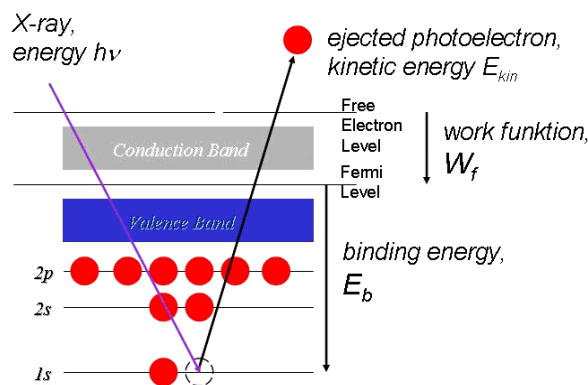


Figure 12. The principle of XPS [15]

Appendix reference

1. R. Boukherroub; X. Wallart; S. Szunerits; B. Marcus; P. Bouvier; M. Mermoux. *Electrochem. Commun.* **2005**, 7, 937.
2. *United States Patent* 6555835.
3. <http://www.iemn.univ-lille1.fr>
4. D. Quéré. *Nature Materials*. **2002**, 1, 14-15.
5. T. Young. *Philos. Trans. R. Soc. London*. **1805**, 95, 65.
6. G. D. Danilatos. *Advances in Electronics and Electron Physics*. **1988**, 71, 109-250.
7. G. D. Danilatos. *Advances in Electronics and Electron Physics*. **1990**, 78, 1-102.
8. www.purdue.edu/REM/rs/sem.htm

9. P. E. West. Introduction to Atomic Force Microscopy Theory Practice Applications. *AFM University*.
10. P. D. Natale; P. Cancio; D. Mazzotti. *Femtosecond Laser Spectroscopy*. **2005**, 109-132.
11. D. Gonçalves; E. A. Irene. *Química Nova Quím.* **2002**, 25, 5.
12. A. J. Anderson. Fundamentals and applications of spectroscopic ellipsometry. *Science University of Richmond*. **1991**.
13. B. V. Crist. *XPS International LLC*. **2005**, 1-2.
14. J. T. Grant; D. Briggs. Surface Analysis by Auger and X-ray Photoelectron Spectroscopy. *IM*. **2003**.
15. www.ifw-dresden.de/.../?searchterm=oxidation

CURRICULUM VITAE

Personal

Date of birth: Nov12, 1983

Nationality: Chinese

Marital status: Single

Tel: +33 (0)3 20 19 79 34

Adress: IRI-IEMN Avenue Poincaré - BP 60069
59652 Villeneuve d'Ascq, France

Education

Sep, 2007-June, 2009: Ph. D. student
Science and Technology University of Lille, France

Sep, 2006-Aug, 2007: Ph.D. student
Shandong University, China

Sep, 2004-Jul, 2006: Master
Shandong University, China

Sep, 2000-Jul, 2004: B.Sc.
Shandong University, China

PUBLICATIONS

1. **WANG Mei**, LI Mu Sen, BOUKHERROUB Rabah, SZUNERITS Sabine.
Electropolymerization on boron doped diamond interfaces modified with thiophene monomer units.(*submitted*)
2. **WANG Mei**, SIMON Nathalie, DECORSE-PASCANUT Claudia, BOUTTEMY Muriel, ETCHEBERRY Arnaud, LI Musen, BOUKHERROUB Rabah, SZUNERITS

- Sabine. Comparison of the chemical composition and electrochemical properties of boron doped diamond surfaces upon different oxidation processes. *Electrochimica Acta*. (in press)
3. **WANG Mei**, R. DAS Manash, G. PRAIG Vera, LENORMAND Francois, LI Musen, BOUKHERROUB Rabah, SZUNERITS Sabine. Wet-chemical approach for the halogenation of hydrogenated boron-doped diamond electrodes. *Chem. Commun.* **2008**, 6294-6296.
 4. **WANG Mei**, LI Mu Sen, YIN Long Wei, QI Yong Xin, XU Bin, GONG Jian Hong. The microstructures and catalysis of metallic films covering diamond single crystals synthesized from Fe-Ni-C system. *Key Engineering Materials*. **2007**, 353-358, 2774-2777.
 5. R. DAS Manash, **WANG Mei**, SZUNERITS Sabine, GENGEMBRE Léon, BOUKHERROUB Rabah. Clicking ferrocene groups to boron-doped diamond electrodes. *Chem. Commun.* **2009**, 2753-2755.
 6. **WANG Mei**, LI He-sheng, LI Mu-sen, GONG Jian-hong, TIAN Bin. Effect of Boron Contained in the Catalyst on Thermal Stability of Boron-Doped Diamond Single Crystals. *Chinese Journal of High Pressure Physics*. **2008**, 22(2), 215-219.
 7. **WANG Mei**, LI Mu-sen, GONG Jian-hong, LI He-sheng, TIAN Bin. Analysis on reasons of mesh-like structured surface of boron-doped diamond. *Diamond & Abrasives Engineering*. **2008**, 136(1), 19-21.
 8. **WANG Mei**, LI Mu-sen, GONG Zhi-guang, LI He-sheng, TIAN Bin, LIU Lei. Influence on Thermal Stability of lib Type Diamond Single Crystals under High Temperature Annealing. *Heat Treatment of Metals*. **2007**, 32, 466-469.
 9. **WANG Mei**, LI He-sheng, LI Mu-sen, TIAN Bin. Thermal stability comparison of the IIb type and the Ib type diamond. *Journal of Shandong University of Technology*. **2007**, 37(6), 41-43.
 10. **WANG Mei**, LI Mu-sen, GONG Jian-hong. Study on the composition and structure of covering metal film of boron-doped diamond. *Diamond & Abrasives Engineering*. **2005**, 5:1-3.

11. LI He-sheng, QI Yong-xin, GONG Jian-hong, **WANG Mei**, LI Mu-sen. Boride phase-structure in metallic film and the formation of boron-doped diamond single crystal. *Superhard Material Engineering*. **2008**, 20(1), 1-4.
12. SU Li, GONG Jian-hong, LI He-sheng, **WANG Mei**, LI Mu-sen. Influences of boron carbide on synthesis of diamond from Fe-based system. *Industrial diamond*. **2007**, 1, 20-25.
13. LI He-sheng, GONG Jian-hong, **WANG Mei**, LI Mu-sen. Synthesizing Diamond with Sheeted Iron-based Catalyst Accepting Powder Technology. *Journal of Synthetic Crystals*. **2007**, 36(3), 573-577.
14. GONG Jian-hong, LI Mu-sen, Xu Bin, **WANG Mei**, ZHENG Ke-fang. Investigation on the microstructure and behaviors of boron-doped diamond synthesized under Fe-Ni-B catalyst. *Proceedings of International Symposium on Materials Science and Engineering (C)*. **2005**, 2, 1150-1154.

